

Universitat de València
Institut de Ciència Molecular

Doctorat en Química Sostenible

Functional CdSe and CdSe/ZnS nanoparticles
capped with thiols: photophysical and
photochemical properties and applications as
sensors

JORDI AGUILERA SIGALAT

Directoras de tesis: JULIA PÉREZ PRIETO
RAQUEL EUGENIA GALIAN

València 2012

Dña. Julia Pérez Prieto, Profesora Catedrática de Química de la Universitat de València y Dña. Raquel E. Galian, Doctora en Química de la Universitat de València

CERTIFICAN: Que la presente Tesis Doctoral, titulada: **“Functional CdSe and CdSe/ZnS nanoparticles capped with thiols: photophysical and photochemical properties and applications as sensors”** ha sido desarrollada por JORDI AGUILERA SIGALAT en el Instituto de Ciencia Molecular (ICMol) de la Universitat de València.

Julia Pérez Prieto

Raquel E. Galian

“The solution to a problem changes the problem...”

Agradecimientos

a mis padres, a mi abuela, a mi hermana, a mis tíos y primos,
a Fina y a su familia,
a mis directoras de tesis,
a mis amigos,
a mis compañeros.

CONTENTS

1 - INTRODUCTION.....	3
1.1 - Optical properties of CdSe QDs.....	6
1.2 - Core-shell structures.....	9
1.3 - Synthesis of CdSe QDs.....	11
1.4 - Ligands.....	15
1.4.1- Phosphines.....	18
1.4.2- Carboxylic acids.....	19
1.4.3- Amines.....	19
1.4.4- Thiolates.....	22
1.5- The role of the ligands.....	27
2 - AIMS OF THIS THESIS.....	39
3 – SUMMARY OF PUBLISHED ARTICLES RELATED WITH THE THESIS.....	43
3.1-Fluorescence enhancement of amine-capped CdSe/ZnS quantum dots by thiol addition.....	49
3.2 - Highly fluorescent and photostable organic- and water-soluble CdSe/ZnS core-shell quantum dots capped with thiol.....	53
3.3 - Quantum dot/cyclodextrin supramolecular systems based on efficient molecular recognition and their use for sensing.....	59

3.4 - Further insight into the photostability of the pyrene fluorophore in halogenated solvents.....	65
3.5 – Photoluminescence enhancement of CdSe Quantum Dots: a case of organogel-nanoparticle symbiosis	71
4 - CONCLUSIONS.....	79
5 - SUMMARY OF THE THESIS.....	83
6 - JUSTIFICATION OF THE THEME AND ORIGINAL CONTRIBUTION OF THE AUTHOR.....	89
7 - SUMMARY OF THE THESIS IN SPANISH	93
8 - BIBLIOGRAPHY.....	131
9 - PUBLISHED ARTICLES RELATED WITH THE THESIS.....	141
10-PUBLISHED ARTICLES NO RELATED WITH THE THESIS..	275

1 - INTRODUCTION

In the last few years, a new class of hybrid fluorophores with exceptional photophysical properties has been developed: the quantum dots (QDs). These QDs are semiconductor nanocrystals with diameters from 1 to 100 nm, comprising some hundreds to a few thousands of atoms. The core QDs (QD-C) are formed by groups 12-16 (for instance **CdSe**, CdS, CdTe, ZnSe), 13-15 (InP, InAs), or 14-16 (PbSe) elements of the periodic table. A representation of CdSe QD is shown in figure 1.

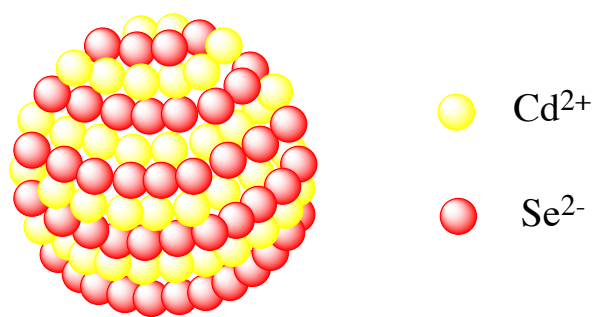
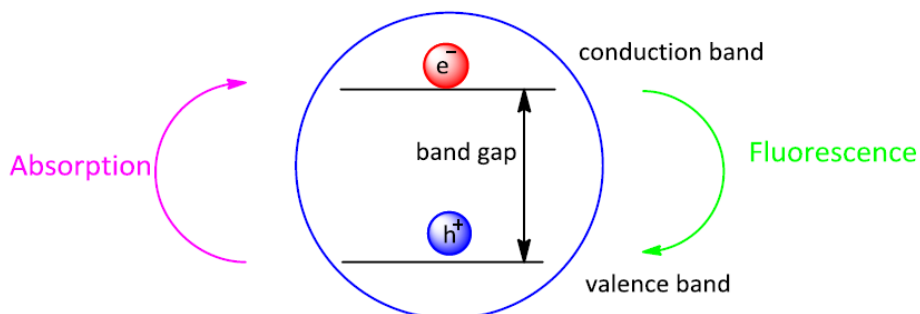


Figure 1 –Illustration of a CdSe QD.

In the nanometre size regime, many physical properties of the semiconductor particles change with respect to the bulk material. In the case of bulk semiconductor, the gap between adjacent energy levels is infinitesimally small, so it is considered as a fixed value (continuous band gap). It is important to mention that, a bulk semiconductor has constant physical properties regarding of his size, while a quantum confinement effect occurs in the nanometre size regime.^{1,2} In a semiconductor nanoparticle, an electron (e^-) can be excited from the valence band to the conduction band by absorption of a photon with an appropriate energy and this process generates a hole (h^+) in the valence band. The formed $e^- - h^+$ pair is called exciton (scheme 1). Recombination of this electron-hole pair results in the fluorescence process.



Scheme 1 - Energy difference between valence and conduction band of the QD and processes of absorption (magenta) and fluorescent emission (green).

The QDs show excellent advantages such as higher photostability, as well as longer lifetimes and higher fluorescence quantum yields than organic fluorophores. All of these *photophysical properties* of the QDs make them of interest for biological, medical and engineering applications.^{3,4,5,6}

1.1 - Optical properties of QDs

The QDs exhibit an UV spectrum showing a peak at longer wavelengths (exciton peak). Due to quantum confinement, the smaller the QD's size, the shorter the wavelength of the exciton peak and, consequently, the fluorescence emission (figure 2 and 3).

A direct estimation of the nanoparticle size (diameter, D) from the maximum in the UV-visible absorbance spectra was published by Peng *et al.* see equation 1:⁷

$$D_{\text{CdSe}}(\text{nm}) = 1.6122 \cdot 10^{-9} \lambda^4 - 2.6575 \cdot 10^{-6} \lambda^3 + 1.6242 \cdot 10^{-3} \lambda^2 - 0.4277 \lambda + 41.57 \quad \text{Eq.1}$$

It is important to say, that while the position of the exciton peak depends on the QD band gap energy (and consequently the QD size), the form and width of

the absorbance band will be influenced by the size's distribution, as well as by the stoichiometry of the Cd/Se atoms in the nanoparticle. Sometimes, the absorbance spectra show small absorption bands at shorter wavelengths; they correspond to excited states of higher energy.⁸

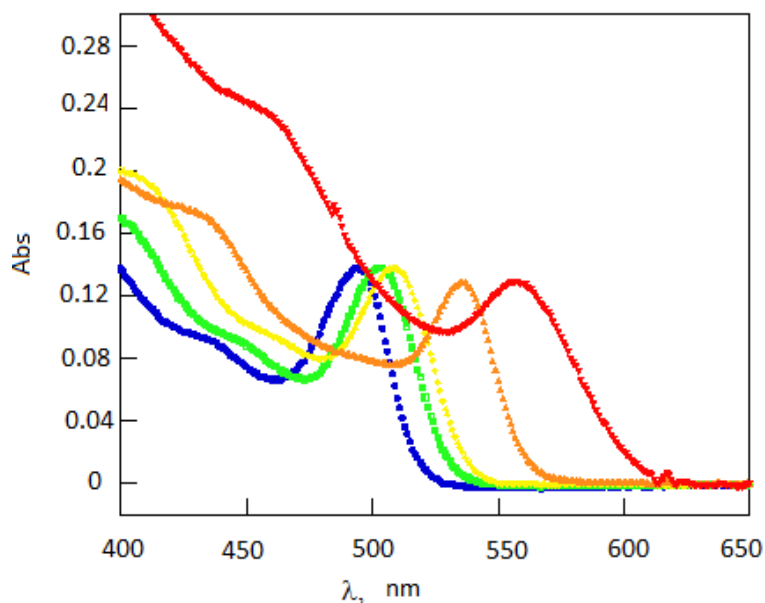


Figure 2 - Absorption spectra of CdSe QDs with different sizes (from ca. 2 nm to ca. 2.5 nm) in toluene.

In addition to this, QDs present high molar extinction coefficients (ϵ), which makes them of special interest in single molecule spectroscopy.⁹ This molar extinction coefficient keeps a relation with the size of the nanoparticle, according to the equation 2 described by Peng *et al*:

$$\epsilon_{\text{CdSe}} (\text{M}^{-1} \cdot \text{cm}^{-1}) = 5857 \cdot D^{2.65} \quad \text{Eq. 2}$$

The fluorescence spectra in figure 3 show very symmetric and narrow emission bands. In addition, QDs present high fluorescence quantum yields, which depend on the quality of the quantum dot. This means that the fluorescence

quantum yield can be reduced as a result of the quenching caused by surface defects (surface trap states).¹⁰ These trap states are imperfections in the regular geometrical arrangement of the atoms in the crystalline structure of the nanoparticle. These imperfections result from deformation of the solid, rapid cooling from high temperature, or high-energy radiation striking the solid, most of them originated in the synthesis of the QDs. Located at single points, along lines, or on whole surfaces in the solid, these defects influence their mechanical, electrical, and optical behaviour.¹¹

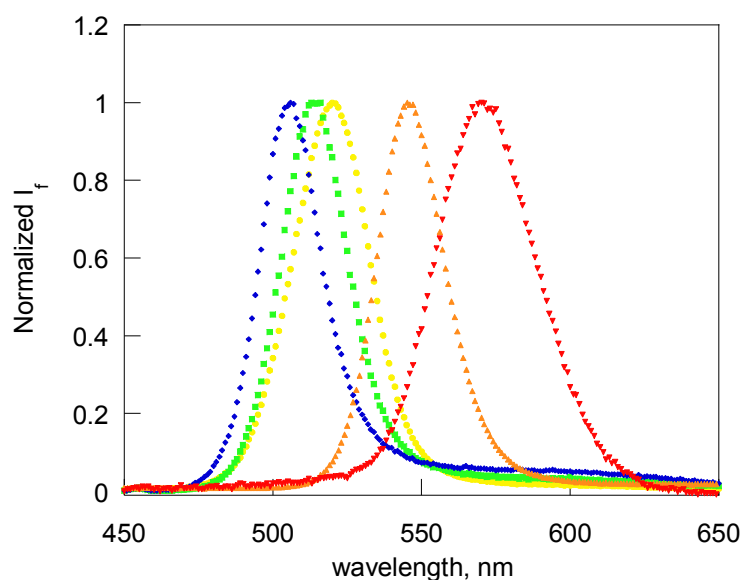


Figure 3 - Normalized emission spectra of CdSe QDs with different sizes (from *ca.* 2 nm to *ca.* 2.5 nm) in toluene.

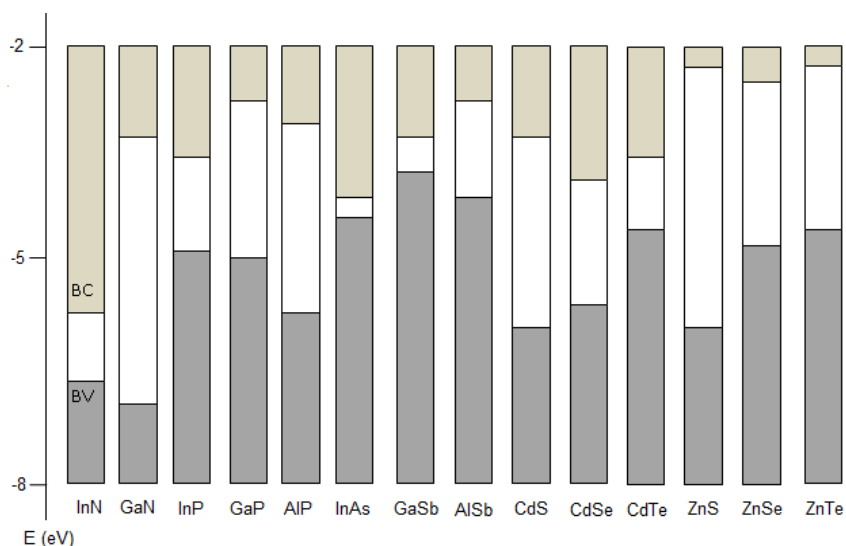
Among the traps states caused during the synthesis are those related with Cd and Se dangling bonds (i.e absence of the Cd or Se in the crystal lattice) or small distortion of the crystal lattice. These trap states can be considerably reduced by a correct passivation of the QD surface. Different kinds of passivation can be used in order to increase the fluorescent quantum yield, but the most

common way is the use of a second semiconductor layer resulting in core-shell systems (QD-CS). This phenomenon will be discussed in the next section.

1.2 - Core-shell structures

The passivation of QD-C with a shell of a second semiconductor is the most used strategy in order to increase the fluorescent quantum yield.^{10,12,13} On one hand, this strategy improves the fluorescence quantum yield and the stability of the QD against photo-oxidation, and on the other hand, it is possible to tune the emission wavelength in a large spectral window by selecting the suitable core and shell material.

Depending on the band gap and the relative position of electronic energy levels of the semiconductors, we can design QD-CS with different functions. These relative positions can be observed in the scheme 2, which represent the band gap of the most used materials employed in the nanocrystal field.



Scheme 2 - Electronic energy levels of selected 13-15 and 12-16 group semiconductors using the valence band offsets¹⁴

Two kinds of QD-CS can be distinguished, called *type I* and *type II* band alignment:

- In the first one, *type I*, the band gap of the shell material is greater than the band gap of the core material, with the valence band of the shell situated below the valence band of the core, and the conduction band of the shell located over the conduction band of the core. This kind of shell plays a crucial role in the emission properties of the QD, because it decreases the non-radiative pathways associated with the trapping of the electron or the hole generated after the absorption of the light by the core. With this passivation, the optical properties of the QD are improved, since the shell separates physically the surface of the core from its surrounding medium, reducing the sensing of the core to the environment, such as water molecules or oxygen. Nanoparticles passivated with this shell are more stable against photodegradation. The most used QD-CS until now is the quantum dot formed by CdSe in the core and ZnS in the shell, denominated commonly as **CdSe/ZnS** QDs (figure 4). The shell growth produce a small red shift (around 5 – 10 nm) in the absorption and emission band spectra of the CdSe. Other kinds of QD-CS *type I* are: CdSe/CdS, CdTe/ZnS, or ZnSe/ZnS among others.

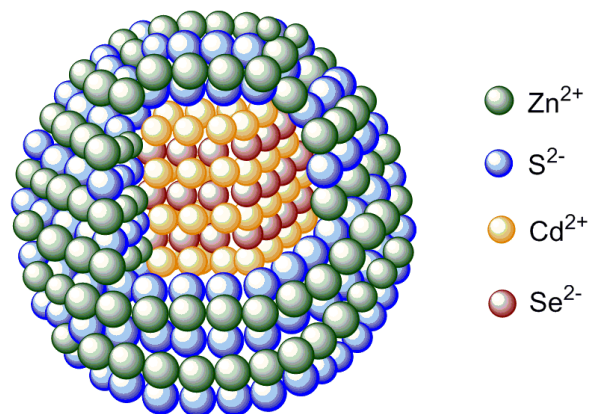


Figure 4 - CdSe/ZnS illustration

- In the second one, *type II*, the valence band or the conduction band edge from the shell material is located among the band gap of the core. The resulting alignment of the bands, leads to a special separation of the hole and the electron in separate regions of the QD-CS structure after the QD absorption of light. This shell produces a significant red shift of the emission wavelength of the QD. These shells are interesting because they allow the tuning of the emission colour using different shell thickness, which is not possible with other kinds of materials. The principal use of these materials is in the synthesis of QDs with emission in the near infrared region. Some examples of this QD-CS are CdTe/CdSe or CdSe/ZnTe QDs. In addition to this, *type II* shells have large photoluminescence decays (in comparison with *type I*) due to the lower overlap of the electron and hole wavefunctions¹⁴ in this system, as the electron or the hole are located in the shell. In addition, a second shell of another semiconductor from *type I* can be used in order to improve the QD fluorescence quantum yield and photostability.

1.3 - Synthesis of CdSe QDs

Nowadays, there are many procedures available for the preparation of QDs. They can be grouped, depending on the reaction temperature, the precursors and ligands used, the type of the shell, QD's shape, etc. To simplify, the procedures have been classified depending on the final media in which the nanoparticle will be solubilized, i.e. organic or aqueous media.

Aqueous media

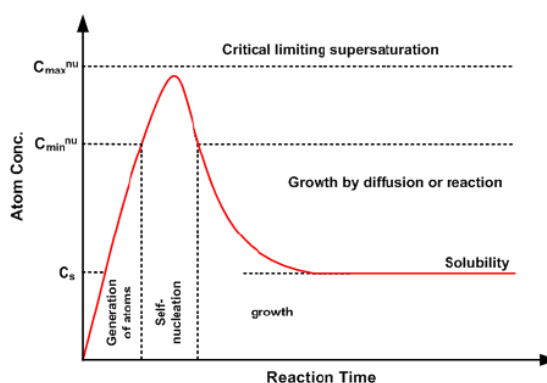
The first methodology for the efficient synthesis of QDs was developed in aqueous media, by precipitating Cd²⁺ ions with the stoichiometric amount of injected H₂S. Then, the solution was activated by adding NaOH and an excess of Cd²⁺ ions.¹⁵ Lately, surfactants or polymers have been used as ligands or

stabilizers.^{16,17} Polymers can bind to the nanoparticle surface and stabilize them (avoiding the agglomeration and precipitation) by steric hindrance or electrostatic repulsion. Some examples are the contributions of Gratzel *et al.*,¹⁸ Henglein *et al.*,^{19,20} Winge *et al.*²¹ or Nozik *et al.*,²² among others.

One of the main problems of water-soluble QDs is the broad size distribution. In order to minimize this problem, several strategies can be found in the literature, such as the size-selective precipitation from solvent-non-solvent mixtures.²³ This methodology, quite simple, is based on the different solubility between small and large nanoparticles. Other techniques are the exclusion chromatography²⁴ and electrophoresis.²⁵

Organic media

Organic-soluble QDs have been synthesized by using high temperature preparation procedures, to obtain monodisperse CdS, CdSe and CdTe nanoparticles. LaMer and Dinegar have demonstrated that the synthesis of monodisperse colloids via homogeneous nucleation requires two separate steps: the formation of the nuclei (nucleation) and the subsequent growth stage.²⁶ This phenomenon is illustrated in the scheme 3.



Scheme 3 - Plot of LaMer's model for the generation of atoms, nucleation, and subsequent growth of colloidal synthesis.²⁷

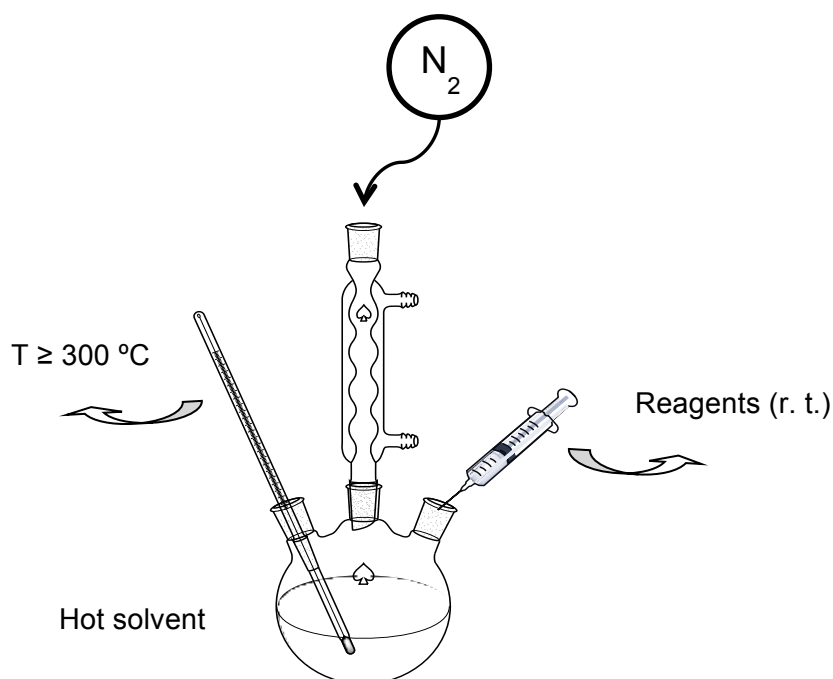
The formation stage comprises three steps: the generation of the atoms, self-nucleation, and the particle growth.

- 1- Initially, the concentration of monomers (minimum subunits of the crystal) increases constantly by generation in situ or by addition from the exterior. It is important to say that no nucleation occurs even above the saturation concentration (C_s)
- 2- When the reaction reaches a degree of supersaturation (C_{\min}^{nu}), the nucleation and formation of stable nuclei take place. Briefly, the consumption rate of the monomer is greater than its production, so that the monomer concentration decrease below C_{\min}^{nu} .
- 3- After that, the subsequent growth stages strongly govern the final morphology of the nanocrystals, determined by the chemical potentials of the different crystallographic faces, which are in turn highly dependent on the reaction environment, such as temperature and solute concentration.

Experimentally, the rapid injection of the reagent into the hot solvent (~ 320 °C) leads to separation of both stages, i.e. the nucleation and growth.²⁸ This methodology, called *hot injection method*, raises the precursor concentration in the reaction flask above the nucleation threshold (scheme 4). The instantaneous nucleation is immediately quenched by the fast cooling of the reaction mixture, since the solution to be injected is added at room temperature or slightly heated (~ 50 °C). The subsequent decrease of the supersaturation after the nucleation burst helps in this quenching.

Another methodology adapted from the synthesis of metallic nanoparticles to be used is the *heating-up method*.²⁹ This method consists in the gradually heating of the reaction mixture to achieve the degree of supersaturation required for the homogeneous nucleation.

In an ideal synthesis, all crystallization nuclei must be created at the same time and with a similar size. Using both methodologies described above, samples with 5 – 10 % standard deviation from the mean size can be obtained.



Scheme 4 - Illustration of the synthesis of QD

The main disadvantage of these methodologies is the use of pyrophoric organometallic precursors, which requires some special experimental precautions. Moreover, due to their high reactivity, it is not possible to synthesize the nanoparticles in a large scale. Recently, the organometallic precursors have been replaced by easy to handle and more environmentally friendly standard reagents. For instance, dimethylcadmium has been substituted by cadmium oxide or cadmium salts (cadmium acetate).³⁰

1.4 - Ligands

The nanoparticle surface must be passivated with organic ligands, allowing the QDs to remain stable in organic solvents or water. For this purpose, the choice of the ligands will be one of the main factors to be considered in the study of QDs and their applications.

The optical properties of the QDs can be modified depending on the ligand, so it will be chosen taking into account the QD application. The ligand can consist of:

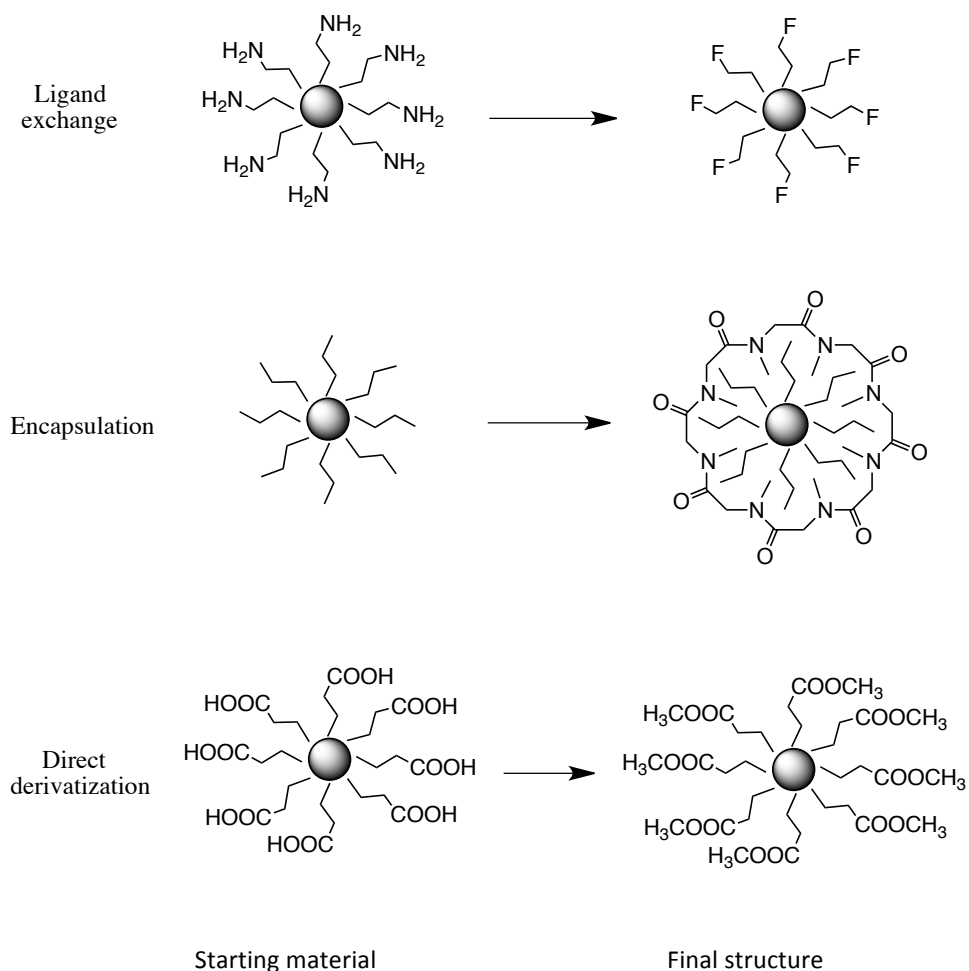
- An anchor group with high affinity for binding to the QD surface.
- A spacer group, such as an alkyl chain, also called linker.
- A functional group or chain with a specific function, for instance, chiral recognition or solubility.

Different techniques can be used for surface functionalization of QDs, such as ligand exchange, encapsulation and/or direct derivatization.³¹ Scheme 5 shows a representation of these methodologies.

Ligand exchange can lead to a loss of the QD fluorescence, but this strategy has been used when the ligand is not stable at the high-temperatures used in the synthesis of the QDs.

Another methodology is the encapsulation of the QD by a shell of organic material, such as a polymers or micelles, which make QDs more soluble in a particular media.³² However, the encapsulation increases the volume of the QD, that is not desirable in many applications or processes, such as in QD used as biosensors or in Förster resonance energy transfer (FRET) processes.

Finally, direct derivatization consists of modification of the QD ligand by means of reactions carried out on the QD periphery (comentar).



Scheme 5 - Comparison between different methods used to modify the QD surface.

Different types of ligands have been used to passivate QDs during their synthesis. The most common are phosphines, carboxylic acids, amines, and thiol/thiolates. In addition, sulphones and lactones have also been added to the QD surface with analytical purposes, though there are few examples in the literature.³³

The effect of the ligands mentioned above on the fluorescence intensity of the QDs is very different. For instance, Mulvaney *et al.*³⁴ have studied the effect of the addition of different ligands (figure 5) to a CdSe QD capped with trioctylphosphine oxide (TOPO). They observed that amines produced the best fluorescence response, while the thiol and the carboxylic acid produced the largest decrease of the QD fluorescence. The use of these common ligands will be discussed in the next section.

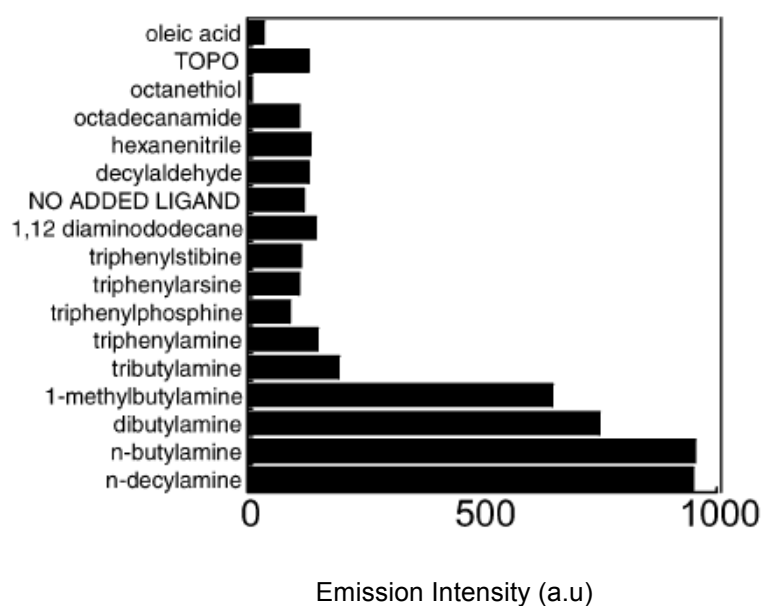


Figure 5 - Fluorescence intensities of 3.1 nm CdSe QD in CHCl₃, 22 h after the addition of different ligands. Image taken from ref. 34.

By analogy with the literature, the nanoparticle functionalized with a ligand will be described such as: QD@ligand

1.4.1 - Phosphines

For several reasons, the most common ligand used in the synthesis of core QDs is trioctylphosphine oxide (TOPO)^{30,35}, scheme 8. The alkyl chains around the QD provide steric repulsion between the nanoparticles and prevent the agglomeration of the QD and their subsequent precipitation. In addition, the bond between the surface of QD and the oxygen of the TOPO is very labile, allowing the ligand exchange in an easy way. Finally, TOPO is very handy and cheap, so we can use high quantity of this ligand to ensure a correct passivation. It is very common to use trioctylphosphine during the QD synthesis in order to solubilize the Se precursor. One of the advantages of the TOPO ligand is the possibility to further functionalize the QD with compounds with alkylic chains by mutual hydrophobic interaction between the carbon chains (encapsulation or interdigitation, figure 6).³⁶ Dioctylphosphine derivatives have been used and proved to be stable at the high temperatures needed for the reactions.³⁷

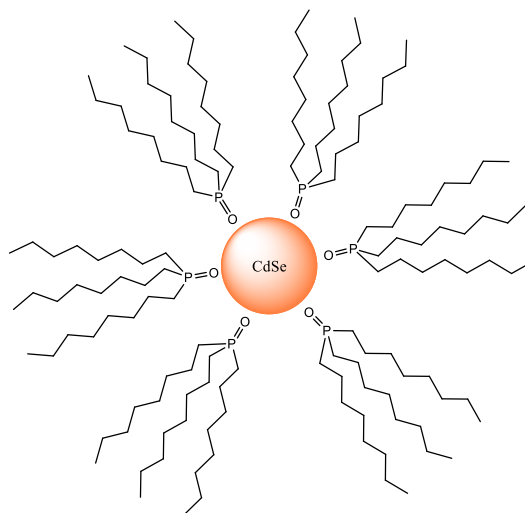


Figure 6 - QD@TOPO structure.

1.4.2 - Carboxylic acids

Organic ligands with a carboxylic acid group can be anchored to the QD surface by the carboxylate group. Generally, addition of carboxylates to QDs produces a drastic decrease of the fluorescence intensity. The main use of this kind of ligands is as analytic and biological labels; for instance, in recognition of several drugs. The interaction between the QD and the carboxylic group is weak enough to allow the release of the ligand from the QD surface. In order to avoid this problem, some researchers have designed a ligand with two carboxylate groups at their focal points which can compensate the carboxylate weak bonding strength.³⁸

1.4.3 - Amines

Amines can also be attached to the surface of the nanoparticle.^{12,39} Several features of the amine can affect the luminescent properties of the QDs, such as the length of the alkyl chain, the number of the substituents of the N atom (steric effect) and the pK_a of the amine. The intensity of this change can be influenced by the size of the nanoparticle. Figure 7 summarizes the change produced on the fluorescence of CdSe QD functionalized with TOPO by the addition of amines with different alkyl chain length and substitution.³⁴

Primary amines increase the intensity emission of the QDs, though the trend between the different chain lengths is still not clear. The luminescence decrease in the following order: primary >> secondary > tertiary amines. The addition of amines to QD capped with TOPO increases the QD fluorescence, up to five times the initial fluorescence in some cases. This effect was observed by Maeda et al.⁴⁰ Another factor to be considered in the fluorescence response of the nanoparticle is the pK_a of the amine added.⁴⁰ The above-mentioned researchers have shown that the fluorescence intensity of the QD increases with the pK_a of the amine, as we can see in figure 8.

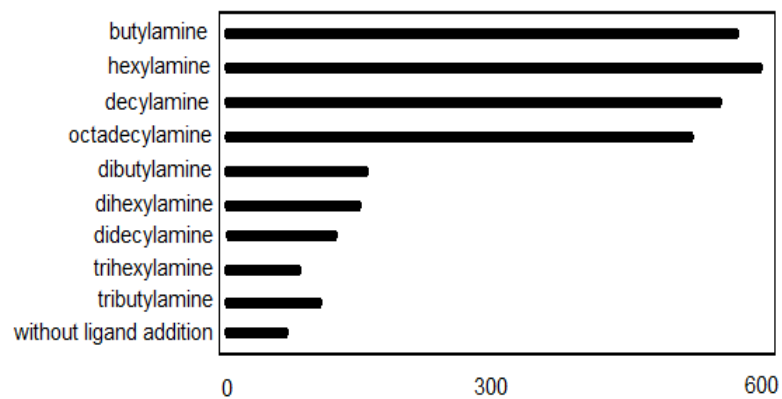


Figure 7 - Relative fluorescence intensity of CdSe QDs capped with TOPO (λ_{max} : 543 nm) in CHCl_3 in the presence of added primary, secondary and tertiary aliphatic amines after equilibration for 22 h. Image taken from ref. 34.

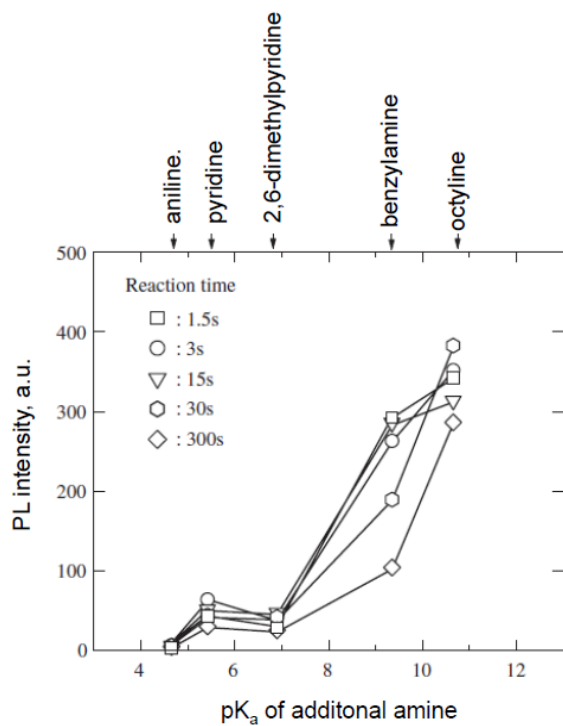


Figure 8 – Fluorescence intensity of QD as a function of the pK_a . Image taken from ref. 40.

Moreover, addition of different amines or direct synthesis with them can affect the maximum of the fluorescence emission, normally to higher frequency (shorter wavelength)⁴⁰. The shift depends on the alkyl chain length and the amino group substituents, as shown in figure 9 and 10.

A special case is the use of pyridine. Ligand exchange of TOPO by pyridine produces “bare” nanocrystals. This is because the interaction between the nanoparticle surface and the pyridine moiety is very weak.⁴¹ In this way, bare-QDs can be dispersed into a conjugated polymer matrix.⁴²

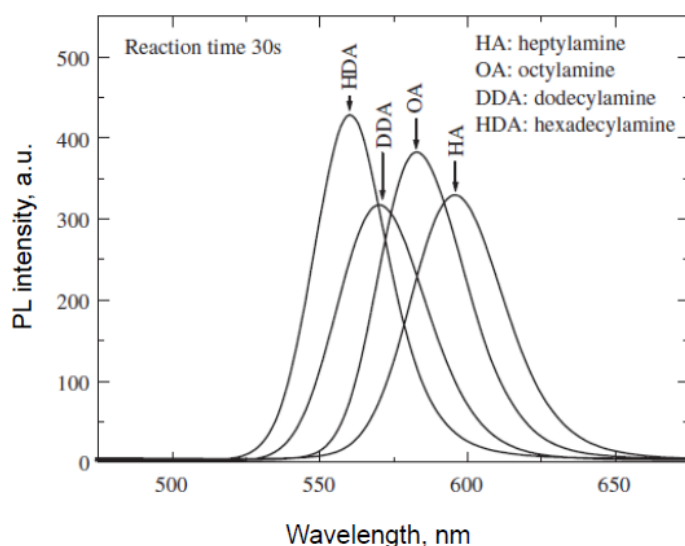


Figure 9 - Fluorescent spectra of CdSe QDs containing primary amines with different alkyl chain lengths. Image taken from ref. 40.

A phosphine-free method has been recently developed, consisting in the use of more environmentally friendly ligands, such as octadecene or octadecylamine, instead phosphines.^{43,44} This approach allows a better control of the reaction conditions while it is cheaper and greener than the phosphine method.

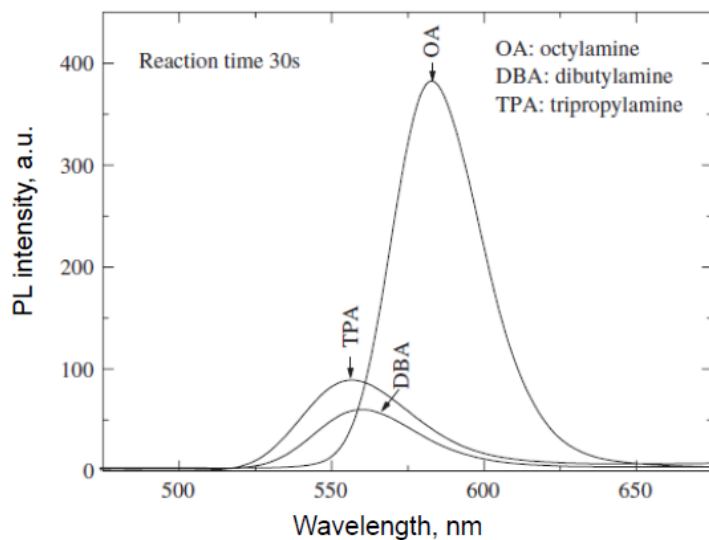


Figure 10 - Fluorescent spectra of CdSe QDs containing alkylamines with different substitution degree. Image taken from ref. 40.

1.4.4 - Thiols / thiolates

Thiols are the most common organic groups used in the passivation of the CdSe core QDs, because of their strong binding to the QD surface. It is well known that aromatic or alkyl thiols produce a remarkable decrease in the fluorescence intensity (figure 11).^{41,45,46}

The quenching of the CdSe QD fluorescence is caused by the transfer of the hole (h^+) from the valence band of the QD to the HOMO of the thiol (non radiative pathway). This is because the HOMO of the thiol is located between the band gap of the CdSe QDs, and after the QD excitation, the hole (h^+) transfer occurs immediately (or in other words, the electron from the thiol is transferred to the QD valence band). This phenomenon is not observed for CdTe QDs (scheme 6) because the valence band of the QD is positioned above of the HOMO of the thiol and, therefore, the trapping of the hole by the thiol is not possible.⁴⁷

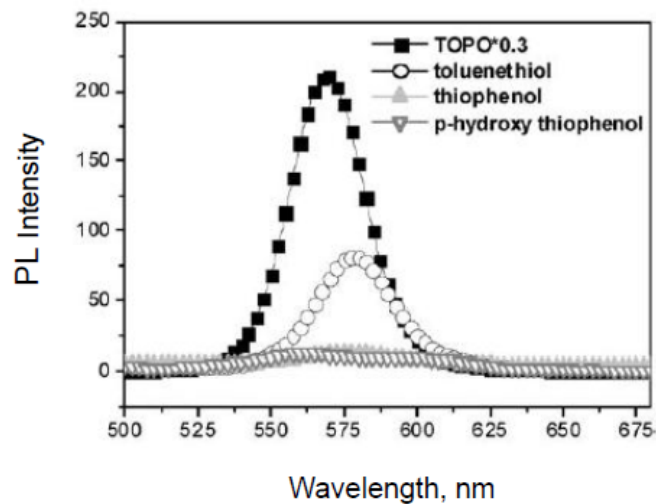
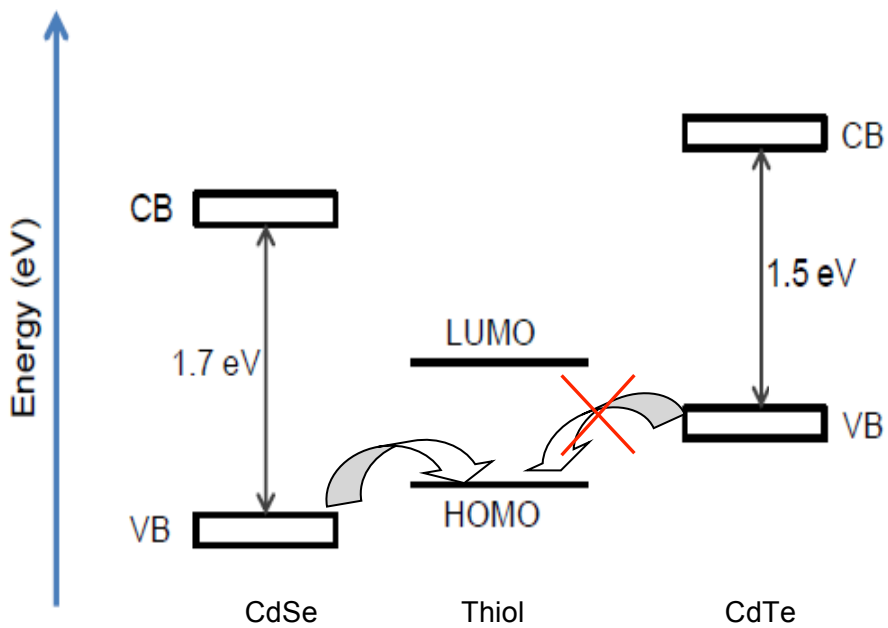


Figure 11 - Fluorescence spectra of CdSe QDs with different aromatic thiol ligands. Image taken from ref. 41.

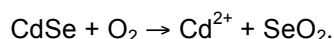


Scheme 6 - Relative positions of CdSe and CdTe band edges versus the HOMO from the thiol.

Although the use of hydrophilic thiols as ligand give rise to water-soluble CdSe QDs, it has been reported that they show low photochemical stability due the following processes: ¹⁰

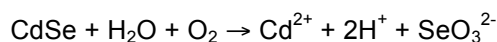
- First, the photocatalytic oxidation of the thiolate occurs on the QD surface. This process can be initiated by the absorption of the light by the nanoparticle, with the consequent oxidation of the thiol to produce thiyl radicals (S[·]), which evolve to disulfides. The formation of disulfides groups is followed by the photoabsorption of water molecules, which produce an enhancement of the fluorescence intensity, due a better passivation of the surface (removal of trapping states).

- Then, the CdSe is partially photooxidized as follow:



This SeO₂ oxide layer causes a better passivation; the layer acts as a second shell of the QDs and eliminates or reduces the surface defects of the QD.

- Finally, the QD undergo photocorrosion and precipitation. The photocorrosion process is described as follow:



When the irradiation time is very long, oxidative dissolution of the QD occurs and SeO₃²⁻ and Cd²⁺ ion are desorbed from the QD surface producing a blue shift of the first exciton absorption peak of the QD (i.e., reduction of its core size). This desorption also causes the precipitation of the QD. Removal of the SeO₂ molecules from the surface exposes new surface defects and lowers the quantum yield. This behaviour is shown in the figure 12. ⁴⁸

In order to improve the stability of thiol-coated semiconductor QDs and to obtain more controllable coupling schemes, some researchers have attempted to link dithiols to the QD surface. In the most cases, dithiols improve the fluorescence properties, however, in some cases they do not produce nanoparticles with better

photostability than the monothiols.⁴⁸

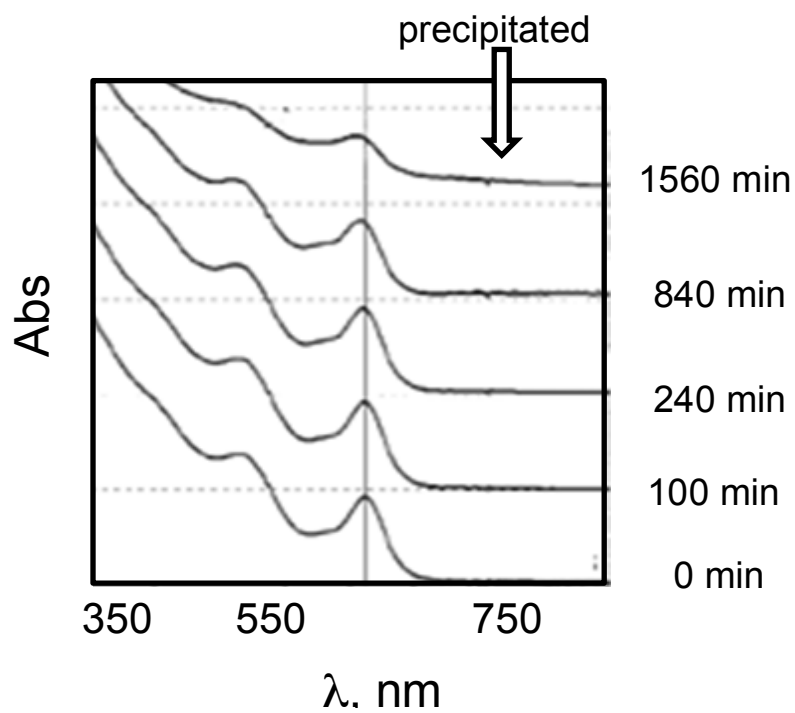


Figure 12 – Precipitation of water-soluble CdSe QDs capped with 11-mercaptoundecanoic acid after 26 h under photooxidation conditions. Image taken from ref. 48.

		<u>Formation energy (Kcal/mol)</u>	
<u>Reaction:</u>		<u>Zn-surface</u>	<u>S-surface</u>
1.- Methane thiol	$\text{H}_3\text{CSH} + \text{ZnS} \rightarrow \text{H}_3\text{CS-ZnS} + \frac{1}{2} \text{H}_2$	7.6	0
2.- Methane thiolate radical	$\text{H}_3\text{CS}\cdot + \text{ZnS} \rightarrow \text{H}_3\text{CS-ZnS}$	46.5	25.1

Table 1 - Binding energies of methane thiol and methane thiyl radical with ZnS.

Pong *et al.* have found that methane thiol cannot covalently bind to the ZnS surface of CdSe/ZnS core-shell QDs, since the total energies of the system were greater than the sum of the clean ZnS slab and methane thiol. However, thiyl radical binds to ZnS, both to Zn or S atoms (46.5 Kcal/mol and 25.1 Kcal/mol, respectively). Table 1 shows the estimated binding energies of thiol and thiyl radical to ZnS surface.^{49,50}

It has been experimentally found that the deprotonated thiols (i.e. thiolates) can bind strongly to ZnS surface.⁵¹ As a consequence, native organic ligands such as phosphines, amines, carboxylic acids, can be exchanged by thiolates. The problem is that this ligand exchange produces a drastic decrease of the QD fluorescence (i.e. the fluorescence quantum yield, ϕ_F , is reduced more than 50%). This behaviour has been explained as due to an exothermic reaction between the thiolate and Zn and S, which produces a significant alteration of the shell. Figure 13 represents this alteration.

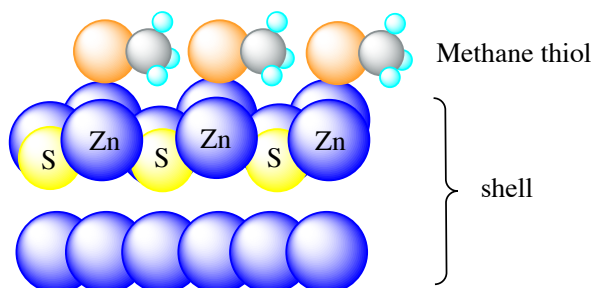


Figure 13 - Binding geometries of methane thiolate on ZnS wurtzite surfaces. For clarity, only the plan and side views of Zn-terminated surface is shown (thiolic sulphur atoms are orange). Notice that Zn atoms are displaced upward when they bind to the thiolate.

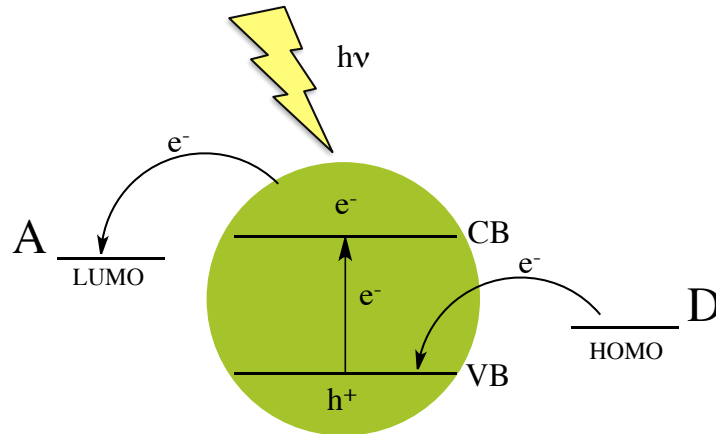
1.5 – The role of the ligands

As it was described in section 1.3, there are different methodologies available in the literature for the preparation of semiconductor nanoparticles, which provide versatile building blocks for nanoscale structures and devices. In order to add functionality to the nanoparticle, different ligands have been used as capping materials (chromophores, polymer), most of them bound to the QDs surface by a thiol moiety. The spherical shape of the nanoparticle allows an elevated number of ligands on the QD surface. Therefore, it is possible to locate high local concentration of a functional group, such as a fluorophores, at the QD periphery.⁵² The ligand can provide not only the desired solubility, i.e. in organic or aqueous media, but also the QD functionality. In addition, the combined action of the QD and the ligand can permit the encapsulation of other molecules bringing them closer to the QD surface. Finally, the functional ligand can reversibly modify the nanoparticles emissive properties and this can be used for sensing applications. The mechanisms involved in this processes can be Photo-induced Electron Transfer (PET) or/and Förster Resonance Energy Transfer (FRET).

The photoexcited QDs can participate in electron transfer process by two different ways (scheme 7):

a- electron transfer from the conduction band to the LUMO of the acceptor molecule (A) with a LUMO energy level less positive than the conduction band potential;

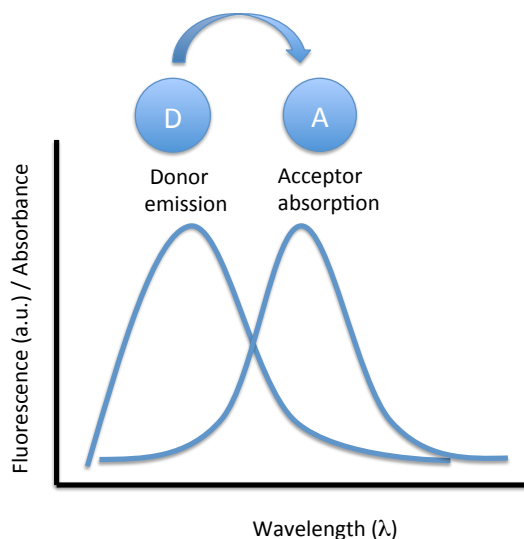
b- electron transfer from the donor molecule (D), with a HOMO energy less positive than the valence band potential, to the hole created in the valence band after excitation of the nanoparticle. In both cases, the electron-hole recombination competes with the electron transfer process leading to a fluorescence quenching.



Scheme 7 – Electron transfer mechanisms in QDs

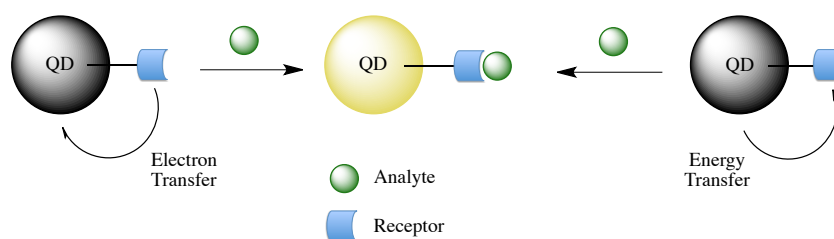
The Förster Resonance Energy Transfer (FRET) between a donor and an acceptor, through a non-radiative dipole-dipole coupling, has been used to monitor sensing events between recognition elements and analytes. The efficiency of FRET depends on (scheme 8):

- i) the distance between the donor and the acceptor (sixth power of the distance)
- ii) the spectral overlap of the donor emission spectrum and the acceptor absorption spectrum
- iii) the relative orientation of the donor emission dipole moment and the acceptor absorption dipole moment



Scheme 8 – Spectral overlap between D and A in a FRET process.

The QDs can operate as fluorescent chemosensors using either electron or energy transfer mechanisms. Conjugation of QDs with sensitive organic ligands as receptors has been used for sensing applications. The fluorescence quenching can occur either through an electron or an energy transfer process depending on the receptor nature. Association of the receptor with an analyte can suppress the electron or the energy process and switch on the fluorescence of the QD (scheme 9).

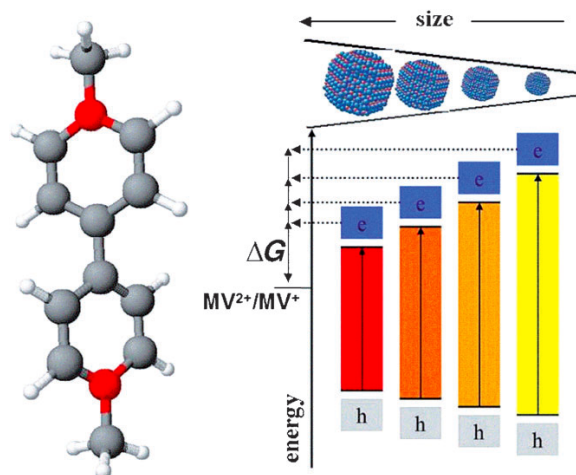


Scheme 9 - The interaction of the analyte with the functionalized QD determines the fluorescence properties of the system.

Photo-induced electron transfer (PET)

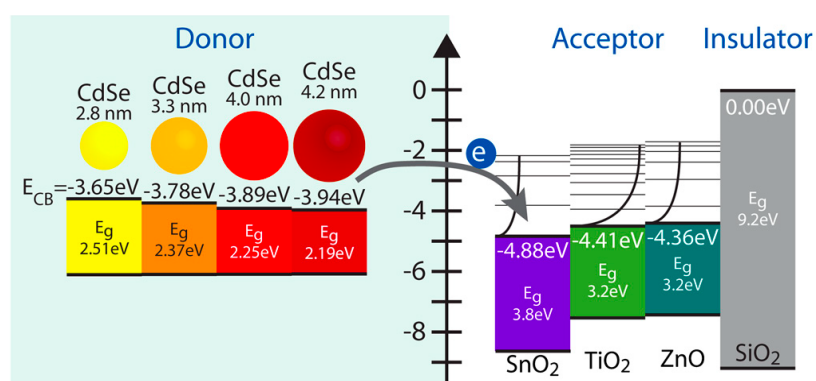
Several researchers have described the interaction between the QD and the ligand in which the electron transfer causes the quenching of the QD fluorescence. This phenomenon depends on the redox potential of the functional ligand and the nanoparticle, which is totally related to the QDs size. PET processes have been reported for both core and core-shell QDs, but only in the case of core QDs, the nanoparticles can act in both directions, i.e. as an electron donor or as an electron acceptor. In the case of core-shell QDs, the nanoparticle can only act as electron donor, because the hole is largely confined in the core, while the electron can delocalize on the surface.⁵³ For instance, Kamat *et al.*⁵⁴ have reported the effect of the *p*-phenylenediamine (PPD) addition in the fluorescence properties of the CdSe QDs. They have observed a linear dependence between the fluorescence quenching of the QD and PPD concentration. The addition of linear amine, such as butylamine among others, enhances the emission yield. This fact suggests that PPD can intercept one of the charge carriers, interrupting the radiative recombination of the exciton. Taking into account the oxidation potential of the PPD and the band gap position of the nanoparticle, they attribute this quenching to an effective scavenging of the photogenerated holes from CdSe surface. Accordingly, they have observed the formation of the PPD cation at the surface of CdSe QD by using the laser flash photolysis technique.

Wachtveitl *et al.*⁵⁵ have studied the ultrafast electron transfer from photoexcited CdSe QDs to methylviologen as electron acceptor (MV^{2+}). They have observed an important dependence of the ET rate with the size of the nanoparticle; the higher the QDs size the lower the ET rate and the ΔG of the process (scheme 10). The formation of MV^+ (absorption spectrum between 600 and 750 nm) was detected by laser flash photolysis at 565 nm.



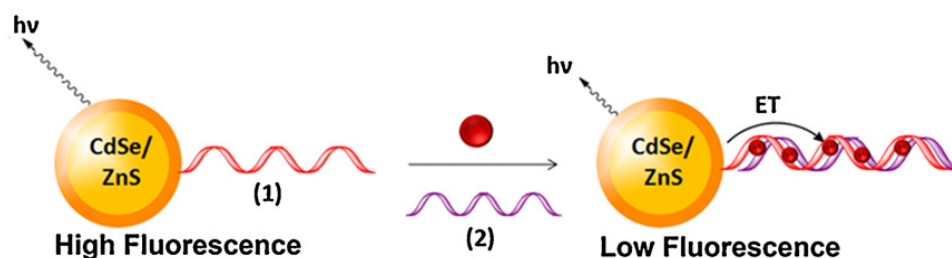
Scheme 10 - Schematic representation of the energetic situation in the QD/MV²⁺ coupled system vs the variation of the QD size.

Photoinduced electron transfer from the QDs as electron donor to semiconductor metal oxide (MOs) as acceptor has been also reported by Kamat *et al.*⁵⁶ This process is possible because the conduction band of the MO is located between the band gap energy of the QDs (scheme 11). This system showed several advantages compared with dye sensitizers and could be used for photovoltaic devices fabrication.



Scheme 11 - Diagram of the relative electronic energy differences between CdSe donating species and MO accepting species for all CdSe-MO combinations.

Photo-induced electron transfer can be used for sensing of analytes such as oligonucleotides and proteins. Functionalized CdSe/ZnS QDs, with a thiolated nucleic acid, have been reported by Willner *et al.*⁵⁷ and were used for the detection of DNA based on a fluorescence-quenching assay. This method involves the PET process between the QDs and doxorubicin in the presence of a complementary nucleic acid (scheme 12), because this molecule can intercalate into duplex DNA. The redox potential of doxorubicin is located between the valence and the conduction band of the QD and, therefore, can accept the electron from the conduction band after the QD excitation.

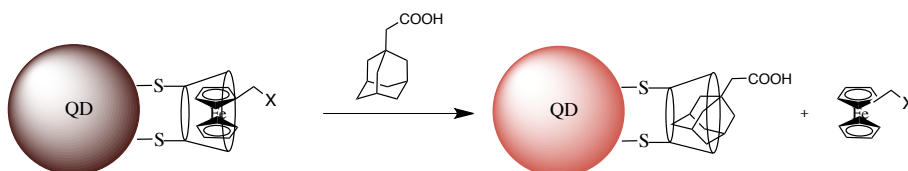


Scheme 12 - Detection of DNA (2) by using a nucleic acid functionalized QDs (1) and doxorubicin (red ball) as the quencher.

There are different molecular receptor, such as cyclodextrins, calixarenes and crown-ethers, used for analytical sensing of various substrates. Fluorescent properties of the receptors capped nanoparticles can be tuned by the binding of the analytes to the cavity of the receptor to form host-guest complexes.

Liu *et al.*⁵⁸ have developed a water-soluble nano-hybrid system based on the use of thiol- β -cyclodextrin as capping receptor of CdS QDs. The modified β -CD can encapsulate organic molecules inside its hydrophobic cavity, as is the case of ferrocene. This complex causes a reversible fluorescent quenching of the QDs by electron transfer mechanism. The addition of adamantane carboxylic acid produces a recovery of the initial fluorescence due to the competitive binding of the

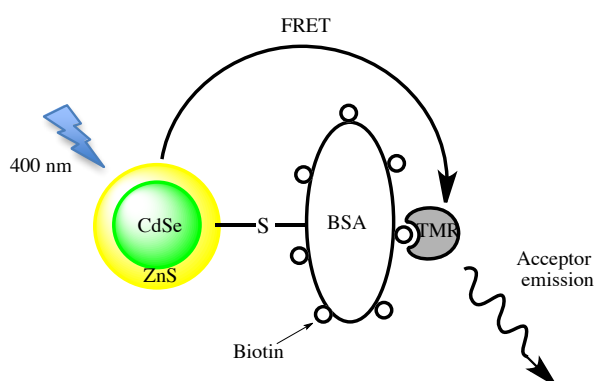
analyte to the β -CD cavity, which has a higher association constant than the ferrocene (scheme 13). This methodology was used to test adamantane carboxylic acid by suppression of the PET between the QD and ferrocene.



Scheme 13 - Detection of adamantane carboxylic acid by PET in CdS QDs.

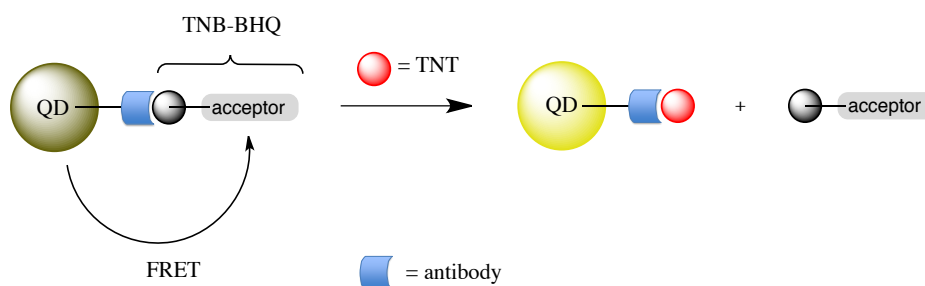
Föster Resonance Energy Transfer (FRET)

Willard *et al.*⁵⁹ have studied the energy transfer from CdSe/ZnS QDs as energy donor to an organic molecules acceptor in aqueous solution (scheme 14). The fluorescence intensity of a thiolated biotinylated bovine serum albumin CdSe/ZnS QDs was quenched by the addition of a modified streptavidin dye (tetramethylrhodamine, TMR). Interaction between biotin and streptavidin approximate the acceptor to the QDs surface and allow the FRET and as a consequence the intensity of TMR was enhanced. These results can be used for the design of new devices for homogeneous assays of antibody-antigen binding, DNA, proteins, etc.



Scheme 14 - Schematic process of FRET between CdSe/ZnS QDs and TMR.

The FRET principle can be used to recognize and detect small organic molecules. For this purpose, Mattoussi *et al.* synthesized a nanosensor based on FRET process for the detection of explosive 2,4,6-trinitrotoluene (TNT). A functionalized dihydrolipoic acid CdSe/ZnS QD linked to an antibody was able to recognize and bind TNT. ⁶⁰ When the QD linked to a TNT analogue labeled with a quenching dye, namely TNB-BHQ is excited, it transfers the energy to the TNB-BHQ, and the fluorescence of the QD was quenched. However, addition of TNT displace away the TNB-BHQ from the QD, the FRET process is suppressed, and the nanoparticle recovers its fluorescence (scheme 15).



Scheme 15 - FRET process between QD and TNT-dye is suppressed by addition of TNT

Very few studies have been reported for CdSe QDs acting as FRET acceptors. Anikeeva *et al.*⁶¹ have reported FRET from a complex of iridium to CdSe/ZnS QDs. In this case, the emission intensity of CdSe/ZnS QDs increases by 55 % when a 10 % of the complex of iridium is near of the QD surface (figure 14). In addition, the QD emission lifetime increases from 40 ns to 400 ns.

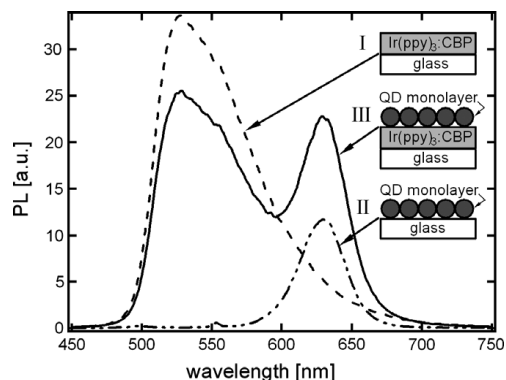


Figure 14 - Fluorescence spectra of samples I, II and III at $\lambda_{\text{ex}} = 395 \text{ nm}$.

Zhong *et al.*⁶² have reported a FRET process from conventional naphthalimide chromophores to CdSe/ZnS core/shell QDs, in which QD acts as energy acceptor. In first place, they functionalized a CdSe/ZnS with a 1,8-naphthalimide and compared the QD fluorescence with and without the naphthalimide. They observed the quenching of the QD emission (energy donor) and the increase of the fluorescence emission of the naphthalimide (energy acceptor, figure 15). They monitored the QD emission at 600 nm ($\lambda_{\text{ex}} = 400 \text{ nm}$) and measured an average lifetime of 13.3 ns for naphthalimide-QD compared to 10.3 for the bare QD. In the case of the naphthalimide ($\lambda_{\text{em}} = 470 \text{ nm}$), the average lifetime was 2.3 ns in the naphthalimide-QD hybrid and 7.8 ns for free naphthalimide. The decrease in the donor lifetime combined with the increase in the acceptor lifetime indicated an efficient FRET process in the naphthalimide-QD hybrid system.

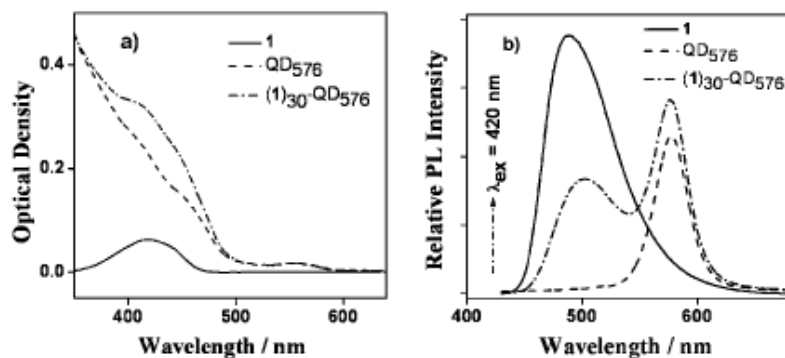
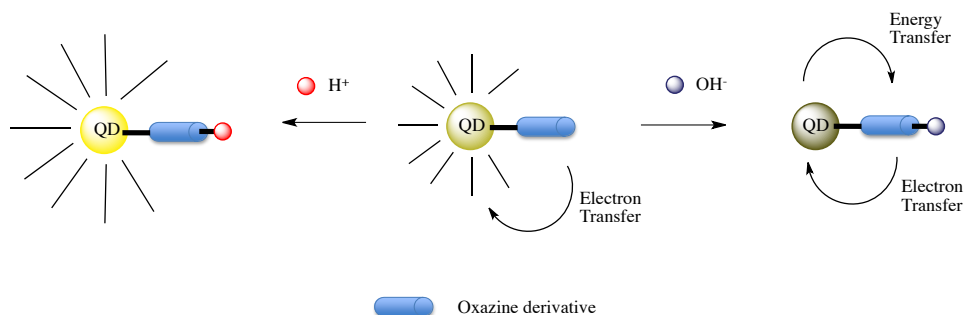


Figure 15 - a) UV/Vis spectra of naphthalimide (1), QD and naphthalimide-QD (1_{30} -QD₅₇₆) assemblies with identical concentrations in CHCl₃. b) The corresponding PL spectra ($\lambda_{\text{ex}} = 420$ nm) at equilibrium state.

Combination of PET and FRET processes

Raymo *et al.*⁶³ have designed an interesting system in which PET and FRET processes were combined. An oxazine derivative was modified with a thiolate group in order to attach it to the nanoparticle surface. This compound behaves as a pH-dependent ligand; in their neutral form, it acts as electron donor, so the fluorescence of the nanoparticle is partially quenched. In their basic form, by addition of Bu₄NOH, it absorbs in the same wavelength region where the QD emits and therefore it acts as energy acceptor. In addition, the basic form modifies the oxidation potential of the neutral oxazine, so that the ligand becomes a better electron donor than in its neutral form. It means, that in presence of base, the QD fluorescence is totally quenched. By contrast, upon adding CF₃CO₂H, the ligand changes to its protonated form, with a notable increase of its redox potential. This change reduces the electron transfer process and enhances the QD fluorescence (scheme 16). The luminescent properties of the nanosystem, which combines FRET and PET process, can be tuned by modification of the pH.



Scheme 16 - Addition of acid to the oxazine derivative prevents the PET. Addition of base modifies the ligand and decreases the QD fluorescence by activation of FRET process and by increase of PET process.

Thiols are one of the most used functional organic groups for the passivation of QDs, because they can attach covalently (as a thiolate) to the QD surface. However, functionalization of both CdSe core and core-shell QDs using thiols as ligands have shown an important decrease in the QD fluorescence quantum yield. Therefore, the design of a new method to obtain highly fluorescent QDs capped with thiols would be beneficial, in order to construct devices for molecular recognition or sensing based in the FRET and PET processes.

2 - AIMS OF THIS THESIS

According with the above-mentioned precedents of the thiol-functionalized CdSe and CdSe/ZnS QDs, the following objectives were proposed:

- To study in detail the effect caused by thiols and thiolates on the fluorescence of CdSe/ZnS QDs, and compare the results with those obtained for CdSe QDs.

- To develop new methodologies for the synthesis of highly fluorescent and photostable organic and water-soluble CdSe/ZnS QDs capped with thiols.

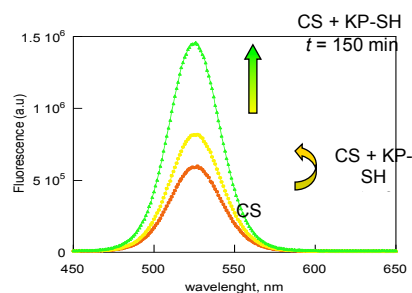
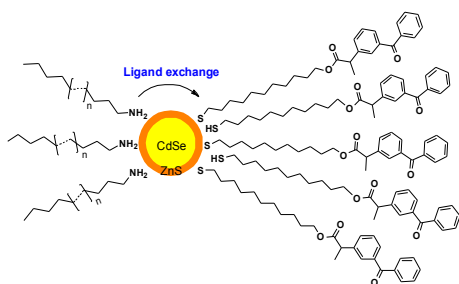
- To design new strategies for the novel, effective, and easy preparation of sensors for molecular recognition, based on particular interactions of the nanoparticles with different analytes.

- To use of nanoparticle as carrier of an organic fluorophore such as pyrene and study its photostability in different chlorinated solvents.

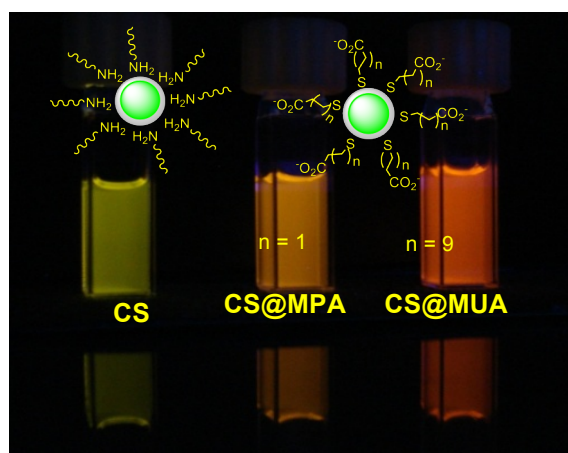
- To study the potential synergistic effect between QDs (core- and core-shell) and an organogelator to obtain fluorescent gels.

**3 - SUMMARY OF PUBLISHED ARTICLES
RELATED WITH THE THESIS**

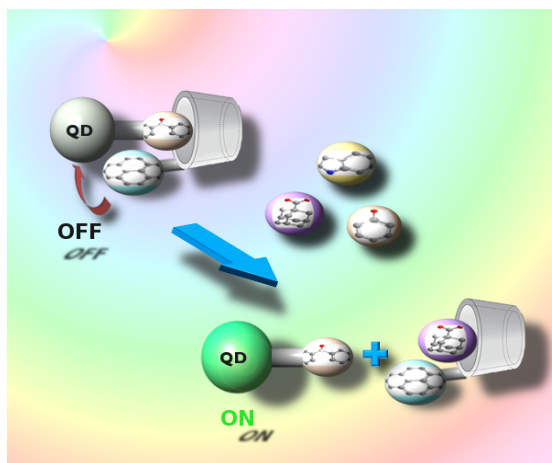
“Fluorescence enhancement of amine-capped CdSe/ZnS quantum dots by thiol addition” Jordi Aguilera-Sigalat, Simon Rocton, Raquel E. Galian, and Julia Pérez-Prieto. *Canadian Journal of Chemistry* **2011**, *89*, 359-363



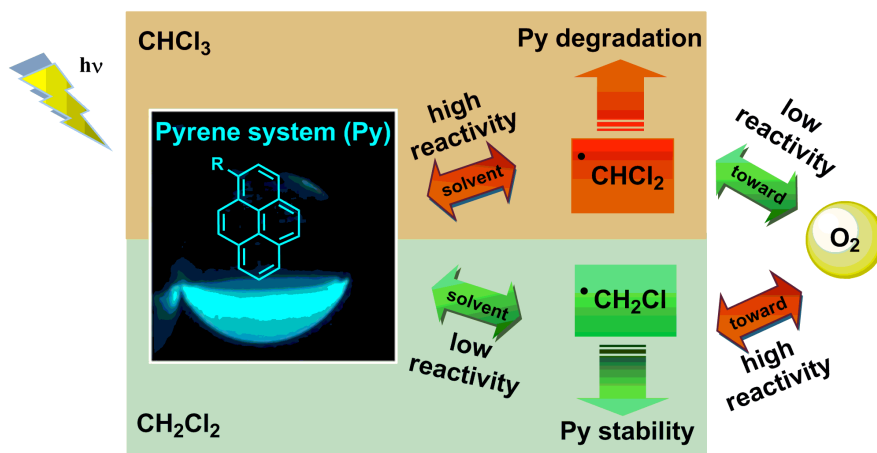
“Highly fluorescent and photostable organic- and water-soluble CdSe/ZnS core-shell quantum dots capped with thiols” Jordi Aguilera-Sigalat, Simon Rocton, Juan F. Sánchez-Royo, Raquel E. Galian, and Julia Pérez-Prieto. *RSC Advances* **2012**, *2*, 1632-1638



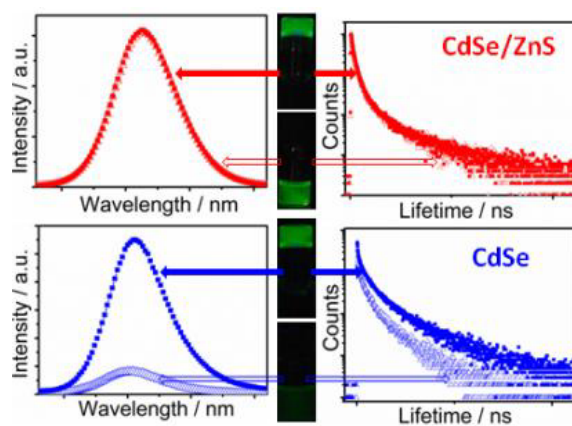
“Quantum dot/cyclodextrin supramolecular systems based on efficient molecular recognition and their use for sensing” Jordi Aguilera-Sigalat, Juan M. Casas-Solvas, Maria C. Morant-Miñana, Antonio Vargas-Berenguel, Raquel E. Galian, and Julia Pérez-Prieto. *Chemical Communications* **2012**, 48, 2573-2575



“Further Insight into the Photostability of the Pyrene Fluorophore in Halogenated Solvents” Jordi Aguilera-Sigalat, Jaime Sanchez-SanMartín, Carlos E. Agudelo-Morales, Elena Zaballos, Raquel E. Galian, and Julia Pérez-Prieto. *ChemPhysChem* **2012**, 13, 835-844



“Photoluminescence enhancement of CdSe Quantum Dots: a case of organogel-nanoparticle symbiosis” Prashant D. Wadhavane, Raquel E. Galian, M. Angeles Izquierdo, Jordi Aguilera-Sigalat, Francisco Galindo, Luciana Schmidt, M. Isabel Burguete, Julia Pérez-Prieto, and Santiago V. Luis. *J. Am. Chem. Soc.* (dx.doi.org/10.1021/ja310508r)



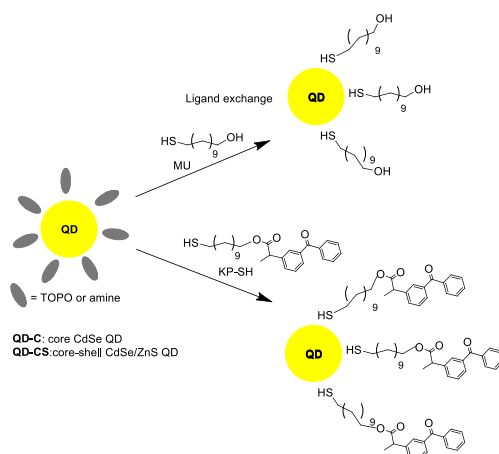
3.1 - “Fluorescence enhancement of amine-capped CdSe/ZnS quantum dots by thiol addition”

Addition of thiols to CdSe core QDs produces a decrease of their fluorescence properties, due to the hole-trapping capacity of thiol molecules.^{48,64} Curiously, a similar effect has been reported for CdSe/ZnS core-shell QDs, where the ZnS should protect the core from fluorescence quenching. This has been attributed to the formation of thiolates in water, which causes new hole trap states.

In this contribution, we seek to better understand the role of the thiols on the fluorescence of organic-soluble core- and core-shell QDs. For this purpose, we have studied the QD emission in the presence of two different alkyl thiols: 11-mercapto-1-undecanol (MU) and a thiol functionalized with a benzophenone chromophore (KP-SH). The benzophenone moiety has been selected in order to add functionality to the QD, using a long carbon chain as a linker to avoid the fluorescence quenching of the nanoparticle, and MU was chosen as pattern ligand. Core QDs have been synthesized with TOPO and TOP as organic ligands; while core-shell QDs possess a long-chain amine as capping material. In addition to this, we have used different sizes of QDs, as well as different thiol concentrations.

First, we have studied the effect of the thiol addition to home-made core CdSe QDs at different concentrations of thiols using steady-state absorption and fluorescence spectroscopy (scheme 17). No changes of the QD absorption, were observed. Surprisingly, an important dependence of the QD emission trend with the thiol concentration was observed. High thiol:QD concentration ratios (above 1000:1), led to a remarkable quenching for all CdSe QDs sizes. By contrast, when the thiol:QD concentration ratio was lower (below 700:1), two different phenomena were observed a fluorescence enhancement and the presence of a broad photoluminescence band at longer wavelength than the exciton emission wavelength, this emission has been ascribed to the creation of new surface states with emissive properties.⁴⁶ This behaviour was observed with different thiols and different nanoparticles sizes (2.5 nm and 3.4 nm).

Then we studied the effect of the thiol addition on the fluorescence of core-shell CdSe/ZnS QDs, purchased from Evident Technologies (QD-CS, www.evidentech.com). These QD-CS were capped with long-chain amines (octadecylamine, ODA). In this case, the addition of different thiols produced a surprising increase of the fluorescence quantum yield, independently of the QD/thiol molar ratio of thiol added. This behaviour was in contrast with the effect reported for the thiolates.⁶⁵ Control experiments were carried out to discard the possibility that the different behaviour between the CdSe and CdSe/ZnS here studied was due to the different capping ligand. ODA was added to CdSe@TOPO, with the consequent increase of the QD fluorescence. Subsequently, MU was added and a high quenching of the fluorescence was observed (figure 16). Hence, amines were not responsible for the different behaviour between the core and core-shell QDs to the addition of thiols.



Scheme 17 - Exchange of TOPO/TOP (core QDs) and amine (core-shell QDs) by thiol compounds.

The behaviour of the CdSe QDs to thiol addition has been previously connected with surface defects. Low thiol concentrations can passivate better the QD surface, whilst high thiols concentrations produce a drastic decrease in the fluorescence emission due to the generation of new surface defects.

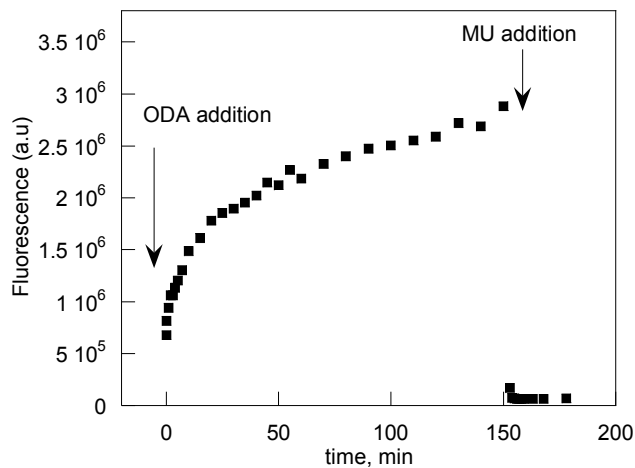


Figure 16 - Time-dependence of the fluorescence intensity of CdSe@TOPO upon addition of ODA followed by addition of mercaptoundecanol 150 min later; [amine]/[QD] = 2200 and [thiol]/[QD]=1800.

By contrast, we found that the addition of thiols to core-shell CdSe/ZnS QDs enhanced their emission properties. To better understand the nature of the thiol binding to the QD, two samples (A and B) containing QD-CS and KP-SH were maintained for 2 hours (CS@KP_{2h}) and 48 h (CS@KP_{48h}) in deaerated chloroform. This experiment allows to follow the reaction versus the time. Both solutions exhibited higher fluorescence than QD-CS. However, after washing treatment (the QD washed and centrifuged) to remove the ligand excess not covalently bound, the emission intensity of CS@KP_{48h} was higher than CS@KP_{2h}. Therefore, this washing of the thiol-capped QDs resulted in a loss of unbound (encapsulated) thiol, which produce lower emission than the original QD. The red-shift emission (4 nm) observed before washing indicates the binding of the thiols to the QD surface. These results demonstrated that the replacement of amines by thiols on the core-shell QDs surface produce better surface passivation of the QD emission. In

addition, the higher fluorescence of CS@KP_{48h} than CS@KP_{2h} suggested that thiolate binding to the QD surface is non-detrimental for the QD emission.

In summary, these results demonstrated that, while addition thiols drastically decrease the fluorescence of the CdSe core QDs, they increase the emission properties of highly fluorescent amine-capped CdSe/ZnS core-shell QDs.

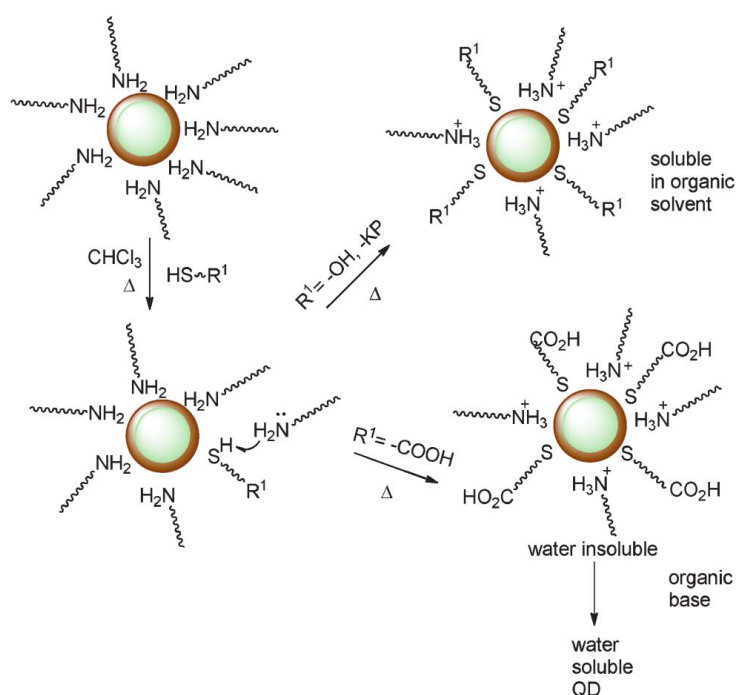
3.2 - “Highly fluorescent and photostable organic- and water-soluble CdSe/ZnS core-shell quantum dots capped with thiols”

Theoretical calculations have shown that thiols cannot bind to the ZnS surface in CdSe/ZnS QDs, however, thiolate binding is thermodynamically favored.⁵¹ However, ligand exchange of TOPO or amine by thiolates produces a drastic decrease of the fluorescence quantum yield due to the high exothermicity of the reaction.^{49,50,51} Nevertheless, we have demonstrated in the previous article that, at room temperature, thiol addition to highly fluorescent CdSe/ZnS QDs capped with a long chain primary amine produces an increase on the QD emission, though the QDs lose the fluorescence intensity after washing, indicating some removal of the encapsulated thiols.⁶⁶ Interestingly, the observation of a red-shifted QD emission suggested that part of these thiols are chemisorbed to the QD surface. The amine ligands apparently act as Lewis bases abstracting the proton of the thiol at the same time that the thiol is anchored to the ZnS as thiolate. Therefore our hypothesis for the present work was that the chemisorption of the thiol to the ZnS surface could be favoured by heating. We report here that chemisorption of thiols to CdSe/ZnS core-shell QDs helped by the amine ligands of the QDs can even improve their emission performance.

The methodology to obtain CdSe/ZnS QDs capped with thiols was as follows:

- First, we prepared the thiol derivatives used to solubilize the QDs either in organic or in water media. A ketoprofen derivative functionalized with a mercapto group (KP-SH) was synthesized using the methodology described by *Ohara et al.*⁶⁷ and was used for the synthesis of organic-soluble QDs. On the other hand, commercial mercaptoundecanoic acid (MUA) and mercaptopropionic (MPA) acid were used to obtain water-soluble QDs.

- Then, the synthesis of the core-shell QDs capped with thiols was carried out from commercial QDs with amine ligands, QD-CS (purchased from Evident Technologies or Ocean Nanotech), by using a simple procedure. The thiol/QD mixture was heated at reflux in chloroform for 48 h in the darkness and absence of air. In the case of the ketoprofen-capped QDs (CS@KP), they were purified by precipitation from MeOH and later they were re-dissolved in toluene. In the case of the water-soluble QDs, they precipitated from CHCl_3 and were washed in the same solvent for several times. Their solubility in water was increased by addition of tetramethylammonium hydroxide and mild heating (scheme 18).



Scheme 18 - Heterobifunctional ligands used in this work and schematic preparation of the organic- and water-soluble QDs.

The $^1\text{H-NMR}$ spectrum of the new nanoparticles showed the typical broad signals of the ligands attached to the QDs, particularly those protons close to the QD surface.^{68,69} In addition to this, the presence of a triplet at 3.3 ppm, ascribed to the CH_2 attached to the N of protonated amine ligands, was observed. These species can be formed by the abstraction of a proton from the thiol by the amine, which acts as a Lewis base.

The UV-Vis spectra showed the first exciton peak of the CS@KP at the same wavelength than QD-CS. In addition, high-resolution transmission electronic microscopy (HRTEM) images showed that the nanoparticles kept their size and crystallinity after functionalization. Remarkably, the fluorescence of CS@KP showed much higher fluorescence quantum yield (in some cases, increase of 50%) than in the case of the precursor QD-CS, while nanoparticles soluble in water maintained the same fluorescence yield (figure 17). These facts demonstrated that the chemisorption of the thiol to the QD surface did not show a negative effect on the QD emission.

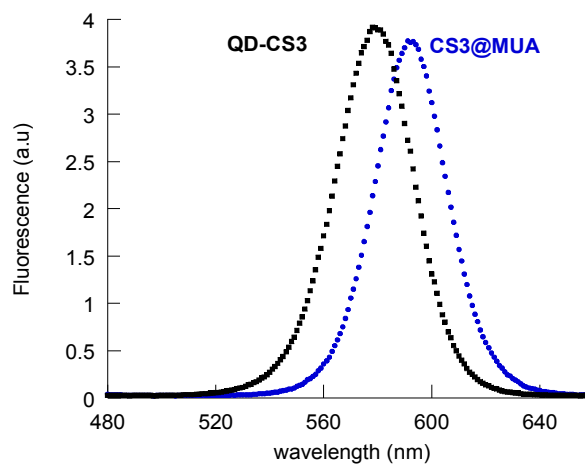


Figure 17 - Comparative fluorescence spectra ($\lambda_{\text{ex}} = 450 \text{ nm}$) of a deaerated toluene solution of commercial QD-CS (black) and a water solution of CS@MUA (blue). The absorbance of the samples at 450 nm was 0.1.

We have confirmed this chemisorption of the thiol to the ZnS surface by IR spectra by comparing the precursor and the final nanoparticle spectra with that of the free thiol ligand. In the nanoparticles capped with thiol, the stretching vibration mode of the thiol group (ca. 2569 cm^{-1}) was not present.

In addition, X-ray photoelectron spectroscopy (XPS) was used, since it provides information of the chemical environment of selected atoms. We compared the original CdSe/ZnS capped with amine versus CdSe/ZnS capped with thiol (organic- and water-soluble QDs), and versus the free thiols (KP-SH and MUA). A core-shell QD prepared by reacting QD-CS with KP-SH at room temperature (CS@KP_{rt}) was also studied. Cd 3d spectra of these compounds are shown in figure 18A. The binding energy of the Cd was similar for all core-shell QD. A new component in the case of QD functionalized with KP or MUA was observed, ascribed to the presence of N 1s of ammonium salts. Regarding the S 2s spectrum (figure 18B), KP-SH showed a peak at 227.4 eV ascribed to the thiol group, while QD-CS presented a peak at 225.7 eV. In the case of CS@KP_{rt} the band was very similar. However, in the case of CS@KP the band shifted to a lower energy (225.3 eV). When this peak was deconvoluted, a new component, shifted to a lower value than the free thiol, was observed (224.4 eV vs 227.4 eV). This peak is attributed to the chemisorption of KP-SH to the QD surface.

In order to check the generality of this methodology to prepare highly fluorescent QDs with QD-S covalent bonds, a home-made TOPO-capped CdSe/ZnS QD prepared using the methodology described by Bawendi *et al.*⁷⁰ with some modifications was synthesized.⁷¹ Then, this QD was treated with an excess of ODA (ratio QD:ODA 1:5000) in order to carry out a ligand exchange of TOPO by ODA. In this way, we obtained CdSe/ZnS@ODA QD. This was treated following the same methodology that we described above to produce CdSe/ZnS QDs capped with thiols. After its characterization, we found that the new nanoparticles showed also high fluorescence quantum yield.

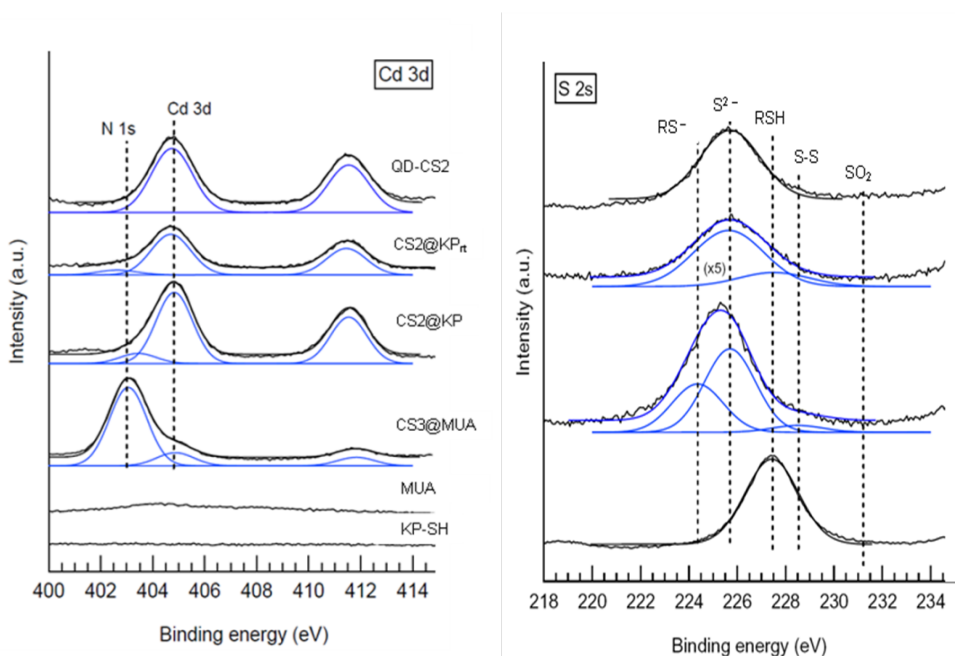


Figure 18 – A) XPS spectra of Cd 3d and N 1s for the QDs. B) top to bottom: XPS spectra of S 2s for QD-CS, CS@KP_{rt}, CS@KP, and KP-SH

In addition, the replacement of the amine capping ligand of core-shell QDs purchased from another company (Ocean NanoTech) by KP-SH thiol (CS@KP₁) and the KP-S⁻ thiolate (CS@KP₂) was also performed. CS@KP₁ was prepared following our strategy, while CS@KP₂ was prepared as follows: KP-SH was treated with an organic base in order to produce the corresponding thiolate (KP-S⁻); which was then added to a solution of the commercial QD-CS. Surprisingly, after the work-up, the CS@KP₁ showed a decrease in their fluorescence of only 8%, while CS@KP₂ showed a drastic decrease of the QD emission (39%).

The ligand exchange procedure was also studied in a home-made amine capped CdSe/ZnS core-shell QDs. In first place, a TOPO-capped QDs was prepared. After that, the amine-capped QDs were obtained using the above-mentioned methodology. The fluorescent quantum yield of the thiol-capped QDs

increase up to 13% in relation with their precursor capped with amine, demonstrating the generality of this methodology.

Finally, we tested the photostability of the nanoparticles capped with thiols, and it was compared with that of their precursor (figure 19). Surprisingly, both water- and organic-soluble CdSe/ZnS capped with thiols, showed a higher photostability than the commercial QDs when they were irradiated for five hours with visible light under aerobic and anaerobic conditions, because QDs are well-covalently bound as thiolates to the ZnS shell, and this prevents disulfide formation and, therefore, QD precipitation.¹⁰

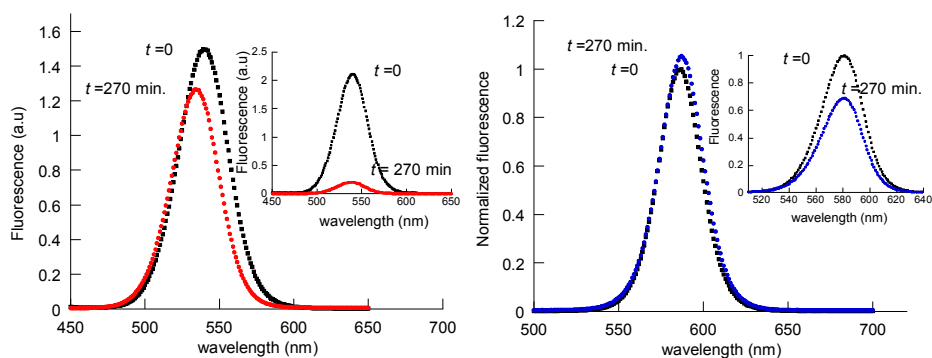


Figure 19 – Left, normalized fluorescence spectra of deaerated toluene solutions of CS@KP, before (■) and after (●) 270 min irradiation at $\lambda > 400$ nm. Inset: comparative fluorescence spectra of QD-CS. Right, Normalized fluorescence spectra of aerated toluene solutions of CS@MPA, before (■) and after (●) 270 min irradiation at $\lambda > 400$ nm. Inset: comparative fluorescence spectra of QD-CS in toluene.

In summary, we have demonstrated that replacement of amine ligands by thiols to lead to either organic-soluble or water-soluble QDs can be performed under mild conditions preserving or enhancing not only the emission properties of the nanoparticles but also their photostability.

3.3 - “Quantum dot/cyclodextrin supramolecular systems based on efficient molecular recognition and their use for sensing”

CdSe/ZnS are highly fluorescent systems that can be used for molecular recognition or sensing of different analytes.

β -Cyclodextrin (β -CD) is a cyclic oligosaccharide containing seven D-glucopyranose units linked by α -(1 \rightarrow 4) bonds. It possesses a toroid structure with the larger opening containing the secondary hydroxyl groups, whilst the smaller opening contains the primary hydroxyl groups. Due to this disposition, the interior of the cyclodextrin is considerably less hydrophilic than the aqueous solution, and can host a variety of hydrophobic compounds (formation of inclusion complexes).
72,73

There are examples in the literature where QDs have been modified with cyclodextrins in order to chemically detect different analytes,^{74,58} by means of either Förster resonance energy transfer (FRET) or photoinduced electron transfer (PET) mechanisms.

In this work, we focused in a new strategy to obtain an effective sensor, based on the molecular recognition between a QD and a β -CD, that showed a fluorescence increase in response to different analytes.

First, we prepared a ketoprofen-capped CdSe/ZnS QD (CS@KP) as we have described in the previous article,⁵⁷ and β -CD was modified with a pyrene unit, the 3-(pyren-1-yl) prop-2-ynyl, on its secondary face (CD-Py). We selected these compounds for two reasons:

- The association constant of β -CD with ketoprofen is quite or pretty high (K_a ca. 3000 M⁻¹).⁷⁵

- The potential capacity of the 3-(pyren-1-yl) prop-2-ynyl moiety to quench the QD emission.

Thus, the effective capping of CS@KP by CD-Py led to the QD/CD supramolecular system (CS@KP/CD-Py, figure 20). The encapsulation of the QD by the CD allows the system solubilisation in polar media (acetonitrile:water 3:1).

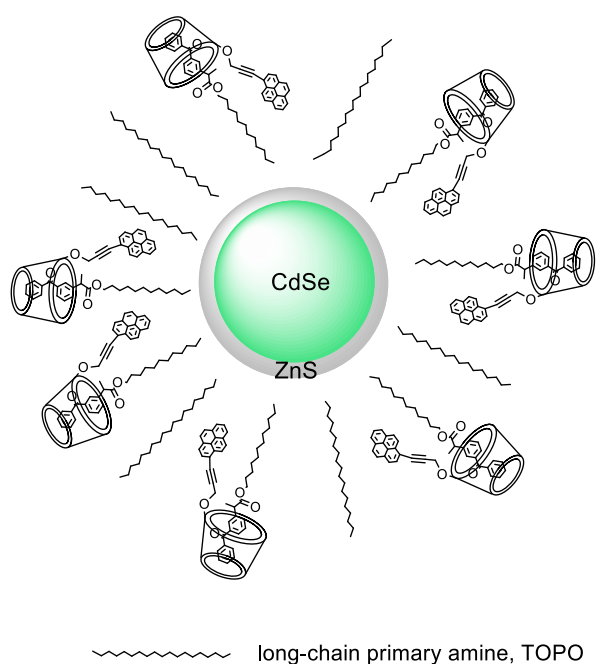


Figure 20 - CS@KP/ CD-Py system

In order to confirm the location of the pyrene moieties in the QD@KP/CD-Py system, transient absorption measurements of the pyrene systems (QD@KP/CD-Py, CD-Py) were performed.⁷⁶ Laser flash photolysis (Nd/YAG, 355nm) of CD-Py showed the formation of the pyrene triplet (λ_{max} at 430 nm, τ ca. 6 μs) and the pyrene radical cation (λ_{max} at 490 nm, τ ca. 31 μs). In the case of the supramolecular system, pyrene radical cation yield and lifetime showed a strong decrease, while the pyrene triplet yield and lifetime showed a high increase. These

results are in agreement with the location of the pyrene moieties of CD-Py within the organic capping ligand of the CS@KP QDs, pointing toward the QD surface, due to the high sensibility of the pyrene to the polarity of the media.

The supramolecular system was prepared by adding a toluene solution of QD to an acetonitrile/water solution of CD-Py (QD:CD-Py = 1/1000). After stabilization, the significant quenching of the QD emission indicates the formation of CS@KP/CD-Py system, which showed a blue-shifted QD emission compared to that CS@KP (figure 21).

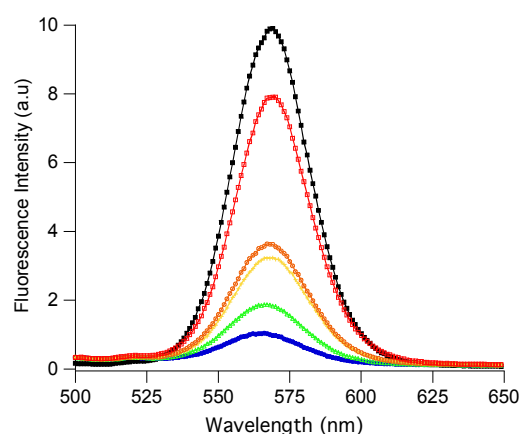


Figure 21. Fluorescence spectra of a deaerated acetonitrile/water (3/1) solutions of CS@KP (■), CS@KP/β-CD-Py ([CS] = 5×10^{-9} M, [β-CD-Py] = 5×10^{-6} M) before (●) and after addition of benzophenone: (2.5×10^{-6} M, ▲), (5×10^{-6} M, +), (1×10^{-5} M, ○) and (2.5×10^{-5} M, □), $\lambda_{\text{ex}} = 450$ nm. The luminescence was recorded after equilibration in ultrasounds 10 min.

The addition of the analyte can cause a competitive association with the CD cavity and, as a consequence, the increase of the QD emission (figure 16) by moving the pyrene (the quencher) away from the QD surface. Among the studied analytes were benzophenone derivatives, phenols, indole, indole derivatives, and adamantane carboxylic acid (figure 22). The different recovery in the QD fluorescence after addition of analytes demonstrates the selectivity of this system.

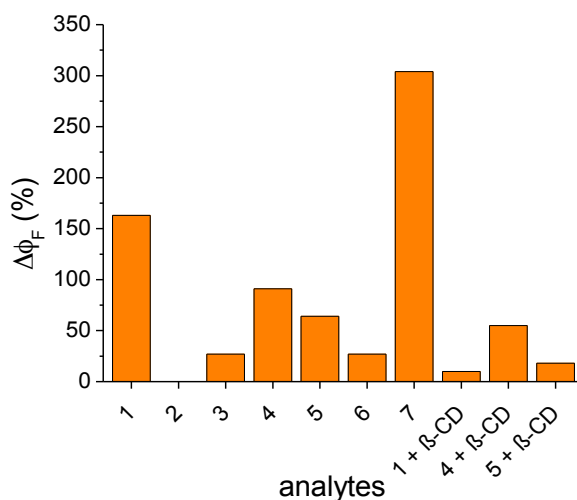


Figure 22 - Effect of the addition of different analytes (1- benzophenone, 2- ketoprofen, 3- ketoprofen methyl ester, 4- phenol, 5- indole, 6- 7-methyl indol, 7- adamantane carboxylic acid) on the fluorescence ($\lambda_{ex} = 450$ nm) of deaerated acetonitrile/water (3/1) solution of CS@KP/ β -CD-Py. The ligand/QD molar ratio was 1000/1. Competitive effect of β -CD for analyte 1, 4 and 5 was also analysed. The luminescence was recorded after equilibration in ultrasounds for 10 min.

Finally, we were able to recover individually the three elements used in the molecular recognition experiment: ketoprofen-capped CdSe/ZnS QDs, the β -cyclodextrin with the pyrene and the analyte. Addition of toluene to the mixture of CS@KP/ β -CD-Py system (ACN/H₂O) with the analyte caused the separation of the solution in two phases, the migration of the acetonitrile to the toluene phase (top), and the separation of the QD in the interphase, because its low solubility in toluene/acetonitrile and the aqueous phase. Subsequently, the organic phase was separated and evaporated; the ¹H-NMR spectrum of the residue showed the recovery of the analyte. Then, toluene was added to the remaining aqueous phase to lead to the QD transfer to toluene; the fluorescence spectrum of the organic

phase demonstrated the recovery of CS@KP, while MS/GC and $^1\text{H-NMR}$ of the aqueous phase corroborated the recovery of CD-Py (figure 23).

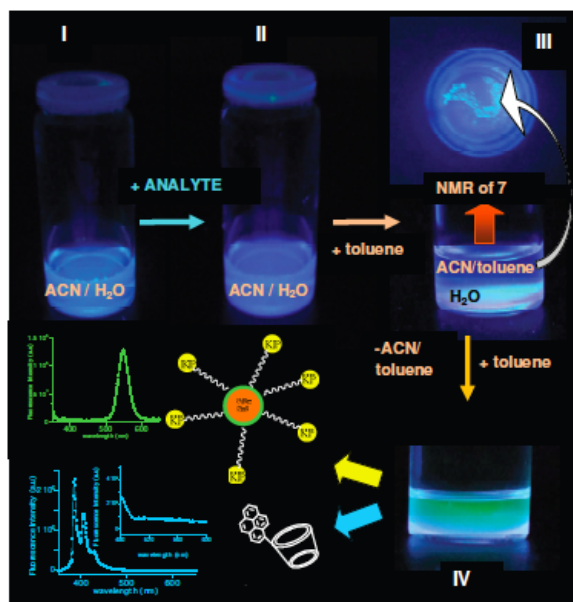


Figure 23 – Recovery of the QD, β -CD-Py and adamantane carboxylic acid (7) once the molecular recognition was completed.

In conclusion, we have prepared a supramolecular QD/CD system, which can be used as effective molecular sensor for different analytes. Moreover, all the components of the assay (CS@KP, β -CD-Py, and the analyte) can be recovered individually, which is highly desirable both from the commercial and environmental points of view.

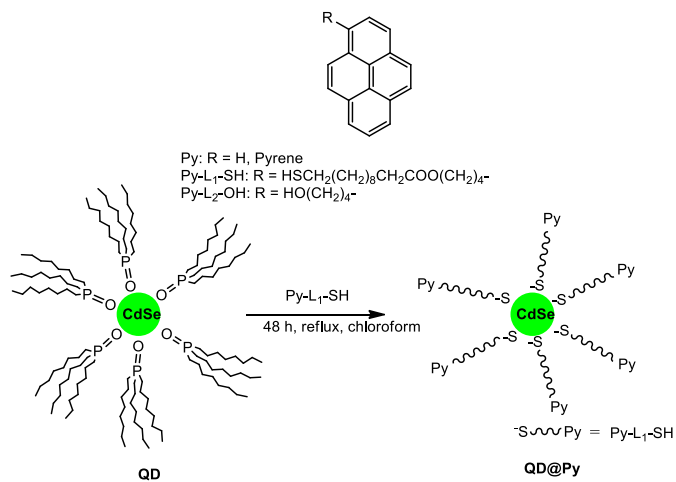
3.4 - “Further Insight into the Photostability of the Pyrene Fluorophore in Halogenated Solvents”

Pyrene chromophore is a polycyclic aromatic hydrocarbon, PAH, used as probe and in fluorescent chemosensors. Some researchers have observed that pyrene experiences important photodegradation in several media, such as dissolved in methanol or acids, or adsorbed in cellulose, among others, that can have a drastic effect on the accuracy of the analysis under consideration.^{77,78,79} In particular, pyrene chromophores in halogenated solvents is a great concern.⁸⁰ In addition, pyrene photostability in chloroform is lower in oxygen than in nitrogen atmosphere.

Spherical QDs have a large surface-to-volume ratio and allow to locate large number of molecules in their periphery. The same number of molecules could not be placed in a flat surface due to the repulsive forces or steric hindrance between them.

The aim of this work was to compare the photodegradation in halogenated solvents (CHCl_3 , CH_2Cl_2) of the pyrene chromophore free in solution with that of pyrene adsorbed to CdSe QD. We have studied and analyzed the photostability of pyrene, a CdSe QD capped with a pyrene derivative (QD@Py) and two alkylpyrene derivatives, Py-L₁-SH y Py-L₂-OH, one of them being the QD ligand (scheme 19).

For this purpose, we prepared a pyrene-functionalized CdSe QD (QD@Py) with a high local concentration of Py-L₁-SH pyrene derivative in their surface, evidenced by the considerable pyrene excimer formation ca. 480 nm (figure 24).



Scheme 19 - Structures of pyrene, pyrene derivatives and synthesis of the QD@Py.

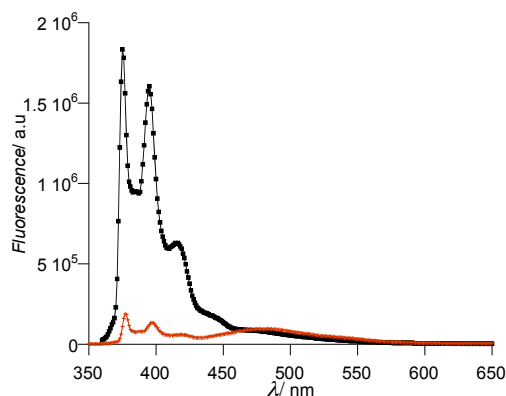


Figure 24 - Fluorescence spectra of toluene solutions of Py-L₂-OH (black) and QD@Py (red) under anaerobic conditions. The samples were adjusted at the same absorbance at 355 nm.

Photophysical studies of these systems and the analysis of the photoproducts were carried out using different techniques such as steady-state absorption and fluorescence, nuclear magnetic resonance (¹H-NMR, ¹³C-NMR, COSY, HMQC and HMBC), and Fourier transformed infrared (FTIR) spectroscopies, high-resolution transmission electronic microscopy (HRTEM), and gas chromatography–mass (GC-MS) spectrometry.

First, we irradiated aerated chloroform solutions of pyrene, pyrenebutanol and QD@Py using UV-A lamps.

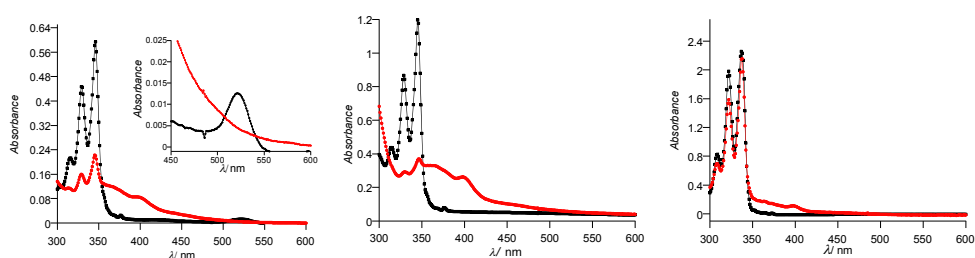


Figure 25 – Left, absorption spectra of aerated chloroform solutions of QD@Py before (black) and after (red) UV-A lamp irradiation for 30 min. Centre, absorption spectra of aerated chloroform solutions of pyrenebutanol before (black) and after (red) UV-A lamp irradiation for 60 min. Right, absorption spectra of aerated chloroform solutions of pyrene before (black) and after (red) UV-A lamp irradiation for 60 min.

The absorption and emission spectra of QD@Py showed the drastic transformation of the pyrene after a brief irradiation with UV-A lamps (only aerated solutions is showed in figure 25). The fluorescence spectra of QD@Py system irradiated for 30 min showed a new structured band (λ_{max} at 399 and 420 nm), red-shifted compared to that of the pyrene moiety, together with broad-bands (λ_{max} 450 and 490 nm, figure 26).

For comparative purposes, the stability of pyrene and pyrenebutanol was also studied. The absorption spectra (figure 25) showed analogue transformations as observed for QD@Py. The fluorescence spectra of pyrenebutanol showed structured bands (λ_{max} at 395 and 420) and red-shifted broad emission bands (λ_{max} 440 and 450-525 nm). However, for pyrene, the fluorescence spectra showed a structured band with λ_{max} at ca. 388 and 408 nm, a broad band at λ_{max} ca. 450 nm, and a band from 450 to 600 nm showing a well-structured shape (figure 26).

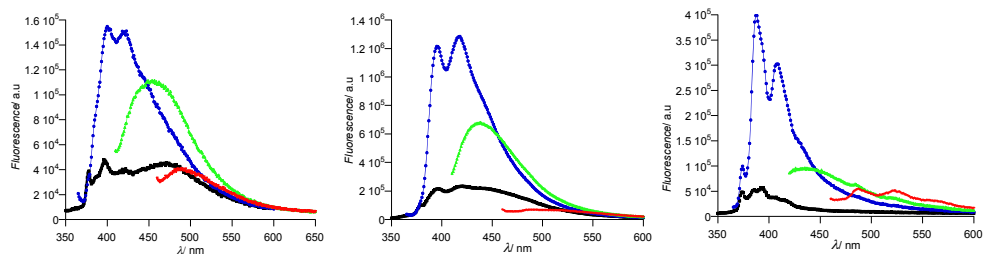


Figure 26 – Emission spectra of aerated chloroform solutions of A) QD@Py, B) pyrenebutanol, and C) pyrene after 30 min UV-A-lamp irradiation for QD@Py and 60 min UV-A-lamp for pyrenebutanol and pyrene. All spectra were recorded at λ_{ex} 313 nm (black), 355 nm (blue), 400 nm (green), and 450 nm (red).

Secondly, the experiments were carried out in amylene-free dichloromethane. Irradiation of the three systems in aerated dichloromethane showed high photostability of the pyrene chromophore in this solvent (figure 27).

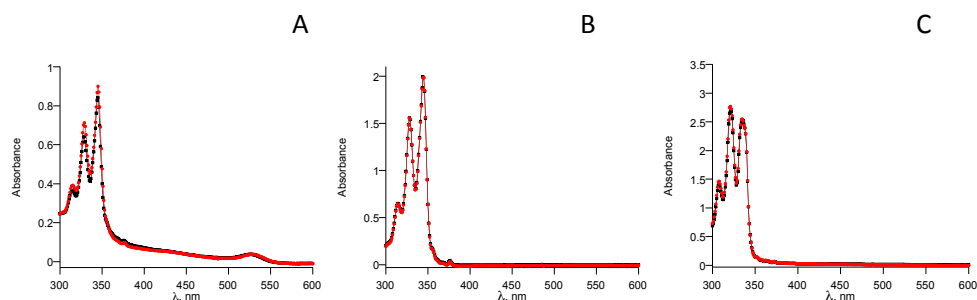
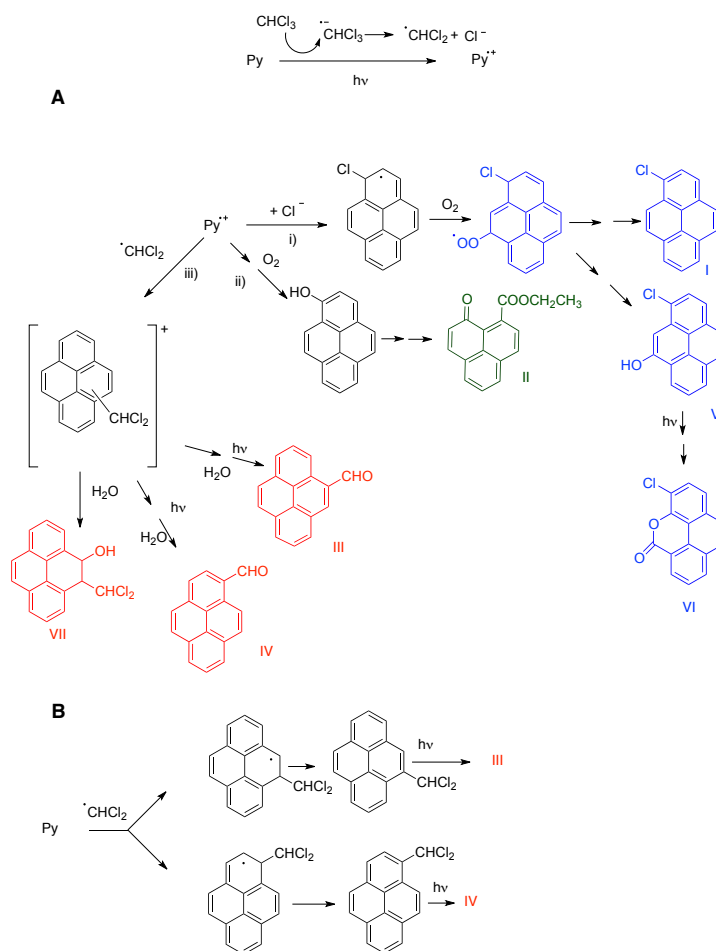


Figure 27. Absorption spectra of QD@Py (A), Py-L₂-OH (B), and Py (C) in amylene-free dichloromethane before (black) and after 50 minutes (red) UVA-lamp illumination in the presence of air.

Finally, a large amount of pyrene was irradiated in chloroform under UV-lamps in order to determine the nature of the photoproducts. Column chromatography made it possible the separation of the more abundant photoproducts and one in trace amounts easy-to-follow in the separation due its strong green fluorescence (compound VI, see proposed structures in scheme 20).

These products were characterized by $^1\text{H-NMR}$, $^{13}\text{C-NMR}$, COSY, HMQC, HMBC, FTIR and GC-MS.

The possible mechanism of this photooxidation is very complex (scheme 20). It seems that electron transfer from the pyrene excited state to the halogenated solvent produce the haloalkane radical anion and the radical cation of the pyrene. The rapid dissociation of the haloalkane radical anion into $\cdot\text{CHCl}_2$ and Cl^- prevents the rapid back-electron transfer to the pyrene radical cation. Then, the pyrene radical cation could react with the Cl^- , O_2 or $\cdot\text{CHCl}_2$ to give rise the subsequent photoreaction to produce eventually the photoproducts.



Scheme 20 - Mechanistic proposal for the photodegradation of pyrene

The higher photostability of pyrene in dichloromethane and the fact that pyrenecarbaldehydes were the main photoproducts in the degradation of pyrene in CHCl_3 suggests that the responsible species in this transformation is the haloalkane radical, and not the chloride anion. Actually, the photodegradation of pyrene is faster in distilled chloroform. The reason of the high stability of the pyrene in dichloromethane could be due the lower reactivity of $\cdot\text{CHCl}_2$ towards pyrene and the high reactivity towards oxygen.

In summary, the results of these studies evidenced that chloroform combined with light produces a high photodegradation of pyrene systems. Dichloromethyl radicals are the main species responsible for such transformations. Surprisingly, the use of dichloromethane is a suitable alternative to chloroform because the chloromethyl radicals hardly react with pyrene moieties. In addition, we demonstrate that the pyrene structures supported on QDs do not show a better photostability than the free pyrene structure.

3.5 - “Photoluminescence enhancement of CdSe Quantum Dots: a case of organogel-nanoparticle symbiosis”

An organogel is a non-glassy organic material based on self-assembly of the structural molecules via non-covalent interactions. These systems have potential applications such as cosmetics, food conservation, and supporting environment for different kinds of nanoparticles providing stability and spatial organization to the inorganic material.

In addition, quantum dots can be used in the development of fluorescent organogels due to their highly fluorescent properties. There are very few examples combining organogels with CdSe and CdSe/ZnS QDs. Bardelang *et al.*⁸¹ have prepared CdSe/ZnS QD-peptide nanocomposites using ultrasonic bath, while Zhou and You⁸² have reported the design of CdSe and CdSe/ZnS hybrid material by sonication using a hyperbranched molecule. Wadhavane *et al.*⁸³ have reported the potential applications of QD-doped organogels as chemical sensors of gases.

Here we report the photophysical characterization of a hybrid system comprising an organogel, which arises from a pseudopeptidic macrocycle **1** (figure 28) and different types of QDs, such as CdSe core and CdSe/ZnS core-shell QDs capped with trioctylphosphine (TOPO) or octadecylamine (ODA).

The organogelator **1** was selected because of its i) ability to self-assemble in toluene, ii) stability in the experimental conditions, and iii) transparency of the resulting organogel for the optical characterization. For the preparation of the system, the organogel was dissolved in toluene and heated to the boiling point temperature of the solvent to completely dissolve the organogelator **1**. After that, different concentrations of QDs were added and the system was cooled to room temperature. It is important to mention that the QD-organogels obtained by addition of the QDs after solubilization of **1** preserved the QD photophysical properties better than if the QD-organogels were obtained by directly mixing **1** with the QDs

and toluene, followed by heating the system. This is attributed to the poor stability of the QDs at high temperatures. Remarkably, the gelation without the QDs showed that the system needed more quantity of organogel, compared with that in the presence of the QD, to be stable.

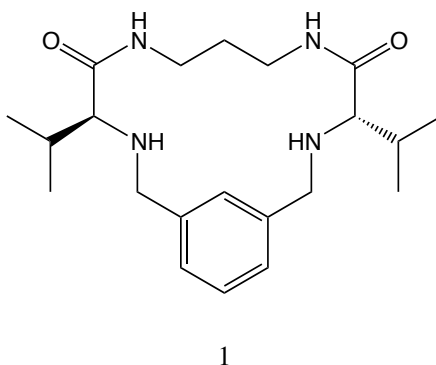


Figure 28 – Chemical structure of organogelator 1

The photophysical characterization of the QD-organogel showed two trends depending the presence or the absence of the ZnS shell:

- The fluorescent emission of CdSe/ZnS QDs was preserved. This has been attributed to the role of the shell, which efficiently passivate the CdSe surface defects.

- A considerable emission enhancement of CdSe QD emission was observed (up to 528%). This enhancement could be attributed to the removal of trap states, but this is not the main contribution, as we will see in the time-resolved fluorescence analysis.

The QD-organogel system was highly stable, and preserves the initial fluorescence after 5 h since its formation. Thermoreversibility studies showed that the QD fluorescence was conserved after heating and cooling the system for 5 cycles (figure 29).

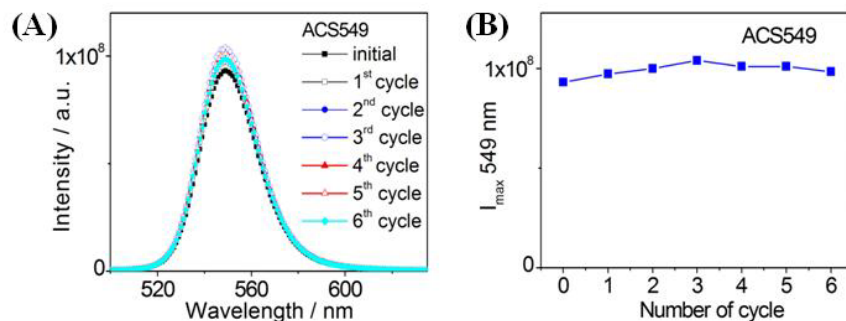


Figure 29 - A) Emission spectra of a core-shell QD capped with amine (CS@ODA) in toluene containing organogelator **1** ($\lambda_{exc} = 465$ nm). B) Plots of the emission intensity at the maximum emission wavelength after each cycle of melting-gelation.

Time-resolved fluorescence spectroscopy made it possible to study the effect of the gelator concentration on the QD lifetime. Two main trends for fluorescence lifetimes were observed. On the one hand, the fluorescence lifetimes and their contributions follow the same pattern for each core-shell QD regardless the presence of organogelator **1**. On the other hand, the fluorescence lifetimes of the core QDs increased after addition of organogelator **1**. Regarding the average lifetime, the core-shell QDs were not affected by the organogelator, but the core QD average lifetime was increased by a 1.5 – 1.7 factor in the presence of organogelator.

Then, the dependence of the emission properties of core-QD on the concentration of organogelator was studied. A small increase of the emission intensity and the fluorescence lifetime was observed in the presence of low concentrations of **1**. When the concentrations were higher than 4 mM, the emission intensity showed an enormous increase of the emission intensity while the fluorescence lifetime did not increase (figure 30A). Afterwards, we compared the radiative rate constant (k_r) and the non-radiative rate constant (k_{nr}) of the QD regarding the concentration of the organogelator. For this purpose, equations 3 and 4 were used.

$$\phi = \frac{k_r}{k_r + k_{nr}} \quad \text{Eq. 3}$$

$$\tau_f = \frac{1}{k_r + k_{nr}} \quad \text{Eq. 4}$$

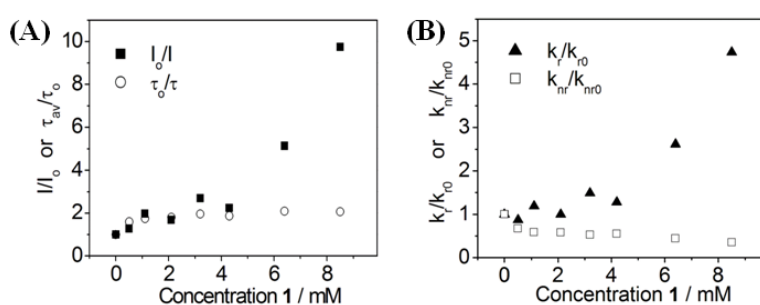


Figure 30 - A) Relative change in the emission intensity and the lifetime of CdSe capped with TOPO vs concentration of organogel 1. B) Relative change in the radiative rate constants and non-radiative constant of CdSe capped with TOPO vs concentration of organogelator 1.

Figure 30B shows that the increase in the QD fluorescence correlated well with the increase of the radiative constant, while the non-radiative constant was not significantly affected by the concentration of the organogel. This latter constant is related with the surface defects of the QD and plays a minor role in the increase of the fluorescence of the QD.

The macrocycle **1** contains amide and amine groups, as well as hydrophobic moieties in its chemical structure. Amides can participate in the stabilization of the nanoparticles,³⁴ and it is well known that amines have an important effect in the fluorescence properties of the QDs. In addition, the organogelator **1** can undergo ligand interdigitation with QD ligands because of its multifunctional organic groups. This process could affect the QD properties during the gelation to

generate organogels with better properties (symbiotic effect). For this reason, NMR and IR studies were carried out to get insight into the interaction of the macrocycle **1** with the QD.

The ^1H -NMR of the organogelator showed a typical broadening of its signals in the presence of the QD, even in conditions of no gelation (figure 31). Comparatively, the organogel signals underwent considerably higher displacement in the presence of TOPO, but without any broadening. This suggests that the organogel cannot interact with the TOPO oxygen atom after attached to the QD surface.

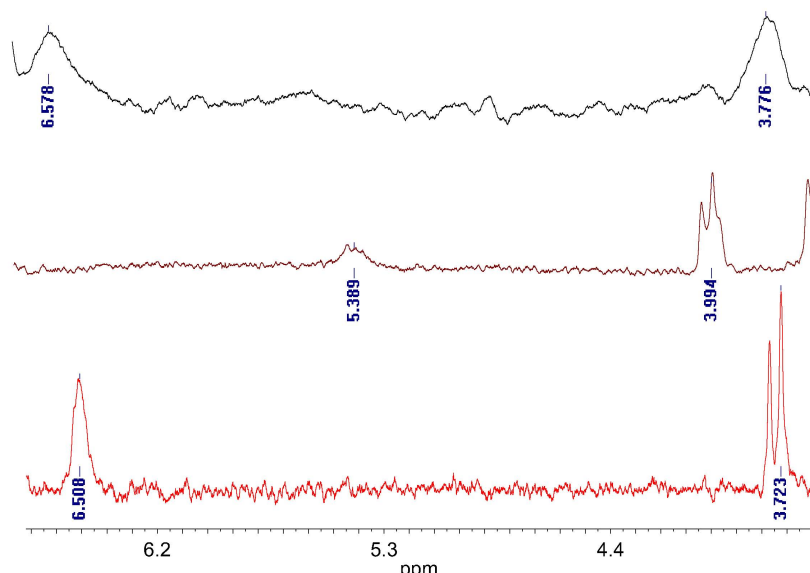


Figure 31 - Bottom to top: Amplification between 3.6 ppm and 6.7 ppm of the ^1H -NMR spectrum of the macrocycle **1** in deuterated toluene, compared with those of the macrocycle **1** in the presence of TOPO (macrocycle/TOPO molar ratio of 1000/1) and in the presence of QD@TOPO QDs.

The ^{31}P -NMR spectra of QD and QD-organogel (in conditions of no gelation) also showed a characteristic broadening of the TOPO signals, and their corresponding shifting to highfield compared to those of TOPO, which corroborate the interaction between QD and organogel before the gelation process (figure 32). In addition, the free TOPO signals were not detected in the mixture, indicating the absence of ligand exchange between TOPO and the organogel.

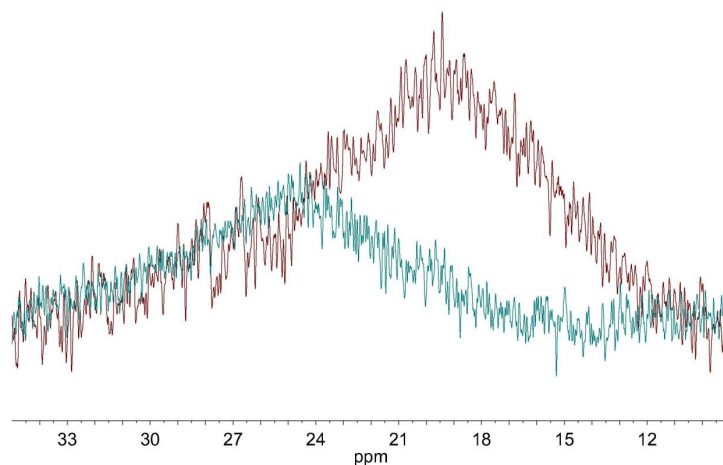


Figure 32 - ^{31}P -NMR spectra in deuterated toluene of QD@TOPO in the absence (—) and in the presence of the macrocycle **1** (—).

The IR studies also showed the interactions of the QD and the organogel. The more significant signals (N-H bands at 3300 cm^{-1} , C-H bond at 3100 cm^{-1}) are displaced for the QD/organogelator mixture respect to that of the organogel in absence of QD (figure 33). Moreover, these effects were evident even before the formation of the organogel (figure 34).

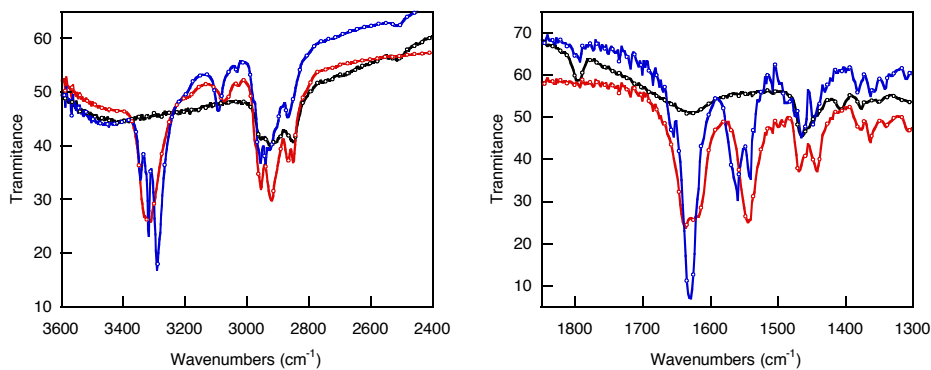


Figure 33 - Comparative IR spectra of organogelator (—), QD@TOPO (—), and organogelator-QD@TOPO mixture (—) using KBr. Left: region from 3600 to 2400 cm^{-1} and Right: region from 2400 to 1300 cm^{-1} . Conditions of gelation. Ratio QD/organogelator 1/50.

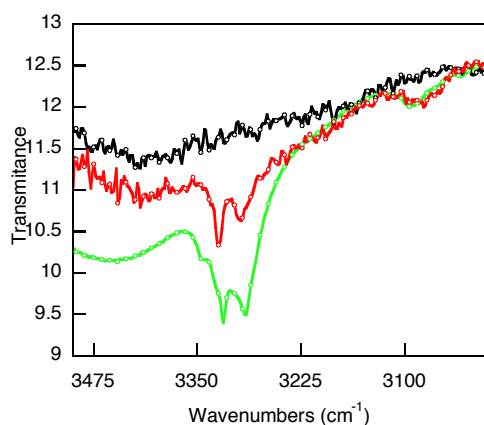


Figure 34 - Comparative IR spectra in toluene of organogelator (—), QD@TOP (—), and organogelator-QD@TOPO mixture (—) using KBr. Conditions of no gelation. Ratio QD/organogelator 1/50.

The atomic force microscopy (AFM) revealed no changes in the organogel, regardless the presence or absence of QD. This means that the morphology of the

fibrillar network formed by organogelator **1** is preserved. In addition, TEM images showed that nanoparticles were well dispersed in the organogel fibers, and the QD do not form aggregates. These results demonstrated that QDs did not destabilize the fibrillar network in the organogel. Usually, organogel have been described as supramolecular systems composed of a series of pools of solvent in which QDs can move as in a solution, but this does not explain the increase in the QD fluorescence, which starts before the critical concentration of gelator (*cgc*). The fact that the *cgc* for mixtures of QDs and organogel was lower than the *cgc* for the organogelator **1** alone indicated that the QD was acting as nucleation sites of the gelator, which favored a high local concentration of the gelator, and consequently, the gelation process. The symbiosis of the organogelator/QD combination is attributed to interdigitation of the organogelator **1** and the QDs organic ligand.

Regarding the increase in the k_r of CdSe QDs at high gelator concentration can be attributed to the decrease of energy transfer and reabsorption processes between the QDs as consequence of the immobilization in the fibrillar network of the gelator, but if this were true, both CdSe and CdSe/ZnS should increase the QD emission. Alternatively, the increase in the refractive index of the medium after gelation for CdSe QDs could be responsible of the increase of the radiative rate constant.⁸⁴

In summary, these results have shown the symbiosis between CdSe core and CdSe/ZnS core-shell capped with different ligands and the organogelator **1**. The formation of the organogel is favored in the presence of the QDs, i.e., it is possible to prepare the gel by reducing the concentration of the organogelator. Regarding the QD, the enormous increase of the fluorescence intensity in the case of core-QDs is remarkable. Thus, highly, transparent, stable, and the fluorescent systems can be prepared easily by heating the organogel in toluene and cooling it to room temperature in the presence of the QD. To our knowledge, this is the first time where the interaction between an organogel and a QD has been reported. Moreover, this has been demonstrated by using simple and accessible methodologies, such as IR and NMR spectroscopies.

4 - CONCLUSIONS

The results obtained in this thesis give rise to the following conclusions:

- Addition of thiols to organic soluble CdSe QDs causes a decrease in the luminescence properties of the nanoparticles. However, an important fluorescence enhancement was observed for organic soluble amine-capped CdSe/ZnS QDs.
- The replacement of amine ligands by alkyl thiol ligands to synthesize CdSe/ZnS@thiol under mild heating in chloroform results in QDs with high fluorescence properties. Amine ligands seem to play a key role in this observation, due to their basicity which allows a slow deprotonation of the thiol ligand to take place close to the nanoparticle surface. As a result, the thiolate binds to the ZnS shell causing a minimum of surface alteration. This methodology has been applied successfully for the synthesis of nanoparticles soluble in organic and aqueous media. Moreover, these new nanoparticles show better stability and photostability than the original QDs. These results are of great interest for the design of new functional QDs, whose applications require highly fluorescent, photostable, and small-sized QDs.
- It has been possible to prepare a supramolecular system based on a ketoprofen-functionalized CdSe/ZnS nanoparticle and β -cyclodextrin modified with a pyrene unit. This system has been successfully used for molecular recognition of different analytes. A strategy for recovery of all components separately, which is highly desirable from the viewpoint of the green chemistry, was developed.
- The pyrene photostability (free or supported on the QDs) is poor in chloroform due to the light-induced formation of the dichloromethyl radicals from chloroform. Dichloromethane has been proposed as

an alternative solvent because chloromethyl radicals hardly react with pyrene structures.

- It is possible to prepare highly fluorescent organogels by combining a pseudopeptidic macrocycle and different types of non-commercial CdSe and CdSe/ZnS QDs. On the one hand, the organogel preserve (CdSe/ZnS QDs) or increase (CdSe QDs) the photoluminescent properties of the QDs, and on the other hand, it is possible to reduce the critical concentration of the organogelator needed to form stable and thermoreversible organogels.

5 - SUMMARY OF THE THESIS

This thesis focuses on the symbiotic effect between CdSe/ZnS core-shell QDs or CdSe core QDs and their organic ligands, and the advantages of this effect to improve the functionality of the QD or/and of the ligand, or create a new functionality of the device. Thus,

1. the nanoparticle surface capping with organic ligands can allow the QD i) to remain stable in organic solvents or water, by providing steric or ionic repulsion between the nanoparticles, ii) to preserve/enhance their emissive properties (passivation of the surface defects, isolation from quenchers), and/or iii) to add functionality to the nanoparticle.
2. the spherical shape of the nanoparticle makes the location of an elevated number of ligands on the QD surface possible. Therefore, it is possible to have a high local concentration of a functional group at the QD periphery, in an otherwise diluted solution.
3. the combined action of the QD and the ligand can permit the encapsulation/interdigitation of other molecules, bringing them closer to the QD surface. In addition, the functional ligand can reversibly modify the nanoparticles emissive properties and this can be used, for example, for sensing applications.

There is great interest on the passivation of CdSe core and CdSe/ZnS core-shell QDs with organic ligands possessing a mercapto group at one end, because of the high affinity of this anchoring group to the QD surface, mainly when it is as thiolate. Nevertheless, exchange of the ligands of the QDs (usually prepared with amino ligands) by thiol (core) or thiolates (core-shell) causes a remarkable reduction of the luminescent properties of both type of QDs. In the case of the core QDs, the thiol traps the hole of the excited QD, and therefore prevents the electron-hole recombination. The low emission of the core-shell QD has been attributed to the alteration of the QD shell during the ligand exchange.

We have developed a new strategy to obtain highly fluorescent organic-soluble and water-soluble CdSe/ZnS QDs passivated with thiolates, based on the chemisorption of thiols on the QD surface. In this strategy the QD amine native

ligand plays a key role, by dissociating the thiol in the vicinity to the QD surface. The replacement of the long chain amines by thiols was performed under mild conditions, and it allows preserve or even improve the QD luminescent properties. This methodology was tested in home-made and commercially available nanoparticles. Moreover, the QDs were more photostable than those capped with amine.

These results are of interest for constructing new devices of application in sensing or molecular recognition, based on energy or electron transfer processes. Thus, that strategy was used in the preparation of highly fluorescent water-soluble CdSe/ZnS QDs capped with a bifunctional ligand, with a mercapto group (the anchoring group) at one end and a benzophenone moiety at the other. The QD was used to develop a supramolecular system, based on ketoprofen-functionalized CdSe/ZnS QDs and pyrene-modified cyclodextrin (CD). The ketoprofen units play a key role, ensuring the molecular recognition between the nanoparticle and the cyclodextrin and, at the same time, places the pyrene unit near to the nanoparticle surface, resulting in QD fluorescence quenching. This symbiotic effect was successfully used for molecular sensing of different analytes. The sensing of this easy-to-prepare and effective hybrid system is based in the recovery of the QD fluorescence intensity in response to different analytes. In addition of this, the methodology proposed allows the individual recovery of all the components used in the mentioned system, which is highly desirable both from the commercial and environmental points of view.

As stated before, the QD can be used as nano-carrier of a functional group, leading to increase of the local concentration of the functional group in an otherwise diluted solution. In this thesis, CdSe QDs were used as carriers of pyrene moieties, and, as a consequence, making the formation of the pyrene excimer possible by using a very low concentration of the pyrene ligand. The CdSe QD luminescence was drastically reduced by using a pyrene ligand with mercapto group as the anchoring group. The system was used to study the influence of the QD on the photostability of the pyrene in chlorinated solvents and the results were

compared to those of the free pyrene. These studies evidenced that the combination of chloroform and light produces a high photodegradation of all the pyrene systems, while they were highly stable in dichloromethane.

Finally, we studied highly fluorescent QDs-organogels prepared from a pseudopeptidic macrocycle and both types of QDs, i.e. CdSe and CdSe/ZnS capped with different ligands. These hybrid organogels were easily prepared, by heating the organogelator in toluene, followed by the addition of the QDs and the cooling of the system to room temperature. The presence of the QD in the organogel system decreases the critical concentration of the gelator needed to form stable and thermoreversible organogels, without affecting significantly the internal fibrillar network of the organogel. In addition, the effect of the organogel on the luminescent properties of the QDs depends on the presence of the ZnS shell. The photophysical properties of CdSe/ZnS core-shell QDs are preserved in the organogel media, while in the case of CdSe core QDs, an enormous increase of the fluorescence intensity was observed. We demonstrate that the macrocycle interacts with the CdSe QD ligand even before gelation, by using common methodologies, such as IR and NMR spectroscopies. This is the first time that the interaction between an organogel and a QD has been reported.

**6 - JUSTIFICATION OF THE THEME AND ORIGINAL
CONTRIBUTION OF THE AUTHOR**

This thesis has been developed in the Photochemistry Reactivity Group, Molecular Science Institute (ICMol) at University of Valencia under the supervision of Julia Pérez-Prieto and Raquel E. Galian. Since 2007, the group has been working in the field of semiconductor nanocrystals, such as CdSe and CdSe/ZnS quantum dots and metallic nanoparticles, such as Ag and Au.

The group has reported several studies on the photocatalytic modification of the size of semiconductor (controlled size reduction) and metal nanoparticles (controlled size increase) as well as on a photocatalyzed seeding of gold nanoparticles. With respect QDs, the group has been focused in the design and the applications of new functionalized quantum dots. As a preliminary step the group was interested in the use of thiols as organic ligands, since they can strongly bind to the nanoparticle surface and be used to add functionality to the system. The main challenge of this work was to keep or improve the luminescent properties of the nanoparticle after the functionalization with thiol ligands. The articles described in this thesis have been published in different journals with an impact factor up to 9.9, indicating the interest of our results.

The knowledge obtained during these years will allow the group to design versatile QDs as sensors, probes, etc., as well as new assembly of QDs with different supramolecular systems, such as organogels.

During the development of this thesis, Jordi Aguilera-Sigalat, has gained experience in the synthesis, purification, and characterization of core and core-shell quantum dots. This experience was necessary to add functionality to the QDs successfully. He has done most of the experimental work of the herein described results. The preparation and the measurements of absorbance, fluorescence, laser flash photolysis, and FTIR spectroscopies have been done at the ICMol within the group of Julia Pérez-Prieto. The NMR measurements were carried out in the central services of the University of Valencia, using Bruker Advances DPX 300 or 400 when more accumulation times were required. In addition, the technical staff of the central services at the University of Valencia has made the HR-TEM and XPS spectroscopy measurements. In the case of the article "Quantum dot/cyclodextrin

supramolecular systems based on efficient molecular recognition and their use for sensing”, the functionalized cyclodextrin has been prepared at the University of Almeria by Juan M. Casas-Solvas and Antonio Vargas-Berenguel, and the preliminary studies were done by Maria C. Morant-Miñana, who finished her PhD in the group in 2008. For the article “Further Insight into the Photostability of the Pyrene Fluorophore in Halogenated Solvents”, Dr. Elena Zaballos has contributed in the treatment of the results and isolation of the photoproducts because of her great knowledge in organic chemistry. For the article “Photoluminescence enhancement of CdSe Quantum Dots: a case of organogel-nanoparticle symbiosis”, the preparation of the organogelator and the steady state and time resolved fluorescence studies, as well as the AFM and TEM, analysis of the QD-organogel systems were performed at the University of Jaume I (Castellón).

7 – SUMMARY OF THE THESIS IN SPANISH

Objetivos de la tesis doctoral.

Teniendo en cuenta los precedentes sobre las nanopartículas semiconductoras ("quantum dots", QD) del tipo CdSe ("core", QD-core) y CdSe/ZnS ("core/shell", QD-core/shell) funcionalizadas con tioles, se plantearon los siguientes objetivos:

- Estudiar detalladamente el efecto que provoca la adición de tioles y tiolatos sobre la fluorescencia de los QD-core/shell de CdSe/ZnS y comparar los resultados obtenidos con los efectos que produce sobre los QD-core de CdSe.
- Desarrollar nuevas metodologías para la síntesis de QD-core/shell de CdSe/ZnS funcionalizados con tioles, solubles en medios orgánicos y acuosos y que sean altamente fluorescentes y fotoestables.
- Diseñar nuevas estrategias para la preparación de sensores fáciles de preparar y efectivos para el reconocimiento molecular, basados en interacciones específicas de la nanopartícula con diferentes analitos.
- Usar las nanopartículas como soporte de fluoróforos orgánicos, tales como pireno, y estudiar su fotoestabilidad en diferentes disolventes clorados.
- Estudiar el posible efecto sinérgico entre las nanopartículas de CdSe (CdSe-core y CdSe/ZnS-core/shell) y un organogelante para la obtención de geles fluorescentes.

Metodología de los artículos relacionados con la tesis doctoral.

Fluorescence enhancement of amine-capped CdSe/ZnS quantum dots by thiol addition

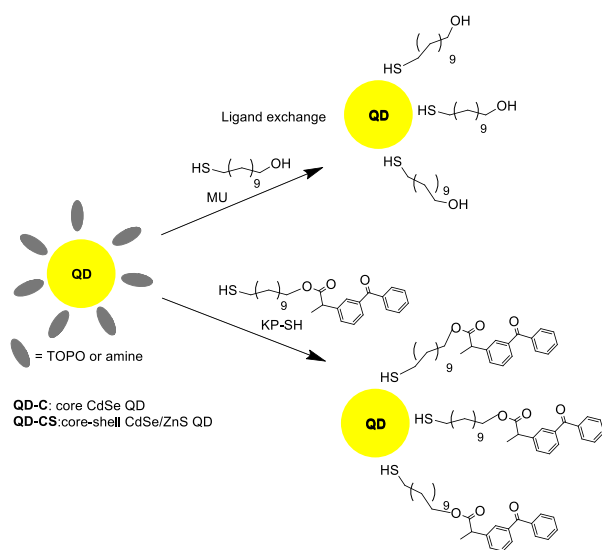
(*Canadian Journal of Chemistry* **2011**, *89*, 359-363).

La adición de tioles a QD-core de CdSe provoca una disminución en sus propiedades fluorescentes, debido a la capacidad de los tioles para atrapar los huecos generados en el QD después de la absorción de luz. Curiosamente, un efecto similar ha sido descrito para los QD-core/shell de CdSe/ZnS, en las cuales la corteza de ZnS debería proteger al núcleo de CdSe de la desactivación de su fluorescencia.

En este artículo, estudiamos el efecto que provoca la adición de tioles en la fluorescencia de los QDs de CdSe y CdSe/ZnS. Para ello, se estudia la emisión fluorescente de estas nanopartículas en presencia de diferentes alquiltioles, tales como el 11-mercapto-1-undecanol (MU) y un tiol funcionalizado con un cromóforo de benzofenona, KP-SH (esquema 21). El QD de CdSe ha sido sintetizado utilizando TOPO y TOP como ligandos orgánicos; mientras que el QD de CdSe/ZnS posee una amina primaria de cadena larga. Para el estudio se han utilizado nanopartículas de diferente tamaño (entre 2 y 3 nm).

En primer lugar, se ha estudiado el efecto que provoca la adición de los tioles a QDs de CdSe-core en sus propiedades fluorescentes, utilizando diferentes concentraciones de tiol y tamaños de nanopartícula. Para estos estudios se emplean las técnicas espectroscópicas de absorción y de fluorescencia en estado estacionario. Mientras que los espectros de absorción no mostraron cambios significativos, los espectros de fluorescencia evidenciaron una dependencia de la emisión del QD respecto de la concentración de tiol. Relaciones molares de QD/ligando por encima de 1/1000, producen una drástica disminución de la fluorescencia para todos los tamaños de nanopartícula; mientras que cuando se

usaron relaciones por debajo de 1/700, se observaron dos fenómenos: un aumento de la fluorescencia y nuevas bandas a mayores longitudes de onda que la emisión del QD, relacionadas con los defectos de superficie.⁴⁴ Este comportamiento se observó utilizando diferentes tamaños de nanopartícula (2.5 y 3.4 nm).



Esquema 21 - Intercambio de ligando TOPO/TOP (core QDs) y amina (core-shell QDs) por los diferentes tioles (MU, KP-SH).

Posteriormente, se estudió el efecto que produce la adición de los tioles en las propiedades fluorescentes de los QDs de CdSe/ZnS comerciales, los cuales poseen octadecilamina (ODA) como ligando. En este caso, la adición de tioles provoca un aumento de la fluorescencia, independientemente de la relación QD/ligando. Estas observaciones contradicen los resultados encontrados en la literatura.⁶⁴ Para determinar si el diferente comportamiento entre los QDs de CdSe y los QDs de CdSe/ZnS se debe a la diferente naturaleza de sus ligandos, se adicionó un exceso de ODA a una muestra de CdSe funcionalizada con TOPO, observándose un aumento considerable de la fluorescencia del QD. Una vez

estabilizada la muestra, se adicionó el tiol y se observó una gran disminución de la fluorescencia (figura 35). Así pues, se concluyó que la amina como ligando no es la responsable del diferente comportamiento entre los QDs de CdSe y los de CdSe/ZnS a la adición de tioles.

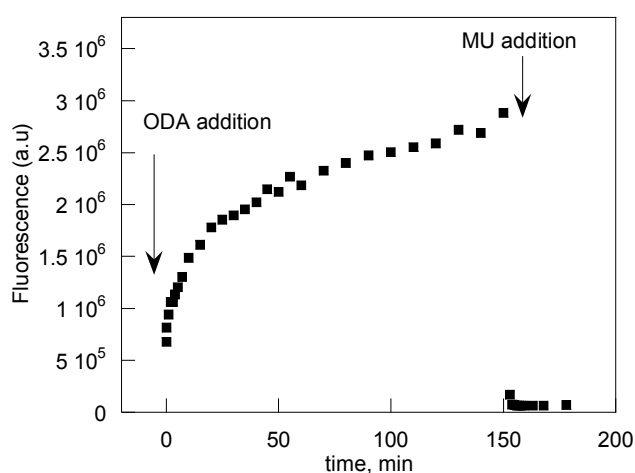


Figura 35 - Intensidad de fluorescencia del QD tras la adición de octadecilamina seguida de la adición de MU.

Estos resultados demuestran que las propiedades fluorescentes de los QDs de CdSe están condicionadas por los defectos de superficie. Bajas concentraciones de tioles ayudan a una mejor pasivación de la superficie de la nanopartícula. Altas concentraciones de tioles producen drásticas disminuciones de la fluorescencia del QD.

Por otro lado, la adición de tioles a QDs de CdSe/ZnS mejora sus propiedades fluorescentes. Con el fin de entender mejor la naturaleza del enlace entre el tiol y el QD, se adicionó KP-SH a dos muestras (A y B) que contenían QD de CdSe/ZnS. La muestra A se dejó reaccionar durante 2 horas (CS@KP_{2h}) mientras que la muestra B se dejó durante 48 horas (CS@KP_{48h}). Ambas soluciones mostraron mayor fluorescencia que el QD precursor. Sin embargo,

después de los lavados, el CS@KP_{48h} mostró mayor fluorescencia que el CS@KP_{2h}. La intensidad de fluorescencia de las muestras disminuyó con respecto al QD de CdSe/ZnS original después de realizar una serie de lavados, debido a una pérdida parcial del tiol encapsulado. Sin embargo, estas muestras mostraron un desplazamiento hacia el rojo del máximo de fluorescencia del QD, lo que reflejó la unión de tioles a la superficie de ZnS. Estos resultados demuestran que el intercambio de ligando amina por tiol en la superficie de los QDs de CdSe/ZnS produce una mejor pasivación de la fluorescencia de los mismos. Además, la mayor fluorescencia de CS@KP_{48h} respecto CS@KP_{2h} sugiere que los tioles unidos a la superficie del QD no son perjudiciales para la fluorescencia del QD.

En resumen, estos resultados demostraron que la adición de tioles QDs de CdSe causa una drástica disminución de la fluorescencia. Sin embargo, la adición de tioles a QDs de CdSe/ZnS funcionalizados con aminas aumenta la fluorescencia de los QDs.

Highly fluorescent and photostable organic- and water-soluble CdSe/ZnS core-shell quantum dots capped with thiols

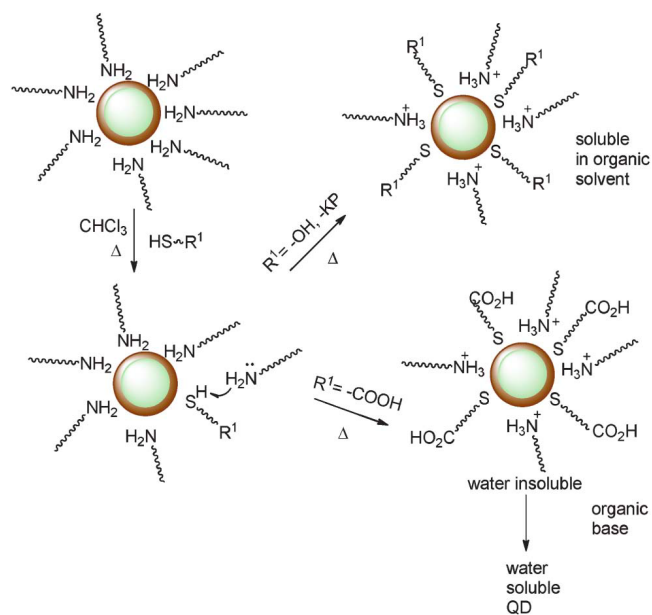
(*RSC Advances* **2012**, 2, 1632-1638)

Cálculos teóricos demuestran que los tioles no pueden unirse a la superficie de ZnS, pero sin embargo, los tiolatos, se unen fácilmente a esta superficie. El intercambio de amina o TOPO por tiolatos produce una drástica disminución de la fluorescencia del QD debido a la gran exotermicidad de la reacción. En el artículo anterior se observó que la adición de tioles, a temperatura ambiente, a QDs de CdSe/ZnS altamente fluorescentes funcionalizados con aminas primarias de cadena larga producía un aumento en su fluorescencia, aunque después de los lavados se observó que hay una disminución de la fluorescencia del QD, debido a la eliminación de parte de los tioles encapsulados. Curiosamente, un desplazamiento del máximo de fluorescencia sugirió que parte de los tioles fueron quimiadsorbidos en la superficie del QD. Aparentemente, las aminas actúan como bases de Lewis disociando el tiol, el cual se une a la superficie de ZnS como tiolato. En este trabajo nos planteamos si la quimiadsorción del tiol a la superficie de ZnS podría estar favorecida por condiciones suaves de reacción y la presencia de ligandos amina, con el fin de obtener QDs con mejores propiedades fluorescentes de estos.

La metodología para obtener QDs de CdSe/ZnS funcionalizados con tioles se describe a continuación:

- En primer lugar, se prepararon los tioles que utilizaremos posteriormente para solubilizar las nanopartículas en medios orgánicos. Para ello, se sintetizó un derivado del ketoprofeno funcionalizado con un grupo mercapto (KP-SH), siguiendo la metodología descrita por Ohara *et al.*⁶⁷ Para la síntesis de los QD en medios acuosos se usaron el ácido mercaptoundecanoico (MUA) y el ácido mercaptopropiónico (MPA).

- Después, se llevó a cabo la síntesis de los QD-core/shell funcionalizados con tioles a partir de nanopartículas de CdSe/ZnS funcionalizadas con aminas (QD-CS, Evident Technologies o Ocean NanoTech). La mezcla tiol/QD se calentó a reflujo en cloroformo durante 48 h en la oscuridad y atmósfera de nitrógeno. Los QDs funcionalizados con ketoprofeno (CS@KP) se purificaron precipitándolos en metanol, y finalmente se redisolviaron en tolueno. En el caso de los QDs solubles en medios acuosos, MUA (CS@MUA) y MPA (CS@MPA), se precipitaron de cloroformo y se redisolviaron en agua. La solubilidad de estos QDs se incrementó al adicionar una base orgánica débil (el hidróxido de tetrametilamonio), y calentando ligeramente la muestra (esquema 22).



Esquema 22 - Preparación de los QDs solubles en medios orgánicos y acuosos.

En el espectro de resonancia magnética nuclear de protón ($^1\text{H-NMR}$) de las nuevas nanopartículas se observó el típico ensanchamiento de las señales del ligando,^{57,58} especialmente de aquellos protones cercanos a la superficie del QD. Además apareció una nueva señal, un triplete a 3.3 ppm asignado al CH_2 unido al nitrógeno de un ligando amino protonado. Ésta especie se formaría por abstracción de un protón del tiol por parte de la amina, que se comportaría como una base de Lewis.

En el espectro UV-vis se observó que el pico del primer excitón del CS@KP apareció a la misma longitud de onda que el QD precursor. Además, en las imágenes de alta resolución del microscopio electrónico de transmisión no se observó cambio del tamaño ni cristalinidad de los QDs después de la funcionalización. Es importante destacar que la fluorescencia de CS@KP fue mucho mayor (hasta un 50 %) que la fluorescencia de los QD-CS de partida, mientras que las nanopartículas solubles en agua mantuvieron la misma fluorescencia (figura 36).

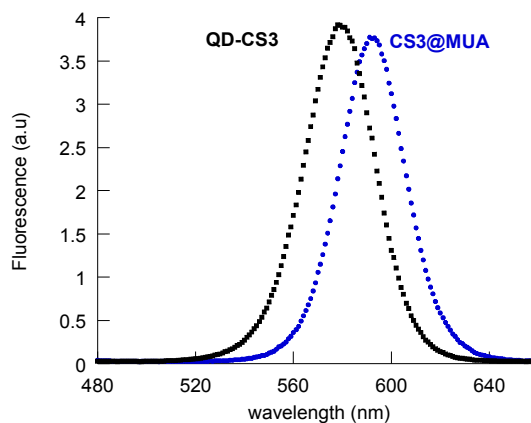


Figura 36 – Espectros de fluorescencia comparativos en N_2 de QD-CS en tolueno (negro) y CS@MUA en agua (azul).

La quimiadsorción del tiol a la superficie de ZnS se pudo confirmar por espectroscopia infrarroja (IR), ya que en las nanopartículas funcionalizadas con tioles, no se observó la banda S-H del grupo tiol (aproximadamente a 2569 cm^{-1}).

Además, se usó la técnica de espectroscopía fotoelectrónica por rayos X (XPS), la cual proporciona información del entorno químico de un átomo. Se compararon los espectros de las nanopartículas funcionalizadas con tiolatos con los de sus nanopartículas precursoras (con ligandos aminas) y con los ligandos libres. Además, también se estudió un QD preparado a partir de un QD-CS y KP-SH a temperatura ambiente (CS@KP_{rt}). El espectro 3d del Cd de estos compuestos se muestra en la figura 37. Las energías de enlace del Cd fueron similares para todos los QD-core/shell. Se observó un nuevo componente en el caso del CS@KP y CS@MUA , adscrito a la presencia del N 1s de las sales de amonio. En el caso del espectro S 2s (figura 37), el KP-SH mostró un pico a 227.4 eV correspondiente al grupo tiol, mientras que el QD-CS presentó un pico centrado a 225.7 eV relacionada con el ZnS. Además, mientras la banda del CS@KP_{rt} apareció a una energía de enlace muy similar a la del shell, la banda se desplazó a menores energías (225.3 eV) para el CS@KP . La deconvolución de este pico mostró un nuevo componente desplazado a menores energías que el tiol libre (224.4 eV frente a 227 eV) y pudo ser atribuido a la quimiadsorción del KP-SH a la superficie del QD.

Para comprobar la versatilidad de esta técnica para preparar QDs altamente fluorescentes con enlaces covalentes QD-S, se sintetizaron nanopartículas de CdSe/ZnS funcionalizadas con TOPO, siguiendo la metodología descrita por Bawendi y colaboradores⁵⁵ con algunas modificaciones. Estos QD se trataron con un exceso de ODA (QD:ODA 1:5000) con el fin de intercambiar el TOPO por ODA. Posteriormente, éstas nanopartículas se funcionalizaron con tioles siguiendo la metodología descrita anteriormente. Estas nanopartículas mostraron altos rendimientos cuánticos de fluorescencia, al igual que las nanopartículas comerciales.

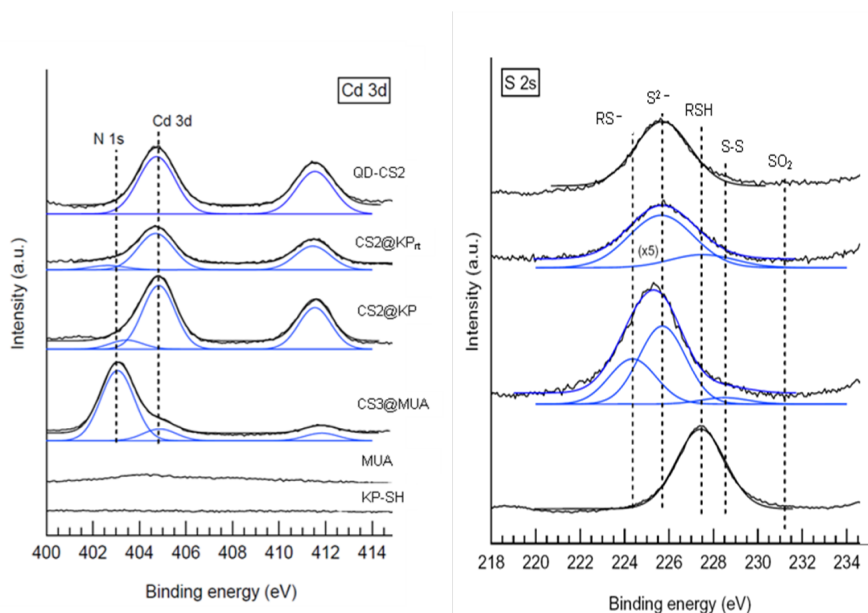


Figura 37 – Izquierda, espectro de XPS del Cd 3d y del N 1s para los QDs. Derecha, de arriba a abajo: espectro de XPS del S 2s para QD-CS, CS@KP_{rt}, CS@KP, y KP-SH.

Además, se llevó a cabo el intercambio de los ligandos amina de un QD-CS adquirido a otra compañía con un tiol, KP-SH (CS@KP₁) y un tiolato, KP-S⁻ (CS@KP₂). CS@KP₁ se preparó siguiendo nuestra metodología, mientras que CS@KP₂ se preparó como se detalla a continuación: KP-SH se trató con una base orgánica para producir el correspondiente tiolato (KP-S⁻). Este se adicionó al QD-CS y se calentó a reflujo de cloroformo durante 48 h en la oscuridad y atmósfera de nitrógeno. Los QDs se lavaron con MeOH y se redisolieron en tolueno. Sorprendentemente, el CS@KP₁ mostró una ligera pérdida de fluorescencia (8 %), mientras que CS@KP₂ mostró una drástica disminución de su fluorescencia (39%).

El mismo procedimiento de intercambio de ligandos fue realizado utilizando un QD de CdSe/ZnS@amina preparado en el laboratorio. Para ello, se sintetizaron QDs de CdSe/ZnS pasivados con TOPO, el cual se intercambió por ODA (CS@ODA) y posteriormente por tioles. El rendimiento cuántico de

fluorescencia de los QDs funcionalizados con tiolatos aumentó hasta un 13% en relación con su precursor funcionalizado con amina, demostrando la generalidad de esta metodología.

Finalmente, se estudió la fotoestabilidad de estas nuevas nanopartículas en comparación con la de sus precursoras (figura 38). Sorprendentemente, las nuevas nanopartículas solubles en medios acuoso y orgánico presentan mayor fotoestabilidad que sus precursoras, debido a que los QDs se encuentran unidos covalentemente como tiolatos a la superficie de ZnS, evitando la formación de disulfuro y, por lo tanto, la precipitación del QD.¹⁰

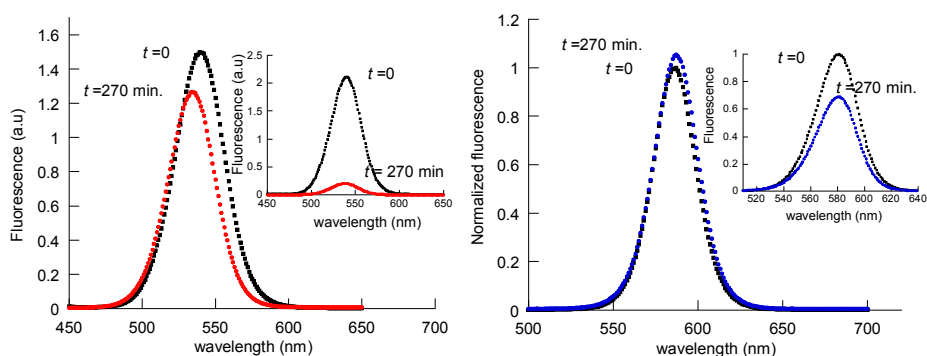


Figura 38 – Izquierda, espectro de fluorescencia en tolueno y aire de CS@KP, antes (■) y después (●) de 270 min de la irradiación a $\lambda > 400$ nm. Recuadro: Espectro de fluorescencia comparativo del QD-CS comercial. Derecha, espectro de fluorescencia en tolueno y N_2 de CS@MPA, antes (■) y después (●) de 270 min de irradiación a $\lambda > 400$ nm. Recuadro: Espectro de fluorescencia comparativo del QD-CS en tolueno.

En resumen, hemos demostrado que el intercambio de ligandos amina por tioles para obtener QDs solubles en medios orgánicos o acuosos puede llevarse a cabo bajo condiciones de reacción suaves, manteniendo o incrementando sus rendimientos cuánticos de fluorescencia y su fotoestabilidad.

Quantum dot/cyclodextrin supramolecular systems based on efficient molecular recognition and their use for sensing

(*Chemical Communications* **2012**, 48, 2573-2575).

Los QDs de CdSe/ZnS son sistemas altamente fluorescentes que pueden ser usados para el reconocimiento molecular o para la detección de diferentes analitos.

Las β -ciclodextrinas (β -CD) son oligosacáridos cíclicos que contienen siete unidades de D-glucopiranosas unidas por enlaces α -(1 \rightarrow 4). Estas β -CD poseen una cavidad toroidal en la que la cara grande contiene los grupos hidroxilo secundarios, mientras que la cara pequeña contiene los grupos hidroxilo primarios. Debido a esta disposición, la cavidad interior de la ciclodextrina es menos hidrofílica que el agua, lo cual permite formar gran cantidad de complejos de inclusión.⁶¹

En la bibliografía aparecen algunos estudios en los que utilizan QDs funcionalizados con ciclodextrinas para la detección de diferentes analitos, a través de la transferencia de energía de resonancia de Förster (FRET) o transferencia electrónica fotoinducida.

En este trabajo, se diseñó una nueva estrategia para obtener un sensor efectivo basado en el reconocimiento molecular de un QD por una β -ciclodextrina, el cual mostró un aumento de fluorescencia como respuesta a la adición de diferentes analitos.

En primer lugar, se sintetizó un QD de CdSe/ZnS funcionalizado con ketoprofeno (CS@KP,) tal y como se describió en el artículo anterior,⁷¹ y una β -ciclodextrina modificada con una unidad de pireno, el 3-(piren-1-il)prop-2-inilo, en su cara grande (esquema 39). Se eligieron estos compuestos por dos razones:

- La constante de asociación entre la β -CD y el pireno es considerablemente alta (K_a aprox. 3000 M^{-1})

- El 3-(piren-1-il) prop-2-inilo podría desactivar la fluorescencia del QD

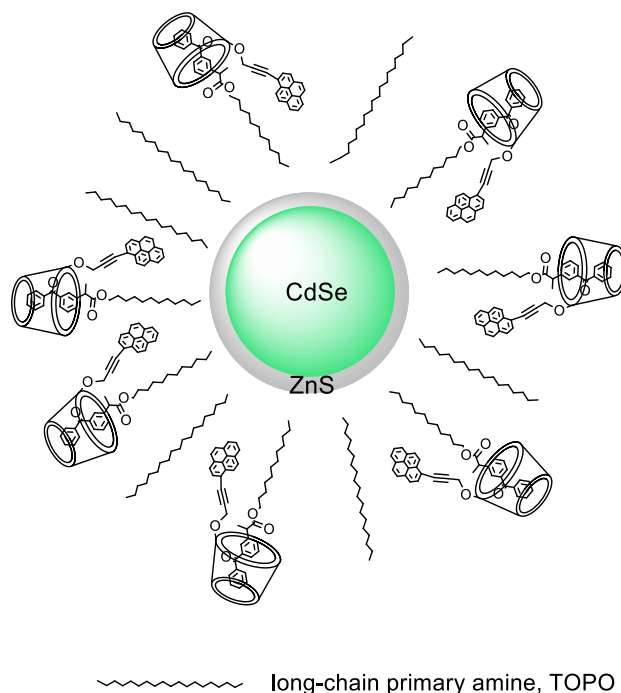


Figura 39 – Sistema supramolecular CS@KP/CD-Py.

Así, la encapsulación del KP en la cavidad de la ciclodextrina dio lugar al sistema supramolecular (CS@KP/CD-Py, esquema 39), soluble en medios acuosos (acetonitrilo:agua 3:1).

Con el fin de determinar la localización del pireno en el sistema de CS@KP/CD-Py, se llevaron a cabo estudios de fotólisis de destello laser (Nd / YAG, 355 nm) de los sistemas pireno (QD@KP/CD-Py y CD-Py). Se observó la formación del triplete del pireno (λ_{max} a 430 nm, τ aprox. 6 μs) y el catión radical del pireno (λ_{max} a 490 nm, τ aprox. 31 μs). En el caso del sistema supramolecular, el rendimiento del pireno catión radical y su tiempo de vida medio disminuyeron considerablemente (10 μs), mientras que el rendimiento del triplete del pireno y su

tiempo de vida aumentaron de forma notoria (24 μ s). Estos resultados indicaron que el pireno se situaba cerca de la superficie del QDs, es decir, entre las capas de ligando del CS@KP.

El sistema supramolecular se preparó adicionando una disolución de QD en tolueno a una disolución de CD-Py en acetonitrilo/agua (QD:CD-Py = 1:1000). Una vez estabilizado el sistema, se observó una disminución importante de la emisión del QD y un desplazamiento del máximo de emisión hacia el azul (figura 40).

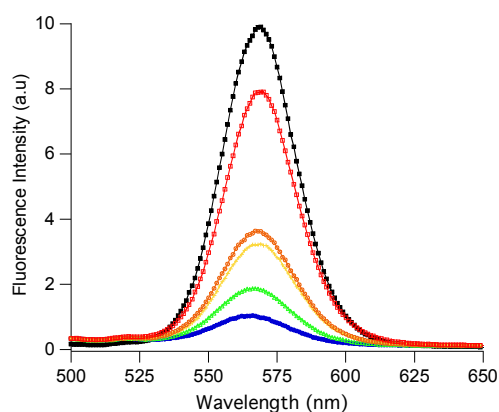


Figura 40. Espectro de fluorescencia en N_2 en acetonitrilo/agua (3/1) de CS@KP (■), CS@KP/ β -CD-Py ([CS] = 5×10^{-9} M, [β -CD-Py] = 5×10^{-6} M) antes (●) y después de la adición de benzofenona: (2.5×10^{-6} M, ▲), (5×10^{-6} M, +), (1×10^{-5} M, ○) y (2.5×10^{-5} M, □), λ_{ex} = 450 nm. Relación molar analito/QD 1000/1.

La adición de diferentes analitos al sistema causó un aumento de la fluorescencia debido a la asociación competitiva frente al ketoprofeno dentro de la cavidad de la CD. La asociación QD/analito provoca un alejamiento del CD-Py de la superficie del QD, con el consiguiente aumento de la fluorescencia de la

nanopartícula. Los analitos estudiados han sido benzofenona, indoles y derivados, fenoles y el ácido adamantano carboxílico (figura 41).

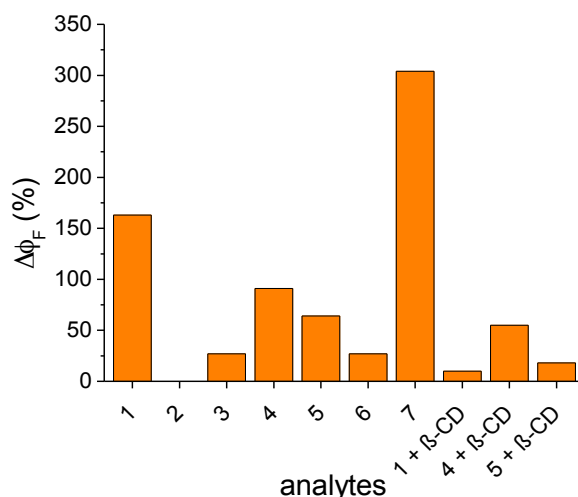


Figura 41 – Efecto de la adición de diferentes analitos (1- benzofenona, 2- ketoprofeno, 3- éster metílico del ketoprofeno, 4- fenol , 5- indol, 6- 7-metil indol , 7- ácido adamantano carboxílico) en la fluorescencia ($\lambda_{ex} = 450$ nm) de una disolución en acetonitrilo/agua (3/1) de CS@KP/ β -CD-Py en atmosfera de N_2 . Efecto competitivo de la β -CD para los analitos 1, 4 y 5.

Una vez realizado el estudio, se diseñó una metodología para recuperar individualmente los tres elementos usados en el análisis, es decir, el CS@KP, la β -ciclodextrina y el analito. La adición de tolueno a la mezcla del sistema CS@KP/ β -CD-Py (ACN/ H_2O) con el analito provocó la separación de la solución en dos fases: la migración del acetonitrilo a la fase de tolueno (parte superior) y la separación de la QD en la interfase, debido a su baja solubilidad tanto en la fase tolueno/acetonitrilo como en la fase acuosa. Posteriormente, se separó y se evaporó la fase orgánica. El espectro de 1H -RMN del residuo indicó la recuperación del analito. A continuación, se añadió tolueno a la fase acuosa, lo que condujo a la transferencia del QD a la fase del tolueno. El análisis por

espectroscopia de fluorescencia de la fase orgánica mostró la recuperación de CS@KP. Finalmente, el análisis por GC/MS y ¹H-RMN de la fase acuosa corroboró la recuperación de CD-Py (figura 42).

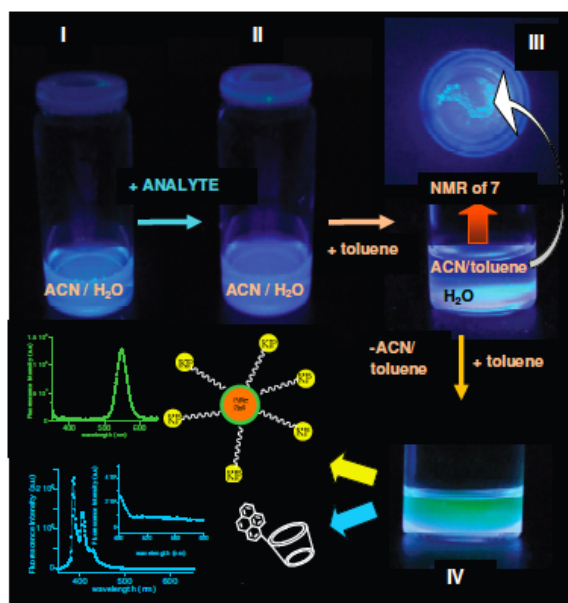


Figura 42 – Recuperación del QD, de la β -CD-Py y del adamantano (7) una vez completado el proceso de reconocimiento molecular.

En resumen, se ha diseñado un sistema supramolecular de QD/CD que puede ser utilizado como un sensor molecular efectivo para diferentes analitos. Además, todos los componentes han sido recuperados individualmente, lo cual es de vital interés desde el punto de vista medioambiental.

Further Insight into the Photostability of the Pyrene Fluorophore in Halogenated Solvents

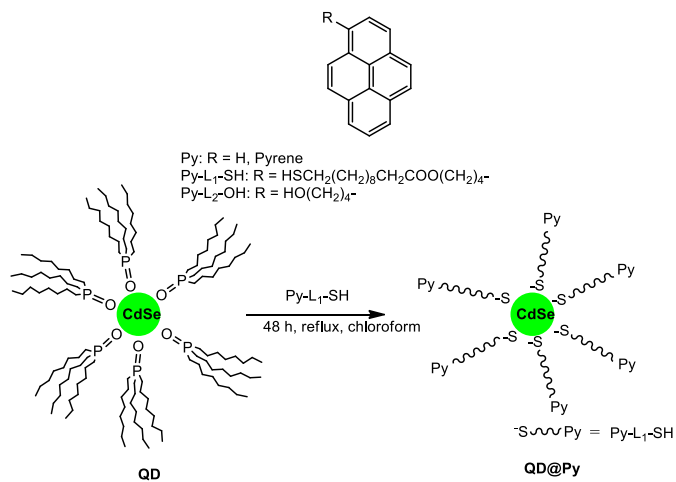
(*ChemPhysChem* **2012**, *13*, 835-844).

El pireno es un hidrocarburo policíclico aromático, PAH, usado ampliamente como sensor químico. Se ha observado que el pireno sufre una importante degradación en diferentes medios, tales como metanol o ácidos, o adsorbido en celulosa, lo cual puede desvirtuar el análisis realizado. El uso del cromóforo pireno en disolventes halogenados es motivo de especial preocupación. Además, se ha encontrado que la fotoestabilidad del pireno en cloroformo es menor en atmósfera de oxígeno que en nitrógeno.

Por otra parte, la forma esférica de los QDs les confiere un alta relación superficie-volumen lo que permite obtener una alta concentración local de ligandos en su periferia.

El objetivo de este trabajo es comparar la fotodegradación en diferentes disolventes halogenados (CHCl_3 y CH_2Cl_2) del pireno libre en disolución con la del pireno en la periferia de los QDs de CdSe. Así pues, se ha estudiado y analizado la fotoestabilidad del pireno, de un derivado del pireno unido a la superficie de los QDs y dos derivados alquilpirenos, Py-L₁-SH y Py-L₂-OH, siendo uno de ellos el ligando del QD (esquema 23).

En primer lugar, se prepararon nanopartículas de CdSe funcionalizadas con moléculas de pireno (QD@Py). La observación de la emisión del excímero del pireno indicó una alta concentración local de pireno sobre la nanopartícula (figura 43).



Esquema 23 - Estructuras del pireno, los derivados del pireno y del QD@Py.

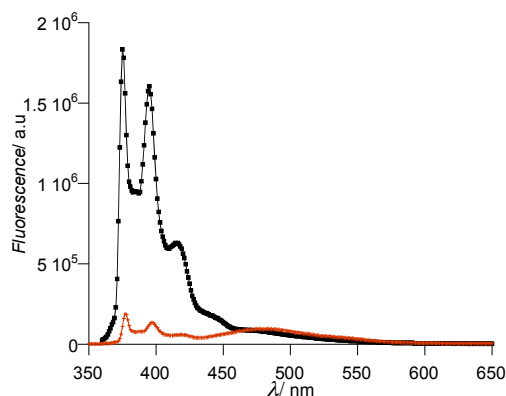


Figura 43 – Espectro de fluorescencia del pirenobutanol (negro) y del QD@Py (rojo) en condiciones anaeróbicas. Las muestras están ajustadas a la misma absorbancia a 355 nm.

Los estudios fotofísicos de los sistemas de pireno y el análisis de los fotoproductos generados se llevó a cabo usando las diferentes técnicas analíticas de absorción y fluorescencia de estado estacionario, resonancia magnética nuclear (¹H-NMR, ¹³C-NMR, COSY, HMQC, y HMBC), espectroscopia infrarroja (FTIR), microscopia electrónica de transmisión de alta resolución (HRTEM), y espectrometría de gases-masas (GC-MS).

Primero, las disoluciones en cloroformo del pireno, pirenobutanol y QD@Py se irradiaron (lámparas UV-A) en atmósfera de aire.

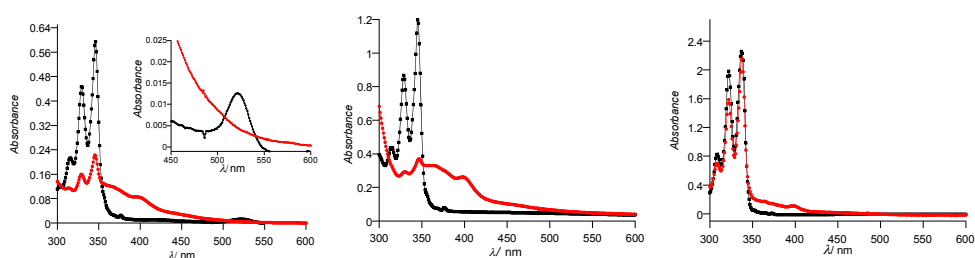


Figura 44 – Izquierda, espectro de absorción en cloroformo y aire de QD@Py, antes (negro) y después (rojo) de la irradiación con lámparas UV-A durante 30 min. Centro, espectro de absorción en cloroformo y aire del pirenobutanol, antes (negro) y después (rojo) de la irradiación en lámparas UV-A durante 60 min. Derecha, espectro de absorción en cloroformo y aire del pireno, antes (negro) y después (rojo) de la irradiación con lámparas UV-A durante 60 min.

El espectro de absorción y emisión del QD@Py mostró la elevada transformación del pireno después de 30 minutos de irradiación con lámparas UV-A (figura 44). Así, el espectro de fluorescencia del QD@Py irradiado evidenció nuevas bandas estructuradas con λ_{max} a 399 y 420 nm (figure 45), desplazadas hacia el rojo en comparación con las bandas del pireno, además de la aparición de bandas anchas (λ_{max} a 450 y 490 nm).

Con fines comparativos, se estudió la estabilidad del pireno y del pirenobutanol. El espectro de absorción (figura 44) mostró una degradación análoga a la del QD@Py. En el espectro de fluorescencia del pirenobutanol irradiado aparecieron bandas a λ_{max} a 395 y 420 nm y bandas anchas desplazadas hacia el rojo (λ_{max} a 440 y 450-525 nm, figura 45). Sin embargo, para el pireno, el espectro de fluorescencia mostró bandas con λ_{max} aprox. a 338 y 408 nm, y una banda ancha λ_{max} a 450 nm, y una banda estructurada entre 450 y 600 nm.

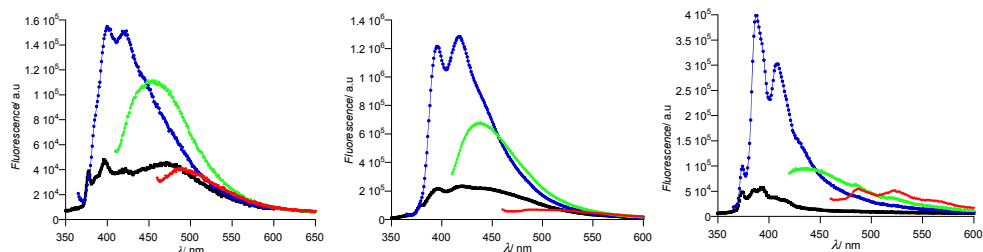


Figura 45 – Espectros de emisión en aire de izquierda) QD@Py, centro) pirenobutanol, y derecha) pireno después de irradiación con lámparas UV-A del QD@Py (30 min), para el pirenobutanol (60 min) y el pireno (60 min). Los espectros fueron registrados a longitudes de excitación (λ_{ex}): λ_{ex} 313 nm (negro), 355 nm (azul), 400 nm (verde), y 450 nm (rojo).

Después, se realizaron las irradiaciones de las muestras en diclorometano destilado (libre de amileno). La irradiación de los tres sistemas en diclorometano mostró la alta fotoestabilidad del pireno en este disolvente (figura 46).

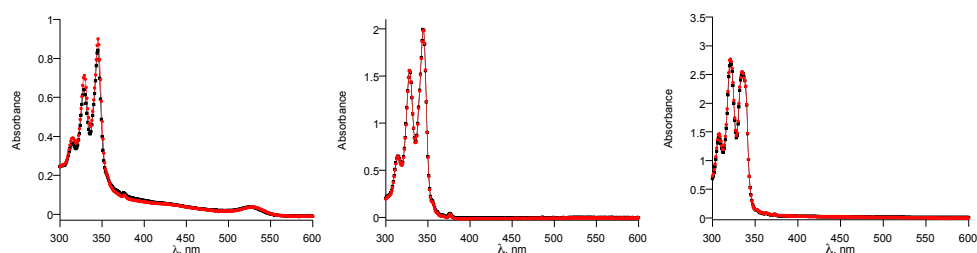
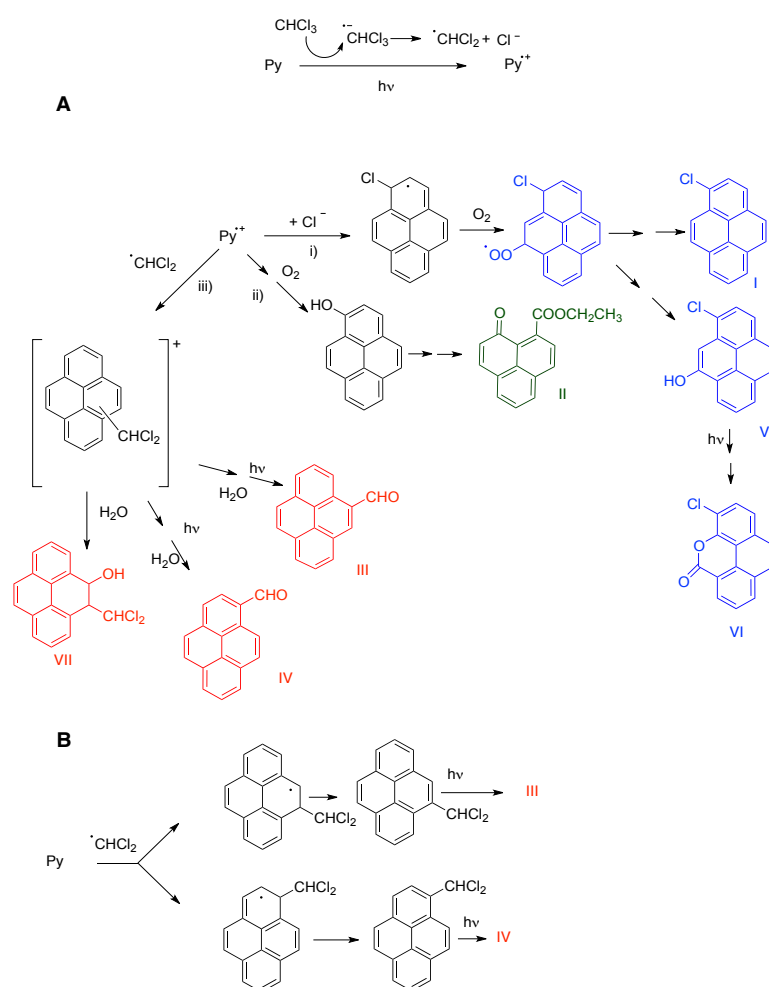


Figura 46 – Espectros de absorción de QD@Py (izquierda), Py-L₂-OH (centro), y Py (derecha) en diclorometano libre de amileno, antes (negro) y después (rojo) de su irradiación en atmósfera de aire y con lámparas UV-A.

Finalmente, se irradió gran cantidad de pireno en cloroformo con lámparas UV-A con el fin de analizar los fotoproductos generados. La cromatografía de columna permitió separar los fotoproductos más abundantes, así como trazas de un compuesto, el cual fue fácil de seguir y separar por cromatografía debido a su elevada fluorescencia.

El mecanismo propuesto para la transformación del pireno se indica en el esquema 31. La transferencia electrónica desde el pireno excitado al disolvente halogenado daría lugar al anión radical del haloalcano y al cation radical del pireno. En el caso del cloroformo, la rápida disociación del anión radical del haloalcano en $\cdot\text{CHCl}_2$ y Cl^- evitaría la rápida transferencia electrónica de este al cation radical del pireno. Posteriormente, el cation radical del pireno reaccionaría con el Cl^- , O_2 o $\cdot\text{CHCl}_2$ (esquema 24).



Esquema 24 – Mecanismo propuesto para la fotodegradación del pireno.

La alta fotoestabilidad del pireno en diclorometano junto con el hecho de que los carbaldehídos fueron los principales fotoproductos en la degradación del pireno en cloroformo sugirió que el radical del haloalcano, y no el anión cloruro, es la especie mayoritariamente responsable de la transformación del pireno. De hecho, el pireno se degrada mas rápidamente en cloroformo destilado. Así pues, la alta estabilidad de los cromóforos de pireno en diclorometano parece ser debido a la baja reactividad de los radicales $\text{CH}_2\text{Cl}\cdot$ hacia el pireno, además de su alta reactividad hacia el oxígeno, comparado con la de los radicales $\text{CHCl}_2\cdot$.

En resumen, los resultados obtenidos en estos estudios indicaron que la combinación del cloroformo con la luz provoca una alta fotodegradación de los cromóforos de pireno, causada principalmente por los radicales diclorometilo. Sorprendentemente, el uso de diclorometano mostró ser una buena alternativa al cloroformo debido a que los radicales clorometilo apenas reaccionaron con las estructuras de pireno. Además, se demostró que los cromóforos de pireno soportados en QDs no presentaron mejor fotoestabilidad que la de los cromóforos libres.

Photoluminescence enhancement of CdSe Quantum Dots: a case of organogel-nanoparticle

(Journal of the American Chemical Society, dx.doi.org/10.1021/ja310508r)

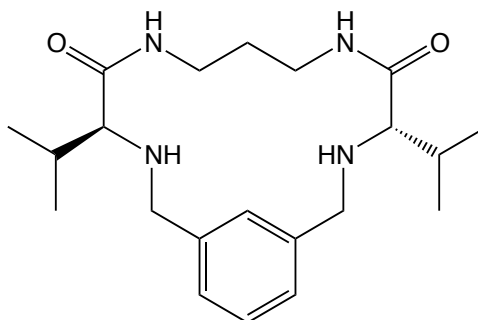
Los organogeles son materiales orgánicos basados en el autoensamblaje de moléculas mediante interacciones no covalentes. Estos sistemas tienen aplicaciones en cosméticos, conservantes alimenticios o como soportes de diferentes tipos de nanopartículas confiriéndoles estabilidad y organización espacial.

Los QDs pueden ser usados para el desarrollo de organogeles fluorescentes debido a sus altos rendimientos cuánticos de fluorescencia. Existen pocos ejemplos donde se combinen QDs de CdSe y CdSe/ZnS con organogeles. Bardelang *et al.*⁸¹ han preparado un sistema basado en la combinación de un péptido y un QD de CdSe/ZnS mediante ultrasonidos. Por otro lado, Zhou *et al.*⁸² han diseñado un material híbrido basado en la combinación de QDs de CdSe y CdSe/ZnS y una molécula hiperramificada.

En este trabajo, presentamos la preparación y caracterización de sistemas híbridos que combinan el macrociclo pseudopeptídico **1** (figura 47) con diferentes tipos de QD (CdSe y CdSe/ZnS) funcionalizados con diferentes ligandos (TOPO y ODA).

La elección del organogelante **1** se debió a tres factores: su capacidad de autoensamblaje en tolueno, su estabilidad en las condiciones experimentales y la transparencia de los organogeles resultantes necesaria para la caracterización óptica. Para la preparación del sistema, el organogel se disolvió en tolueno y se calentó a la temperatura de ebullición del disolvente hasta la completa disolución de **1**. Posteriormente, se adicionó el QD y se enfrió la mezcla a temperatura ambiente hasta la gelificación. Este método de trabajo proporcionó mejores resultados que cuando el sistema se obtuvo mezclando previamente el QD con el

organogelante **1**, seguido del calentamiento la mezcla y de su posterior enfriamiento, debido a la baja estabilidad de los QDs a altas temperaturas.



1

Figura 47 - Estructura química del organogel 1.

La caracterización fotofísica del sistema QD-organogel mostró diferentes tendencias dependiendo de la presencia o ausencia de ZnS:

- La fluorescencia de los QD de CdSe/ZnS se conserva, debido a la existencia de la corteza de ZnS que pasiva la superficie del CdSe.
- En el caso de los QDs de CdSe, se observó un gran aumento de la fluorescencia (hasta un 528%). Aunque se podría pensar que este comportamiento podría ser debido a la pasivación de los defectos de superficie, no es así, como se analizará posteriormente en estudios de fluorescencia resueltos en el tiempo.

El sistema QD-organogel presentó una gran estabilidad; mantuvo su fluorescencia inicial después de 5 horas desde su preparación. Estudios de termoreversibilidad demostraron que la fluorescencia del QD se mantiene después de 6 ciclos de calentar y enfriar el organogel híbrido (figura 48).

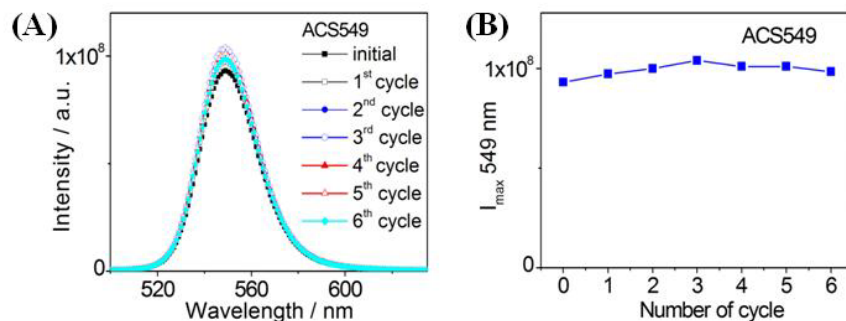


Figura 48 - A) Espectros de emisión de muestras preparadas en tolueno que contienen QDs de CdSe/ZnS funcionalizados con amina (CS@ODA) y el organogel **1** ($\lambda_{\text{exc}} = 465$ nm). B) Gráfico de la intensidad de emisión a la longitud de onda del máximo de emisión después de cada ciclo de fusión-gelificación.

Los estudios de espectroscopía de fluorescencia de tiempo resuelto mostraron el efecto de la concentración del macrociclo **1** sobre el tiempo de vida del QD. Estos estudios revelaron dos tendencias. En primer lugar, los tiempos de vida de fluorescencia y sus contribuciones relativas siguieron el mismo patrón en los QDs de CdSe/ZnS, independientemente de la presencia del organogel. En segundo lugar, se observó un aumento de los tiempos de vida de fluorescencia de los QDs de CdSe. Además, el tiempo de vida medio no se vio afectado en el caso de los QDs de CdSe/ZnS. Sin embargo, para los QDs de CdSe, el tiempo de vida medio aumentó en presencia del organogel entre un 1.5 y 1.7.

Posteriormente, se realizó un experimento para determinar la dependencia de las fluorescencia de los QDs de CdSe respecto de la concentración del macrociclo **1**. Se observó que a pequeñas concentraciones de **1**, se produce un pequeño aumento de la intensidad y del tiempo de vida de fluorescencia. En cambio a concentraciones de organogel mayores de 4 mM, la fluorescencia del QD aumentó drásticamente, mientras que el tiempo de vida apenas se vio modificado (figura 49A). A continuación, se realizó una comparación de la dependencia de la constante radiativa (k_r) y la constante no radiativa (k_{nr}) con la

concentración del organogel, utilizando las ecuaciones 5 y 6. La figura 49B muestra que el incremento en la fluorescencia del QD está relacionado con el incremento de la constante radiativa, mientras que la constante no radiativa no se afecta significativamente por la concentración de organogel. La k_{nr} está relacionada con los defectos de superficie del QD y presentó una menor participación en el aumento de la fluorescencia del QD.

$$\phi = \frac{k_r}{k_r + k_{nr}} \quad \text{Eq. 5}$$

$$\tau_f = \frac{1}{k_r + k_{nr}} \quad \text{Eq. 6}$$

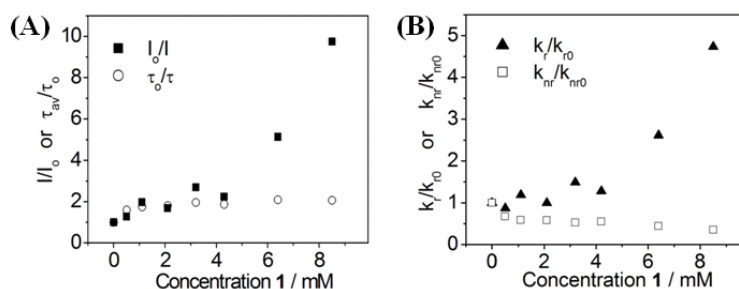


Figura 49 – A) Relación de los cambios de las intensidades y tiempos de vida de emisión de CdSe@TOPO frente a la concentración del organogel. B) Relación entre la constantes radiativa y no radiativa de CdSe@TOPO frente a la concentración del organogel.

El macrociclo **1** contiene grupos amida y amina, así como partes hidrofóbicas en su estructura química. Las amidas pueden participar en la estabilización de las nanopartículas³⁴ y las aminas tienen un efecto importante en las propiedades fluorescentes de los QDs. Además, el macrociclo **1** puede dar lugar a una interdigitalización con los ligandos del QD. Este proceso podría afectar a las propiedades del QD durante la gelificación dando lugar a organogeles con mejores propiedades (efecto simbiótico). Para determinar la existencia de tal interacción, se llevaron a cabo estudios de RMN y de IR de muestras macrociclo **1**/QD de CdSe con concentraciones de macrociclo menores a la de gelificación.

Estudios de resonancia magnética nuclear de protón ($^1\text{H-NMR}$) mostraron el típico ensanchamiento de las señales del organogel en presencia del QD de CdSe, en condiciones de no gelificación (figura 50). Con fines comparativos, se incluye el espectro del macrociclo **1** en presencia de TOPO, donde se observa que las señales de protón de **1** aparecen considerablemente desplazadas a campo bajo respecto a las del macrociclo **1** en tolueno, pero no se observó ningún ensanchamiento.

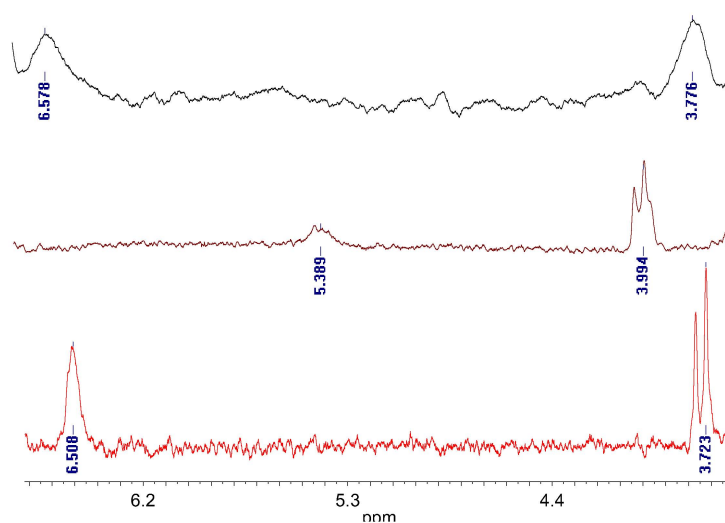


Figura 50 – De abajo a arriba: Ampliación entre 3.6 ppm y 6.7 ppm del espectro de $^1\text{H-NMR}$ del macrociclo **1** en tolueno deuterado, comparado con el macrociclo **1** en presencia de TOPO (ratio macrociclo/TOPO de 1000/1) y en presencia de QD@TOPO. Condiciones de no gelificación.

En estas condiciones, los espectros de resonancia magnética nuclear de fósforo ($^{31}\text{P-NMR}$) del QD de CdSe y QD-organogel, mostraron un ensanchamiento de la señal del TOPO, además de un considerable desplazamiento. Este desplazamiento fue aún mayor en QD@TOPO. Estos resultados indicaron una interacción entre el QD y el organogel antes de la gelación (figura 51). Además, no observaron las señales del TOPO libre, lo que indicó que no tuvo lugar el intercambio de ligando entre el TOPO y el organogel.

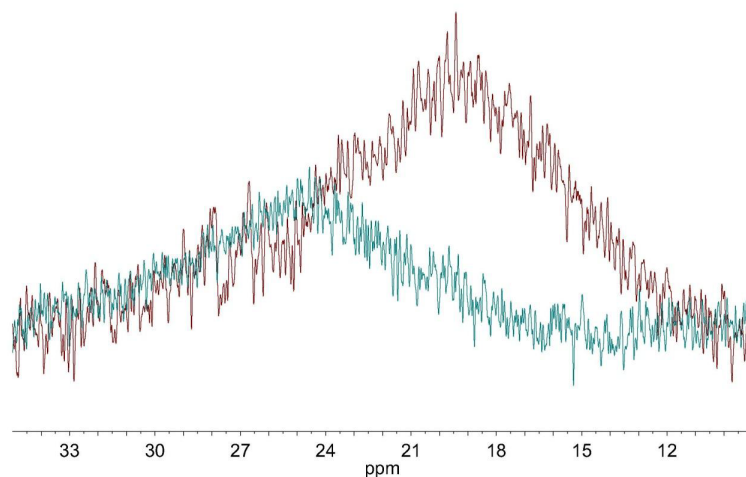


Figura 51 – Espectro de ^{31}P -NMR en tolueno deuterado de QD@TOPO en ausencia (—) y en presencia del macrociclo **1** (—). Condiciones de no gelificación.

Los estudios de espectroscopia infrarroja (IR) muestran la interacción entre el QD@TOPO de CdSe y el organogel. En la figura 52 se observa como las señales más significativas (3300 cm^{-1} , y 3100 cm^{-1} correspondientes a N-H y C-H respectivamente) se desplazan en la mezcla QD/organogel respecto al organogel en ausencia de QD. La figura 53 muestra que este efecto puede observarse incluso antes de la formación del organogel.

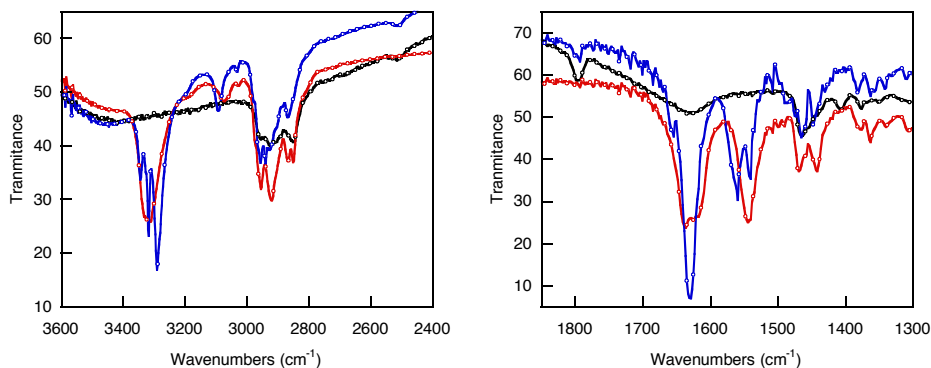


Figura 52 – Espectros comparativos de IR del organogel (—), QD@TOPO (—), y QD@TOPO/organogel (—) en KBr. Izquierda: región desde 3600 a 2400 cm^{-1} Derecha: región desde 2400 a 1300 cm^{-1} . Condiciones de gelificación.

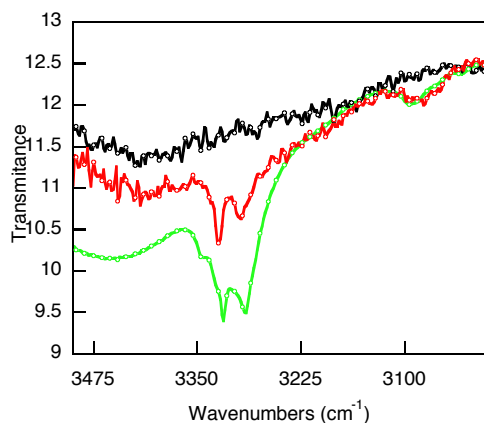


Figure 53 - Espectro IR comparativo del organogel (—), QD@TOPO (—), y QD@TOPO/organogel (—) en KBr. Condiciones de no gelificación.

Los estudios de microscopia de fuerza atómica (AFM) mostraron que la estructura fibrilar se mantiene tras la formación del QD-organogel. Las imágenes obtenidas en el microscopio electrónico de transmisión (TEM) mostraron que las

nanopartículas se dispersaron aleatoriamente por las fibras del organogel, manteniendo su tamaño y su forma cristalina. Estos resultados demostraron que los QDs no desestabilizan la estructura fibrilar del organogel. Generalmente, los organogeles se ha descrito como sistemas supramoleculares compuestos de una serie de “*piscinas de disolvente*” en los cuales los QDs se podrían mover como si estuviesen en una disolución. Sin embargo, esto no explicaría el aumento de la fluorescencia de los QDs, incluso en condiciones previas a la gelificación. El hecho de que la concentración crítica de gelante (*cgc*) para mezclas de QDs y organogeles fuese menor que la *cgc* para el gelante sólo, indica que el QD actúa como *lugares de nucleación*, al favorecer una alta concentración local del gelante en la superficie del QD y por lo tanto facilitar el proceso de gelificación. Por lo tanto, el efecto simbiótico estabilizante de la combinación organogel/QD se atribuye a una interdigitalización del macrociclo **1** y los ligandos del QD.

El incremento en la k_r en los QDs de CdSe a altas concentraciones del organogel no se puede interpretar como una disminución en los procesos de transferencia de energía y de reabsorción entre los QDs como consecuencia de su inmovilización en la red fibrilar del gelante, ya que si así fuese, tanto en los QDs de CdSe como los QDs de CdSe/ZnS debería observarse dicho incremento. No obstante, el incremento del índice de refracción después de la gelificación de los QDs de CdSe podría contribuir al aumento de la constante radiativa.

En resumen, estos resultados demostraron la simbiosis entre los CdSe QDs y el organogelante **1**. La formación del organogel se favoreció en presencia de QD, ya que se necesitó menos cantidad para su gelificación y las propiedades fluorescentes de los QDs aumentaron en el caso del core CdSe. Sistemas altamente fluorescentes, transparentes y estables pueden ser preparados de manera rápida y fácil por calentamiento del organogel en tolueno y posterior enfriamiento a temperatura ambiente en presencia del QD.

Conclusiones

Los resultados obtenidos en esta tesis dan lugar a las siguientes conclusiones:

- La adición de tioles a QDs de CdSe solubles en medios orgánicos provoca una disminución de la fluorescencia de las nanopartículas. Sin embargo, para los CdSe/ZnS funcionalizados con aminas se observa un importante aumento de las propiedades fluorescentes tras la adición de tioles.
- El intercambio de ligandos amina por alquiltioles para sintetizar CdSe/ZnS@tioles QDs calentando suavemente la mezcla de reacción produce QDs altamente fluorescentes. Las aminas tienen un importante papel en esta observación, puesto que su basicidad permite una suave desprotonación del tiol cerca de la superficie del QD. Como resultado de esto, el tiolato se une a la superficie de ZnS con una mínima alteración de la superficie. Esta metodología ha sido aplicada con éxito para la síntesis de nanopartículas solubles en medios orgánicos y acuosos. Además, estas nanopartículas son más (foto)estables que sus precursoras. Estos resultados son de gran interés para el diseño de nuevos QDs funcionales, altamente fluorescentes, fotoestables y de pequeño tamaño.
- Se ha preparado un sistema supramolecular basado en una nanopartícula de CdSe/ZnS funcionalizada con ketoprofeno y una β -ciclodextrina modificada con una molécula de pireno. Este sistema ha sido utilizado de forma eficiente para el reconocimiento molecular de diferentes analitos. Además, se ha diseñado una estrategia de

recuperación de todos los componentes, lo que hace el sistema económico y sostenible.

- La fotoestabilidad del pireno (libre o soportado en QDs) es más baja en cloroformo debido a la formación de radicales diclorometilo bajo irradiación. Se propone el uso de diclorometano como disolvente alternativo debido a que los radicales clorometilo apenas degradan las estructuras de pireno.
- Ha sido posible preparar organogeles altamente fluorescentes combinando un macrociclo pseudopeptídico y diferentes tipos de QDs de CdSe y CdSe/ZnS. Por un lado, el organogel conserva (CdSe/ZnS) o aumenta (CdSe) las propiedades fotoluminiscentes de los QDs, y por otro lado, es posible reducir la concentración crítica necesaria de organogel un sistema estable y termorreversible.

Resumen de la tesis

Esta tesis se centra en el efecto simbiótico entre los QDs de CdSe o CdSe/ZnS y sus ligandos orgánicos, y las ventajas de este efecto para mejorar la funcionalidad del QD y/o del ligando, o crear una nueva funcionalidad del sistema. Así :

1. la superficie de las nanopartícula recubierta con ligandos orgánicos puede permitir al QD i) permanecer estable en disolventes orgánicos o acuosos, debido a la repulsión estérica o iónica entre las nanopartículas, ii) mantener o aumentar sus propiedades emisivas (pasivación de los defectos de superficie, aumento de distancia entre nanopartícula y moléculas desactivadoras), y/o iii) para proporcionar funcionalidad a la nanopartícula.

2. la forma esférica de la nanopartícula favorece la localización de un elevado número de ligandos en la superficie del QD. Por lo tanto, es posible tener una alta concentración local de un grupo funcional en la periferia QD, incluso en solución diluidas.

3. la acción combinada del QD y el ligando puede permitir la encapsulación o interdigitalización de otras moléculas, acercándolas a la superficie del QD. Además, el ligando funcional puede modificar reversiblemente las propiedades emisivas de las nanopartículas y esto ser utilizado para la detección de analitos, entre otras aplicaciones.

Existe una gran interés en la pasivación de los QDs de CdSe y CdSe/ZnS con ligandos orgánicos que poseen en uno de sus extremos un grupo mercapto debido a la alta afinidad de este grupo por la superficie del QD, principalmente cuando está como tiolato. Sin embargo, el intercambio de ligandos de los QDs (generalmente preparados con ligandos amino) por tiol (QDs tipo core) o tiolatos (QDs tipo core-shell) produce una considerable reducción de las propiedades luminiscentes de ambos QDs. En el caso de los QDs tipo core, el tiol atrapa el

hueco formado tras la excitación del QD, y por lo tanto evita la recombinación electrón-hueco. La baja emisión del QD tipo core-shell es atribuida a una alteración en la superficie del QD durante intercambio de ligando.

Durante esta tesis, hemos desarrollado una nueva estrategia para obtener QDs de CdSe/ZnS pasivados con tiolatos, altamente fluorescentes, solubles en medios orgánicos y en agua, basada en la quimisorción de tioles en la superficie QD. En esta estrategia el ligando nativo amina del QD juega un papel clave, ya que ayuda a la disociación el tiol cerca de la superficie QD. La sustitución de las aminas de cadena larga por tioles se llevó a cabo bajo condiciones de reacción suaves, lo que permite preservar o incluso mejorar las propiedades luminiscentes de los QD. Esta metodología se llevo a cabo con éxito tanto en nanopartículas sintetizadas en el laboratorio como en aquellas disponibles comercialmente. Además, estos QDs mostraron mayor fotoestabilidad que los QDs funcionalizados con amina.

Estos resultados son de gran interés para la fabricación de nuevos dispositivos para la detección o reconocimiento molecular, basado en procesos de transferencia de energía o de electrones. Así pues, esta estrategia fue utilizada para la preparación de QDs de CdSe/ZnS, altamente fluorescentes y soluble en agua, pasivados con un ligando bifuncional, con un grupo mercapto (grupo de anclaje) en un extremo y una benzofenona en el otro. Este QD se usó para desarrollar un sistema supramolecular, basado en una nanopartícula de CdSe/ZnS funcionalizada con ketoprofeno y una β -ciclodextrina modificada con una molécula de pireno. Las unidades de ketoprofeno favorecen el reconocimiento molecular entre la nanopartícula y la ciclodextrina y, al mismo tiempo, sitúan la unidad de pireno cerca a la superficie de nanopartículas, provocando la desactivación de la fluorescencia del QD. Este efecto simbiótico se utilizó con éxito para la detección molecular de diferentes analitos. El proceso de detección de este sistema híbrido, eficaz y fácil de preparar, se basa en la recuperación de la intensidad de fluorescencia del QD en respuesta a diferentes analitos. Además, la metodología

diseñada permitió la recuperación individual de todos los componentes utilizados en este sistema, lo cual es muy deseable tanto desde el punto de vista económico como medioambiental.

Como se mencionó anteriormente el QD puede ser utilizado como nano-transportador de un grupo funcional, lo que conduce a un aumento de la concentración local del grupo funcional en una solución diluida. En esta tesis, QDs de CdSe fueron utilizados como soportes de moléculas de pireno, y, como consecuencia, se observó la formación del excímero del pireno utilizando concentraciones muy bajas del ligando pireno. La luminiscencia de los QDs de CdSe se redujo drásticamente debido al uso de un ligando pireno que posee un grupo mercapto como grupo de anclaje. Este sistema fue utilizado para estudiar la influencia del QD en la fotoestabilidad del pireno en diferentes disolventes clorados y se compararon con los resultados obtenidos con pireno libre. Estos estudios demuestran que la combinación de cloroformo y la luz produce una alta fotodegradación de todos los sistemas de pireno, mientras que en diclorometano son altamente estables.

Finalmente, se estudiaron sistemas híbridos QD-organogel, altamente fluorescentes, a partir de un macrociclo pseudopeptídico, y ambos tipos de QDs (CdSe y CdSe/ZnS pasivados con diferentes ligandos). Estos organogeles híbridos se prepararon fácilmente por calentamiento del organogelante en tolueno, seguido de la adición de los QDs y del posterior enfriamiento del sistema a temperatura ambiente. La presencia del QD en el sistema QD-organogel disminuye la concentración crítica del organogelante necesaria para formar los organogeles estables y termorreversibles, sin afectar significativamente el interior de la red fibrilar del organogel. Además, el efecto del organogelante en las propiedades luminiscentes de los QDs depende de la presencia de la capa de ZnS. Las propiedades fotofísicas de los QDs de CdSe/ZnS se mantuvieron en el

medio organogel, mientras que en el caso de los QDs de CdSe se observó un importante aumento de la intensidad de fluorescencia. Demostramos que el macrociclo interactúa con los ligandos del QD de CdSe incluso antes de la gelificación, mediante el uso de metodologías usuales, tales como IR y RMN. Esta es la primera vez que se reporta la interacción entre un organogel y un QD.

8 - BIBLIOGRAPHY

- (1) Brus, L. E. *Journal of Chemical Physics* **1984**, *80*, 4403-4409.
- (2) Bawendi, M. G.; Steigerwald, M.; Brus, L. *Annual Review Of Physical Chemistry* **1990**, *41*, 477-496.
- (3) Hyldahl, M. G.; Bailey, S. T.; Wittmershaus, B. P. *Solar Energy* **2009**, *83*, 566-573.
- (4) Michalet, X.; Pinaud, F. F.; Bentolila, L. A.; Tsay, J. M.; Doose, S.; Li, J. J.; Sundaresan, G.; Wu, A. M.; Gambhir, S. S.; Weiss, S. *Science* **2005**, *307*, 538-544.
- (5) Alivisatos, P. *Nature Biotechnology* **2004**, *22*, 47-52.
- (6) Chen, F.; Gerion, D. *Nano Letters* **2004**, *4*, 1827-1832.
- (7) Yu, W. W.; Qu, L.; Guo, W.; Peng, X. *Chemistry of Materials* **2003**, *15*, 2854-2860.
- (8) Norris, D. J.; Sacra, A.; Murray, C. B.; Bawendi, M. G. *Physical Review Letters* **1994**, *72*, 2612-2615.
- (9) Maye, M. M.; Gang, O.; Cotlet, M. *Chemical Communications* **2010**, *46*, 6111-6113.
- (10) Carrillo-Carrion, C.; Cardenas, S.; Simonet, B. M.; Valcarcel, M. *Chemical Communications* **2009**, 5214-5226.
- (11) Fu, H.; Zunger, A. *Physical Review B* **1997**, *56*, 1496-1508.
- (12) Talapin, D. V.; Rogach, A. L.; Kornowski, A.; Haase, M.; Weller, H. *Nano Letters* **2001**, *1*, 207-211.
- (13) Borchert, H.; Talapin, D. V.; McGinley, C.; Adam, S.; Lobo, A.; Castro, A. R. B. d.; Moller, T.; Weller, H. *The Journal of Chemical Physics* **2003**, *119*, 1800-1807.
- (14) Wei, S.-H.; Zunger, A. *Applied Physics Letters* **1998**, *72*, 2011-2013.

- (15) Xu, J.; Birke, R. L.; Lombardi, J. R. *Journal of the American Chemical Society* **1987**, *109*, 5645-5649.
- (16) Fojtik, A.; Weller, H.; Koch, U.; Henglein, A. *Berichte der Bunsengesellschaft für physikalische Chemie* **1984**, *88*, 969-977.
- (17) Spanhel, L.; Haase, M.; Weller, H.; Henglein, A. *Journal of the American Chemical Society* **1987**, *109*, 5649-5655.
- (18) Ramsden, J. J.; Gratzel, M. *Journal of the Chemical Society, Faraday Transactions 1: Physical Chemistry in Condensed Phases* **1984**, *80*, 919-933.
- (19) Weller, H.; Fojtik, A.; Henglein, A. *Chemical Physics Letters* **1985**, *117*, 485-488.
- (20) Resch, U.; Weller, H.; Henglein, A. *Langmuir* **1989**, *5*, 1015-1020.
- (21) Dameron, C. T.; Reese, R. N.; Mehra, R. K.; Kortan, A. R.; Carroll, P. J.; Steigerwald, M. L.; Brus, L. E.; Winge, D. R. *Nature* **1989**, *338*, 596-597.
- (22) Rajh, T.; Micic, O. I.; Nozik, A. J. *Journal Name: Journal of Physical Chemistry; (United States); Journal Volume: 97:46* **1993**, Medium: X; Size: Pages: 11999-12003.
- (23) Chemseddine, A.; Weller, H. *Berichte der Bunsengesellschaft für physikalische Chemie* **1993**, *97*, 636-638.
- (24) Fischer, C. H.; Weller, H.; Fojtik, A.; Lume-Pereira, C.; Janata, E.; Henglein, A. *Berichte der Bunsengesellschaft für physikalische Chemie* **1986**, *90*, 46-49.
- (25) Fischer, C. H.; Weller, H.; Katsikas, L.; Henglein, A. *Langmuir* **1989**, *5*, 429-432.
- (26) LaMer, V. K.; Dinegar, R. H. *Journal of the American Chemical Society* **1950**, *72*, 4847-4854.

- (27) Brandreth, D. A.; Otterstedt, J.-E. *Small particles technology* New York, 1998.
- (28) de Mello Donegá, C.; Liljeroth, P.; Vanmaekelbergh, D. *Small* **2005**, *1*, 1152-1162.
- (29) Park, J.; Joo, J.; Kwon, S. G.; Jang, Y.; Hyeon, T. *Angewandte Chemie International Edition* **2007**, *46*, 4630-4660.
- (30) Peng, Z. A.; Peng, X. *Journal of the American Chemical Society* **2000**, *123*, 183-184.
- (31) Hammer, N.; Emrick, T.; Barnes, M. *Nanoscale Research Letters* **2007**, *2*, 282 - 290.
- (32) Dubertret, B.; Skourides, P.; Norris, D. J.; Noireaux, V.; Brivanlou, A. H.; Libchaber, A. *Science* **2002**, *298*, 1759-1762.
- (33) Galian, R. E.; Guardia, M. d. I. *TrAC Trends in Analytical Chemistry* **2009**, *28*, 279-291.
- (34) Bullen, C.; Mulvaney, P. *Langmuir* **2006**, *22*, 3007-3013.
- (35) Murray, C. B.; Norris, D. J.; Bawendi, M. G. *Journal of the American Chemical Society* **1993**, *115*, 8706-8715.
- (36) Janczewski, D.; Tomczak, N.; Han, M.-Y.; Vancso, G. J. *Nat. Protocols* **2011**, *6*, 1546-1553.
- (37) Skaff, H.; Sill, K.; Emrick, T. *Journal of the American Chemical Society* **2004**, *126*, 11322-11325.
- (38) Liu, Y.; Kim, M.; Wang, Y.; Wang, Y. A.; Peng, X. *Langmuir* **2006**, *22*, 6341-6345.
- (39) Yuan, C.-T.; Chou, W.-C.; Chen, Y.-N.; Chou, J.-W.; Chuu, D.-S.; Lin, C.-A. J.; Li, J. K.; Chang, W. H.; Shen, J.-L. *The Journal of Physical Chemistry C* **2007**, *111*, 15166-15172.

- (40) Nose, K.; Fujita, H.; Omata, T.; Otsuka-Yao-Matsuo, S.; Nakamura, H.; Maeda, H. *Journal of Luminescence* **2007**, *126*, 21-26.
- (41) Liu, I. S.; Lo, H.-H.; Chien, C.-T.; Lin, Y.-Y.; Chen, C.-W.; Chen, Y.-F.; Su, W.-F.; Liou, S.-C. *Journal of Materials Chemistry* **2008**, *18*, 675-682.
- (42) Huynh, W. U.; Dittmer, J. J.; Alivisatos, A. P. *Science* **2002**, *295*, 2425-2427.
- (43) Shen, H.; Wang, H.; Tang, Z.; Niu, J. Z.; Lou, S.; Du, Z.; Li, L. S. *CrystEngComm* **2009**, *11*, 1733-1738.
- (44) Chen, X.; Hutchison, J.; Dobson, P.; Wakefield, G. *Journal of Materials Science* **2009**, *44*, 285-292.
- (45) Susumu, K.; Oh, E.; Delehanty, J. B.; Blanco-Canosa, J. B.; Johnson, B. J.; Jain, V.; Hervey, W. J.; Algar, W. R.; Boeneman, K.; Dawson, P. E.; Medintz, I. L. *Journal of the American Chemical Society* **2011**, *133*, 9480-9496.
- (46) Kalyuzhny, G.; Murray, R. W. *The Journal of Physical Chemistry B* **2005**, *109*, 7012-7021.
- (47) Wuister, S. F.; de Mello Donegá, C.; Meijerink, A. *The Journal of Physical Chemistry B* **2004**, *108*, 17393-17397.
- (48) Aldana, J.; Wang, Y. A.; Peng, X. *Journal of the American Chemical Society* **2001**, *123*, 8844-8850.
- (49) Liu, W.; Choi, H. S.; Zimmer, J. P.; Tanaka, E.; Frangioni, J. V.; Bawendi, M. *Journal of the American Chemical Society* **2007**, *129*, 14530-14531.
- (50) Breus, V. V.; Heyes, C. D.; Nienhaus, G. U. *The Journal of Physical Chemistry C* **2007**, *111*, 18589-18594.
- (51) Pong, B.-K.; Trout, B. L.; Lee, J.-Y. *Langmuir* **2008**, *24*, 5270-5276.
- (52) Agudelo-Morales, C. E.; Galian, R. E.; Pérez-Prieto, J. *Analytical Chemistry*, *84*, 8083-8087.

- (53) van Embden, J.; Jasieniak, J.; Gómez, D. E.; Mulvaney, P.; Giersig, M. *Australian Journal of Chemistry* **2007**, *60*, 457-471.
- (54) Sharma, S. N.; Pillai, Z. S.; Kamat, P. V. *The Journal of Physical Chemistry B* **2003**, *107*, 10088-10093.
- (55) Scholz, F.; Dworak, L.; Matylitsky, V. V.; Wachtveitl, J. *Chemphyschem : a European journal of chemical physics and physical chemistry*, *12*, 2255-2259.
- (56) Tvrđy, K.; Frantsuzov, P. A.; Kamat, P. V. *Proceedings of the National Academy of Sciences*, *108*, 29-34.
- (57) Raichlin, S.; Sharon, E.; Freeman, R.; Tzfati, Y.; Willner, I. *Biosensors and Bioelectronics*, *26*, 4681-4689.
- (58) Palaniappan, K.; Hackney, S. A.; Liu, J. *Chemical Communications* **2004**, 2704-2705.
- (59) Willard, D. M.; Carillo, L. L.; Jung, J.; Van Orden, A. *Nano Letters* **2001**, *1*, 469-474.
- (60) Goldman, E. R.; Medintz, I. L.; Whitley, J. L.; Hayhurst, A.; Clapp, A. R.; Uyeda, H. T.; Deschamps, J. R.; Lassman, M. E.; Mattoussi, H. *J Am Chem Soc* **2005**, *127*, 6744-51.
- (61) Achermann, M.; Petruska, M. A.; Kos, S.; Smith, D. L.; Koleske, D. D.; Klimov, V. I. *Nature* **2004**, *429*, 642-646.
- (62) Xu, H.; Huang, X.; Zhang, W.; Chen, G.; Zhu, W.; Zhong, X. *Chemphyschem : a European journal of chemical physics and physical chemistry*, *11*, 3167-3171.
- (63) Tomasulo, M.; Yildiz, I.; Kaanumalle, S. L.; Raymo, F. i. M. *Langmuir* **2006**, *22*, 10284-10290.
- (64) Billone, P. S.; Maretta, L.; Maurel, V.; Scaiano, J. C. *Journal of the American Chemical Society* **2007**, *129*, 14150-14151.

- (65) Algar, W. R.; Krull, U. J. *ChemPhysChem* **2007**, *8*, 561-568.
- (66) Aguilera-Sigalat, J.; Rocton, S.; Galian, R. E.; Pérez-Prieto, J. *Canadian Journal of Chemistry* **2011**, *89*, 359-363.
- (67) Ishihara, K.; Ohara, S.; Yamamoto, H. *Science* **2000**, *290*, 1140-1142.
- (68) Ji, X.; Copenhaver, D.; Sichmeller, C.; Peng, X. *Journal of the American Chemical Society* **2008**, *130*, 5726-5735.
- (69) Owen, J. S.; Park, J.; Trudeau, P.-E.; Alivisatos, A. P. *Journal of the American Chemical Society* **2008**, *130*, 12279-12281.
- (70) Dabbousi, B. O.; Rodriguez-Viejo, J.; Mikulec, F. V.; Heine, J. R.; Mattoussi, H.; Ober, R.; Jensen, K. F.; Bawendi, M. G. *The Journal of Physical Chemistry B* **1997**, *101*, 9463-9475.
- (71) Aguilera-Sigalat, J.; Rocton, S.; Sanchez-Royo, J. F.; Galian, R. E.; Perez-Prieto, J. *RSC Advances* **2012**, *2*, 1632-1638.
- (72) D'Souza, V. T.; Lipkowitz, K. B. *Chemical Reviews* **1998**, *98*, 1741-1742.
- (73) Chen, X.; Hong, L.; You, X.; Wang, Y.; Zou, G.; Su, W.; Zhang, Q. *Chemical Communications* **2009**, 1356-1358.
- (74) Freeman, R.; Finder, T.; Bahshi, L.; Willner, I. *Nano Letters* **2009**, *9*, 2073-2076.
- (75) Marconi, G.; Mezzina, E.; Manet, I.; Manoli, F.; Zambelli, B.; Monti, S. *Photochemical & Photobiological Sciences* **2011**, *10*, 48-59.
- (76) Bohne, C.; Abuin, E. B.; Scaiano, J. C. *Journal of the American Chemical Society* **1990**, *112*, 4226-4231.
- (77) Sun, Y.-P.; Ma, B.; Lawson, G. E.; Bunker, C. E.; Rollins, H. W. *Analytica Chimica Acta* **1996**, *319*, 379-386.

- (78) Kubát, P.; Civiš, S.; Muck, A.; Barek, J.; Zima, J. *Journal of Photochemistry and Photobiology A: Chemistry* **2000**, *132*, 33-36.
- (79) Reyes, C. A.; Medina, M.; Crespo-Hernandez, C.; Cedeno, M. Z.; Arce, R.; Rosario, O.; Steffenson, D. M.; Ivanov, I. N.; Sigman, M. E.; Dabestani, R. *Environmental Science & Technology* **1999**, *34*, 415-421.
- (80) Chen, W.; Durning, C. J.; Turro, N. J. *Macromolecules* **1999**, *32*, 4151-4153.
- (81) Bardelang, D.; Zaman, M. B.; Moudrakovski, I. L.; Pawsey, S.; Margeson, J. C.; Wang, D.; Wu, X.; Ripmeester, J. A.; Ratcliffe, C. I.; Yu, K. *Advanced Materials* **2008**, *20*, 4517-4520.
- (82) Yan, J.-J.; Wang, H.; Zhou, Q.-H.; You, Y.-Z. *Macromolecules*, *44*, 4306-4312.
- (83) Wadhavane, P. D.; Izquierdo, M. A.; Galindo, F.; Burguete, M. I.; Luis, S. V. *Soft Matter*, *8*, 4373-4381.
- (84) Vidyasagar, A.; Handore, K.; Sureshan, K. M. *Angewandte Chemie International Edition*, *50*, 8021-8024.

9 – PUBLISHED ARTICLES RELATED WITH THE THESIS

Fluorescence enhancement of amine-capped CdSe/ZnS quantum dots by thiol addition

Jordi Aguilera-Sigalat, Simon Rocton, Raquel E. Galian, and Julia Pérez-Prieto

Abstract: The present communication reports that while addition of alkyl thiols drastically reduces the fluorescence of CdSe core quantum dots, it actually enhances the emission properties of already highly fluorescent amine-capped CdSe/ZnS core-shell quantum dots.

Key words: CdSe/ZnS, core shell, fluorescence, ligand exchange, quantum dot.

Résumé : On montre dans ce travail que, alors que l'addition d'alkylthiols diminue d'une façon drastique la fluorescence des points quantiques d'un coeur CdSe, cette addition augmente en fait les propriétés d'émission de fluorescence déjà très élevées des points quantiques de la couche d'un coeur CdSe/ZnS chapeauté par une amine.

Mots-clés : CdSe/ZnS, couche d'un cœur, fluorescence, échange de ligand, point quantique.

[Traduit par la Rédaction]

Introduction

Quantum dots (QDs) have unique optical properties¹ that make them of interest for biological, medical, and engineering applications. They are highly fluorescent systems compared with organic dyes, though different factors, such as growth conditions, post-illumination treatment, the nature of the capping ligand, and storage conditions, seem to affect their fluorescence quantum yield (Φ_F). Some of these factors may induce the appearance of defects on the QD surface, producing an additional nonradiative pathway due to trapping of the electron or the hole generated after the absorption of light. To reduce the number of defects and, consequently, increase the Φ_F , good QD surface passivation is needed. This can be accomplished by adding an inorganic shell or using long-chain organic surfactants.¹

With regard to using an inorganic shell as coating, a higher band gap material (ZnS, ZnSe, CdS) has been used to prepare core-shell QDs that have, in general, a much higher Φ_F .^{2,3}

With respect to ligands, trioctylphosphine (TOP) and trioctylphosphine oxide (TOPO) are the most common ligands used in the synthesis of QDs.^{1,2,4} However, the exchange of the phosphine ligands by fatty amines leads to an enhancement of the Φ_F of the resulting nanoparticle.⁵ Functional thiol ligands have also been used as capping material to make QDs water-soluble and to add functionality to the nanoparticle.⁶ Thiol ligands can replace TOPO and amine ligands and bind more strongly to the QD surface,^{7,8} but such

exchange decreases the Φ_F of CdSe core QDs.^{5,8,9} This behavior has been attributed to the hole-trapping capacity of thiol molecules.¹⁰

Curiously, in the case of CdSe/ZnS core-shell QDs, where the shell should avoid the QD emission quenching by electron donors,¹¹ ligand exchange of TOPO by hydrophilic thiols to achieve water-soluble QDs also leads to a decrease in Φ_F . This has been explained by formation of thiolates in water, and such thiolates somehow add new hole trap states.^{7,12}

To gain insight into the effect of thiols (rather than thiolates) on the fluorescence of organic-soluble core-shell QDs, we studied the QD emission in the presence of two model alkyl thiols: 11-mercapto-1-undecanol (MU) and a thiol functionalized with a benzophenone chromophore (KP-SH) (Scheme 1). For comparison purposes, studies using CdSe core QDs were also performed. We analyzed the influence of the native ligand (TOPO or TOP for CdSe and a long-chain amine for CdSe/ZnS) used as capping material, the QD size, and the thiol concentration on the variation of the QD fluorescence. Our results demonstrated that the CdSe and CdSe/ZnS QDs presented a different response to the addition of the assayed thiols.

Results and discussion

CdSe core QDs (QD-C) capped with TOPO and TOP ligands were synthesized according to the methodology reported by Peng and Peng.^{4a} The size of the nanoparticles

Received 31 March 2010. Accepted 3 October 2010. Published on the NRC Research Press Web site at canjchem.nrc.ca on 25 February 2011.

This article is part of a Special Issue dedicated to Professor J. C. Scaiano on the occasion of his 65th birthday.

J. Aguilera-Sigalat, S. Rocton, and J. Pérez-Prieto.² Instituto de Ciencia Molecular (ICMol), Universidad de Valencia, Catedrático José Beltrán 2, 46980 Paterna, Valencia, Spain.

R.E. Galian.¹ Departamento de Química Analítica, ICMol, Dr. Moliner 50, 46100 Burjassot, Spain.

¹Corresponding author (e-mail: raquel.galian@uv.es).

²Corresponding author (e-mail: Julia.perez@uv.es).

Fig. 2. Fluorescence spectra of a deaerated toluene solution of QD-C1 (2.9 $\mu\text{mol/L}$) before (\circ), immediately after (\bullet), and 90 min after (\blacksquare) the addition of MU (1.57 mmol/L); $[\text{MU}]/[\text{QD-C1}] = 540$.

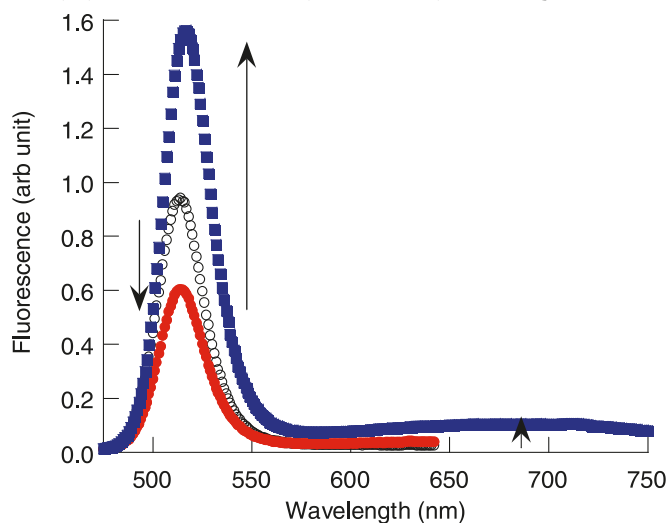
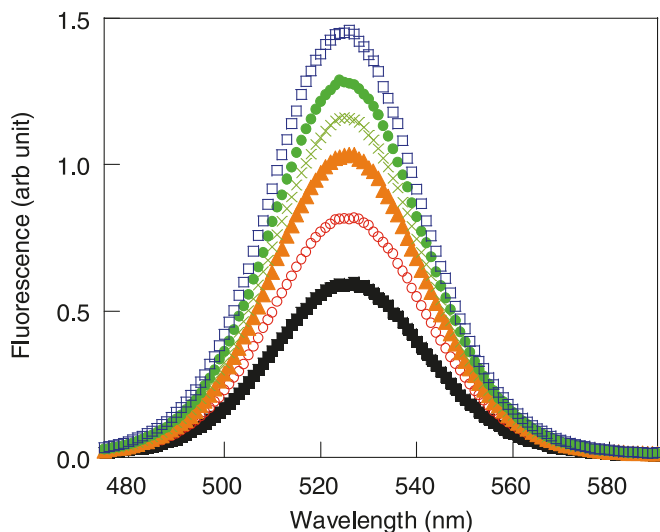


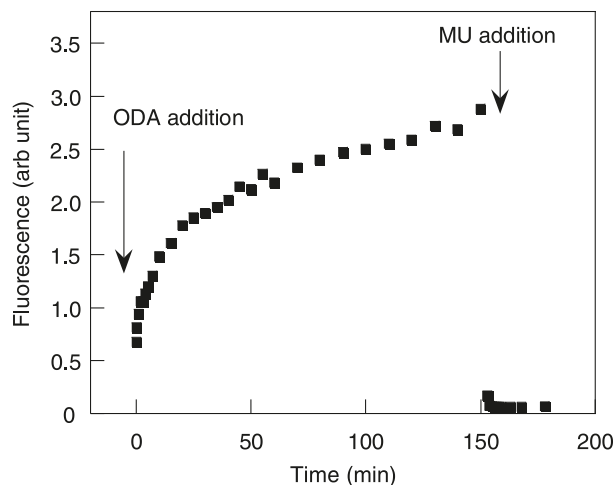
Fig. 3. Fluorescence spectra of a deaerated toluene solution of QD-CS1 in the absence (\blacksquare , $[\text{QD}] = 0.5 \mu\text{mol/L}$) and in the presence of KP-SH ($[\text{KP-SH}]/[\text{QD}] = 3600$), the latter being registered 0 (\circ), 10 (\blacktriangle), 30 (\times), 60 (\bullet), and 150 (\square) min after the addition of the thiol.



of the core-shell QDs upon thiol addition contrasts with the effect reported for the thiolates.^{17,18}

Control experiments were performed to rule out the possibility that the different nature of the native ligand (TOPO in core QDs and a long-chain amine in core-shell QDs) was the origin of the different response to thiol addition of the core and core-shell QDs. So, the effect of the addition of octadecylamine (ODA), followed by MU 150 min later, on the QD-C1 fluorescence was monitored (Fig. 4). The addition of ODA to QD-C1 led to a considerable enhancement of the QD emission (+3.28) in a time-dependent process (Figs. 4 and S7). This increase was in agreement with the higher fluorescence quantum yield of amine-coated QDs compared with TOPO- or TOP-coated QDs.^{4b} The exchange kinetics has been interpreted as being due to a combination

Fig. 4. Time dependence of the fluorescence intensity of QD-C1 (2.9 $\mu\text{mol/L}$) upon addition of ODA (6.5 mmol/L) followed by addition of MU (5.2 mmol/L) 150 min later; $[\text{amine}]/[\text{QD}] = 2200$ and $[\text{thiol}]/[\text{QD}] = 1800$.



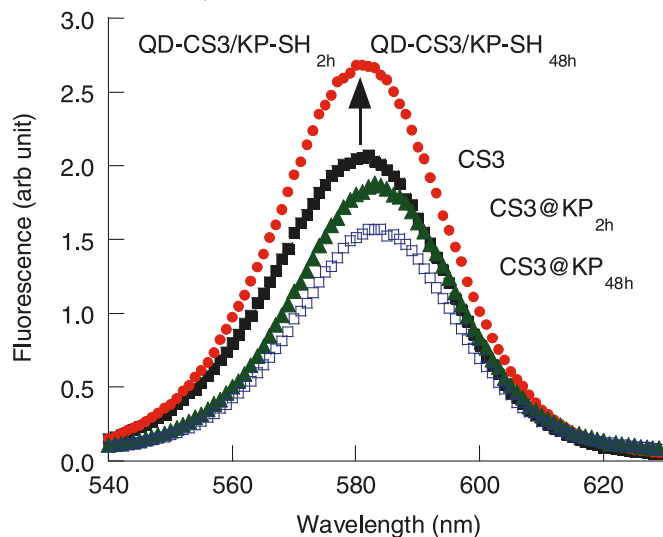
of ligand binding to vacant surface sites on CdSe QDs (fast coordination) and the ligand exchange itself (a slower process). After an equilibrium was reached, addition of MU caused a drastic decrease in the fluorescence emission of the system because the amine was replaced by the thiol ligand (Figs. 4 and S8). Therefore, the presence of amine as a native capping ligand (QD-CS) instead of TOPO (QD-C) is not responsible for the different behavior produced by thiol addition to these QDs.

The time-dependent fluorescence quenching observed for CdSe has been previously used as a tool to measure the exchange kinetics of native ligands for thiols on the CdSe surface.⁸ Therefore, the changes in QD emission intensities were recorded as a time function, from which the kinetic rate constants (k_{LE} , Table 1) for the ligand exchange (TOPO, CdSe; amine, CdSe/ZnS) were calculated (see details in Figs. S9–S14 in the Supplementary data). The values for the addition of KP-SH were two times higher than those for the addition of MU, which is indicative of a higher replacement of a bulkier ligand.

To gain insight into the nature of the thiol binding to the QD, we prepared two samples (A and B) containing QD-CS3 (λ_{max} exciton peak at 520 nm, 48.1×10^{-9} mol) and KP-SH (2.4×10^{-4} mol) in deaerated chloroform (50 mL). They were maintained at room temperature for 2 h (sample A) and 48 h (sample B). After almost total solvent evaporation (2 mL) and the addition of methanol (30 mL), the samples were centrifugated at 8000 rpm (20 800g) for 20 min at 20 °C and the supernatants were decanted. The nanoparticles were dissolved in chloroform (2 mL) and the purification process was repeated twice, finally leading to CS3@KP_{2h} and CS3@KP_{48h} nanoparticles.

Both QD-CS3/KP-SH solutions exhibited a higher fluorescence than QD-CS3, and their emission maxima shifted slightly (1 nm) towards the red compared with that of QD-CS3 (Fig. 5). Remarkably, the emission of the cleansed QDs, CS3@KP_{2h} and CS3@KP_{48h}, was lower than that of QD-CS3 (Fig. 5), and the maxima were located at 542 nm (4 nm red-shifted compared with QD-CS3).¹⁹ Therefore,

Fig. 5. Comparative fluorescence spectra of deaerated toluene solutions of QD-CS3 (■), QD-CS3/KP-SH (5×10^3 molar ratio) 2 h and 48 h after addition of the thiol (●), and cleansed CS3@KP_{2h} (▲) and CS3@KP_{48h} (□).



washing of the thiol-capped QDs resulted in a loss of the unbound (encapsulated) thiol and produced QDs with an emission lower than that of the initial core-shell QDs. The red-shifted emission exhibited by CS3@KP_{2h} and CS3@KP_{48h} indicated some thiol binding to the QD surface with time.

These results demonstrated that the replacement of amines by thiols on the core-shell QD surface resulted in better protection of the QD emission. The thiols encapsulated within the QD ligands were responsible for the fluorescence enhancement. In addition, the higher emission of CS3@KP_{48h} QDs than of CS3@KP_{2h} QDs suggested that thiolate binding to the QD surface appeared to be, at the least, non-detrimental for the QD emission.

Theoretical calculations have shown that thiol binding to ZnS surfaces is endothermic, while thiolate binding is a spontaneous process that can cause an alteration of the ZnS surface.²⁰ Consequently, we suggest that the replacement of amine ligands by thiols in the CdSe/ZnS QDs could benefit from the basicity of the amine ligands, allowing slow deprotonation of the thiol ligands to take place close to the nanoparticle surface and eventually resulting in thiolate binding to the shell with minimum surface alteration.

In summary, our results demonstrate that while addition of thiols drastically reduces the fluorescence of CdSe core QDs, it actually enhances the emission properties of already highly fluorescent amine-capped CdSe/ZnS core-shell QDs.

Supplementary data

Supplementary data (Table S1, Figs. S1–S15) are available with the article through the journal Web site (www.nrcresearchpress.com/cjc).

Acknowledgements

The authors thank Ministerio de Ciencia y Tecnología (Project CTQ2008-06777-CO2-01 contract granted to J.A.-

S., and RyC contract granted to R.E.G), Generalitat Valenciana (Project ACOMP/2009/334), and Universidad de Valencia (Project UV-AE-09-5805) for their support.

References

- (1) Alivisatos, A. P. *J. Phys. Chem.* **1996**, *100* (31), 13226. doi:10.1021/jp9535506.
- (2) Carrillo-Carrión, C.; Cárdenas, S.; Simonet, B. M.; Valcárcel, M. *Chem. Commun. (Camb.)* **2009**, (35): 5214. doi:10.1039/b904381k.
- (3) (a) Liu, Y.; Kim, M.; Wang, M.; Wang, Y. A.; Peng, X. *Langmuir* **2006**, *22* (14), 6341. doi:10.1021/la052747e.; (b) Hines, M. A.; Guyot-Sionnest, P. *J. Phys. Chem.* **1996**, *100* (2), 468. doi:10.1021/jp9530562.
- (4) (a) Peng, Z. A.; Peng, X. *J. Am. Chem. Soc.* **2001**, *123* (1), 183. doi:10.1021/ja003633m.; (b) Talapin, D. V.; Rogach, A. L.; Kornowski, A.; Haase, M.; Weller, H. *Nano Lett.* **2001**, *1* (4), 207. doi:10.1021/nl0155126.
- (5) Bullen, C.; Mulvaney, P. *Langmuir* **2006**, *22* (7), 3007. doi:10.1021/la051898e.
- (6) Galian, R. E.; de la Guardia, M. *Trends Analyt. Chem.* **2009**, *28* (3), 279. doi:10.1016/j.trac.2008.12.001.
- (7) Breus, V.; Heyes, C. D.; Nienhaus, G. U. *J. Phys. Chem. C* **2007**, *111* (50), 18589. doi:10.1021/jp075848p.
- (8) Koole, R.; Schapotschnikow, P.; de Mello Donega, C.; Vlugt, T. J. H.; Meijerink, A. *ACS Nano* **2008**, *2* (8), 1703. doi:10.1021/nn8003247.
- (9) Munro, A. M.; Plante, H. J.-L.; Ng, M. S.; Ginger, D. S. *J. Phys. Chem. C* **2007**, *111* (17), 6220. doi:10.1021/jp068733e.
- (10) (a) For the photocatalytic role of CdSe QDs in the formation of disulfides, see: Aldana, J.; Wang, A. Y.; Peng, X. *J. Am. Chem. Soc.* **2001**, *123* (36), 8844. doi:10.1021/ja016424q.; (b) however, disulfide bond cleavage on the surface of CdSe QDs has also been reported: Billone, P. S.; Maretti, L.; Maurel, V.; Scaiano, J. C. *J. Am. Chem. Soc.* **2007**, *129* (46), 14150. doi:10.1021/ja076118y.
- (11) Dabbousi, B. O.; Rodriguez-Viejo, J.; Mikulec, F. V.; Heine, J. R.; Mattoussi, H.; Ober, R.; Jensen, K. F.; Bawendi, M. G. *J. Phys. Chem. B* **1997**, *101* (46), 9463. doi:10.1021/jp971091y.
- (12) (a) Jeong, S.; Achermann, M.; Nanda, J.; Ivanov, S.; Klimov, V. I.; Hollingsworth, J. A. *J. Am. Chem. Soc.* **2005**, *127* (29), 10126. doi:10.1021/ja042591p.; (b) Hohng, S.; Ha, T. *J. Am. Chem. Soc.* **2004**, *126* (5), 1324. doi:10.1021/ja039686w.
- (13) Yu, W. W.; Qu, L.; Guo, W.; Peng, X. *Chem. Mater.* **2003**, *15* (14), 2854. doi:10.1021/cm034081k.
- (14) MU was transformed into KP-SH following the Yamamoto procedure: Ishihara, K.; Nakayama, M.; Ohara, S.; Yamamoto, H. *Synlett* **2001**, *2001* (7), 1117. doi:10.1055/s-2001-15156.
- (15) Kalyuzhny, G.; Murray, R. W. *J. Phys. Chem. B* **2005**, *109* (15), 7012. doi:10.1021/jp045352x.
- (16) Commercial core-shell quantum dots were purchased from Evidenttech. They possess a fluorescence quantum yield higher than 50%.
- (17) Algar, W. R.; Krull, U. J. *ChemPhysChem* **2007**, *8* (4), 561. doi:10.1002/cphc.200600686.
- (18) In fact, addition of MU as thiolate to QS-CS3 nanoparticles led to a decrease in their fluorescence (see Fig. S6 in the Supplementary data).
- (19) Full width at half maximum: 40 nm (QD-CS3), 39 nm (KP-

SH/QD-CS3), and 38 nm (CS3@KP). In addition, Fig. S15 in the Supplementary data shows the $^1\text{H-NMR}$ spectrum of KP-SH/QD-CS3, CS3@KP_{48h}, and the collected supernatants after washing of the QDs.

(20) Pong, B.-K.; Trout, B. L.; Lee, J.-Y. *Langmuir* **2008**, *24* (10), 5270. doi:10.1021/la703431j.

Fluorescence enhancement of amine capped CdSe/ZnS quantum dots by thiol addition

Jordi Aguilera-Sigalat, Simon Rocton, Raquel E. Galian and Julia Pérez-Prieto

Electronic Supplementary Information

TABLE OF CONTENTS

Title	page
Table S1: Maximum in the UV-visible absorption and fluorescence (into parenthesis) spectra of core (QD-C1) and core-shell (QD-CS1 and QD-CS2) QDs upon the addition of MU and KP-SH.	S2
Figure S1: Fluorescence spectra of a deaerated toluene solution of QD-C1 before and after addition of KP-SH	
Figure S2: Fluorescence spectra of a deaerated toluene solution of QD-C1 before and after addition of KP-SH	S3
Figure S3: Fluorescence spectra of a deaerated toluene solution of QD-CS2 before and after the addition of KP-SH	S4
Figure S4: Fluorescence spectra of a deaerated toluene solution of QD-CS1 before and after the addition of MU	S5
Figure S5: Fluorescence spectra of a deaerated toluene solution of QD-CS2 before and after addition of MU	S6
Figure S6 : Fluorescence spectra of a deaerated toluene solution of QD-CS3 (0.47 μ M) before (■) and after addition of MU thiolate (2.1 mM): 0 min (●), and 120 min later (▲); [thiolate]/[QD-CS]= 4500	S7
Figure S7-S8: Fluorescence spectra of a deaerated toluene solution of QD-C1 before and after the addition of octadecylamine and after subsequent addition of MU	S8
Procedure for the calculation of ligand exchange rate constant	S9
Figure S9: Time-dependence of the QD-C1 fluorescence intensity upon addition of MU .	S10
Figure S10: Time-dependence of the QD-C1 fluorescence intensity upon addition of KP-SH .	
Figure S11: Time-dependence of the QD-CS1 fluorescence intensity upon addition of MU .	S11
Figure S12: Time-dependence of the QD-CS1 fluorescence intensity upon addition of KP-SH .	
Figure S13: Time-dependence of the QD-CS2 fluorescence intensity upon addition of MU .	S12
Figure S14: Time-dependence of the QD-CS2 fluorescence intensity upon addition of KP-SH .	
Figure S15: $^1\text{H-NMR}$ spectra of i) KP-SH , ii) a mixture of KP-SH and QD-CS3 core-shell maintained 48 h at room temperature, iii) the collected supernatants after washing of the QDs, and i) the cleansed QDs.	S13

Table S1: Maximum in the UV-visible absorption and fluorescence (into parenthesis) spectra of core (QD-C1) and core-shell (QD-CS1 and QD-CS2) QDs upon the addition of MU and KP-SH.

QD / Thiol System	Without thiol	In the presence of thiol ^a
QD-C1	513 (524)	
QD-C1 / MU		511 (521)
QD-C1 / KP-SH		513 (524)
QD-CS1	504 (524)	
QD-CS1 / MU		504 (522)
QD-CS1 / KP-SH		504 (524)
QD-CS2	565 (581)	
QD-CS2 / MU		563 (581)
QD-CS2 / KP-SH		565 (580)

^a Fluorescence measured 2 h after the addition of the thiol.

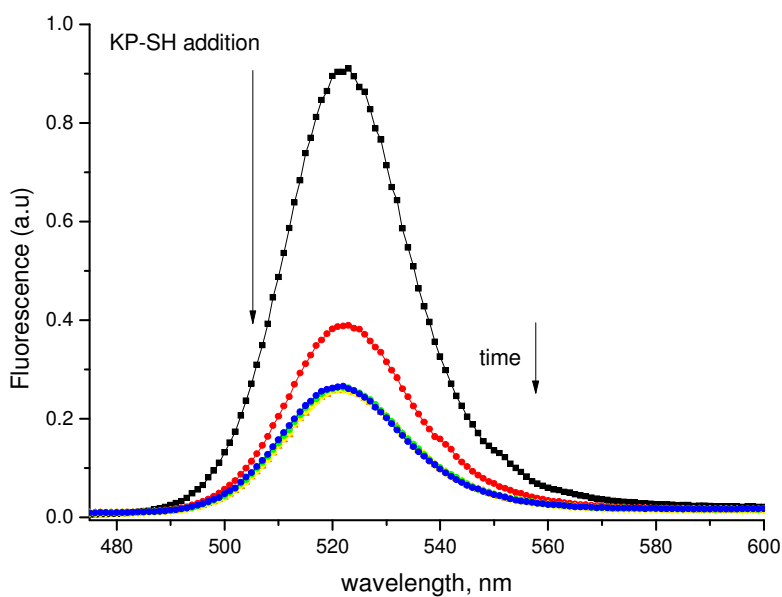


Figure S1: Fluorescence spectra of a deaerated toluene solution of **QD-C1** (2.9 μ M) before (■) and after addition of **KP-SH** (18 mM): 0 min (●), 22 min (▲), 32 min (◆), 52 min (●) and 120 min (●) later; $[\text{KP-SH}]/[\text{QD-C1}] = 6200$.

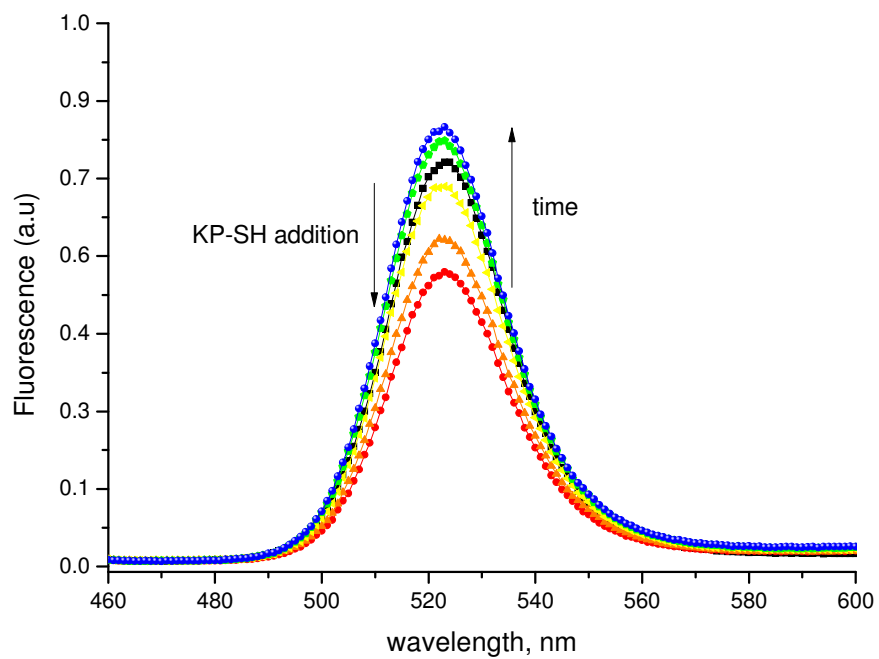


Figure S2: Fluorescence spectra of a deaerated toluene solution of **QD-C1** ($2.9 \mu\text{M}$) before (■) and after addition of **KP-SH** (1.8 mM): 0 min (●), 10 min (▲), 30 min (◆), 60 min (●) and 90 min (●) later; $[\text{KP-SH}]/[\text{QD-C1}] = 620$.

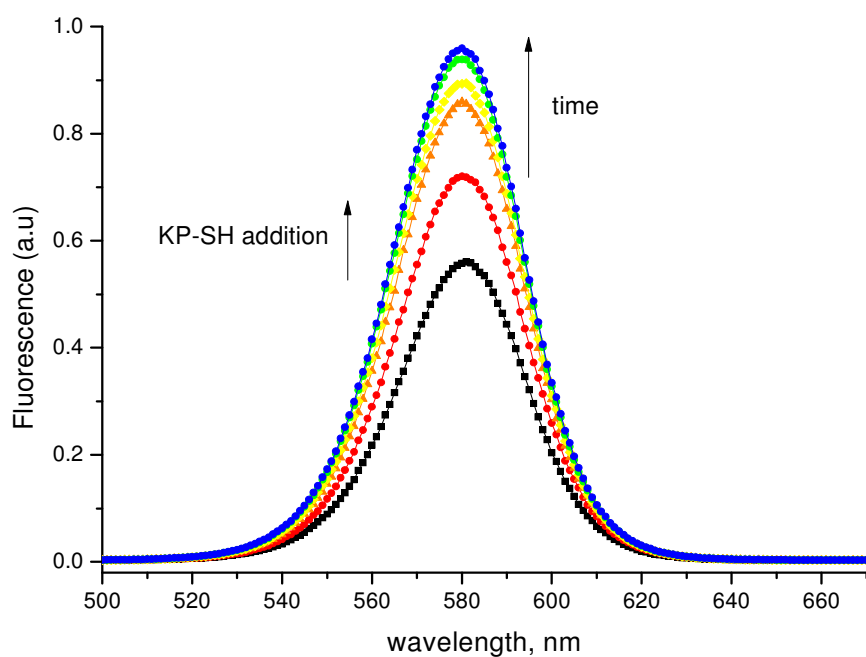


Figure S3: Fluorescence spectra of a deaerated toluene solution of **QD-CS2** ($0.4 \mu\text{M}$) before (■) and after the addition of **KP-SH** (1.8 mM): 0 min (●), 10 min (▲), 30 min (◆), 50 min (●) and 70 min (●) later; $[\text{KP-SH}]/[\text{QD-CS2}] = 4500$.

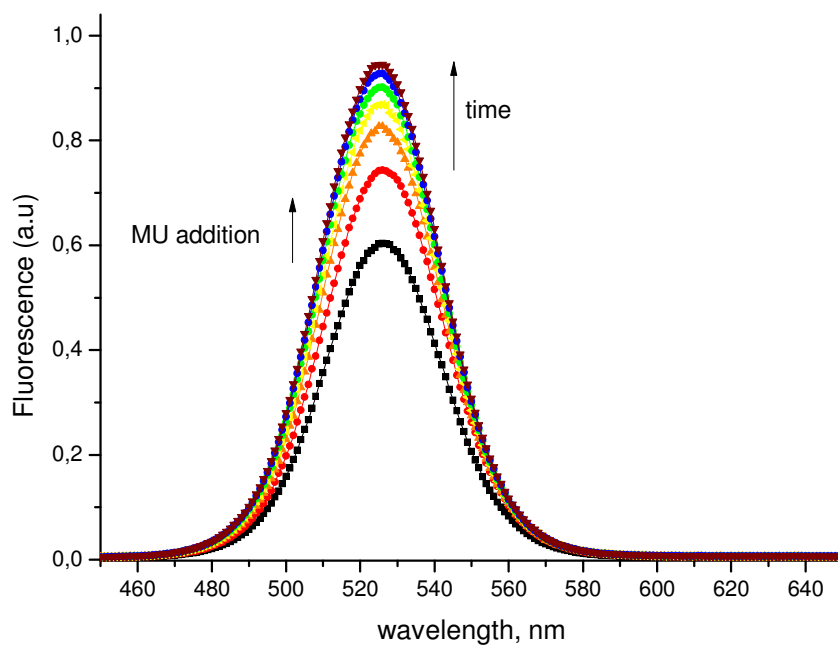


Figure S4: Fluorescence spectra of a deaerated toluene solution of **QD-CS1** ($1.7\mu\text{M}$) before (■) and after the addition of **MU** (5 mM): 0 (●), 10 (▲), 30 (◆), 60 (●), 90 (●), and 140 (▼); $[\text{MU}]/[\text{QD-CS1}] = 2940$.

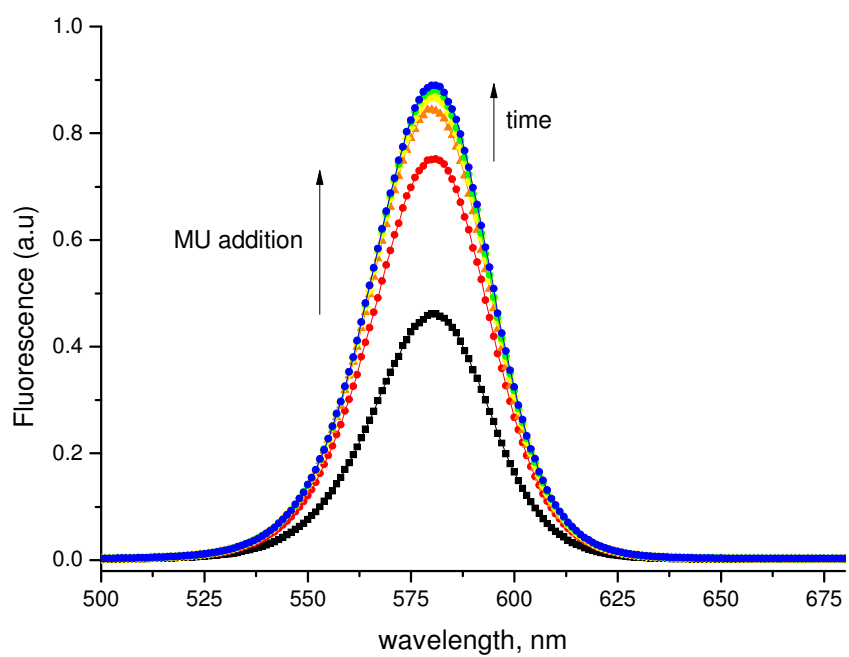


Figure S5: Fluorescence spectra of a deaerated toluene solution of **QD-CS2** (0.4 μM) before (■) and after addition of **MU** (5 mM): 0 (●), 10 min (▲), 30 min (◆), 50 min (●), and 70 min (●) later; $[\text{MU}]/[\text{QD-CS2}] = 12500$.

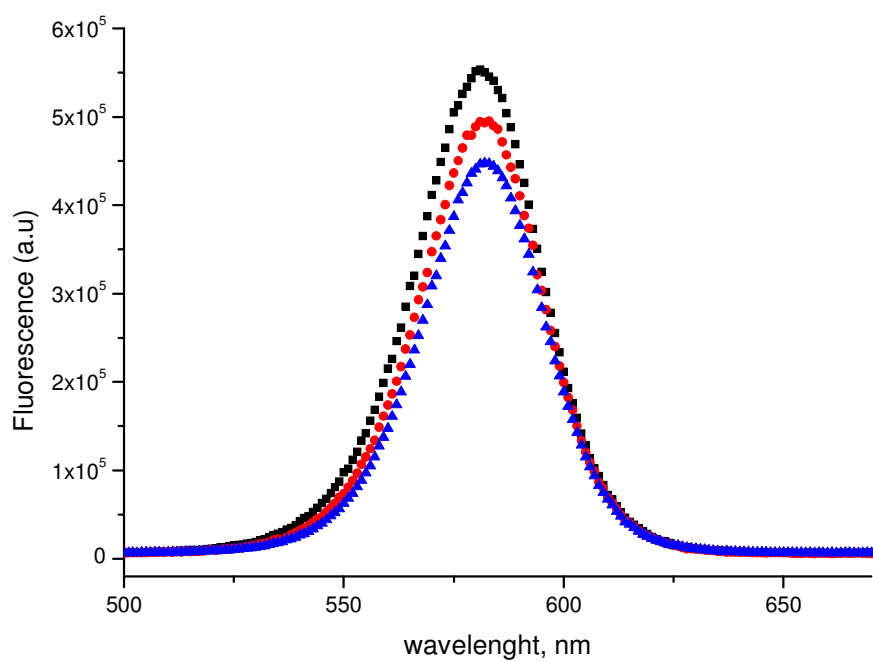


Figure S6 : Fluorescence spectra of a deaerated toluene solution of **QD-CS3** (0.47 μM) before (■) and after addition of MU thiolate (2.1 mM): 0 min (●), and 120 min later (▲); [thiolate]/[QD-CS3]= 4500

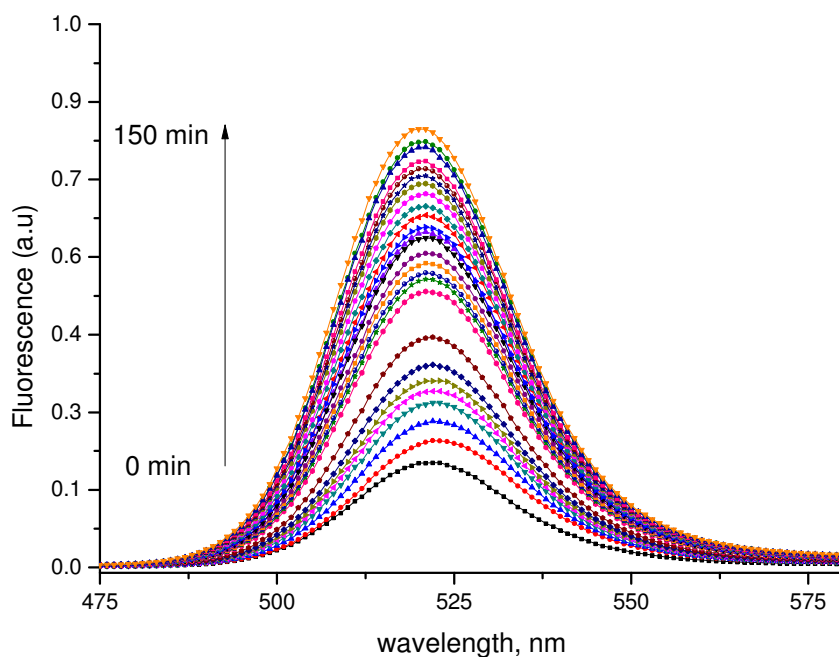


Figure S7: Fluorescence spectra of a deaerated toluene solution of **QD-C1** ($2.9 \mu\text{M}$) before (\blacksquare) and after the addition of octadecylamine (6.5 mM); $t = 150 \text{ min}$ (\blacktriangledown); $[\text{octadecylamine}]/[\text{QD-C1}] = 2240$.

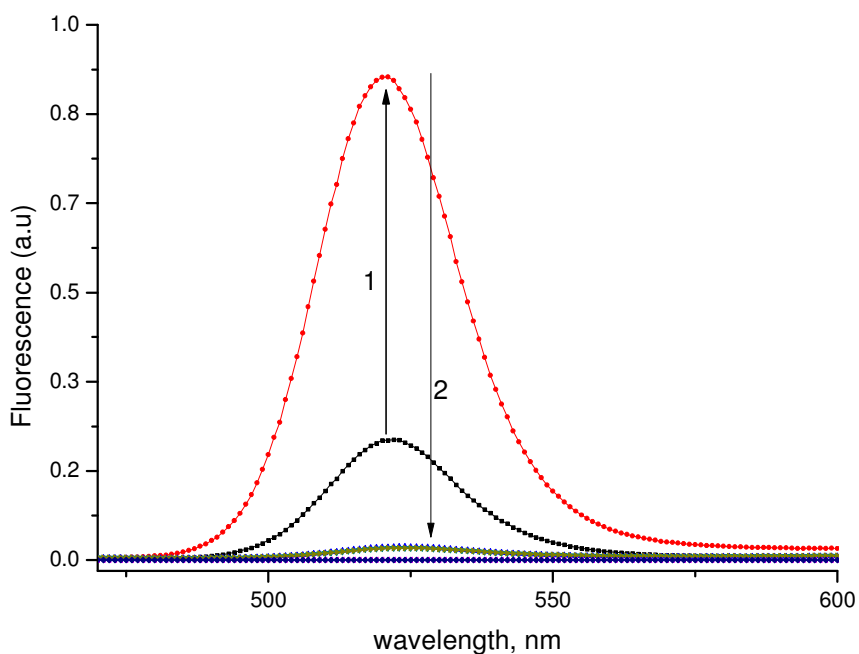


Figure S8: Fluorescence spectra of a deaerated toluene solution of **QD-C1** ($2.9 \mu\text{M}$) before (\blacksquare), and after the addition of octadecylamine (6.5 mM , \bullet) recorded 150 min later, followed by addition of **MU** (5.2 mM , \blacksquare); $[\text{octadecylamine}]/[\text{QD-C1}] = 2200$ and $[\text{MU}]/[\text{QD-C1}] = 1800$.

Procedure for the calculation of ligand exchange rate constant:

In order to obtain the rate constant of the ligand exchange, equation (1) was used.

$$\ln \frac{I_{inf}-I_t}{I_{inf}-I_0} = k_{obs} \cdot t \quad (\text{eq. 1})$$

where I_{inf} , I_0 , and I_t correspond to the intensity of fluorescence at the plateau, time zero and time t after the addition of the thiol, respectively. The slope of the graph of $\ln (I_{inf}-I_t/I_{inf}-I_0)$ vs. time gives the kinetic constant k_{obs} . The rate constant of ligand exchange (k_{LE}) was obtained from $k_{obs} = k_{LE} \times [\text{thiol}]$ (see inset in Figure S8-S13 for all QD/thiol systems).

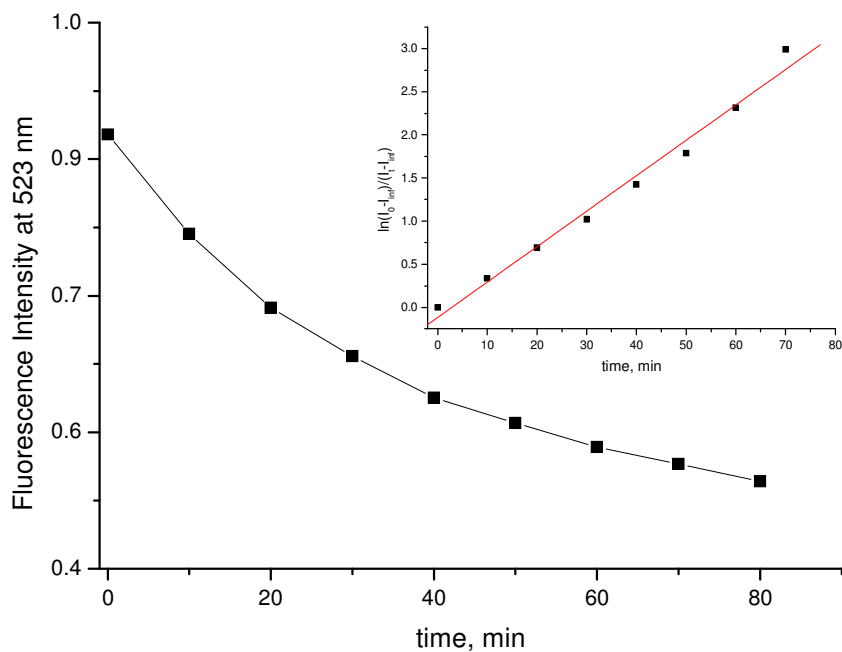


Figure S9: Time-dependence of the **QD-C1** fluorescence intensity upon addition of **MU**. Inset: Linear fitting according to equation 1 used for the k_{LE} constant determination.

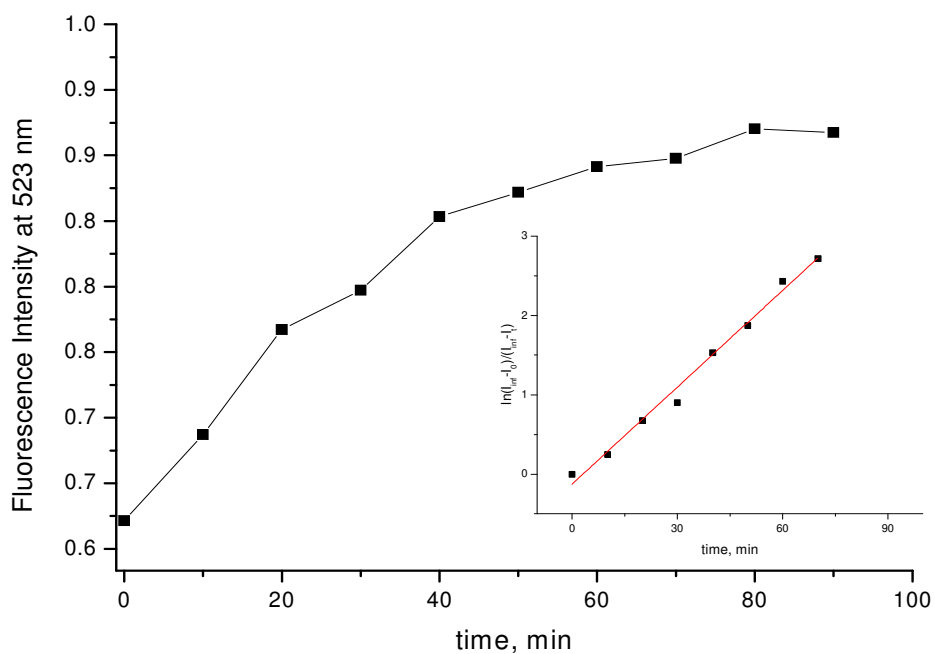


Figure S10: Time-dependence of the **QD-C1** fluorescence intensity upon addition of **KP-SH**. Inset: Linear fitting according to equation 1 used for the k_{LE} constant determination.

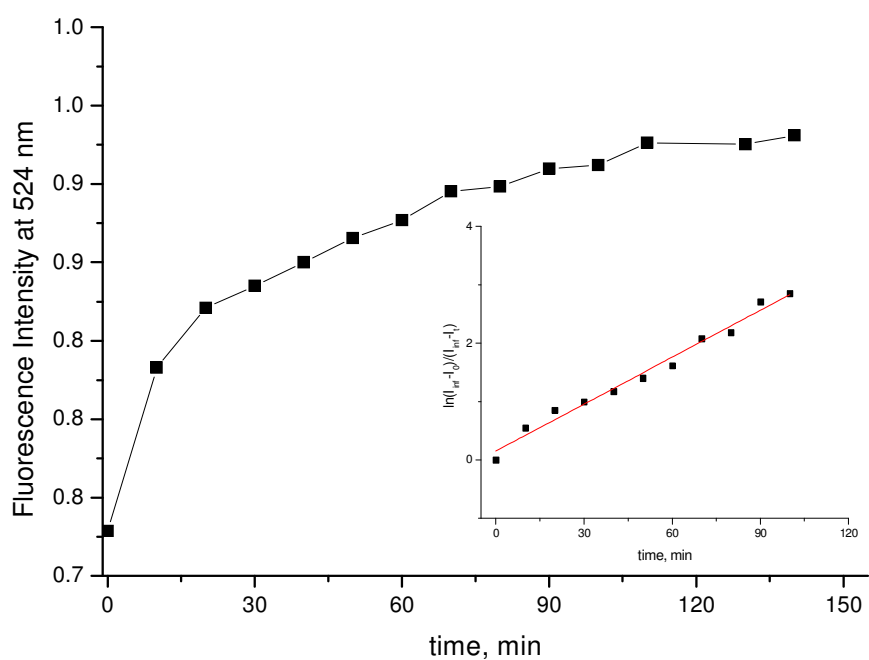


Figure S11: Time-dependence of the **QD-CS1** fluorescence intensity upon addition of **MU**. Inset: Linear fitting according to equation 1 used for the k_{LE} constant determination.

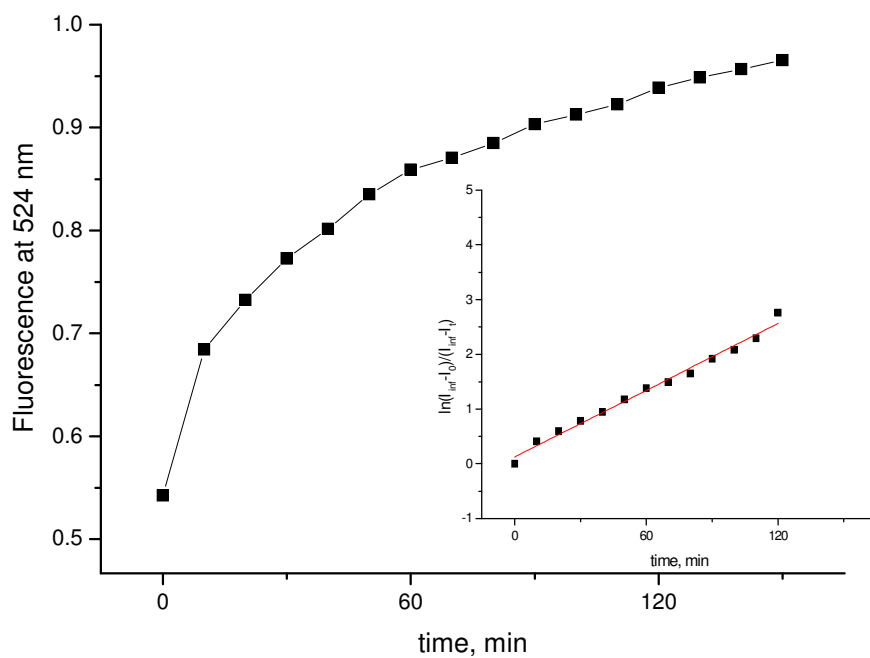


Figure S12: Time-dependence of the **QD-CS1** fluorescence intensity upon addition of **KP-SH**. Inset: Linear fitting according to equation 1 used for the k_{LE} constant determination.

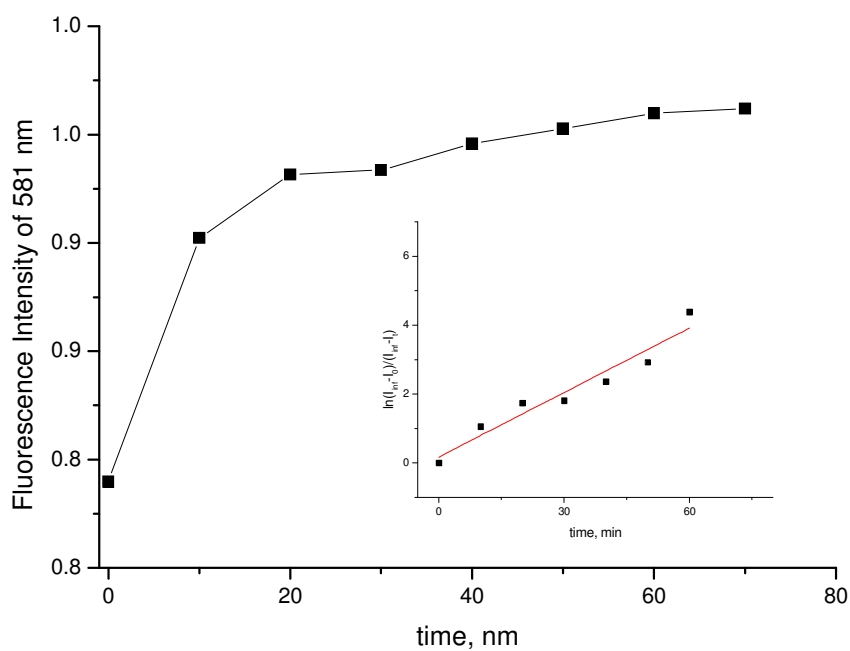


Figure S13: Time-dependence of the **QD-CS2** fluorescence intensity upon addition of **MU**. Inset: Linear fitting according to equation 1 used for the K_{LE} constant determination.

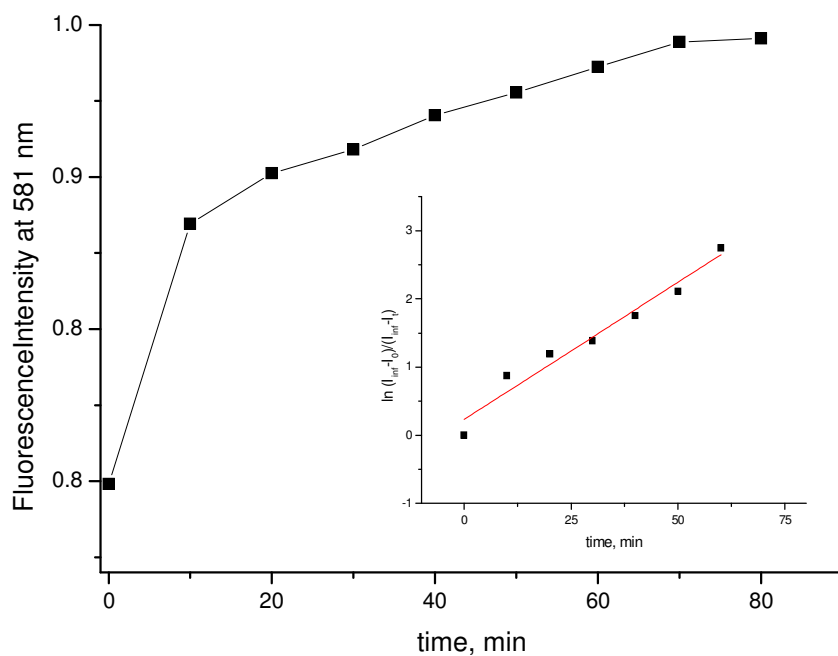


Figure S14: Time-dependence of the **QD-CS2** fluorescence intensity upon addition of **KP-SH**. Inset: Linear fitting according to equation 1 used for the k_{LE} constant determination.

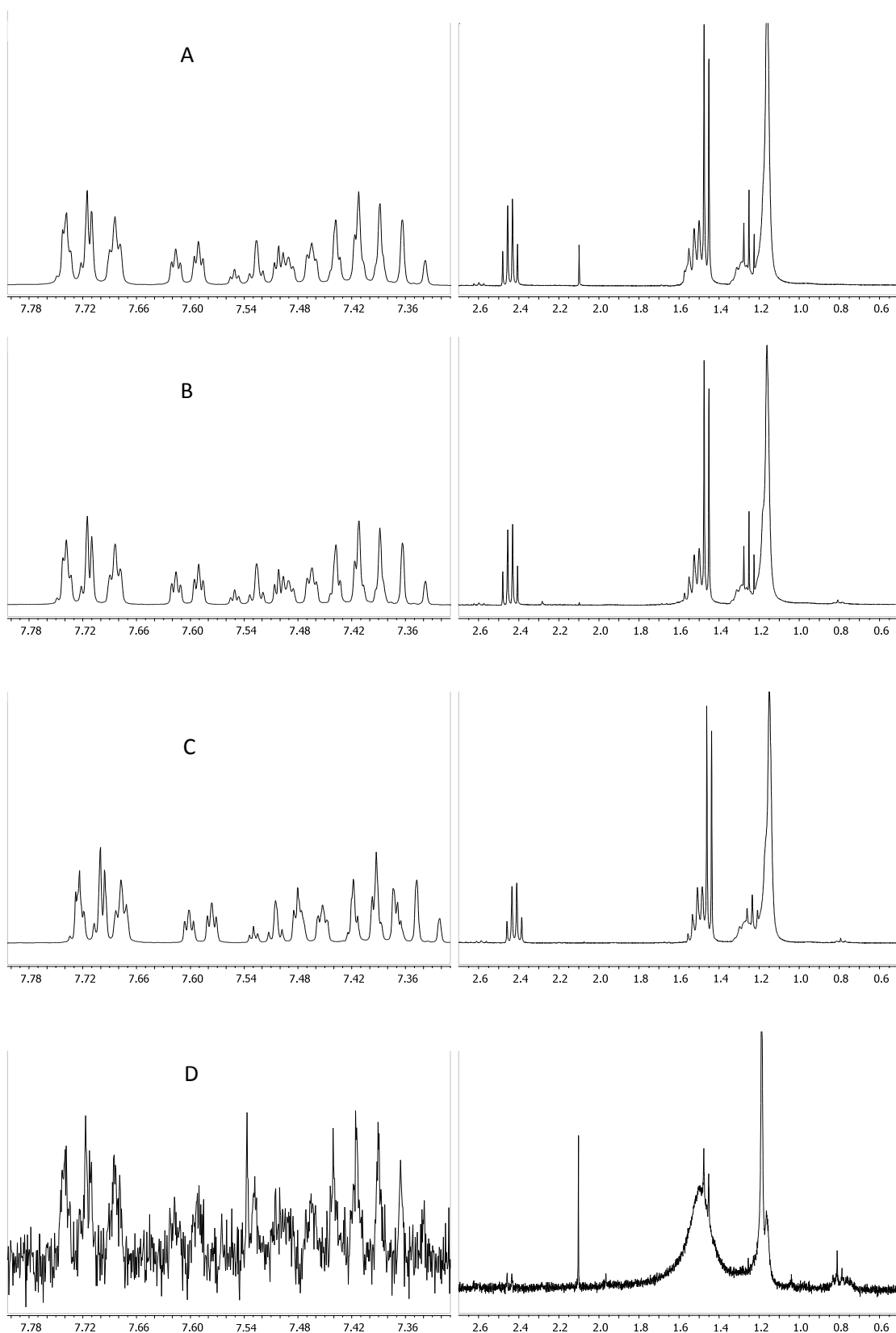


Figure S15: ^1H -NMR spectra of i) KP-SH (**A**), ii) a mixture of KP-SH and QD-CS3 core-shell (5×10^5 molar ratio) maintained 48 h at room temperature (**B**), iii) the collected supernatants after washing of the QDs (**C**), and iv) the cleansed QDs (**D**); aromatic region has been amplified ($\times 7.5$).

Cite this: *RSC Advances*, 2012, 2, 1632–1638

www.rsc.org/advances

PAPER

Highly fluorescent and photostable organic- and water-soluble CdSe/ZnS core-shell quantum dots capped with thiols†

Jordi Aguilera-Sigalat,^a Simon Rocton,^a Juan F. Sánchez-Royo,^b Raquel E. Galian*^{ac} and Julia Pérez-Prieto*^{aa}

Received 2nd November 2011, Accepted 3rd November 2011

DOI: 10.1039/c1ra01005k

Highly fluorescent organic- and water-soluble CdSe/ZnS core-shell quantum dots (QDs) with thiol ligands chemisorbed on the QD surface were synthesized by the replacement of amine ligands by alkyl thiols under very mild conditions. The QDs exhibited an even greater photostability than the initial core-shell amine capped QDs.

1. Introduction

Core-shell CdSe/ZnS quantum dots (QDs) are highly fluorescent systems compared with organic dyes which makes them of interest for biological, medical, and engineering applications¹. The ZnS shell plays a crucial role in their emission properties;² it decreases non-radiative pathways associated with the trapping of the electron or the hole generated after the absorption of light by the CdSe core. In addition, the shell enhances the chemical- and photo-stability of the QDs.

CdSe/ZnS nanoparticles are further passivated with organic ligands to allow them to remain stable as colloidal solutions in organic solvent and water. Organic-soluble QDs are required for optoelectronic applications, while water-soluble QDs are needed for biological applications. Trioctylphosphine (TOP) and trioctylphosphine oxide (TOPO), as well as fatty amines, are the most common ligands used in the synthesis of QDs.^{2,3}

Theoretical calculations have shown that thiols cannot bind to the ZnS surface.⁴ By contrast, functional deprotonated thiols (thiolates) have been used as a capping material to make QDs water soluble and to add functionality to the nanoparticle. Thiolate ligands can replace TOPO and amine ligands and thus bind to the surface of CdSe/ZnS QDs more strongly, but such exchange produces QDs with drastically diminished fluorescence quantum yield (Φ_F of more than 50% reduction).⁵ This has been explained as being due to a spontaneous binding of thiolates to the ZnS surface, causing a significant alteration of the surface.⁴ In addition, it has been reported that QDs capped with thiolates are vulnerable to photooxidation.⁶

Here we report that the chemisorption of thiols to CdSe/ZnS core-shell QDs helped by the amine ligands of the QDs can even improve their emission performance. This strategy was applied to the preparation of highly fluorescent organic- and water-soluble QDs that exhibited a higher photostability than the initial amine-capped QDs.

Model heterobifunctional ligands, 11-mercaptoundecanol (MU), 11-mercaptoundecanoic acid (MUA), 3-mercaptopropionic acid (MPA), and the ester of ketoprofen with MU (KP-SH)⁷ were used for these studies (Scheme 1). In addition, different sized CdSe/ZnS core-shell QDs capped with long-chain primary amines were used. These QDs were homemade or were purchased from different commercial sources (Table S1, ESI†).

2. Experimental section

2.1 Materials

All reagents were commercially available and used as received. The 11-mercaptoundecanol (MU), 11-mercaptoundecanoic acid (MUA), and 3-mercaptopropionic acid (MPA) were purchased from Sigma-Aldrich. Core-shell QDs capped with long-chain primary amine were purchased from Evident Technologies (www.evidenttech.com) and from Ocean NanoTech (www.oceannanotech.com). Solvents for chromatography (ethyl acetate and hexane) were reagent grade and used without further purification. ¹H-NMR (CDCl₃) spectra were recorded on a 300 MHz spectrometer. The sample was dissolved in deuterated chloroform. Data of ¹H-NMR are reported as follows: chemical shift (ppm), multiplicity [singlet (s), doublet (d), triplet (t), quartet (q) or multiplet (m)], and coupling constant (Hz).

2.2 Characterization

UV-vis spectra of the samples were recorded using quartz cuvettes in a UV-visible spectrophotometer: Agilent 8453E. Steady-state fluorescence spectra were measured on a spectrofluorometer PTI, equipped with a lamp power supply (LPS-220B, motor driver (MD-5020), Brytebox PTI and working at room temperature. The Felix 32 Analysis software was used to

^aMolecular Science Institute (ICMOL), University of Valencia, Catedrático José Beltrán 2, 46980 Paterna, Valencia, Spain.

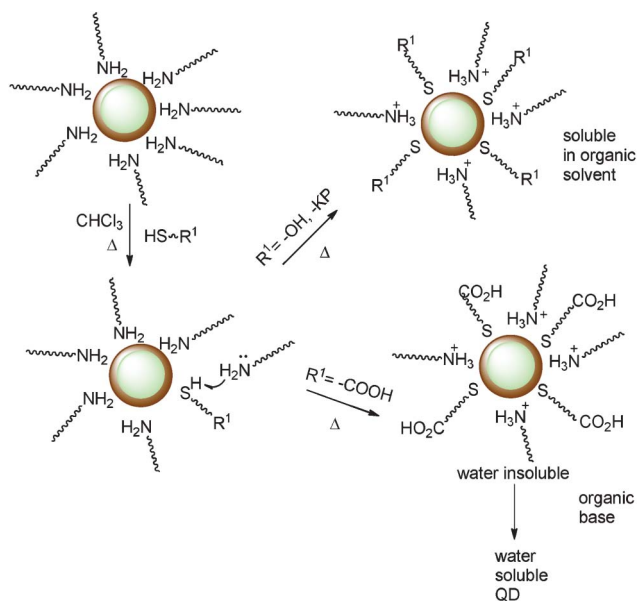
E-mail: julia.perez@uv.es; Fax: 34-963543576; Tel: 34-963543050

^bMaterials Science Institute, University of Valencia, Dr. Moliner 50, 46100 Burjassot, Valencia, Spain

^cDepartment of Analytical Chemistry, ICMOL/Research Building, University of Valencia, Dr. Moliner 50, 46100 Burjassot, Valencia

E-mail: raquel.galian@uv.es; Fax: 34-963543273; Tel: 34-963544307

† Electronic supplementary information (ESI) available: additional emission spectra of the QDs before and after irradiation under nitrogen and air atmosphere, UV-visible spectra, HRTEM images, XPS spectra, and physical data of the QDs. See DOI: 10.1039/c1ra01005k



Scheme 1 Heterobifunctional ligands used in this work and schematic preparation of the organic- and water-soluble QDs.

register the data. The excitation wavelength for the emission spectra was fixed at 400 nm. Images from the QDs were obtained by high resolution tunnelling electron microscopy (HRTEM, FEI Tecnai G2 F20) at an accelerating voltage of 200 kV. Samples were prepared by dropping the colloidal solution on a Lacey Formvar/carbon-coated copper grid. The digital analysis of the HRTEM micrographs was done using digital Micrograph™ 1.80.70 for GMS by Gatan. X-ray photoemission (XPS) measurements were performed in an ESCALAB 210 multianalysis system (base pressure 1.0×10^{-10} mbar) from Thermo VG Scientific available in our laboratory. Photoelectrons were excited with the Mg-K α line. The hemispheric photoelectron analyzer worked with pass energy of 20 eV. In order to compare all spectra recorded, we selected the C 1s core level attributable to C–C or C–H bonds as a reference, whose binding energy was fixed to 284.5 eV. Infrared measurements were performed on a Fourier Transformation-Infrared Spectrometer NICOLET 5700 (Thermo Electron Corporation).

2.3 Synthesis of 11-mercaptoundecyl 2-(3-benzoylphenyl)propanoate (KP-SH)

The KP-SH ligand was prepared following an esterification method described in the literature.⁷ In brief, ketoprofen (500 mg, 2.0 mmol) and 11-mercapto-1-undecanol (402 mg, 2.0 mmol) were dissolved in anhydride toluene (24 mL). A complex of hafnium/THF (1.8 mg) was added and the mixture was heated for 48 h under azeotropic reflux conditions to remove water through a Soxhlet thimble with 3 Å molecular sieves. In order to quench the reaction, 1 mL of water was added. The product was purified by column chromatography performed on silica gel 60 (230–400 mesh) using a 10 : 1 mixture of hexane : ethyl acetate. The compound was obtained in a 81% yield. ¹H NMR (300 MHz, CDCl₃): δ 1.00–1.34 (m, 14H), 1.25 (t, $J = 7.7$ Hz; 1H), 1.45–1.57 (m, 7H), 2.43 (q, $J = 7.1$ Hz; 2H), 3.73 (q, $J = 7.2$ Hz; 1H), 3.99 (t, $J = 6.7$ Hz; 2H), 7.33–7.55 (m, 5H), 7.60 (dt, $J = 6.2$ Hz, $J = 1.5$ Hz; 1H), 7.67–7.75 (m, 3H) ppm.

2.4 Steady-state irradiations

Photochemical irradiations were carried out in a Luzchem photoreactor equipped with 10 lamps of $\lambda > 400$ nm (λ_{max} at 420 nm) under either nitrogen or air atmosphere using toluene or water as the solvent. The samples were placed in Pyrex tube, dissolved in the adequate solvent and purged with dry nitrogen over a period of 10–15 min prior to irradiation.

2.5 Synthesis of QD-CS6

Fluorescent CdSe nanocrystals were synthesized using the procedure described by Peng *et al.* with some modifications.⁸ Briefly, a mixture of 0.2 mmol of CdO, 0.7 mmol of tetradecylphosphonic acid (TDPA), and 9.1 mmol of TOPO was heated gradually up to 320 °C in a three-neck flask under N₂ flow. The reaction was maintained at this temperature for 10–15 min, until the solution was clear. Then, the reaction was cooled to 270 °C, and 1.2 mL of the SeTOP was quickly injected (SeTOP mixture was prepared by the addition of 0.3 mmol of Se and 3.4 mmol of TOP under N₂ flow at 70 °C). When the reaction turned orange (indicative of a size of *ca.* 2.5 nm), the nanocrystals were precipitated in cool MeOH and purified several times by centrifugation with MeOH to remove the excess of starting materials. Finally, the QDs were re-dispersed in toluene.

The synthesis of core-shell QDs (CdSe/ZnS) was done following M. G. Bawendi's procedure with some modifications.² For a typical reaction, 5 g of TOPO was heated up to 190 °C in a three-neck flask for 2 h under Ar flow. Then, the solution was cooled to 60 °C and 0.5 mL of TOP was added into the flask. After that, 2 mL of CdSe QD was added and the reaction was heated to 140 °C. Then, the shell was added drop-wise for 10 min.

For the shell, 440 μ L of ZnEt₂, 65 μ L of (TMS)₂S, and 2600 μ L of TOP were mixed in a glove box under N₂ flow. Then, the reaction was cooled to 90 °C and kept at this temperature for 3 h. For the purification, the CdSe/ZnS QDs were precipitated in MeOH several times. Finally, QD-CS6 was redissolved in toluene.

2.6 Synthesis of QD-CS7

In order to obtain a core-shell QD covered with amine ligands (QD-CS7) a ligand exchange methodology was applied. Typically, 2 mL of QD-CS6 and 431 mg of ODA (QD : ligand molar ratio of 1 : 5000) were added in a flask and the mixture was heated under reflux in chloroform for 48 h using a N₂ flow and in absence of light. Then, the reaction was cooled down to room temperature. For the purification, the nanocrystals were precipitated in MeOH several times. Finally, the QDs were dissolved in toluene.

2.7 Thiol binding to QD-CS5

QD-CS5 (0.5 mL) and 68 mg of KP-SH (QD : ligand molar ratio of 1 : 5000) were added in a flask and heated up to reflux in 25 mL of chloroform for 48 h, under N₂ flow in an absence of light. Then, the reaction was cooled down to room temperature. For the purification, the nanocrystals were precipitated in MeOH several times. Finally, the QDs were dissolved in toluene.

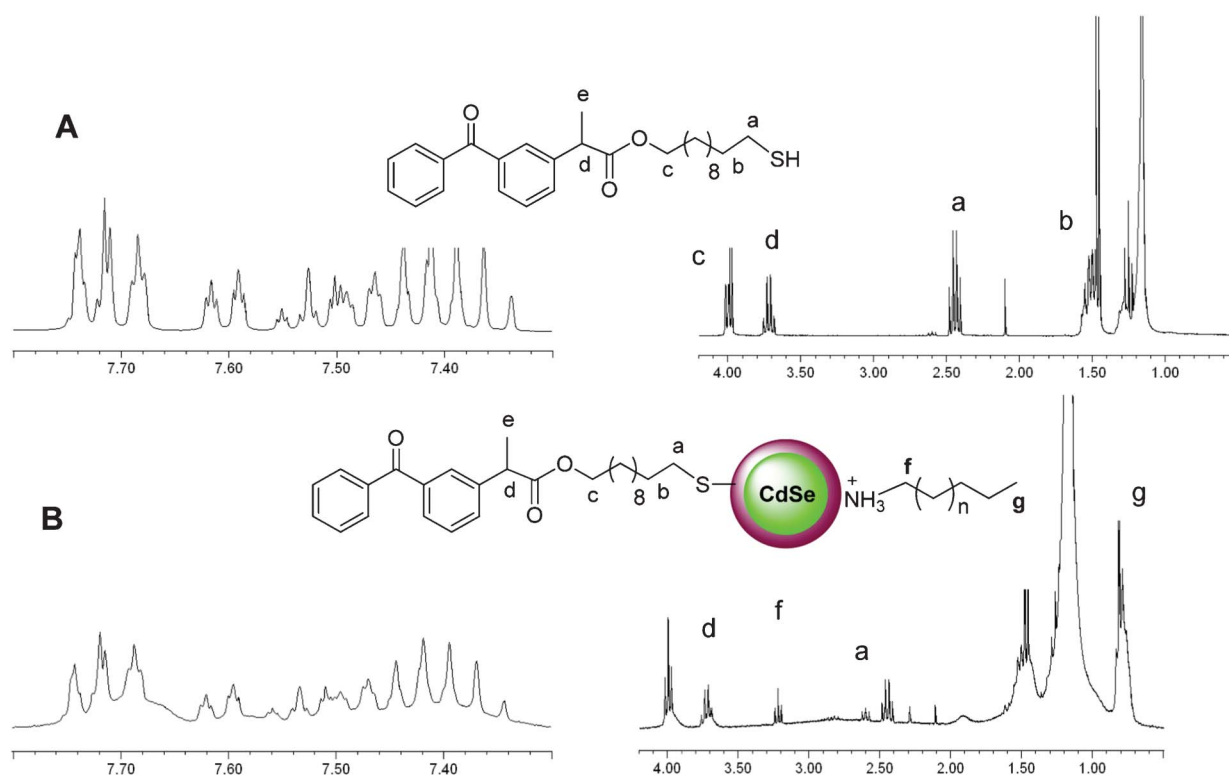


Fig. 1 $^1\text{H-NMR}$ spectrum of A) KP-SH and B) CS1@KP. The most significant signals are highlighted.

2.8 Ligand exchange of the QD-CS5 ligand by thiolate

KP thiolate (KP-S^-) was prepared by stirring a mixture of 68 mg of MU and 56 mg of tetramethylammonium hydroxide (TMOH) in 1 mL of chloroform at room temperature for 1 h. This solution was added to 0.5 mL of QD-CS5 (QD : thiolate molar ratio of 1 : 5000) in 25 mL of chloroform and the mixture was heated under reflux, in N_2 flow and absence of light, for 48 h. Then, the reaction was cooled down to room temperature. For the purification, the nanocrystals were precipitated in MeOH several times. Finally, the QDs were dissolved in toluene.

3. Results and discussion

First, different sized CdSe/ZnS core-shell QDs capped with a fatty amine (QD-CS1, QD-CS2, and QD-CS3 with λ_{max} exciton peaks at 509, 521, and 564 nm, respectively (Table S1, ESI †)), were purchased from Evident and used in these studies.

A chloroform solution (25 mL) of QD-CS1 (5.46×10^{-7} mmol) and KP-SH (2.65×10^{-3} mmol, [thiol]/[QD] = 4859 molar ratio) was heated to reflux under nitrogen atmosphere for 48 h. After almost total solvent evaporation (2 mL) and the addition of methanol (30 mL), the samples were centrifuged at 8000 rpm for 20 min at 25 $^\circ\text{C}$ and the supernatant was decanted. The nanoparticles (CS1@KP) were dissolved in toluene (1 mL) and the purification process was repeated three times. The $^1\text{H-NMR}$ spectrum of CS1@KP (Fig. 1B) showed a broadening of the ligand signals together with those of freely soluble ligands; the presence of a triplet at 3.3 ppm, ascribed to the CH_2 attached to the N of protonated amine ligands (Fig. 1) was detected. It is well known that a ligand strongly bound to colloidal nanocrystals

shows broad $^1\text{H-NMR}$ signals, especially those of the protons close to the QD surface.⁹

The UV-visible spectrum of CS1@KP QDs exhibited the first exciton peak at the same position as the QD-CS1 QDs, *i.e.*, QD functionalization did not produce any change in the first exciton peak (Fig. 2). High resolution transmission electron microscopy (HRTEM) images showed that CS1@KP maintained the size and the crystallinity of QD-CS1 (Fig. 3 and Fig. S1 in the ESI †). Interestingly, these QDs exhibited a higher Φ_{F} (+ 50%) than the amine capped precursor (Fig. 4, Table S1, ESI †),^{10,11,12}

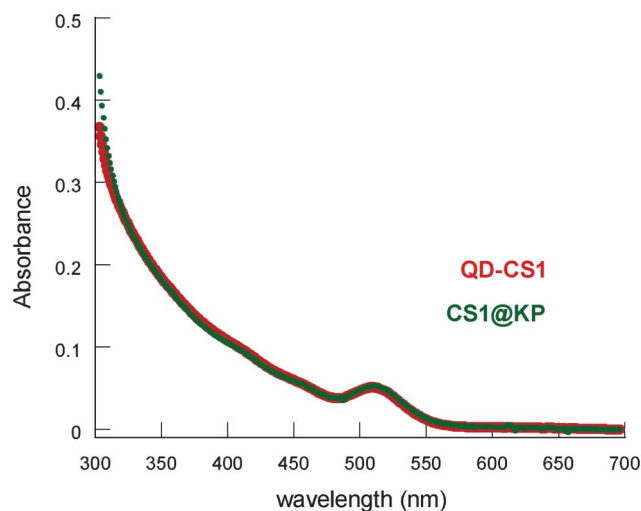


Fig. 2 UV- visible absorption spectrum of QD-CS1 and CS1@KP in toluene.

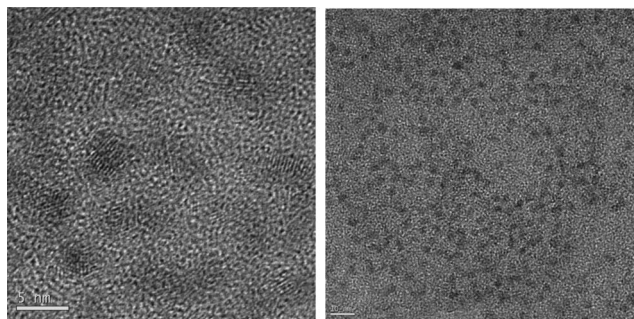


Fig. 3 High Resolution Transmission Electron Microscopy images of **CS1@KP**, (2.3 ± 0.2 nm).

demonstrating that the chemisorption of the thiol to the QD surface does not have a detrimental effect on the QD emission.

Similar results were observed when reacting **QD-CS2** (48.1×10^{-9} moles) with **KP-SH** (2.4×10^{-4} moles) to produce **CS2@KP** (Fig. S2, ESI,† Φ_F increase of 16.5%) and when using **MU** as a capping ligand (Fig. S3, ESI,†). The increase of the Φ_F was higher for the smaller QDs, which is probably associated with a higher surface ligand-to-QD size ratio in the case of smaller-sized nanoparticles.

The same strategy was applied for the preparation of QD-CS nanoparticles decorated with carboxy groups. Thus, a chloroform solution of **QD-CS3** (1.4×10^{-7} moles) was heated under reflux in the presence of **MUA** and **MPA** (7.0×10^{-4} moles) for 48 h. After the above-mentioned work-up, the QDs were placed in water and their solubility was increased by addition of tetramethylammonium hydroxide (10 : 1 v/v water: salt solution 0.1M) and mild heating (40 °C) for several minutes, leading to stable colloids of **CS3@MUA** and **CS3@MPA**. The absorption spectrum of **CS3@MUA** showed a clear red-shifted exciton peak (7 nm shift), while such variation was only of 2 nm for **CS3@MPA**. The solvatochromic effect is expected to induce a redshift as the solvent dielectric constant (ϵ) increases from 4.8 (chloroform) to 78 (water).¹³ The HRTEM images showed an average size of 3.1 ± 0.3 nm and 3.3 ± 0.3 nm for **QD-CS3** and **CS3@MPA** QDs, respectively, (Fig. S4, ESI†). The emission bandwidth of the new water-soluble QDs was narrower than that

of their precursor (Table S1). In addition, the Stokes shift of the thiol capped QDs was greater than that of the amine capped QDs.

Interestingly, the water soluble QDs exhibited a Φ_F of 54% (**CS3@MUA**, Fig. 5) and 45% (**CS3@MPA**, Fig. S5, ESI,†); *i.e.* ligand exchange and water solubilization led to a decrease in the Φ_F of less than 29% (Table S1).

These results indicated that the replacement of the amine ligands by thiols under the described conditions resulted in well-passivated QDs. Lee *et al.*⁴ have reported that the replacement of TOPO ligands by MPA thiolates in considerably larger sized CdSe/ZnS QDs (5.2 nm, λ_{max} at 610 nm) can give rise to QDs with a high photoluminescence performance if using an MPA thiolate soluble in chloroform and avoiding the presence of water. However, this only applied to small thiolate concentrations. In fact, high concentrations of thiolate were detrimental to Φ_F and produced non-fluorescent QDs. We performed control experiments to determine the effect of the addition of such organic-soluble thiolates to QD-CS3 QDs, and found a drastic decrease of the QD fluorescence. Therefore, we reason that the exchange of the amine ligands by thiols in our studies could benefit from the basicity of the amines after their release from the QD surface, polarizing the thiol S–H bond¹⁴ and increasing the nucleophilicity of the thiol (Scheme 1). Consequently, chemisorption of the thiol to the core-shell QD surface would occur under very mild conditions.

To confirm the chemisorption of thiol to the core-shell QDs under the described mild conditions, the infrared spectra of **KP-SH**, **CS2@KP**, **QD-CS2**, and that of a freshly-prepared mixture of **QD-CS2** and **KP-SH** were compared (Fig. S6, ESI,†). The stretching vibration mode of the thiol group of **KP-SH** at *ca.* = 2569 cm^{-1} was also present in the **QD-CS/KP-SH** mixture, but vanished in **CS2@KP**.

In addition, X-ray photoelectron spectroscopy (XPS) was used, since it provides the binding energy of a core-level electron of an atom in the solid.¹⁵ This energy depends on the potential energy at that position, which in turn depends on the chemical environment of the atom. Hence, an organic-soluble QD, **CS2@KP**, and a water-soluble QD, **CS3@MUA**, were analyzed by XPS and the data were compared with those for **KP-SH**,

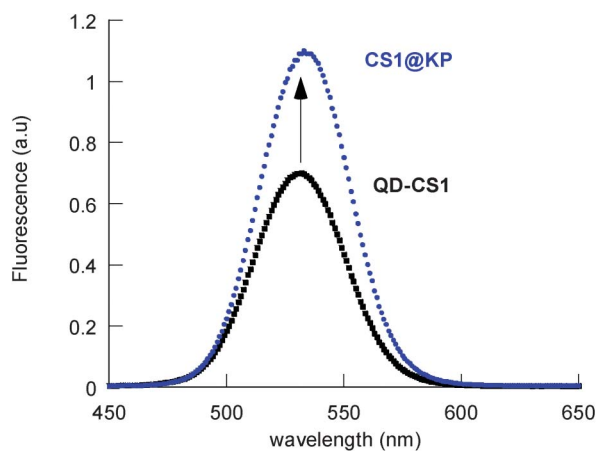


Fig. 4 Comparative fluorescence spectrum of A: a deaerated toluene solution of **QD-CS1** (■) and **CS1@KP** (●).

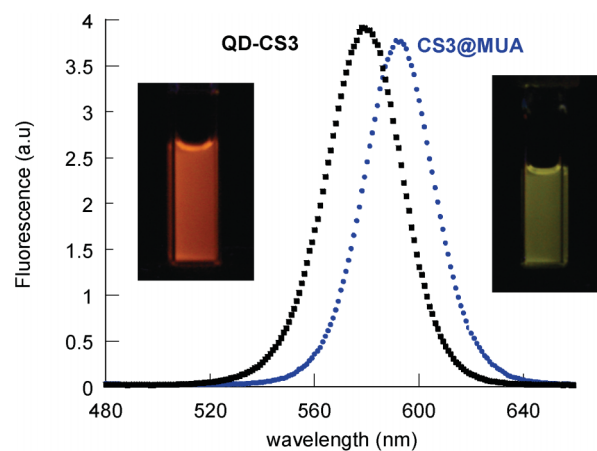


Fig. 5 Comparative fluorescence spectra of a deaerated toluene solution of **QD-CS3** (■) and a water solution of **CS3@MUA** (●).

MUA, and a core-shell QD (QD-CS2), as well as those for a core-shell QD prepared by reacting QD-CS2 (48.1×10^{-9} moles) with KP-SH (2.4×10^{-4} moles) at room temperature, CS2@KP_{rt}.

The Cd 3d spectrum splits by the spin-orbital coupling into the 3d 3/2 (404.7 eV) and 3d 5/2 (411.4 eV) components, with a typical splitting magnitude of 6.7 eV. The binding energy of the Cd was very similar for all the core-shell QDs, QD-CS2, CS2@KP_{rt}, CS2@KP, and CS3@MUA (Fig. 6). Except for QD-CS2, deconvolution of the spectrum gave, besides the 3d 3/2 Cd contribution, a new component with a binding energy at *ca.* 403 eV. This was the main contribution for CS3@MUA, and it was ascribed to the presence of NIs of ammonium salts.¹⁶ In agreement with this, while the C 1s spectrum (not shown) of MUA exhibited a component at 288.8 eV that was attributed to the carboxylic moiety, CS3@MUA presented a peak at 287.8 eV, ascribed to the carboxylate group.¹⁷

Regarding the S 2s spectrum, KP-SH presented a peak at 227.4 eV ascribed to the thiol group,¹⁷ while QD-CS2 exhibited a peak with binding energy of 225.7 eV, brought about by the ZnS shell (Fig. 7).¹⁸ This band was very similar in the case of CS2@KP_{rt}, but shifted to a lower binding energy (225.3 eV) in the case of CS2@KP (Fig. 7). This can be explained by the contribution of the thiol ligand, chemisorbed on the QD shell. Therefore, this peak was deconvoluted into two separate peaks by using the S 2s spectrum of the initial amine-capped core-shell QD as the reference. The new component shifted considerably to a lower value than that of the unbound thiol (at 224.4 eV *vs.* 227.4 eV) and this may be attributed to the chemisorption of KP-SH to the QD surface;¹⁸ its high contribution (*ca.* 30%) showed a large coverage of the QD surface by KP-SH.

The generality of the methodology to prepare highly fluorescent thiol-capped CdSe/ZnS core-shell QDs to QDs

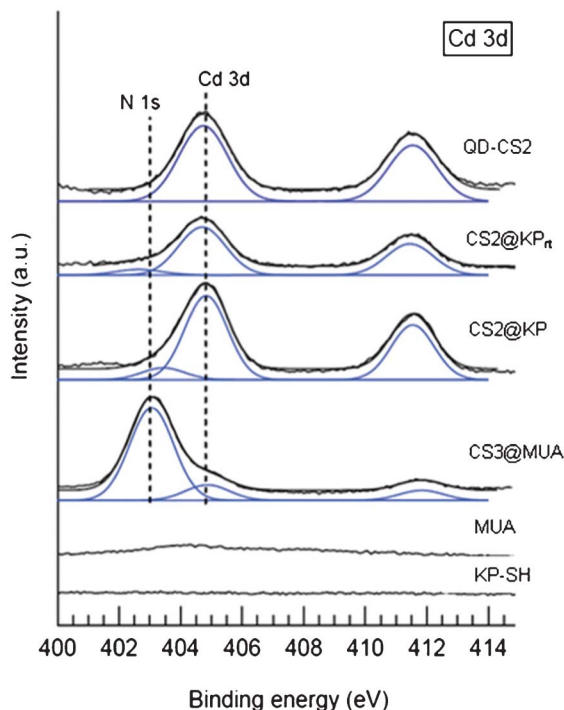


Fig. 6 XPS spectra of Cd 3d and N 1s for QD-CS2, CS2@KP_{rt}, CS2@KP, and CS3@MUA.

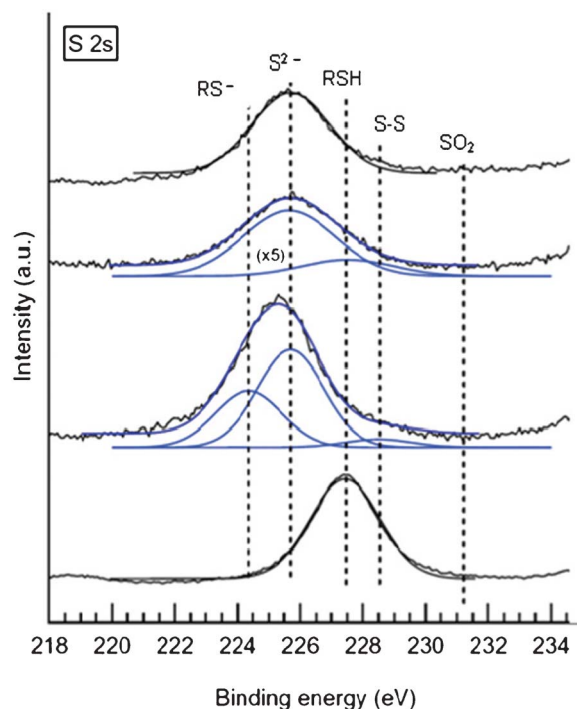


Fig. 7 Top to bottom: XPS spectra of S 2s for QD-CS2, CS2@KP_{rt}, CS2@KP, and KP-SH.

different from those manufactured by Evident was also studied, using homemade QDs as well as QDs purchased from another supplier, specifically from Ocean Nano Tech (QD-CS4: λ_{max} at 503 nm, Φ_{F} of 58% and QD-CS5: λ_{max} at 544 nm, Φ_{F} of 55%), see Table S1, ESI.†

Thus, a homemade TOPO-capped CdSe/ZnS core-shell QD (QD-CS6, 2.8 nm, λ_{max} at 535 nm) was prepared following a previously reported procedure with some modifications (see experimental section). The TOPO ligands of QD-CS6 were replaced by amine ligands by heating a deaerated chloroform solution (25 mL) of QD-CS6 5.46×10^{-7} mmol and octadecylamine (ODA) ([amine]/[QD] = 4859 molar ratio) under reflux for 48 h. The amine-capped QDs (QD-CS7) exhibited its first exciton peak at 535 nm and a Φ_{F} of 31%. The replacement of the capping ligands on QD-CS6 and QD-CS7 by KP-SH was carried out using the above-mentioned strategy to lead to CS6@KP (Φ_{F} of 35%) and CS7@KP (Φ_{F} of 30%), respectively. The S 2s spectrum of CS7@KP (not shown) presented a peak at 224.4 eV ascribed to the chemisorption of KP-SH to the QD, while neither CS6@KP, nor QD-CS6, nor QD-CS7 exhibited a peak with this binding energy. As expected, CS6@KP presented a peak at 227.4 eV ascribed to the thiol group.

In addition, the replacement of the capping ligands on QD-CS5 was performed with the thiol and thiolate form of KP-SH, leading to CS5@KP₁ and CS5@KP₂, respectively. The ¹H-NMR spectrum of both QDs showed the characteristic broadening of the ligand signals. But, while the replacement of the QD capping ligand with the thiol led to a decrease in the Φ_{F} of only 8%, the thiolate produced a drastic decrease (39%) of the QD emission. For further details of these and additional experiments regarding the effect on the emission properties of QD-CS4, QD-CS5, QD-CS6, and QD-CS7 after adding thiols, see Table S2 in ESI.†

Table 1 Physical properties of the CdSe/ZnS QDs capped with thiols and their precursors, before and after irradiation

	λ_{\max} exciton			λ_{\max} emission			Φ_F		
	before irradiation	after irradiation		before irradiation	after irradiation		before irradiation	after irradiation	
		under N ₂	Air		under N ₂	Air		under N ₂	Air
QD-CS2	521	520	520	539	537	538	0.61	0.31	0.22
CS2@KP	520	515	515	540	535	533	0.70	0.44	0.47
QD-CS3	564	564	563	582	581	581	0.63	0.53	0.42
CS3@MUA	571	572	570	595	594	592	0.54	0.52	0.39
CS3@MPA	566	566	567	586	588	587	0.45	0.46	0.49

The photostability of nanoparticles is of great importance in their applications; therefore, the photostability of several of the prepared thiol capped QDs was compared with that of their amine capped precursor. The samples were irradiated ($400 \text{ nm} < \lambda < 700 \text{ nm}$, λ_{\max} at 420 nm , 70 W/m^2) in toluene or water, depending on the solubility of the corresponding QD, under nitrogen or air atmosphere for *ca.* five hours.

Surprisingly, the emission maximum of the QDs experienced only a small blue-shift (up to 6 nm) after 5 h irradiation under air atmosphere (Table 1).¹⁹ Blue-shifts up to 40 nm have been reported for TOPO capped CdSe/ZnS QDs and attributed to photooxidation of the CdSe core.²⁰ For oxidation to take place, oxygen has to diffuse through the ZnS shell. Therefore, our data demonstrated that the CdSe core was well passivated by the ZnS shell in the QDs studied in this research work. The diminished Φ_F of the organic-soluble QDs after their irradiation suggested photooxidation of mainly the ZnS layer,²¹ since it was accompanied by only a slight blue-shift of the emission maximum. In addition, the intensity decrease can be caused by the formation of lattice defects in the core-shell QDs.²¹

In addition, the photostability in air of the QDs covered with chemisorbed thiol ligands was higher than that of the amine-capped CdSe/ZnS QDs (see comparison between QD-CS3 (toluene) and CS3@MPA (water) in Fig. 8, and between QD-CS2 (toluene) and CS2@KP (toluene) in Fig. 9). Moreover, CS3@MPA exhibited an improved fluorescence (10%) after 5 h irradiation. This could be explained by the removal of recombination centers, created during the ligand exchange, by illumination.²²

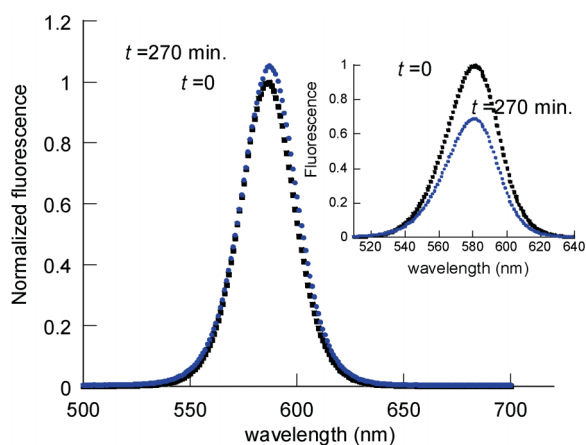


Fig. 8 Normalized fluorescence spectra of aerated solutions of CS3@MPA (water), before (■) and after (●) 270 min irradiation at $\lambda > 400 \text{ nm}$. Inset: comparative fluorescence spectra of QD-CS3 (toluene).

The fluorescence of the amine-capped QDs also drastically decreased after irradiation under anaerobic conditions (though less than under air atmosphere conditions). However, irradiation of CS2@KP, CS3@MUA, and CS3@MPA in the presence or absence of oxygen made little difference and only slightly affected the QD fluorescence performance (Fig. 10, Fig. S7 and S8, ESI,† and Table 1).

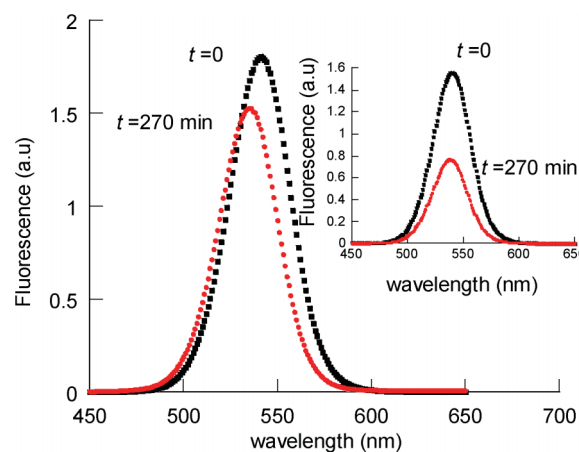


Fig. 9 Normalized fluorescence spectra of aerated toluene solutions of CS2@KP, before (■) and after (●) 270 min irradiation at $\lambda > 400 \text{ nm}$. Inset: comparative fluorescence spectra of QD-CS2.

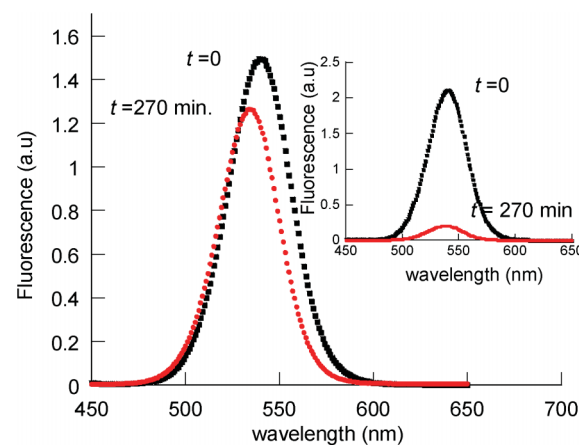


Fig. 10 Normalized fluorescence spectra of deaerated toluene solutions of CS2@KP, before (■) and after (●) 270 min irradiation at $\lambda > 400 \text{ nm}$. Inset: comparative fluorescence spectra of QD-CS2.

4. Conclusions

In summary, we have demonstrated that the replacement of amine ligands by thiols to lead to either organic-soluble or water-soluble QDs can be performed under mild conditions, preserving or enhancing not only the emission properties of the nanoparticles but also their photostability. The QDs remain stable over the six-month study period. These results may help researchers to design new functional QDs for future applications in which highly fluorescent, photostable, and small-sized QDs are required.

Acknowledgements

We thank MEC (Project CTQ2008-06777-CO2-01, contract granted to J. A-S, and RyC contract granted to R.E.G), GVA (Project ACOMP/2009/334), and UVEG (Project UV-AE-09-5805) for their support.

References

- (a) M. G. S. Hyldahl, T. Bailey and B. P. Wittmerhaus, *Sol. Energy*, 2009, **83**, 566; (b) X. Michalet, F. F. Pinaud, L. A. Bentolila, J. M. Tsay, S. Doose, J. J. Li, G. Sundaresan, A. M. Wu, S. S. Gambhir and S. Weiss, *Science*, 2005, **307**, 538; (c) A. P. Alivisatos, *Nat. Biotechnol.*, 2004, **22**, 47; (d) F. Chen and D. Gerion, *Nano Lett.*, 2004, **4**, 1827.
- (a) O. Dabbousi, J. F. Rodriguez-Viejo, V. Mikulec, J. R. Heine, H. Mattoussi, R. Ober, K. F. Jensen and M. G. Bawendi, *J. Phys. Chem. B*, 1997, **101**, 9463; (b) B. M. A. Hines and P. Guyot-Sionnest, *J. Phys. Chem.*, 1996, **100**, 468.
- H. Borchert, D. V. Talapin, C. McGinley, S. Adam, A. Lobo, A. R. B. Castro, T. Möller and H. Weller, *J. Chem. Phys.*, 2003, **119**, 1800.
- B. K. Pong, B.L. Trout and J. Y. Lee, *Langmuir*, 2008, **24**, 5270.
- (a) K. Susumu, E. Oh, J. B. Delehanty, J. B. Blanco-Canosa, B. J. Johnson, V. Jain, W. J. Hervey IV, W. R. Algar, K. Boeneman and P. E. Dawson, *J. Am. Chem. Soc.*, 2011, **133**, 9480; (b) I. L. Medintz, N. D. Abazovic, J. Z. Kuljanin-Jakovljevic and M. I. Comor, *Russ. J. Phys. Chem. A*, 2009, **83**, 1511; (c) W. Liu, H. S. Choi, J. P. Zimmer, E. Tanaka, J. V. Frangioni and M. Bawendi, *J. Am. Chem. Soc.*, 2007, **129**, 14530; (d) V. V. Breus, C. D. Heyes and G. U. Nienhaus, *J. Phys. Chem. C*, 2007, **111**, 18589; (e) R. Gill, I. Wilner, I. Shweky and U. Banin, *J. Phys. Chem. B*, 2005, **109**, 23715.
- J. Aldana, Y. A. Wang and X. Peng, *J. Am. Chem. Soc.*, 2001, **123**, 8844.
- KP-SH was synthesized following the Yamamoto procedure: K. Ishihara, M. Nakayama, S. Ohara, H. Yamamoto, *Synlett*. 2001, **7**, 1117. See ESI for further details.† KP-SH was chosen to prepare thiol-capped QDs since it exhibits ¹H-NMR signals well separated from those of ligands of the commercial or home-made QDs used for these studies. In addition, the benzophenone chromophore of KP-SH does not absorb at 400 nm > λ > 700 nm used for studies of the QD photostability. In addition, as the fluorescence studies show, the benzophenone did not significantly quench the QD emission.
- Z. A. Peng and X. Peng, *J. Am. Chem. Soc.*, 2001, **123**, 183.
- (a) X. Ji, D. Copenhaver, C. Sichmeller and X. Peng, *J. Am. Chem. Soc.*, 2008, **130**, 5726; (b) J. S. Owen, J. Park, P. E. Trudeau and A. P. Alivisatos, *J. Am. Chem. Soc.*, 2008, **130**, 12279.
- Yoon. *et al.* have reported an enhanced emission after binding of cysteine to CdSe/ZnS QDs, but they found indications that cysteine was actually bound to the QD-surface by both its thiol and its amine group. In addition, the enhancement disappeared at high cysteine concentration¹⁰.
- C. Park and T. H. Yoon, *Colloids Surf., B*, 2010, **75**, 472.
- For comparison, a chloroform solution (25 mL) of **QD-CS1** and KP-SH ([thiol]/[QD] = 5000 molar ratio) was maintained at room temperature under nitrogen atmosphere for 48 h. After almost total solvent evaporation (2 mL) and the addition of methanol (30 mL), the samples were centrifuged at 8000 rpm for 20 min at 25 °C and the supernatant was decanted. The nanoparticles (**CS1@KP_r**) were dissolved in toluene (1 mL) and the purification process was repeated three times. The QDs exhibited a lower Φ_F than the amine capped precursor. See also, J. Aguilera-Sigalat, S. Rocton, R. E. Galian and J. Pérez-Prieto, *Can. J. Chem.*, 2011, **89**, 359.
- C. A. Leatherdale and M. G. Bawendi, *Phys. Rev. B: Condens. Matter*, 2001, **63**, 165315.
- G. Zundel, *J. Mol. Struct.*, 1982, **84**, 205.
- A. Lobo, T. Möller, M. Nagel, H. Borchert, S. G. Hickey and H. J. Weller, *J. Phys. Chem. B*, 2005, **109**, 17422.
- (a) G. K. Olivier, D. Shin, J. B. Gilbert, L. M. A. Monzon and J. Frechette, *Langmuir*, 2009, **25**, 2159; (b) A. Adenier, M. M. Chehimi, I. Gallardo J. Pinson and N. Vilà, *Langmuir*, 2004, **20**, 8243; (c) E. Uchida and Y. Ikada, *J. Polymer Sci.*, 1996, **61**, 1365.
- J. J. Park, SHDP, Lacerda, S. K. Stanley, B. M. Vogel, S. Kim, J. F. Douglas, D. Raghavan and A. Karim, *Langmuir*, 2009, **25**, 443.
- This peak was also present in the S 2s spectrum of **CS2@KP_r**. By contrast, **CS2@KP** showed the signal of the disulfide..
- For one example of a slight hypsochromic shift upon photooxidation see L.I. Gurinovich, M.V. Artemév and A.A. Lyutich, *J. Appl. Spectrosc.*, 2006, **73**, 572.
- W. G. J. H. M. Van Sark, P. L. T. M. Frederix, D. J. Van den Heuvel, H. C. Gerritsen, A. A. Bol, J. N. J. Van Lingen, C. de Mello Donegá and A. Meijerink, *J. Phys. Chem. B*, 2001, **105**, 8281.
- W. G. J. H. M. Van Sark, P. L. T. M. Frederix, A. A. Bol, H. C. Gerritsen and A. Meijerink, *ChemPhysChem*, 2002, **3**, 871.
- C. Carrillo-Carrión, S. Cárdenas, B. M. Simonet and M. Valcárcel, *Chem. Commun.*, 2009, 5214.

Highly fluorescent and photostable organic- and water-soluble CdSe/ZnS core-shell quantum dots capped with thiols

Jordi Aguilera-Sigalat, Simon Rocton, Juan F. Sánchez-Royo, Raquel E. Galian* and
Julia Pérez-Prieto*

Supporting Information

TABLE OF CONTENTS

Title	page
Table S1. Physical properties of the CdSe/ZnS QDs capped with thiol and their precursors	S2
Table S2. Maximum in the fluorescence spectra and fluorescence quantum yield of the core-shell QDs upon the addition of the thiol or the thiolate compound. Fluorescence quantum yield calculation.	S3
Figure S1. High resolution transmission electron microscopy images of CS1	S4
Figure S2. Comparative fluorescence spectra of deaerated toluene solutions of QD-CS2 and CS2@KP	
Figure S3. Comparative fluorescence spectra of deaerated toluene solutions of QD-CS2 and CS2@MU .	S5
Figure S4. High resolution transmission electron microscopy images of CS3 (A, 3.1 ± 0.3 nm), CS3@MPA (B, 3.3 ± 0.3).	
Figure S5. Comparative fluorescence spectra of a deaerated toluene solution of QD-CS3 and a water solution CS3@MPA	6
Figure S6. Comparative IR spectra a freshly-prepared mixture of QD-CS2 and KP-SH, QD-CS2 , CS2@KP , and of KP-SH.	
Figure S7. Normalized fluorescence spectra of deaerated solutions of QD-CS3 (toluene) and CS3@MUA (water), before and after 270 min irradiation under 420 nm lamps.	S7
Figure S8. Normalized fluorescence spectra of deaerated aqueous solution CS3@MPA , before (■) and after (●) 270 min irradiation under 420 nm lamps.	S8

Table S1: Physical properties of the CdSe/ZnS QDs capped with thiols and their precursors^a

		λ_{\max} 1 st exciton peak (nm)	D ^b (nm)	λ_{\max} emission peak (nm)	FWHM ^c (nm)	ϕ_F ^d
QD-CS1^e	Evident	509	2.43	531	45 ± 1	0.50
QD-CS2^e	Evident	521	2.64	539	40 ± 1	0.61
QD-CS3^e	Evident	564	3.45	582	34 ± 1	0.63
QD-CS4^e	Ocean	503	2.37	517	36 ± 1	0.58
QD-CS5^e	Ocean	544	2.93	562	33 ± 1	0.55
QD-CS6^e	homemade	535	2.77	543	26 ± 1	0.45
QD-CS7^e	homemade	539	2.84	548	26 ± 1	0.32
CS1@KP	homemade	509		534	44 ± 1	0.75
CS2@KP	homemade	520		540	38 ± 1	0.70
CS6@KP	homemade	537	2.80	546	28 ± 1	0.35
CS7@KP	homemade	538	2.82	547	27 ± 1	0.30
CS3@MUA	homemade	571		595	30 ± 1	0.54
CS3@MPA	homemade	566		586	30 ± 1	0.45

^a The core-shell QD-CS1- QD-CS3 were commercially available (www.evidenttech.com), QD-CS4 and QD-CS5 were purchased from Ocean Nano Teach LLC. ^b The diameter was calculated according to the method of W. W. Yu, L. Qu, W. Guo, X. Peng *Chem. Mater.* 2003, **15**, 2854. ^c Full width at half maximum (FWHM), ^dFluorescence quantum yield obtained using fluoresceine as the standard. ^e Capping ligand: fatty amine and monosubstituted olefin (Evident), fatty amine, oleic acid, and monosubstituted olefin (Ocean), TOPO (QD-CS6), and TOPO and octadecylamine (QD-CS7). ^fThe ¹H-NMR spectrum of the QD showed the presence of monosubstituted olefin.

Table S2: Maximum in the fluorescence spectra (λ_{\max} , nm) and fluorescence quantum yield (Φ_f) of the core-shell QDs upon the addition of the thiol or the thiolate compound.

QD / Thiol System (molar ratio 1:2200)	λ_{\max} emission (nm)	Quantum yield (%)
QD-CS4	517	58
QD-CS4/MU	519	50
QD-CS4/MU thiolate	526	20
QD-CS5	561	55
QD-CS5/MU	562	48
QD-CS5/MU thiolate	565	40
QD-CS5/KP-SH	561	53
QD-CS5/KP-SH thiolate	562	46

^a Fluorescence measured 70 min after the addition of the thiol/thiolate of MU and 140 min for the thiol/thiolate of KP-SH.

Fluorescence Quantum yield Calculation

Quantum dots fluorescence quantum yield ($\Phi_{F,QD}$) was measured by comparing the integrated emission spectra for the QD and fluoresceine according to the following equation (Grabolle, M.; Spieles, M.; Lesnyak V.; Gaponik, N. Eychmüller, A. and Resch-Genger, U.; *Anal.Chem.* 2009, **81**, 6285):

$$\Phi_{F,QD} = \Phi_{F,st} \cdot \frac{F_{QD}}{F_{st}} \cdot \frac{f_{st}(\lambda_{ex})}{f_{QD}(\lambda_{ex})} \cdot \frac{n_{QD}^2}{n_{st}^2}$$

where $\Phi_{F, st}$ is the fluorescence quantum yield of the standard, F is the area under the fluorescence curve, f is the absorption factor at the excitation wavelength (λ_{ex}) and n is the refractive index of the solvent.

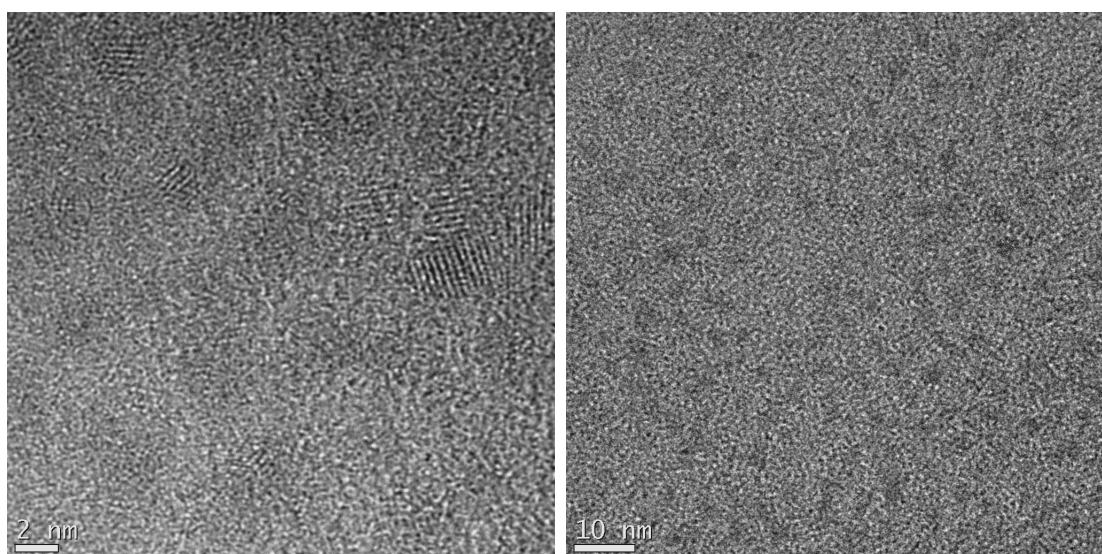


Figure S1: High Resolution Transmission Electron Microscopy images of **CS1** (2.2 ± 0.2 nm)

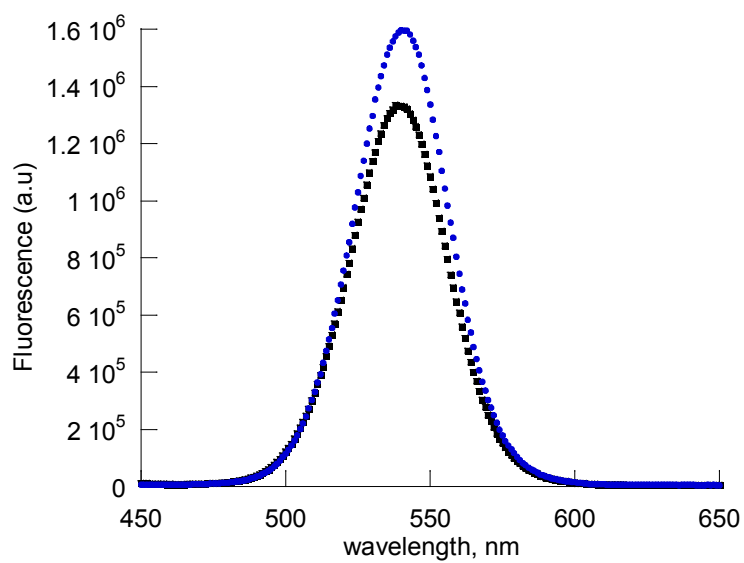


Figure S2: Comparative fluorescence spectra of *deareated* toluene solutions of **QD-CS2** and **CS2@KP**

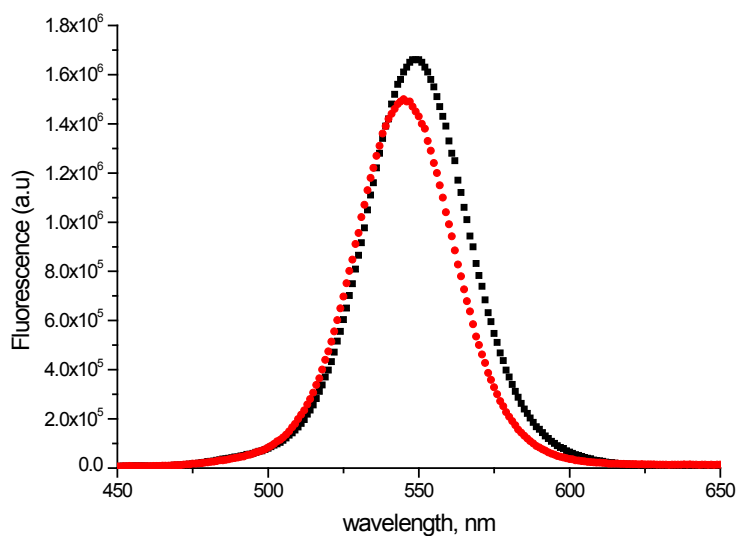


Figure S3 . Comparative fluorescence spectra of *deareated* toluene solutions of **QD-CS2** (●) and **CS2@MU** (■).

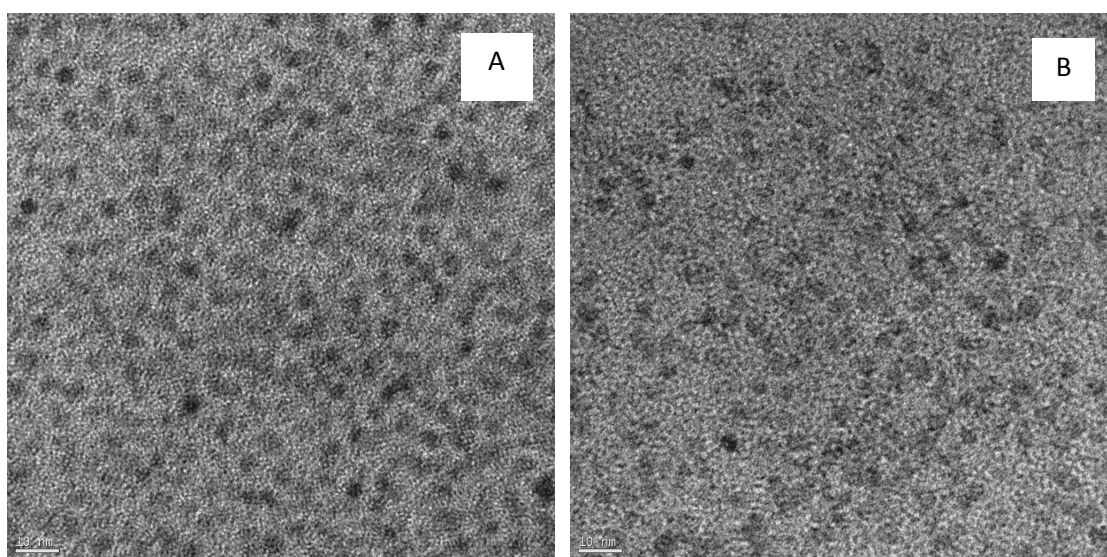


Figure S4: High resolution transmission electron microscopy images of **CS3** (A, 3.1 ± 0.3 nm) and **CS3@MPA** (B, 3.3 ± 0.3 nm), the scale bar is 10 nm.

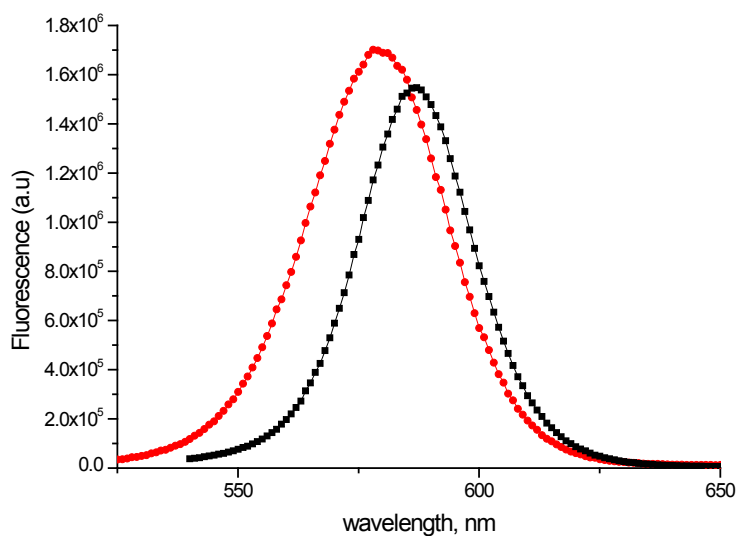


Figure S5. Comparative fluorescence spectra of a *deareated* solution of QD-CS3 (●) and a water solution CS3@MPA (■).

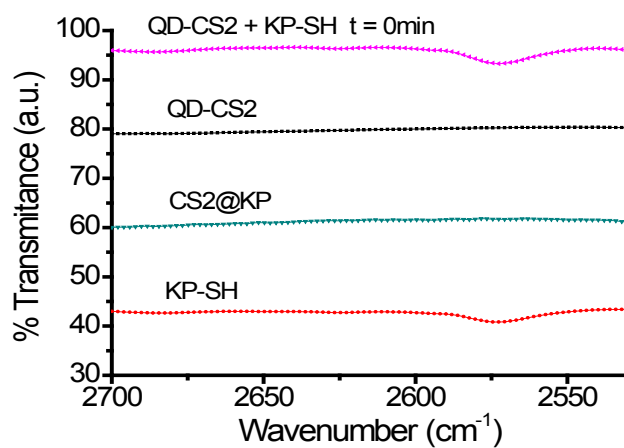


Figure S6. Comparative IR spectra a freshly-prepared mixture of QD-CS2 and KP-SH, QD-CS2, CS2@KP, and of KP-SH.

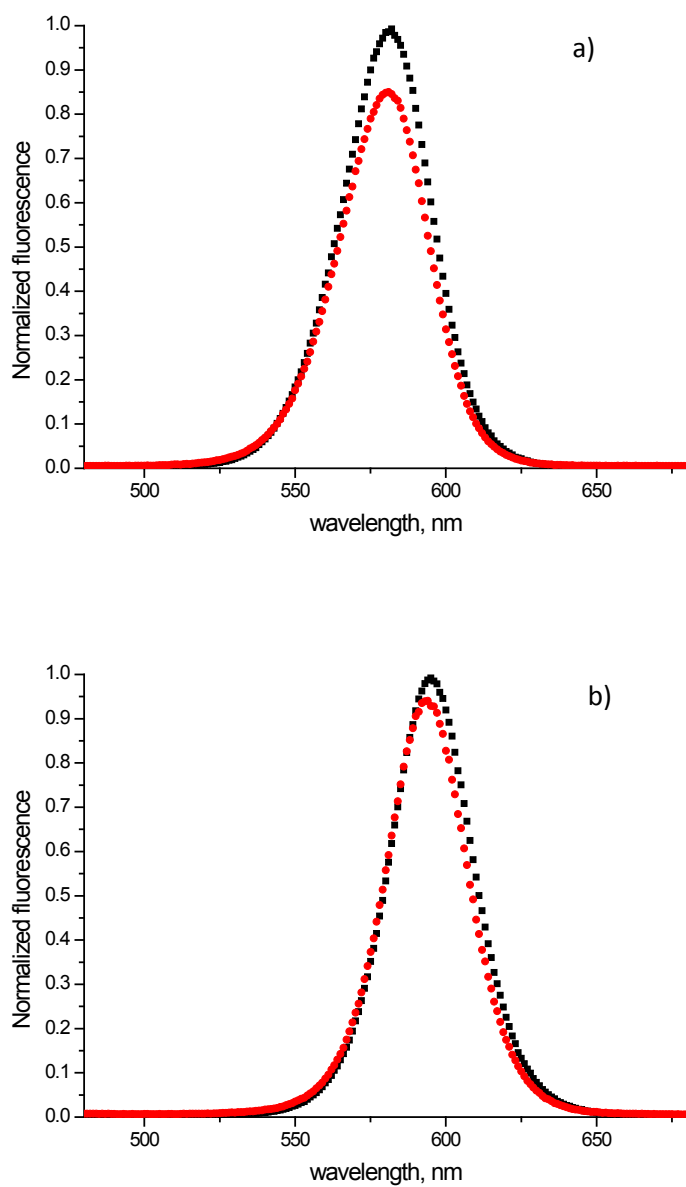


Figure S7. Normalized fluorescence spectra of **deaerated** solutions of a) **QD-CS3** (toluene) and b) **CS3@MUA** (water), before (■) and after (●) 270 min irradiation under 420 nm lamps.

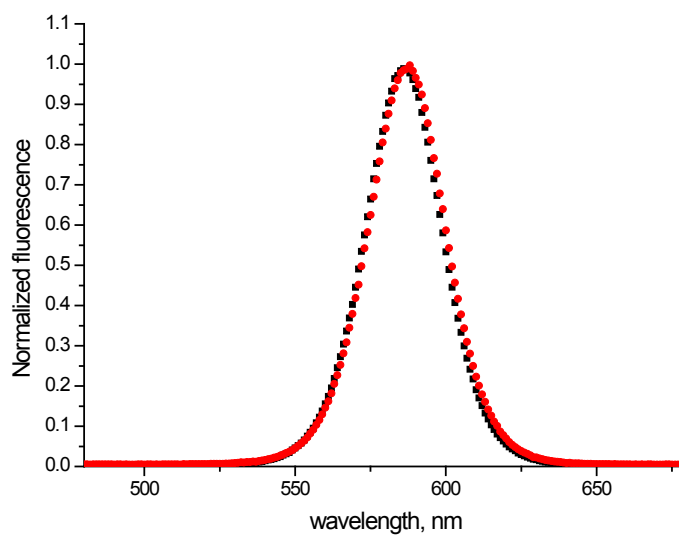


Figure S8. Normalized fluorescence spectra of *deaerated* aqueous solution CS3@MPA, before (■) and after (●) 270 min irradiation under 420 nm lamps.

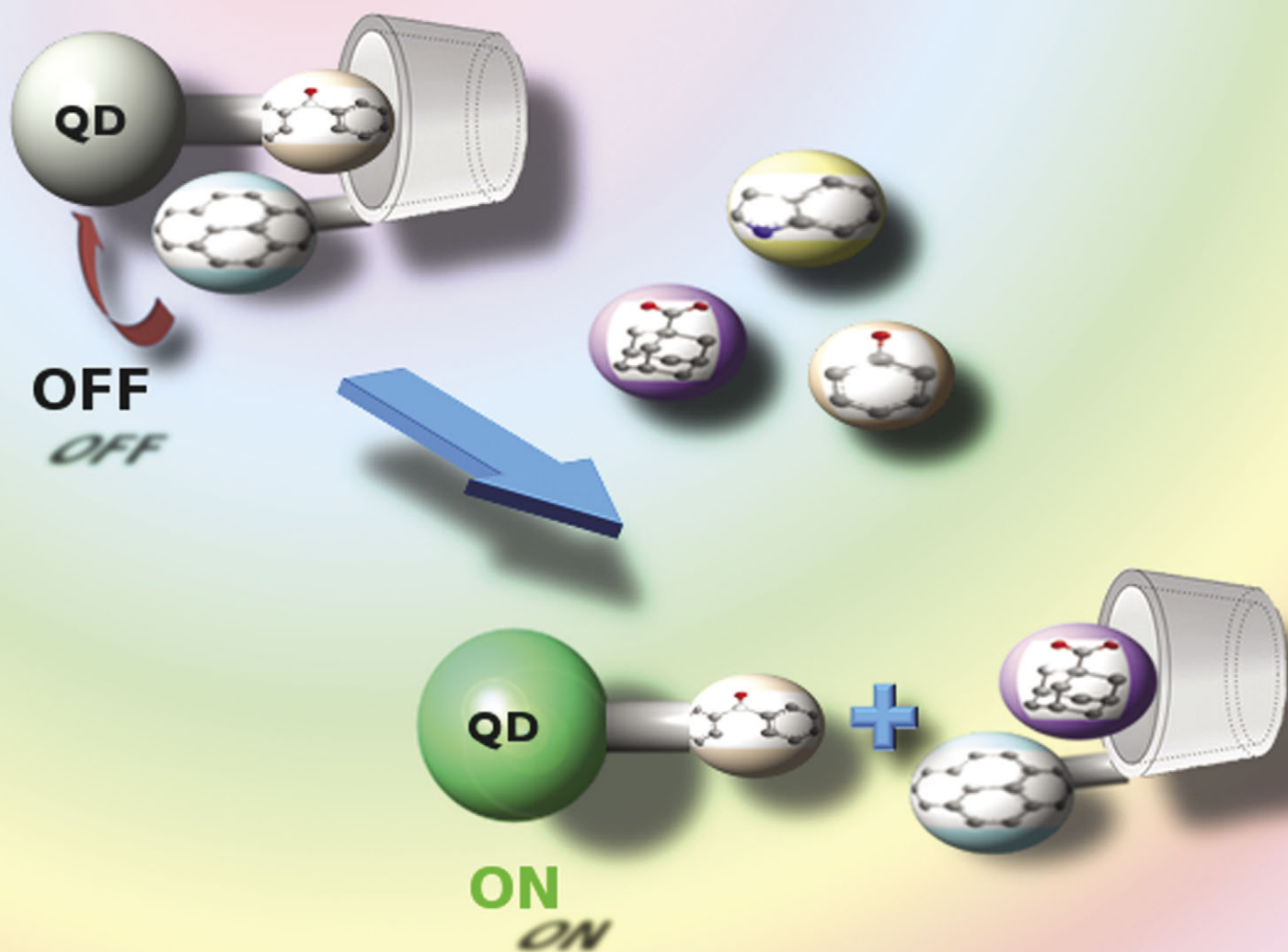
ChemComm

Chemical Communications

www.rsc.org/chemcomm

Volume 48 | Number 20 | 7 March 2012 | Pages 2557–2648

Downloaded by Universidad de Valencia on 14 February 2012
Published on 14 November 2011 on http://pubs.rsc.org | doi:10.1039/C1CC15312A



ISSN 1359-7345

RSC Publishing

COMMUNICATION

Galian and Pérez-Prieto *et al.*

Quantum Dot/Cyclodextrin supramolecular systems based on efficient molecular recognition and their use for sensing

Cite this: *Chem. Commun.*, 2012, **48**, 2573–2575

www.rsc.org/chemcomm

COMMUNICATION

Quantum dot/cyclodextrin supramolecular systems based on efficient molecular recognition and their use for sensing†

Jordi Aguilera-Sigalat,^a Juan M. Casas-Solvas,^b Maria C. Morant-Miñana,^a Antonio Vargas-Berenguel,^b Raquel E. Galian^{*ac} and Julia Pérez-Prieto^{*a}

Received 26th August 2011, Accepted 1st November 2011

DOI: 10.1039/c1cc15312a

A supramolecular system based on ketoprofen functionalised CdSe/ZnS nanoparticles and pyrene-modified β -CD was prepared and successfully used for molecular sensing of different analytes. In addition, a strategy for the individual recovery of all the components of the sensing assay is reported.

Core-shell CdSe/ZnS quantum dots (QDs) are highly fluorescent systems, which makes them of interest for biological, medical, and engineering applications.^{1–4} The ZnS shell plays a crucial role in their emission properties and enhances the chemical- and photo-stability of the QDs. CdSe/ZnS nanoparticles are further passivated with organic ligands which allow them to remain stable as colloidal solutions in organic solvents and water and provide the desired surface functionality.⁵ The application of QDs for biosensing is quite advanced, while their use as optical probes for molecular recognition has hardly been developed.⁶

β -Cyclodextrin (CD) is a cyclic oligosaccharide comprising seven D-glucopyranose units linked by α -(1 \rightarrow 4) bonds. It possesses a relatively rigid torus-shaped structure, which defines an inner hydrophobic cavity rimmed by two hydrophilic openings which are different in diameter, the narrower containing the primary hydroxy groups located on the C-6 of the glucopyranose units and the wider containing the secondary groups located on positions C-2 and C-3 (Fig. S1, ESI†). As a consequence, CD forms inclusion complexes in aqueous solution with a large variety of organic molecules of hydrophobic nature and of suitable size and geometry.^{7–10} In addition to other applications, this feature has been explored for the design and construction of molecular sensors in which the inclusion of the guest molecule triggers a macroscopic signal

which can be detected and quantified.¹¹ Both quantum dots and cyclodextrins have been used in Supramolecular Chemistry.^{11–13}

Chemical sensing systems based on cyclodextrin-coated QDs have been recently designed.^{6,14,15} For example, water-soluble CdSe/ZnS QDs have been prepared by association of the QDs with natural cyclodextrins helped by a sonochemical procedure; subsequent addition of phenols quenches the QD emission.¹⁵ In addition, CD-capped CdSe/ZnS QDs have been prepared *via* covalent binding of an aminophenylboronic-functionalised QD to CD and used for optical sensing of different substrates by means of a fluorescence resonance energy transfer or an electron transfer mechanism.⁶

In this communication, we focus on a new strategy to obtain an easy-to-prepare and effective sensor, based on the molecular recognition between a QD and a CD that exhibits an enhanced fluorescence in response to different analytes.

The protocol used in the present work was to add ketoprofen-capped CdSe/ZnS QDs (CS@KP) to a solution of a CD bearing a pyrene unit on its secondary face (CD-Py, Fig. S1 in ESI†). CD-Py was selected because of the considerable association constant (K_a ca. 3000 M^{-1})¹⁶ of CD with ketoprofen, and the potential capacity of the 3-(pyren-1-yl)prop-2-ynyl moiety to act as a quencher of the QD emission. The effective capping of CS@KP QDs by CD-Py led to QD/CD supramolecular systems (CS@KP/CD-Py, Scheme 1a, Fig. S2, ESI†), which were soluble in aqueous solvents. In the presence of the analyte, competitive association would recover the QD emission by moving the quencher (pyrene) away from the QD surface (Scheme 1b).

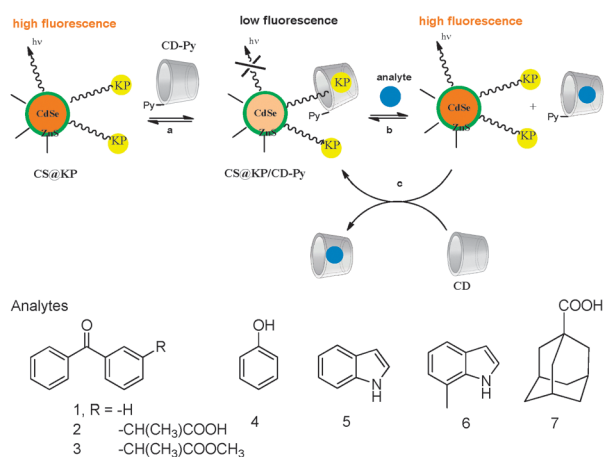
The CD-Py synthesis and characterisation is described in the ESI.† CD-Py exhibited red-shifted UV-absorbance bands compared to those of pyrene (Fig. S3, ESI†) and was soluble in water, DMF, and DMSO. The CS@KP QDs were synthesised by reaction of the bifunctional KP-SH ligand (ester of ketoprofen and 11-mercaptoundecanol) with either commercially available amine-capped CdSe/ZnS QDs from different sources (Evident, CS1; Ocean, CS2) or homemade QDs capped with trioctylphosphine oxide (CS3 and CS4), see experimental details in the ESI.† Table S1 (ESI†) shows the features [average diameter, the maximum of the first exciton (λ_{abs}) and of the emission (λ_{em}) peaks, as well as the fluorescence quantum yield (Φ_f)] of the initial core-shell QDs and that of the CS@KP QDs. ¹H NMR spectra proved that the ligand exchange reactions took place (Fig. S4, ESI†).¹⁷

^a ICMOL, University of Valencia, Catedrático José Beltrán 2, 46980, Paterna, Valencia, Spain. E-mail: julia.perez@uv.es; Fax: +34 963543576; Tel: +34 963543050

^b Área de Química Orgánica, Universidad de Almería, Carretera de Sacramento, 04120, Almería, Spain

^c Department of Analytical Chemistry, University of Valencia, Dr. Moliner 50, 46100, Burjassot, Valencia, Spain. E-mail: raquel.galian@uv.es; Fax: +34 963543274; Tel: +34 963544307

† Electronic supplementary information (ESI) available: Additional absorption, emission, transient absorption and NMR spectra; photo-physical properties of QD and lifetimes of the pyrene systems. Preparation and characterisation of β -CD-Py, KP-SH, home-made CS and CS@KP. See DOI: 10.1039/c1cc15312a



Scheme 1 Structures of CS@KP/CD-Py and of the analytes and protocol for the molecular recognition studies.

The supramolecular systems were prepared by adding 20 μL of a toluene solution of the QD to 3 mL of an acetonitrile/water (3/1) solution of CD-Py (QD/CD-Py = 1/1000) and the system was stabilised over 15 minutes at room temperature (see UV-vis spectra in Fig. S5, ESI[†]). The significant quenching of the QD emission evidenced formation of the CS@KP/CD-Py with the pyrene unit pointing toward the QD surface (Fig. 1A, Table S2, ESI[†]). Comparatively, the emission of the CS@KP QDs remained unchanged or even increased slightly upon addition of the natural CD (Fig. S6A, ESI[†]). Moreover, the supramolecular system exhibited a blue-shifted QD emission when compared to that of CS@KP and CS@KP/CD. The exact quenching mechanism is currently under investigation, but electron transfer reactions involving the 1-pyrenethynyl units and the QD are most likely to be responsible for such a process.¹⁸ Remarkably, the emission of the non-ketoprofen functionalised CS QDs was hardly influenced by capping with CD-Py (Table S2, ESI[†]), suggesting that the association of the CD to the ketoprofen units is essential to stimulate the quenching of the QD fluorescence.

In addition, the fluorescence of the pyrene unit of CD-Py was only slightly affected after formation of CS@KP/CD-Py (Fig. S6B, ESI[†]).

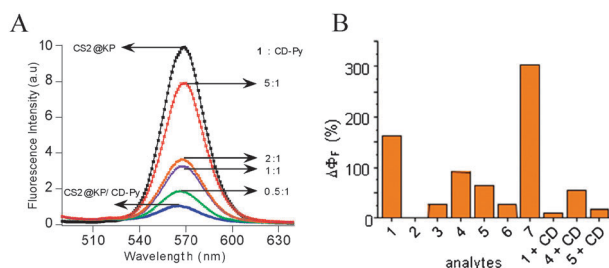


Fig. 1 (A) Fluorescence spectra ($\lambda_{\text{ex}} = 450 \text{ nm}$) of deaerated acetonitrile/water (3/1) solutions of CS2@KP ($5 \times 10^{-9} \text{ M}$, \blacksquare), and CS2@KP/CD-Py (CD-Py/QD molar ratio of 1000), before (\bullet) and after addition of **1**: 1/CD-Py molar ratios of 0.5 : 1 (\blacktriangle), 1 : 1, (\blacktriangledown), 2 : 1 (\circ) and 5 : 1 (\square). (B) Effect of the addition of different analytes (**1** to **7**, $6 \times 10^{-5} \text{ M}$) on the fluorescence ($\lambda_{\text{ex}} = 450 \text{ nm}$) of the solutions of CS2@KP/CD-Py. Competitive effect of CD on analytes **1**, **4** and **5** is also shown. The luminescence of all the samples was recorded after 10 min ultrasound exposure.

Table 1 Lifetimes of the pyrene triplet (${}^3\text{Py}$) and pyrene radical cation (Py^+) of the pyrene systems in $\text{CH}_3\text{CN}/\text{water}$ (3/1)

	${}^3\text{Py}$ $\tau^a/\mu\text{s}$	Py^+ $\tau^b/\mu\text{s}$
CD-Py	6.0 ± 0.8	31 ± 1
CS2@KP/CD-Py	24 ± 1	10 ± 2
1 + CS2@KP/CD-Py ^c	6.4 ± 0.9	27.4 ± 0.6
CS2@KP/CD	5.6 ± 0.2	22 ± 1

^a Measured at 430 nm. ^b Measured at 490 nm. ^c 2 : 1 molar ratio.

The influence of the polarity of the medium on the formation of pyrene radical cations is already known.¹⁹ Therefore, to confirm the location of the pyrene moieties when CD-Py is capping the QDs, we performed transient absorption measurements of the pyrene systems (CD-Py, CS@KP/CD-Py, and CS/CD-Py). Laser flash photolysis (Nd/YAG, 355 nm) of CD-Py led to the formation of the pyrene triplet (λ_{max} at 430 nm, τ ca. 6 μs) and pyrene radical cation (λ_{max} at 490 nm, τ ca. 31 μs), see Table 1 and Fig. S7 and S8 (ESI[†]). Pyrene radical cation yield and lifetime diminished considerably, while the pyrene triplet yield and lifetime increased, in the case of the supramolecular system. These data are in agreement with the location of the pyrene moieties of CD-Py within the organic capping ligand of the CS@KP QDs, pointing toward the QD surface.

Similar experiments were performed with CS/CD-Py and evidenced that the QD had considerably less effect on the yield and lifetime of the pyrene transients (Table 1). This might be attributed to a capping of the QD mainly by the primary face of CD-Py, *i.e.*, with its pyrene units located in the aqueous solution.

Subsequently, we studied the capacity of CS2@KP/CD-Py in molecular sensing, using benzophenone (**1**), ketoprofen (**2**), ketoprofen methyl ester (**3**), phenol (**4**), indole (**5**), 7-methylindole (**6**), and adamantane carboxylic acid (**7**) as analytes; Scheme 1b outlines the protocol for the assay.

The initial fluorescence of CS2@KP ($\Phi_f = 0.51$) was quenched by addition of CD-Py ($\Phi_f = 0.11$; QD/CD-Py molar ratio of 1/1000). Addition of CD had slight effect on the emission properties of CS2@KP/CD-Py (not shown). By contrast, addition of **1** to CS2@KP/CD-Py led to a 5 nm red shift of the λ_{em} and a remarkable enhancement of the QD fluorescence nearly recovering the fluorescence of CS2@KP when using a 1/CD-Py molar ratio of 5 : 1 (see Fig. 1A for different molar ratios), *i.e.*, formation of the host-guest complexes between CD-Py and the analyte caused the release of the cyclodextrin from the QD surface. Consequently, laser flash photolysis experiments showed that the yield and lifetime of the pyrene transients upon addition of **1** to CS2@KP/CD-Py (analyte/supramolecular system molar ratio of 2 : 1, Table 1) were similar to those of CD-Py in $\text{CH}_3\text{CN}/\text{H}_2\text{O}$ (3/1).

Fig. 1B shows the emission response of CS2@KP/CD-Py (QD/CD-Py molar ratio of 1/1000) to a fixed amount ($6 \times 10^{-5} \text{ M}$, CD-Py/analyte molar ratio of 1/2) of the different analytes, demonstrating that the sensing systems can be implemented for many substrates provided that they associate to the cyclodextrin with a binding constant that allows the displacement of the ketoprofen units of the QD. The effect of the addition of CD on the emission of CS2@KP/CD-Py/analyte was also analysed. The emission of the QD decreased because of the

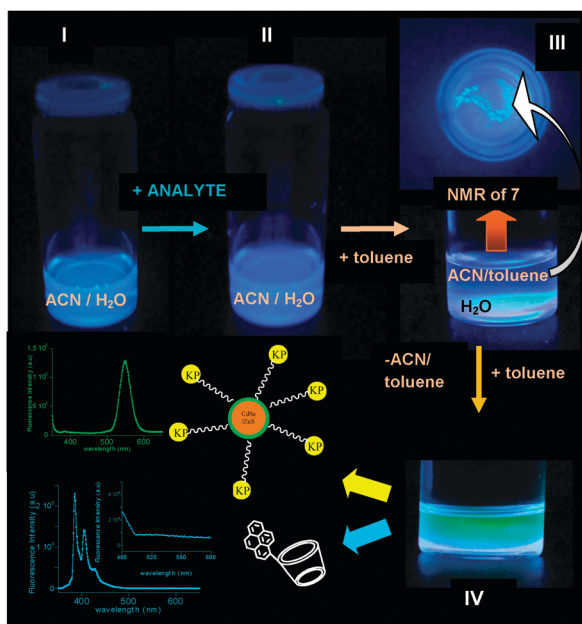


Fig. 2 Recovery of the QD, β -CD-Py, and **7**, once the assay of molecular recognition was complete.

competitive formation of analyte/CD and analyte/CD-Py host-guest complexes (Fig. 1B).

The pyrene-functionalisation of the cyclodextrin secondary face plays a role in its binding ability. Thus, for example, the relative sensitivity of the supramolecular system emission to the presence of analyte **1** vs. analyte **2** was considerably larger than the ratio between the association constants of these analytes with natural CD.^{16,20}

A preliminary assay showed that the presence of a given concentration of benzophenone did not cause an appreciable effect on indole response (Fig. S9, ESI[†]).

Finally, a control experiment was performed on the individual recovery of CD-Py, the QD, and the analyte once the assay of molecular recognition was complete (see Fig. 2). Vial I, containing a 5.25 mL acetonitrile/water (3/1) solution of CD-Py and CS2@KP (3.03×10^{-5} M and 3.03×10^{-8} M, respectively), mainly showed the blue-fluorescence of CD-Py. Vial II corresponded to the molecular recognition assay of analyte **7** (6.06×10^{-5} M, analyte dissolved in 57 μ L of toluene).

Once the molecular recognition experiment was complete, the aim was to recover the three elements. Addition of toluene (250 μ L) to vial II caused separation of the solution into two phases, migration of acetonitrile to the toluene phase, and separation of the QD in the interphase (see vial III, upper view picture), due to the low solubility of the QD in both the organic and the aqueous phases. Then, the organic phase was separated and the solvent evaporated; the ¹H NMR spectrum of the residue demonstrated the recovery of **7** (Fig. S10, ESI[†]). After separation of the organic phase from vial III, addition of 4 mL of toluene led to the QD transfer to the organic solution (vial IV). The fluorescence spectrum of the organic phase evidenced the recovery of CS2@KP (Fig. 2)

while that of the aqueous phase showed the recovery of CD-Py (Fig. 2). The absence of **7** in the aqueous phase was corroborated by ¹H NMR and MS/GC. The experiment was also performed on a large scale (ten-fold) leading to similar results to those described above.

In summary, herein we report a simple preparation of supramolecular QD/CD systems based on the effective recognition between the QD periphery and a β -cyclodextrin with an appended QD quencher (pyrene). The CD can be transferred in and out of the aqueous solution upon complexation and decomplexation with an analyte. The generality of the strategy is demonstrated using quantum dots from different sources (homemade and several commercially available). These studies demonstrate the impressive applicability of these supramolecular QD/CD systems as effective molecular sensors. Moreover, all the components of the assay (CS@KP, CD-Py, and the analyte) can be recovered individually, which is highly desirable both from the commercial and environmental points of view.

We thank MEC (Project CTQ2008-06777-CO2-01, contract granted to J. A.-S., and RyC contract granted to R.E.G), GVA (Project GVACOMP/2011/269), and the Andalusian Government (Consejería de Economía, Innovación y Ciencia-Junta de Andalucía, grants FQM-3141 and FQM-6903) for their support.

Notes and references

- M. G. S. Hyldahl, T. Bailey and B. P. Wittmerhaus, *Sol. Energy*, 2009, **83**, 566.
- X. Michalet, F. F. Pinaud, L. Bentolila, J. M. A. Tsay, S. Doose, J. J. Li, G. Sundaresan, A. M. Wu, S. S. Gambhir and S. Weiss, *Science*, 2005, **307**, 538.
- A. P. Alivisatos, *Nat. Biotechnol.*, 2004, **22**, 47.
- F. Chen and D. Gerion, *Nano Lett.*, 2004, **4**, 1827.
- Y. Chen and Z. Rosenzweig, *Anal. Chem.*, 2002, **74**, 5132.
- R. Freeman, T. Finder, L. Bahshi and I. Willner, *Nano Lett.*, 2009, **9**, 2073.
- Comprehensive Supramolecular Chemistry Cyclodextrins*, ed. J. Szejtli and T. Osa, Pergamon, Berlin, 1996, vol. 3.
- V. T. D'Souza and K. B. Lipkowitz, *Chem. Rev.*, 1998, **98**, 1741.
- Cyclodextrins and Their Complexes*, ed. E. Dodziuk, Wiley-VCH, Weinheim, 2006.
- X. Chen, L. Hong, X. X. You, Y. Wang, G. Zou, W. Su and Q. Zhang, *Chem. Commun.*, 2009, 1356.
- T. Ogoshi and A. Harada, *Sensors*, 2008, **8**, 4961.
- S. Hu, Z. B. Shang and W. J. Jin, *Supramol. Chem.*, 2010, **22**, 554.
- P. Shahgaldian and U. Pieles, *Sensors*, 2006, **6**, 593.
- K. Palaniappan, S. A. Hackney and J. Liu, *Chem. Commun.*, 2004, 2704.
- H. Li and C. Han, *Chem. Mater.*, 2008, **20**, 6053.
- G. Marconi, E. Mezzina, I. Manet, F. Manoli, B. Zambelli and S. Monti, *Photochem. Photobiol. Sci.*, 2011, **10**, 48.
- The broad ¹H NMR signals indicated that the ligand was strongly bound to the QD surface; see: X. Ji, D. Copenhaver, C. Sichmeller and X. Peng, *J. Am. Chem. Soc.*, 2008, **130**, 5726.
- It has been reported that 1-ethynylpyrene is more easily reduced than pyrene ($E_{1/2}$ values of -1.78 V and -2.07 V vs. Ag/AgCl, respectively); A. C. Benniston, A. Harriman, D. J. Lawrie and S. A. Rostron, *Eur. J. Org. Chem.*, 2004, 2272.
- C. Bohne, E. B. Abuin and J. C. Scaiano, *J. Am. Chem. Soc.*, 1990, **112**, 4226.
- G. Perrot, B. Cheng, K. D. Gibson, J. Vala, K. A. Palmer, A. Nayum, B. Maigret and M. A. Scheraga, *J. Comput. Chem.*, 1992, **13**, 1.

Quantum Dot/Cyclodextrin supramolecular systems based on efficient molecular recognition and their use for sensing

Jordi Aguilera-Sigalat, Juan M. Casas-Solvas, Maria C. Morant-Miñana, Antonio Vargas-Berenguel, Raquel E. Galian, and
Julia Pérez-Prieto

Electronic Supplementary Information

TABLE OF CONTENTS

Title	page
Experimental section	S2
Figure S1. Preparation of CD-Py and CS@KP QDs	S6
Figure S2. A CS@KP/CD-Py supramolecular system	S7
Figure S3. Absorption spectrum of a deaerated acetonitrile/water (3/1) solution of CD-Py .	S7
Table S1. Photophysical properties of CS and CS@KP QDs in toluene.	S8
Figure S4. ¹ H-NMR spectrum of CS2@KP in CDCl ₃	S9
Figure S5. Comparative absorbance spectra of deaerated acetonitrile/water (3/1) solutions of CS3@KP and CS3@KP/CD-Py system.	S10
Table S2. Fluorescence properties of CS and CS@KP QDs in ACN/H ₂ O (3/1), both in the presence and in the absence of CD and CD-Py	S11
Figure S6- Comparative fluorescence spectra of deaerated acetonitrile/water (3/1) solutions of CS3@KP, CS3@KP/CD-Py and CS3@KP/CD	S12
Figure S7-S8. Transient absorption spectra of deaerated acetonitrile/water (3/1) solutions of CD-Py and CS2@KP/CD-Py 1.12, 2.72, and 8.8 μs after the laser pulse lamp (355 nm).	S13
Figure S9. Analysis of the response of the CS2@KP/CD-Py fluorescence to increasing amounts of indole in the presence and in the absence of analyte 1	S14
Figure S10. ¹ H-NMR in CDCl ₃ of 7 , recovered in the toluene/acetonitrile organic phase after the molecular sensing assay.	S14
References	S15

Experimental Section

Materials. All reagents were commercially available and used as received. The reagents were purchased from Sigma-Aldrich. Solvents were dried according to literature procedures.¹ Core-shell QDs capped with long-chain primary amine were purchased from Evident Technologies (www.evidenttech.com) and from Ocean NanoTech (www.oceannanotech.com). Solvents for chromatography (ethyl acetate and hexane) were reagent grade and used without further purification. Distilled water (mili-Q) was used for the experiments.

Characterization. TLC was performed on Merck Silica Gel 60 F₂₅₄ aluminium sheets and developed by UV light and ethanolic sulfuric acid (5 % v/v). Flash column chromatography was performed on Merck Silica Gel (230-400 mesh, ASTM). Melting point was measured on a Büchi B-450 melting point apparatus and is uncorrected. Optical rotation was recorded on a Jasco P-1030 polarimeter at room temperature. $[\alpha]_D$ value is given in $10^{-1} \text{ deg cm}^2 \text{ g}^{-1}$. IR spectra were recorded on a Mattson Genesis II FTIR. ¹H, ¹³C and 2D NMR spectra (gCOSY, gHMQC and gHMBC) were recorded on Bruker Avance DPX300 spectrometer equipped with a QNP ¹H/¹³C/¹⁹F/³¹P probe. Standard Bruker software was used for acquisition and processing routines. Chemical shifts are given in ppm and referenced to internal TMS (δ_H and δ_C 0.00). *J* values are given in Hz. MALDI-TOF mass spectrum was recorded on an Applied Biosystems Voyager DR-RP spectrometer using α -cyano-4-hydroxycinnamic acid as matrix.

UV-vis spectra of the samples were recorded using a quartz cuvettes in a UV-visible spectrophotometer Agilent 8453E. Steady-state fluorescence spectra were measured on a spectrofluorometer PTI, equipped with a lamp power supply (LPS-220B, motor driver (MD-5020), Brytebox PTI and working at room temperature. The average diameter value of the nanoparticles was estimated following the Peng *et al.*² procedure. The Felix 32 Analysis software was used to register the data. The excitation wavelength for the emission spectra was fixed at 450 nm for QD excitation and 343

nm for pyrene excitation. Laser flash photolysis (LFP) studies were performed on a pulsed Nd:YAG laser, using 355 nm as excitation source. The pulses width was ca. 10 ns, and the energy was ca. 15 mJ/pulse. A xenon lamp was employed as the detecting light source. The apparatus consisted of the pulsed laser, the Xe lamp, a monochromator, and a photomultiplier (PMT) system. The output signal from the oscilloscope was transferred to a personal computer. Samples of CS (3 mL) were prepared such that they absorbed ca. 0.3 at 355 nm and they were bubbled with N₂ for 10 min.

2^I-O-{3-[1-pyrenyl]-propyn-1-yl}cyclomaltoheptaose. A solution of 1-bromopyrene³ (65 mg, 0.235 mmol) and 2^I-O-propargylcyclomaltoheptaose⁴ (300 mg, 0.256 mmol) in dry piperidine (36 mL) was degassed by bubbling N₂ under sonication for 30 minutes. [Pd(PPh₃)₂Cl₂] (27 mg, 0.024 mmol) was then added and the mixture was heated at 75 °C in the dark. After 30 minutes, CuI (4 mg, 0.024 mmol) was also added before the solution was stirred at that temperature for 17 h in the dark. The solvent was removed by evaporation under vacuum and the crude product was purified by column chromatography (CH₃CN-H₂O-(30 % v/v aq NH₃) 8:2:1) to yield 2^I-O-{3-[1-pyrenyl]-propyn-1-yl}cyclomaltoheptaose (170 mg, 0.122 mmol, 52 %) as a yellowish solid: mp 256 °C dec; [α]_D +46 (c 0.25, H₂O); IR (KBr): 3421, 2926, 1638, 1151, 1116, 1032, 618 cm⁻¹; ¹H NMR (300 MHz; DMSO-*d*₆, ppm) δ 8.61 (d, 1H, *J* = 9.2 Hz, Pyr), 8.38-8.12 (m, 8H, Pyr), 6.03-6.00 (m, 2H, OH), 5.81-5.70 (m, 11H, OH), 5.20 (d, 1H, ³*J* = 3.0 Hz, H-1^I), 4.99 (d, 1H, ²*J* = 16.1 Hz, CHO), 4.91-4.84 (m, 7H, CHO, H^{II-VII}), 4.75 (s, 1H, OH), 4.54-4.44 (m, 6H, OH), 3.92 (t, 1H, *J* = 9.5 Hz, H-3^I), 3.71-3.51 (m, 29H, H-2^I, 3^{II-VII}, 4^I, 6^{I-VII}, 6^{I-VII}), 3.42-3.27 (m, H-2^{II-VII}, 4^{II-VII}, overlapped with HDO); ¹³C NMR (75 MHz; DMSO-*d*₆, ppm) δ 131.3, 131.0, 130.7, 130.5, 129.7, 128.9, 128.5, 127.2, 126.8, 126.0, 125.0, 124.9, 123.5, 123.2, 116.2 (Pyr), 102.0-101.7 (C-1^{II-VII}), 100.0 (C-1^I), 91.5 (CH₂C≡), 84.8 (≡C-Pyr), 82.3, 81.6-81.3 (C-4^{I-VII}), 79.6 (C-2^I), 73.3-71.8, 70.2 (C-2^{II-VII}, 3^{I-VII}, 5^{I-VII}), 60.0-59.9 (C-6^{I-VII}), 59.7 (CH₂O); MALDI-TOF-MS *m/z* calcd for C₆₁H₈₀O₃₅ 1372.45, found 1395.03 (M + Na)⁺.

Synthesis of CS. Fluorescent CdSe nanocrystals were synthesized by Peng *et. al.*⁵ procedure with some modifications. Briefly, a mixture of 2.3 mmol of CdO, 0.7 mmol of TDPA, and 9.1 mmol of TOPO was heated gradually up to 320 °C in a three-neck flask under N₂ flow. The reaction was maintained at this temperature for 10-15 min, until the solution was clear. Then, the reaction was cooled to 270 °C, and 1.2 mL of the SeTOP was quickly injected (SeTOP mixture was prepared by the addition of 0.3 mmol of Se and 3.4 mmol of TOP under N₂ flow at 70 °C). When the reaction turned orange the nanocrystals were precipitated in cool MeOH and purified several times by centrifugation with MeOH to remove the excess of starting materials. Finally, the QDs were re-dispersed in toluene.

The synthesis of core-shell CdSe/ZnS QDs (CS) was done following the Bawendi's procedure⁶ with some modifications. For a typical reaction, 5 g of TOPO were heated up to 190°C in three-neck flask for 2 h under Ar flow. Then, the solution was cooled to 60 °C and 0.5 mL of TOP was added into the flask. After that, 2 mL of QD was added and the reaction was heated to 140 °C. Then, the shell was added drop-wise for 10 min. For the shell, 440 µL of ZnEt₂, 65 µL of (TMS)₂S, and 2600 µL of TOP were mixed in a glove box under N₂ flow. Then, the reaction was cooled to 90 °C and kept at this temperature for 3 h. For the purification, the CdSe/ZnS QDs were precipitated in MeOH several times. Finally, CS was redissolved in toluene.

Synthesis of 11-mercaptoundecyl-2-(3-benzoylphenyl)propanoate (KP-SH). The KP-SH ligand was prepared following an esterification method described in the literature. In brief, ketoprofen (500 mg, 2.0 mmol) and 11-mercapto-1-undecanol (402 mg, 2.0 mmol) were dissolved in anhydride toluene (24 mL). A complex of hafnium/THF (1.8 mg) was added and the mixture was heated for 48 h under azeotropic reflux conditions to remove water through a Soxhlet thimble with 3 Å molecular sieves. In order to quench the reaction, 1 mL of water was added. The product was purified by column

chromatography performed on silica gel 60 (230-400 mesh) using a 10:1 mixture of hexane:ethyl acetate. The compound was obtained in a 81% yield. ^1H NMR (300 MHz, CDCl_3): δ 1.00-1.34 (m, 14H), 1.25 (t, $J=7.7$ Hz; 1H), 1.45-1.57 (m, 7H), 2.43 (q, $J=7.1$ Hz; 2H), 3.73 (q, $J=7.2$ Hz; 1H), 3.99 (t, $J=6.7$ Hz; 2H), 7.33-7.55 (m, 5H), 7.60 (dt, $J=6.2$ Hz, $J=1.5$ Hz; 1H), 7.67-7.75 (m, 3H) ppm.

Ligand exchange of the CS ligand by thiol. For the exchange ligand procedure, 1 mL of CS and 143 mg of KP-SH (molar ratio between CS/ligand is 1/5000) were added in a flask and heated up to reflux in 40 mL of chloroform for 48 h, under N_2 flow in absence of light. Then, the reaction was cooled down to room temperature. For the purification, the nanocrystals were precipitated in MeOH several times. Finally, the CS@KP obtained was dissolved in toluene.

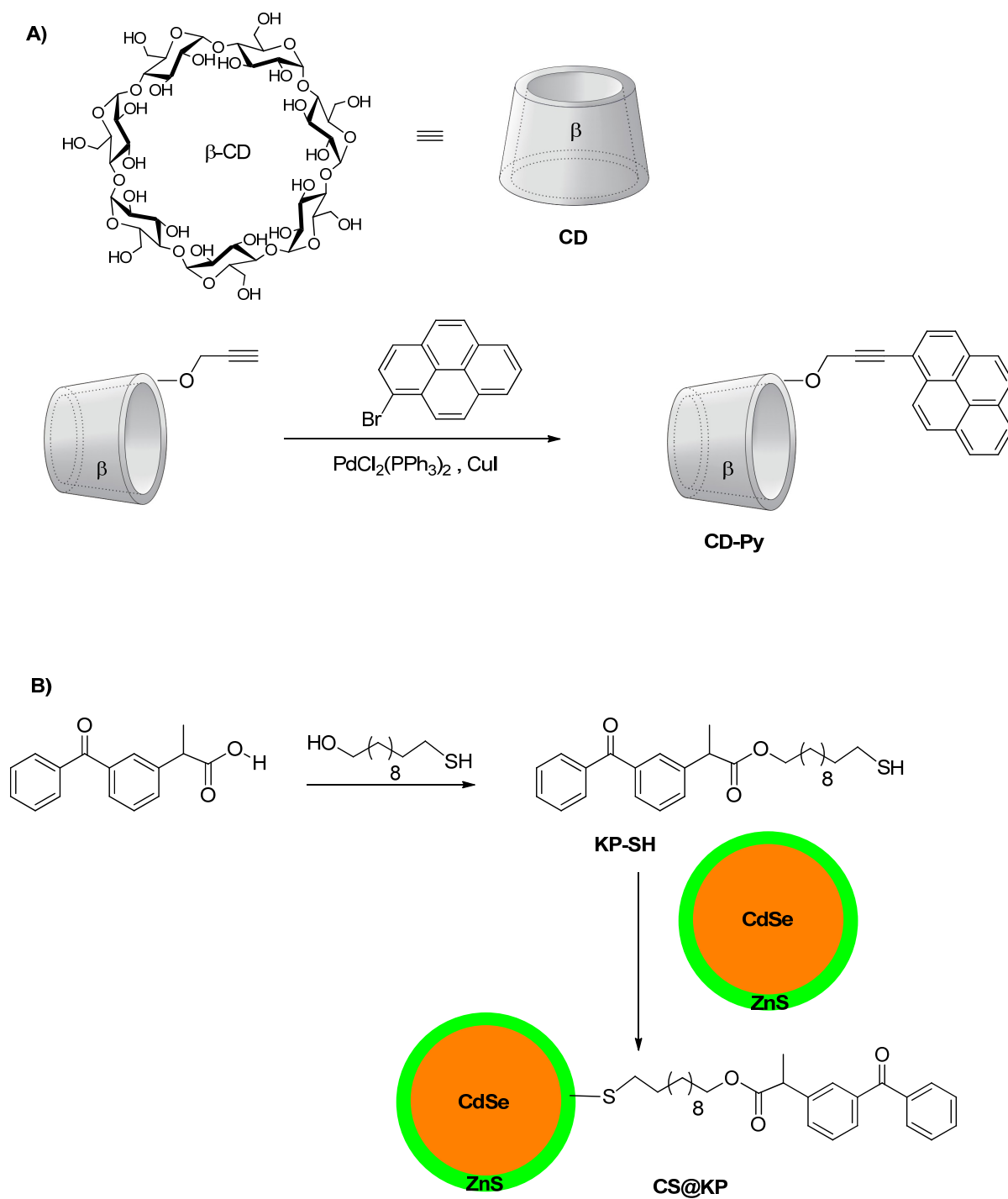


Fig. S1. Preparation of CD-Py and CS@KP QDs

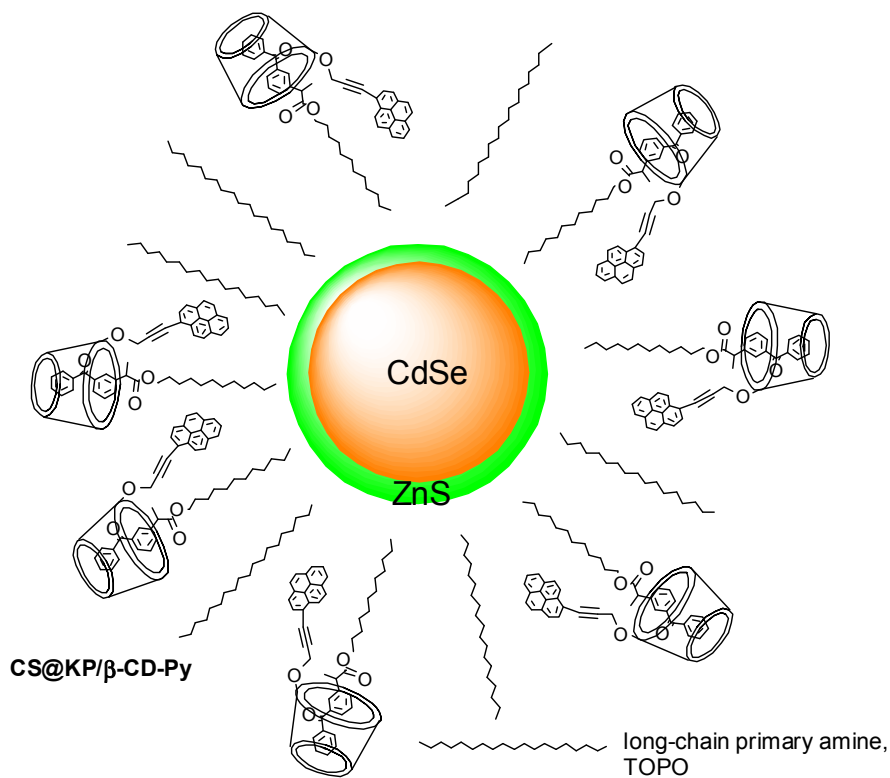


Fig. S2. A CS@KP/CD-Py supramolecular system

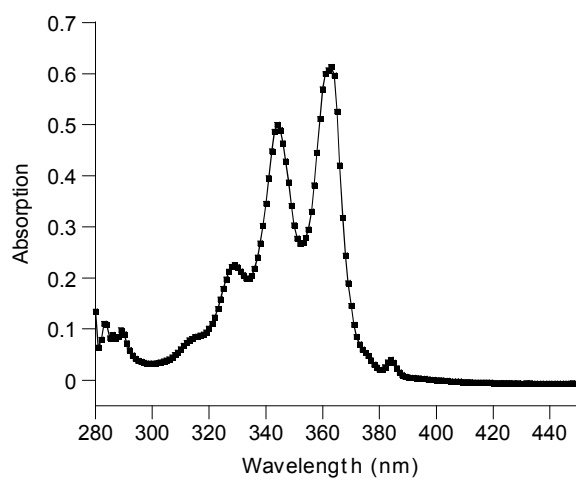


Fig. S3. Absorption spectrum of a deaerated acetonitrile/water (3/1) solution of CD-Py (5×10^{-5} M).

Table S1. Photophysical properties of CS and CS@KP QDs in toluene.

	λ_{abs} (nm)	λ_{em} (nm)	$\phi_{\text{f}}^{\text{a}}$	D (nm)
CS1	521	539	0.61	2.65
CS1@KP	519	541	0.56	2.55
CS2	544	562	0.55	2.93
CS2@KP	543	561	0.51	2.92
CS3	555	571	0.25	3.14
CS3@KP	553	572	0.10	3.10
CS4	541	549	0.34	2.87
CS4@KP	541	550	0.13	2.87

^aQuantum dot fluorescence quantum yield was calculated by comparing the integrated emission spectra of the QD and fluorescein ($\phi_{\text{f}} = 0.87$, NaOH 0.1 M, $\lambda_{\text{exc}} = 465$ nm) according to the procedure described by Resch-Genger *et al.*⁷

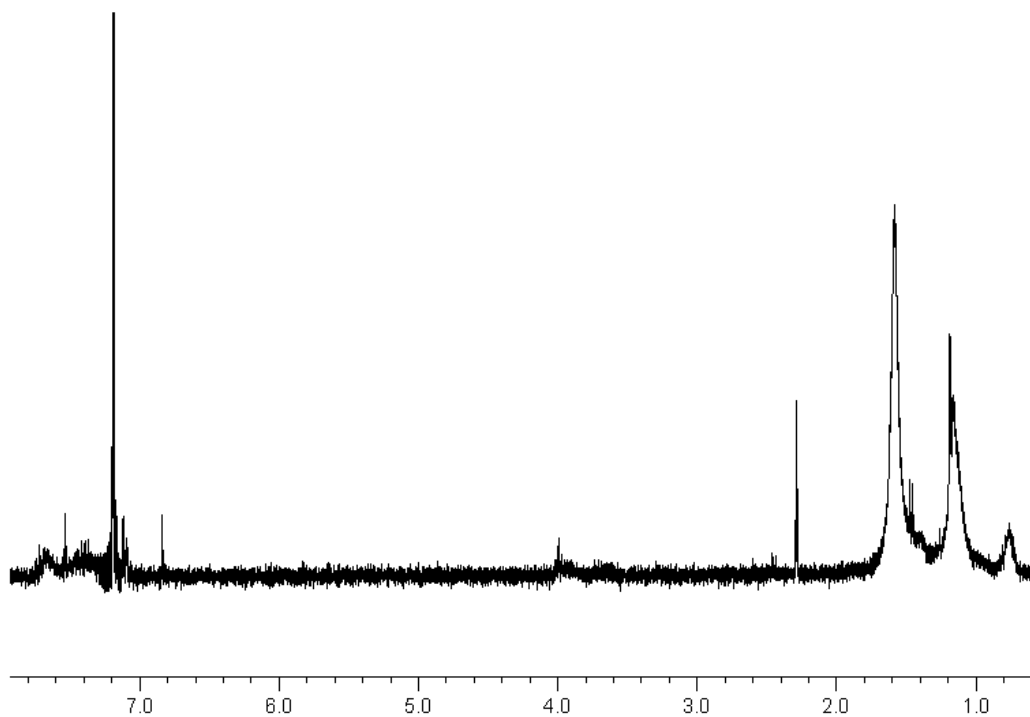


Fig. S4. ¹H-NMR spectrum of CS₂@KP in CDCl₃.

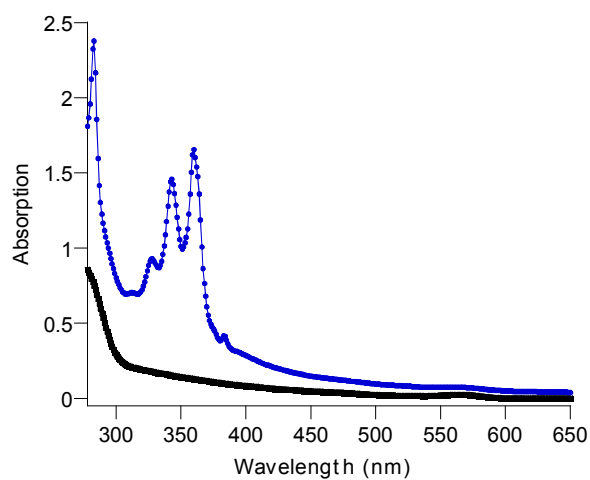


Fig. S5. Comparative absorbance spectra of deaerated acetonitrile/water (3/1) solutions of **CS3@KP** (4×10^{-7} M, ■) and **CS3@KP/CD-Py** system ($[CS] = 4 \times 10^{-7}$ M, ratio CS/CD = 1/1000, ●)

Table S2. Fluorescence properties (quantum yield, Φ_f , and maximum of the emission peak, λ_{em} , of the emission) of CS and CS@KP QDs in ACN/H₂O (3/1), both in the presence and in the absence of CD and CD-Py.

System	(CD/QD molar ratio)	Φ_f^a			λ_{em}^b (nm)		
		-	CD-Py	CD	- ^c	CD-Py	CD
CS1@KP		0.56			549		
	(1000/1)		0.05	0.64		544	548
CS2@KP		0.51			569		
	(1000/1)		0.11	0.53		564	569
CS3@KP		0.10			572		
	(1000/1)		<0.01	0.12		-	572
CS4@KP		0.13			550		
	(1000/1)		<0.01	0.11		-	550
	(3000/1)		<0.01	0.12		-	550
CS2		0.58			551		
	(1000/1)		0.53	0.60		553	-
CS3		0.34					
	(1000/1)		0.31	-	552	551	551

[CS1@KP] = 3.85×10^{-7} M; [CS2@KP] = 3.1×10^{-8} M; [CS3@KP] = 5.2×10^{-7} M; [CS4@KP] = 1.8×10^{-7} M; [CS2] = 4.8×10^{-8} M; [CS3] = 6.3×10^{-8} M. ^aThe fluorescence quantum yield was calculated by following the procedure of Resch-Genger *et al.* (ref. 4 of Supporting Information). ^bMaximum of fluorescence intensity was calculated at $\lambda_{ex} = 450$ nm. ^cThe observed red-shift of the fluorescence maximum of the CS was expected due to a change in the solvent dielectric constant.⁸

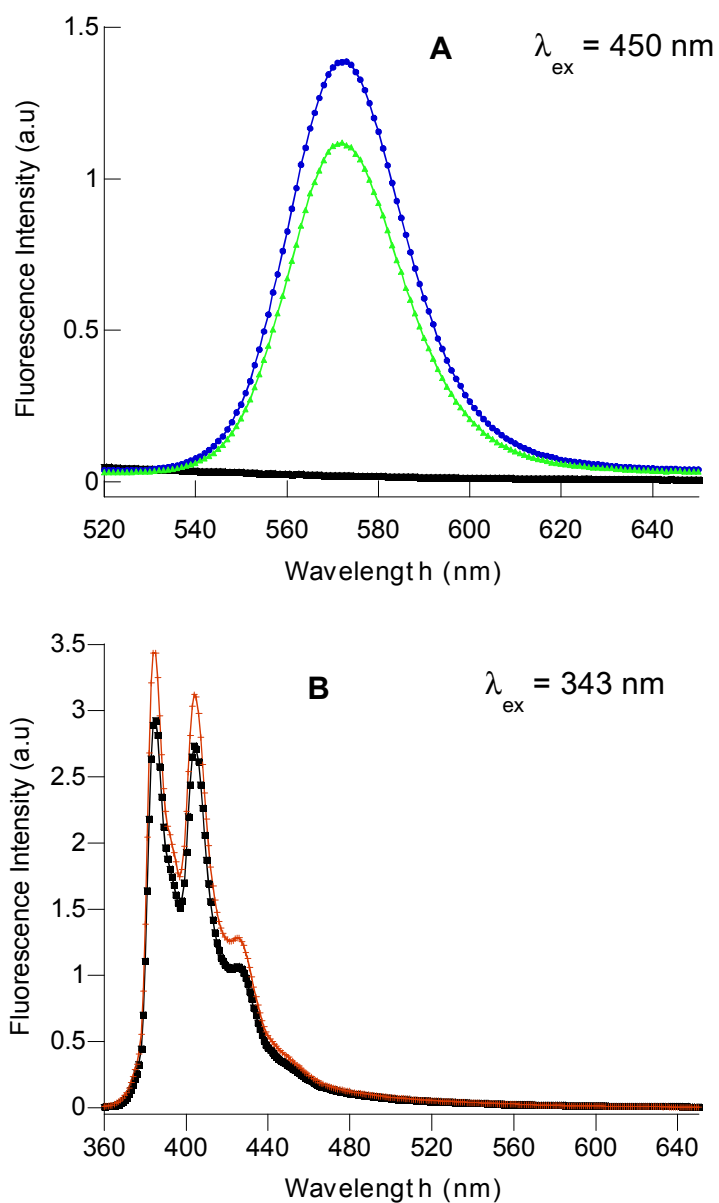


Fig. S6. A: Comparative fluorescence spectra ($\lambda_{ex} = 450 \text{ nm}$) of deaerated acetonitrile/water (3/1) solutions of **CS3@KP** ($4 \times 10^{-7} \text{ M}$, \blacktriangle), **CS3@KP/CD-Py** ($[\text{QD}] = 4 \times 10^{-7} \text{ M}$, $[\text{CD}] = 4 \times 10^{-4} \text{ M}$, \blacksquare), and **CS3@KP/CD** ($[\text{QD}] = 4 \times 10^{-7} \text{ M}$, $[\text{CD}] = 4 \times 10^{-4} \text{ M}$, \bullet). **B:** Comparative fluorescence spectra of deaerated acetonitrile/water (3/1) solutions of **CS3@KP/CD-Py** ($[\text{QD}] = 4 \times 10^{-7} \text{ M}$, $[\text{CD}] = 4 \times 10^{-4} \text{ M}$, \blacksquare) and **CD-Py** ($4 \times 10^{-4} \text{ M}$, $+$) at $\lambda_{ex} = 343 \text{ nm}$.

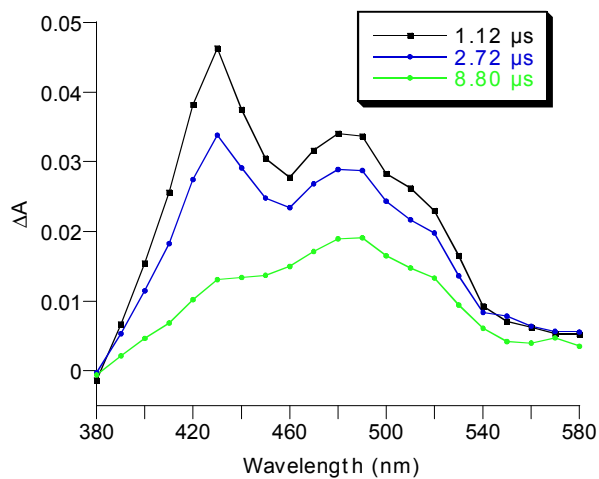


Fig. S7. Transient absorption spectra of a deaerated acetonitrile/water (3/1) solution of **CD-Py** (1.11×10^{-4} M) 1.12, 2.72, and 8.8 μ s after the laser pulse lamp (355 nm).

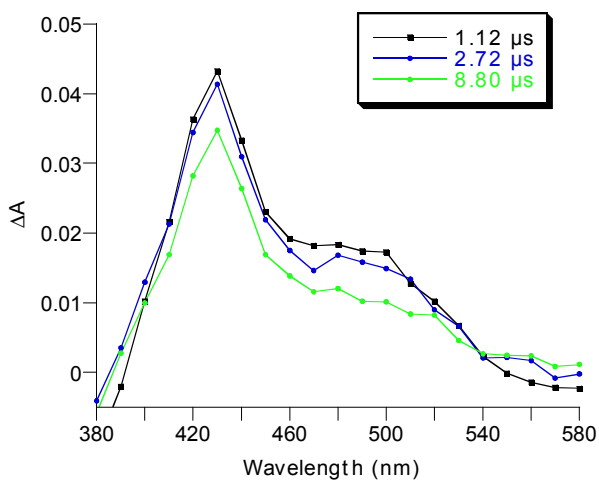


Fig. S8. Transient absorption spectra of a deaerated acetonitrile/water (3/1) solution of **CS₂@KP/CD-Py** ([CS] = 1.11×10^{-7} M, [CD-Py] = 1.11×10^{-4} M) 1.12, 2.72, and 8.8 μ s after the laser pulse lamp (355 nm).

assay.

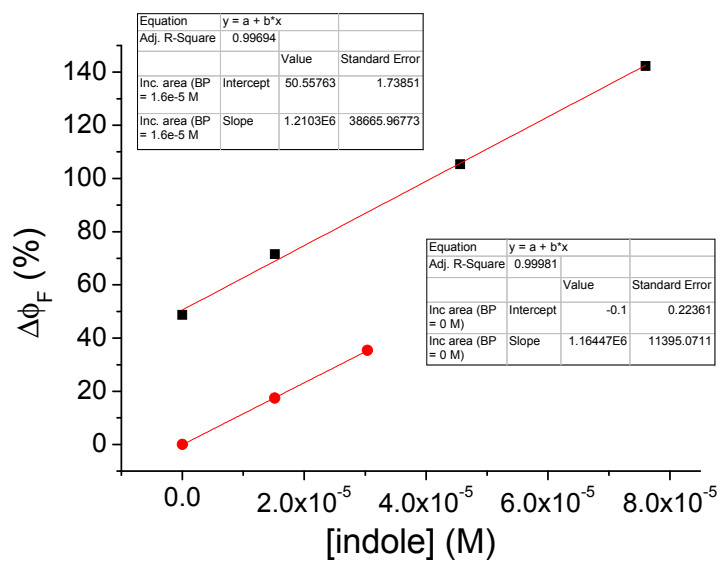


Fig. S9. Analysis of the response of the **CS2@KP/CD-Py** fluorescence to increasing amounts of indole in the presence (■) and in the absence (●) of analyte 1.

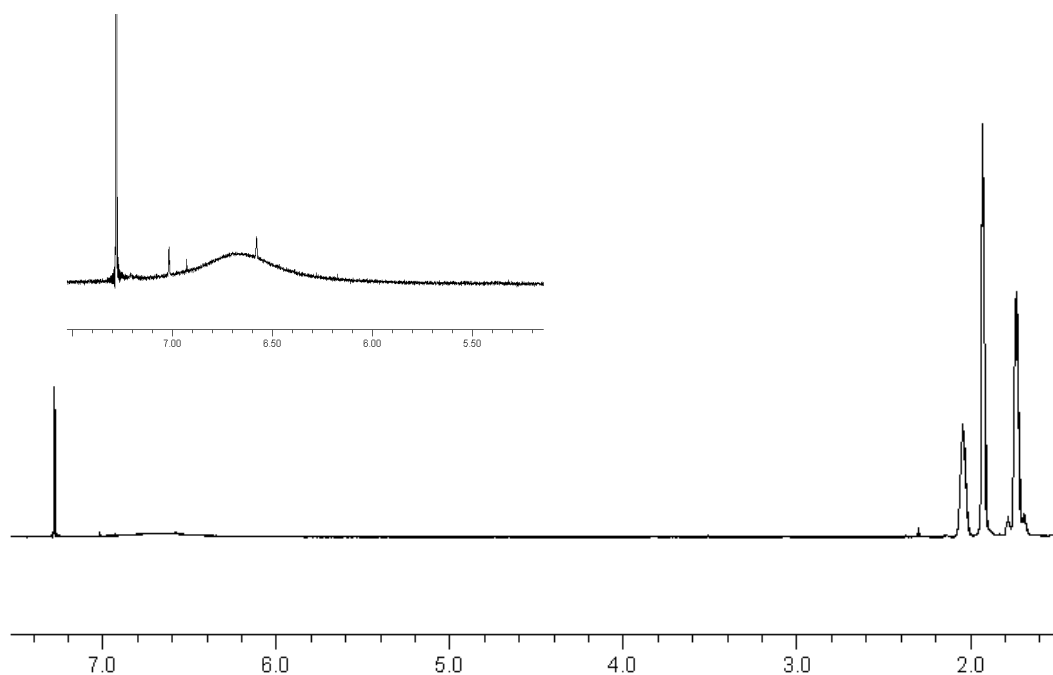


Fig. S10. $^1\text{H-NMR}$ in CDCl_3 of **7**, recovered in the toluene/acetonitrile organic phase after the molecular sensing

REFERENCES

-
- ¹ Perrin, D. D.; Armarego, W. F. L. *Purification of Laboratory Chemicals*, 3rd ed.; Pergamon Press: Oxford, **1989**.
- ² Yu, W. W.; Qu, L.; Guo, W.; Peng, X. *Chem. Mater.* **2003**, *15*, 2854-2860
- ³ Gumprecht, W. H. *Organic Syntheses*, **1968**, *48*, 30-31.
- ⁴ Casas-Solvas, J. M.; Ortiz-Salmerón, E.; Fernández, I.; García-Fuentes, L.; Santoyo-González, F.; Vargas-Berenguel, A. *Chem.-Eur. J.* **2009**, *15*, 8146-8162.
- ⁵ Peng, Z. A.; Peng, X. *J. Am. Chem. Soc.* **2001**, *123*, 183-184
- ⁶ Dabbousi, B. O.; Rodriguez-Viejo, J.; Mikulec, F. V.; Heine, J. R.; Mattoussi, H.; Ober, R.; Jensen, K. F. and Bawendi, M. G.; *J. Phys. Chem. B*, **1997**, *101*, 9463
- ⁷ Grabolle, M.; Spieles, M.; Lesnyak, V.; Gaponik, N.; Eychmüller, A. and Resch-Genger, U.; *Anal. Chem.*, **2009**, *81*, 6285-6294
- ⁸ Leatherdale, C. A.; Bawendi, M. G. *Phys. Rev. B: Condens. Matter Mater. Phys.* **2001**, *63*, 165315.

Further Insight into the Photostability of the Pyrene Fluorophore in Halogenated Solvents

Jordi Aguilera-Sigalat,^[a] Jaime Sanchez-SanMartín,^[a] Carlos E. Agudelo-Morales,^[a] Elena Zaballós,^[b] Raquel E. Galian,^{*,[a, c]} and Julia Pérez-Prieto^{*,[a]}

Pyrene fluorophores of pyrene-functionalized CdSe quantum dots (QD@Py), as well as alkylpyrene and pyrene itself (Py), undergo fast degradation in aerated chloroform under ultraviolet-A (UV-A, $316 < \lambda < 400$ nm) illumination. Steady-state fluorescence studies of irradiated chloroform solutions of QD@Py show formation of new bands, red-shifted compared to that of the pyrene moiety. Similar behaviour is observed for pyrene and the alkylpyrene system. Column chromatography of the pyrene photolysate in chloroform allowed us to isolate photoproducts arising from pyrene degradation, and to obtain information on the structure of the photoproducts responsible for the emission bands. The most predominant photoproducts were those originating from the reaction of pyrene with dichloromethyl radicals. The phototransformation of QD@Py and the alkylpyrene involves mainly detachment of the alkyl chain from the aromatic ring, induced also by dichloromethyl radi-

cals, and oxidation of the alkyl chain at the benzylic position was detected as well. By contrast, these pyrene systems show a high photostability in aerated dichloromethane. Transient absorption measurements showed formation of both pyrene triplet and pyrene radical cation for all pyrene systems in these halogenated solvents. The yield of pyrene radical cations for Py is higher than for QD@Py and the alkylpyrene. In addition, pyrene radical cations were longer-lived in dichloromethane than in chloroform. The reason for the pyrene photostability in dichloromethane is the different reactivity of chloromethyl and dichloromethyl radicals towards pyrene and oxygen. These studies show that the use of dichloromethane can be a suitable alternative to chloroform when the good solubility properties of these halogenated solvents are needed to dissolve pyrene when this chromophore is used as a fluorescent probe.

1. Introduction

Pyrene chromophores are widely used as probes because of 1) their absorption (strength) features, 2) their considerably long singlet lifetime (> 100 ns)^[1] and the information that can be obtained from their fluorescence emission (I_3/I_1 ratio, the excimer-to-monomer ratio, and the polarization value), and 3) their long-lived pyrene radical cation (microsecond scale). Thus, these chromophores have been applied as probes to acquire information about the structure and dynamics of macromolecular systems,^[2–5] surface properties, and adsorption sites. They have also been used in fluorescent chemosensors that can recognize selectively chemical species (ions, oxygen, explosives,...) in potential analytical applications.^[6]

Pyrene undergoes significant photodegradation in several media (adsorbed onto cellulose and silica,^[7] or dissolved in methanol and acetic acid among others^[8–10]), that can have drastic effects on the accuracy of the analysis under consideration. In this respect, there is special concern about the use of this fluorophore in halogenated solvents.^[2] Yamada et al.^[11] have performed gas chromatography-mass spectrometry (GC/MS) analyses of photolysates, resulting from illumination of an mM pyrene chloroform solution using UV ($\lambda > 250$ nm) and sun-light. The formation of two isomeric pyrenecarboxaldehydes (one of them identified as 1-pyrenecarboxaldehyde), 1-chloropyrene, and a monooxygenated adduct of chloropyrene (whose structure is unknown) has been reported. Pyrene showed less photostability in the presence of oxygen than ni-

trogen, leading to a major formation of aldehydes. In spite of that, the pyrene chromophore is still used in chloroform for applications related to its fluorescent properties, because of its good solubility properties.^[12]

Interestingly, even though pyrene quickly transforms into stable photoproducts (whose structures have not been studied) when irradiated ($\lambda_{\text{exc}} = 338$ nm) in CCl_4 ,^[13] its photodegradation quantum yield in dichloromethane^[14] ($\lambda_{\text{exc}} = 311$ nm, high-pressure lamp in combination with an interference filter) is similar to that in water^[15] (1.8×10^{-3} vs 2.1×10^{-3}). The photo-

[a] J. Aguilera-Sigalat, J. Sanchez-SanMartín, C. E. Agudelo-Morales, Dr. R. E. Galian, Dr. J. Pérez-Prieto
Molecular Science Institute (ICMOL)
University of Valencia
C/Catedrático José Beltrán 2, 46980-Paterna, Valencia (Spain)
Fax: (+34) 963543274
E-mail: Julia.perez@uv.es

[b] Dr. E. Zaballós
Department Of Organic Chemistry
University of Valencia
C/Vicent Andrés Estellés sn, 46100-Burjassot, Valencia (Spain)

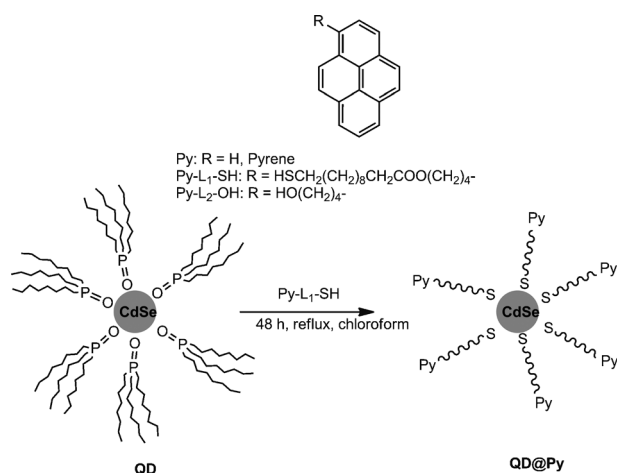
[c] Dr. R. E. Galian
Department of Analytical Chemistry
University of Valencia
C/Dr. Moliner 50, 46100, Burjassot, Valencia (Spain)
E-mail: raquel.galian@uv.es

Supporting information for this article is available on the WWW under <http://dx.doi.org/10.1002/cphc.201100843>.

chemical reaction in halogenated solvents is believed to occur through a pyrene singlet electron transfer to the solvent, followed by the reaction of the pyrene radical cation with the fragmentation products of the radical anion of the haloalkane.^[13] In water, it has been suggested that the first step involves an electron transfer from the excited singlet state of pyrene to molecular oxygen in a contact charge-transfer pair, followed by the reaction of the pyrene radical cation with water, leading to 1-hydroxypyrene as the initial photoproduct. A similar mechanism has been suggested for the photodegradation of pyrene on silica surfaces in the presence of oxygen (under simulated laboratory irradiation conditions and solar irradiation), where 1-hydroxypyrene is generated through the reaction of the pyrene radical cation with physisorbed water.^[10]

There is relatively little known about the structure of pyrene photoproducts in chloroform which renders further investigations on the photostability of pyrene-functionalized nanodevices in this solvent interesting. Such investigations will give information on the photodegradation process in halogenated solvents, so that it might be avoided.

In this study herein, we focus on a CdSe QD-pyrene nanohybrid and analyze its stability under UV-A illumination in chloroform. The influence of the nanoparticle (NP) on the outcome was studied by comparing the results of illuminating the nanohybrid with outcomes from pyrene (Py) and a 1-alkylpyrene analogue (Py-L₂-OH, Scheme 1) under the same reaction conditions. In addition, the photostability of the pyrene systems was also analyzed in dichloromethane.



Scheme 1. Structures of pyrene, Py-L₁-SH, Py-L₂-OH, and QD@Py.

Steady-state irradiations demonstrated the considerable photostability of pyrene systems in dichloromethane under UV-A illumination. Photophysical studies of these systems in chloroform and dichloromethane, together with isolated photoproducts arising from pyrene degradation in chloroform, gave solid information about the actual photodegradation process of pyrene in halogenated solvents.

2. Results and Discussion

2.1. Synthesis of Pyrene-Functionalized CdSe Nanoparticles.

Mercapto-stabilized NPs decorated with pyrene moieties (QD@Py) were prepared by reaction of QD@TOPO (TOPO: triocetyl phosphine oxide) with Py-L₁-SH^[16] (Scheme 1) under chloroform reflux ([thiol]/[QD] = 3375 molar ratio) for 48 h. After purification, the UV/Vis absorption spectrum of QD@Py showed the first exciton peak of the QD at 529 nm, as well as the presence of the pyrene moiety (Figure S1 in the Supporting Information). The size of the nanoparticle obtained by high resolution transmission electron microscopy (HRTEM) was of 2.4 ± 0.4 nm (Figure S2 in the Supporting Information). The ¹H NMR spectrum of QD@Py showed a broadening of the ligand signals, indicating that it is strongly bound to the QD surface (see spectra of Py-L₁-SH and QD@Py in Figures S3A and S3B in the Supporting Information).

2.2. Photophysical Studies

An important deactivation of the QD emission (λ_{\max} at 543 nm) was observed after the exchange of TOPO by a thiol ligand (Figure S4 in the Supporting Information), which may be due to the transfer of a hole from the excited QD to the mercapto group on the QD surface.^[17] In fact, pyrene was the main fluorophore in QD@Py. Figure 1a shows the comparison of the emission spectra of deaerated solutions of Py-L₂-OH and QD@Py in toluene. These samples were adjusted to the same pyrene absorbance at λ_{ex} 355 nm (Abs = 0.4).

These spectra evidenced the high local concentration of pyrene on the QD@Py, leading to Py excimer formation (λ_{\max} at 480 nm), while only monomer emission (λ_{\max} at 376, 396, and 417 nm) was detected for Py-L₂-OH. In addition, the CdSe core QD and oxygen strongly reduced the pyrene fluorescence quantum yield (Figure 1).^[18]

Laser flash photolysis (LFP, Nd:YAG, 355 nm, 10 ns laser pulse) of deaerated chloroform solutions of QD@Py at 355 nm (Abs ca. 0.3) showed the formation of the pyrene triplet (QD@³Py, λ_{\max} ca. 420 nm and $\tau_{\text{T}} = 7.0 \mu\text{s}$, Figure 2a and Table 1). The generation of the pyrene radical cation (QD@Py⁺, λ_{\max} ca. 450 nm, $\tau = 8.2 \mu\text{s}$) was more evident in the presence of air (Figure 2b). Py-L₂-OH led to the same transients (Figure 2c, d), that is, the pyrene triplet (³Py-L₂-OH) and the pyrene

Table 1. Lifetime of the triplet (τ_{T}) and the radical cation (τ_{RC}) of the pyrene systems.

System	τ_{T} [μs]	τ_{RC} [μs]	Solvent
Py	1.81 ± 0.02	4.09 ± 0.05	CHCl ₃
Py-L ₂ -OH	1.88 ± 0.04	7.0 ± 0.5	
QD@Py	7.0 ± 0.5	8.2 ± 0.3	
Py	1.23 ± 0.02	22.1 ± 0.4	CH ₂ Cl ₂
QD@Py	3.7 ± 0.2	24 ± 1	
Py	1.30 ± 0.01	n.d.	THF
Py-L ₂ -OH	9.3 ± 0.1	n.d.	
QD@Py	9.7 ± 0.2	n.d.	

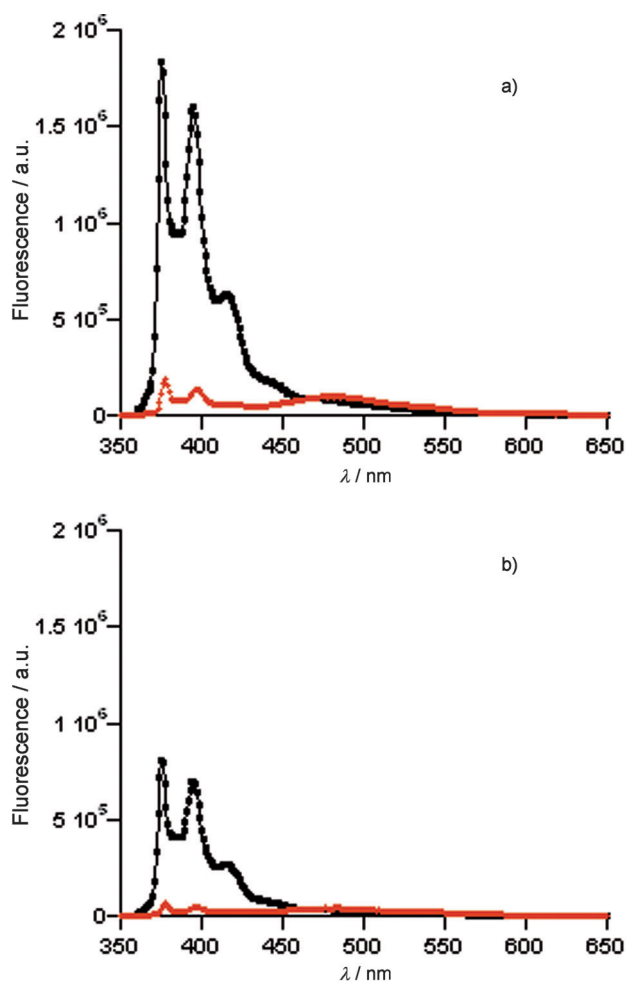


Figure 1. Fluorescence spectra of toluene solutions of Py-L₁-OH (■) and QD@Py (●) under anaerobic (a) and aerobic (b) atmosphere. The samples were adjusted to the same absorbance at 355 nm.

radical cation (Py^{•+}-L₂-OH). ³Py-L₂-OH was obtained in similar yields as from QD@Py, despite the competitive formation of the pyrene excimer in the latter system. This can be attributed to the partial decay of the excimer to produce the pyrene triplet.^[19,20]

The yield of radical cations was higher for Py (Figure 2e), but these species were shorter-lived (4.09 μs) than Py^{•+}-L₂-OH and QD@Py^{•+}. In addition, the pyrene triplet (³Py) lifetime was similar to that of Py-L₂-OH and shorter than that of QD@Py.

As expected, the triplet of all the pyrene systems was shorter-lived in aerated solutions (τ ca. 0.4 μs), while the radical cations showed low reactivity towards oxygen.

Transient absorption measurements were also performed in other solvents, such as dichloromethane. Interestingly, the lifetimes of the radical cations (τ_{RC}) of the pyrene systems (see Py^{•+} and QD@Py^{•+} in Table 1) were much longer in dichloromethane (τ_{RC} ca. 22 μs)^[21] than in chloroform. In addition, the yield of Py^{•+} was 30% lower in dichloromethane. As in the case of chloroform, the pyrene triplet was the main species for the alkylpyrene systems in dichloromethane.^[22] In tetrahydrofuran (THF), the pyrene triplet was the only detected species in all the pyrene systems.

2.3. Photostability Studies of the Pyrene Systems under UV-A-Lamp Irradiation

A Luzchem photoreactor equipped with ten lateral UV-A-lamps, emitting at 316 nm <math>\lambda < 400\text{ nm}</math> and λ_{max} at 351 nm, was used for the irradiation experiments. Samples were irradiated in 1 cm pathway quartz cells.

The photostability of QD@Py was initially analyzed in chloroform, following the changes of the UV/Vis spectra of the NPs. A brief UV-A-lamp irradiation (less than 30 min) of chloroform solutions of QD@Py, in the presence and in the absence of air, caused a drastic transformation of the whole NP. Not only the absorption bands of pyrene strongly decreased, but the exciton peak of the NP was also influenced (Figure 3).

The fluorescence spectra of the QD@Py photolysate showed a new structured band (λ_{max} at 399 and 420 nm), red-shifted compared to that of the pyrene moiety (λ_{max} at 376, 396, and 417 nm), together with broad-bands at longer wavelengths (λ_{max} at ca. 450 and 490 nm, Figure 4).

For comparative purposes, the photostability of Py-L₂-OH and Py under UV-A-lamp illumination was also studied. The absorption spectra of the Py-L₂-OH photolysates (Figures 5a and S5 in the Supporting Information) showed it leads to analogous photoproducts to those of the capping ligand of QD@Py (Figures 3 and S6 in the Supporting Information).

Similarly to the QD@Py photolysate, the emission spectra of the Py-L₂-OH photolysates showed a structured emission band (λ_{max} ca. 395 and 420 nm) together with considerably red-shifted broad emission bands (λ_{max} at 440, and a broad-emission from 450 to 525 nm). By contrast, though the appearance of the emission spectra of the photolysate of Py also evidenced a structured band with maxima at ca. 388 and 408 nm and a broad band at λ_{max} ca. 450 nm, the band from 450 to 600 nm showed a well-structured shape (Figure 5d). The evolution of the fluorescence spectra of the photolysates of the pyrene systems as a function of the irradiation time is shown in Figures S7–S9 in the Supporting Information.

In addition, experiments performed in distilled chloroform showed that the rate of pyrene transformation drastically increases in the absence of the solvent stabilizer (ethanol). Furthermore, Py-L₂-OH was also irradiated in chloroform inside the cell compartment of the spectrofluorometer. The excitation spectrum was monitored at 480 nm after 200 scans. It showed the appearance of a band in the 380–430 nm range. These results are consistent with some photodegradations of the pyrene compound under the excitation conditions typically used for photophysical measurements (Figure S10 in the Supporting Information).^[2]

Remarkably, experiments performed in amylene-free dichloromethane^[23] showed a considerable photostability of the pyrene chromophore as well as of the CdSe core of QD@Py. The QD exciton peak and the pyrene chromophore underwent a transformation that could hardly be perceived (Figure S11 in the Supporting Information) after 50 min of UV-A irradiation in the presence of air. Likewise, Py-L₂-OH and Py showed a high photostability in dichloromethane.

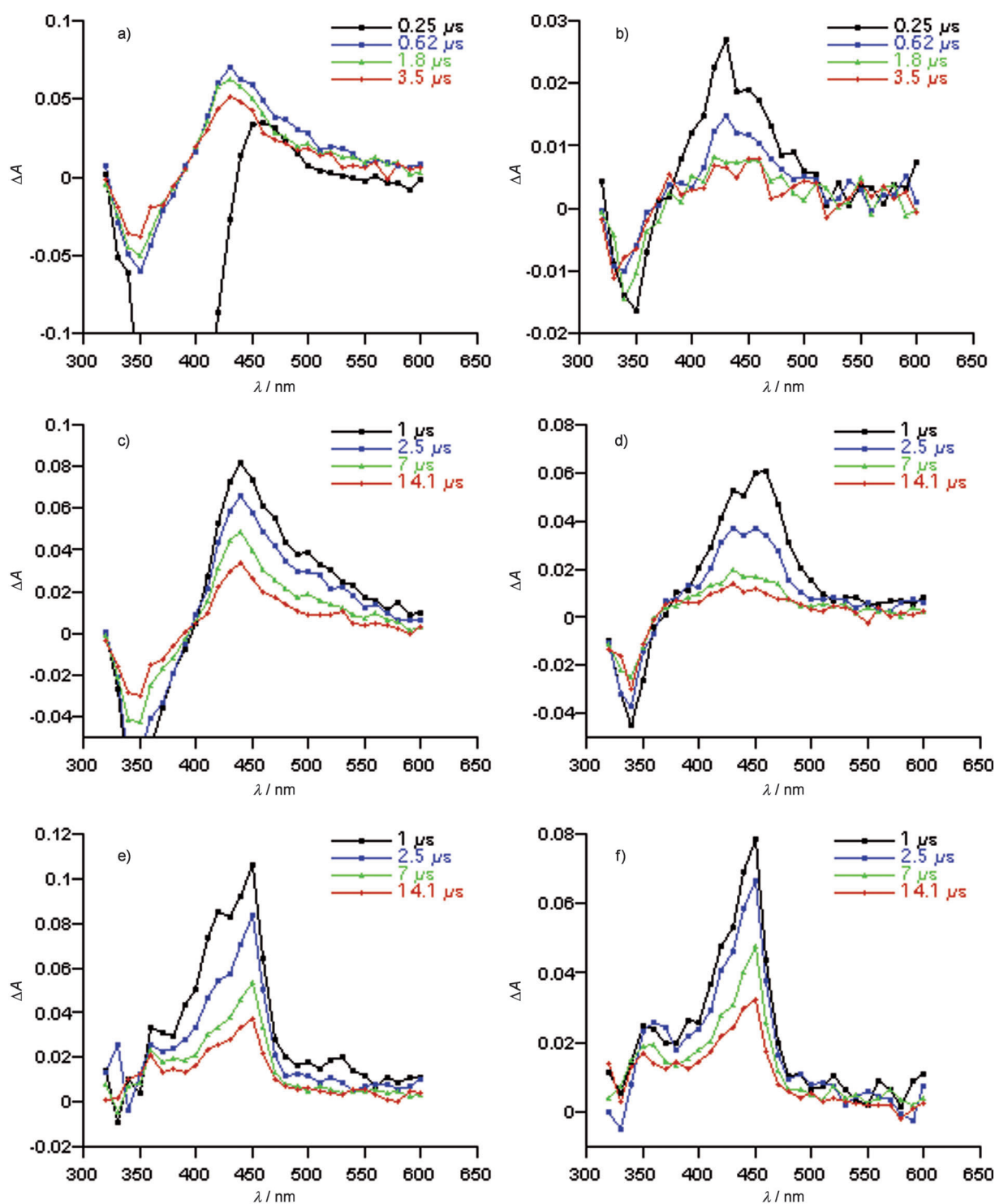


Figure 2. Transient absorption spectra of chloroform solutions of QD@Py (a,b), Py-L₂-OH (c,d), and Py (e,f) recorded under anaerobic (a,c,e) and aerobic (b,d,f) atmosphere. The elapsed time after the laser (355 nm) pulse is indicated. All samples absorbed 0.3 at the laser excitation wavelength.

2.4. Photoproducts Arising from the Lamp Irradiation of the Pyrenes in Chloroform

An aerated chloroform solution of pyrene (100 mL solution, 3.3×10^{-4} M) was irradiated (UV-A-lamps, emitting at $316 < \lambda < 400$) inside the cell in the photoreactor for 12 h. The fluorescence spectra of the photolysate showed a drastic decrease of

Py emission and the formation of photoproducts with emissions at longer wavelengths than pyrene (Figure 6).

The photoproduct mixture was analyzed by GC/MS. The spectrum showed a molecular ion peak of pyrene (m/z 202, 70%), together with peaks at m/z 236 (3%, I), 252 (2%, II), 230 (8%, III), 230 (13%, IV), and 252 (3%, V). The peak at m/z 236 [m/z at 236 (M^+), 200 ($M-HCl$), 118, and 100] was assigned to

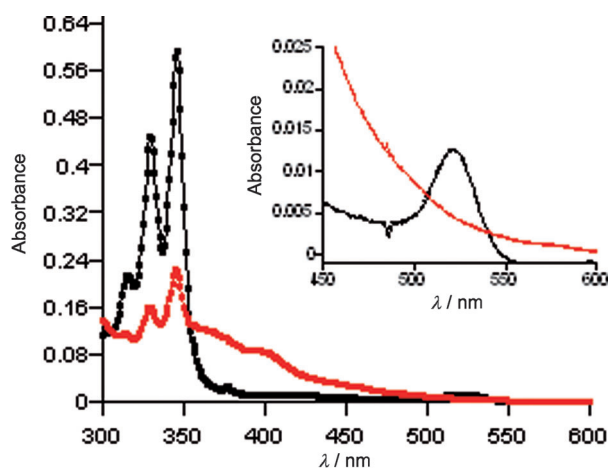


Figure 3. Absorption spectra of chloroform solutions of QD@Py (1.75×10^{-7} M) before (■) and after (●) UV-A-lamp irradiation for 30 min in the presence of air.

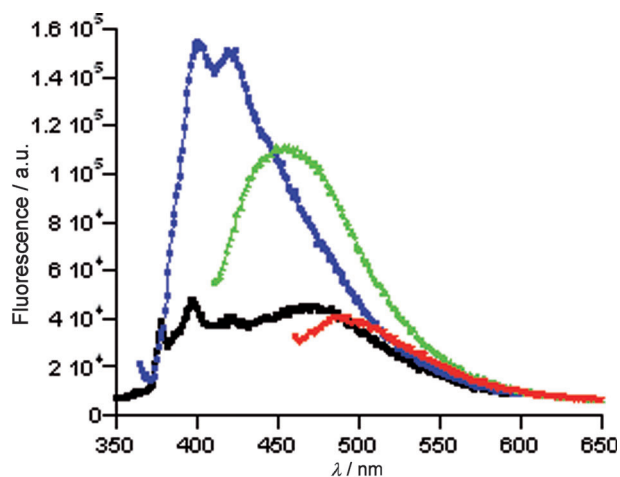


Figure 4. Emission spectra of chloroform solutions of QD@Py (1.75×10^{-7} M) after 30 min UV-A-lamp irradiation in the presence of air. Spectra were recorded at λ_{ex} 313 nm (■), 355 nm (●), 400 nm (▲), and 450 nm (▼).

1-chloropyrene, based on literature data for this compound.^[24] Those at m/z 230 have been ascribed to pyrenecarboxaldehydes (Scheme 2).

The NMR spectrum of the photolysate mainly showed the presence of pyrene, 1-pyrenecarboxaldehyde (IV), and 4-pyrenecarboxaldehyde (III)^[25] (pyrene/aldehyde molar ratio of 2.5/1.0, IV/III molar ratio of 1.5/1.0, see ^1H NMR in Figure S12 in the Supporting Information).^[26]

Column chromatography of the Py photolysate (hexane: ethyl acetate 9:1) made it possible to gain more information on the structure of the photoproducts responsible for the emission bands. They can be classified into three types of products (Scheme 2): 1) those containing a Cl substituent (Type A), 2) those derived from dichloromethyl radical incorporation (Type B), and 3) those without incorporation of species arising from chloroform (Type C).

Figure 7a,b show the absorption and emission spectra of photoproduct V with m/z at 252 for the molecular ion (Fig-

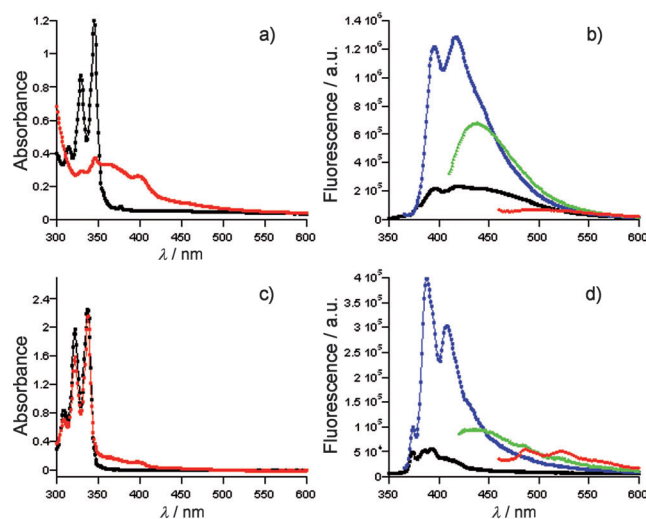


Figure 5. Absorption spectra of 4×10^{-5} M of Py- L_2 -OH (a) and 3.3×10^{-4} M of Py (c) before (■) and after 60 min UVA-lamp illumination in aerated chloroform (●). Emission spectra of Py- L_2 -OH (B) and Py (d) after 60 min UV-A-lamp illumination in aerated chloroform; spectra were recorded at λ_{ex} 313 nm (■), 355 nm (●), 400 nm (▲) and 450 nm (▼).

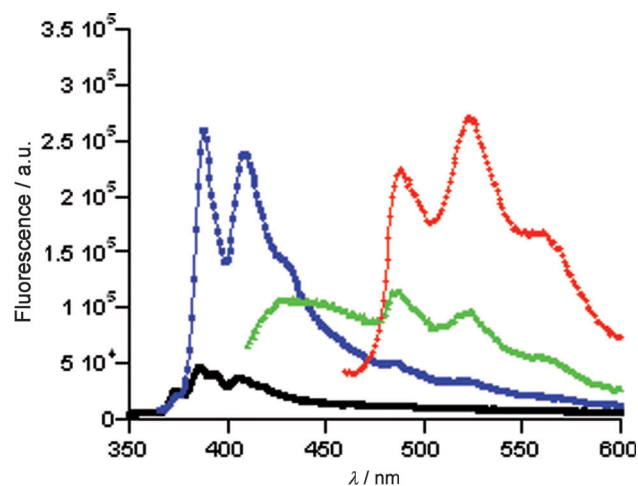
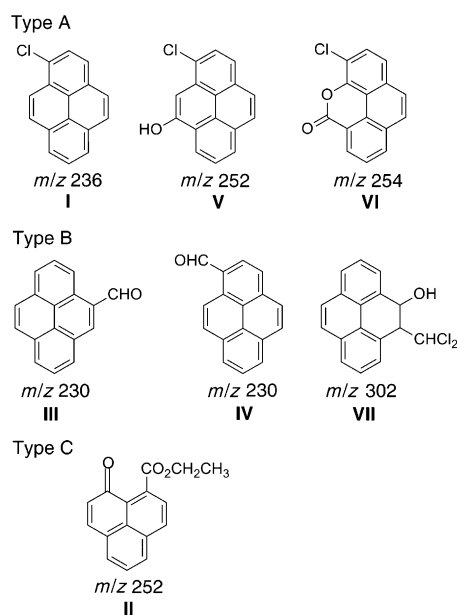


Figure 6. Emission spectra of aerated chloroform solutions of Py (3.3×10^{-4} M) after 12 h UV-A-irradiation; spectra recorded at λ_{ex} 313 nm (■), 355 nm (●), 400 nm (▲), and 450 nm (▼).

ure S13 in the Supporting Information). Its high resolution mass spectrum (HMRS) presented a m/z for $[M+H]^+$ of 253.0415, which agrees with a $\text{C}_{16}\text{H}_{10}\text{OCl}$ molecular formula. This compound exhibits a structured emission at λ_{max} of ca. 390 and 400 nm and a slightly red-shifted absorption spectrum compared to that of Py. These data together with the NMR spectra of compound V (Figures S14–S17 in the Supporting Information) are in agreement with a structure of a chloropyrenol. Control experiments showed that this compound was not generated during irradiation of aerated chloroform solutions of either 1-pyrenol or 1-chloropyrene. A 6-chloropyren-4-ol structure was postulated for compound V (Scheme 2), based on its phototransformation in compound VI.



Scheme 2. Proposed structure for the compounds isolated after lamp irradiation of pyrene in aerated chloroform.

The compound with the structured emission from 460 to 650 nm (λ_{max} at 490, 523, 560 nm, Figure 7d) was not detected in the GC spectrum of the photolysate, but its strong green fluorescence ($\Phi_f = 0.64$ in deaerated CHCl_3) made it possible to follow its formation during pyrene irradiation. This compound presents a considerable absorption in the 370–500 nm region (Figure 7c) and is a bright orange solid. Its structure was established by HRMS, IR, and ^1H NMR (in comparison with published data of 5-H-phenanthro[4,5-bcd]pyran-5-one). Its ^1H NMR spectrum showed signals at 7.72 (d, 9.6 Hz, 1H), 7.83 (d, 9.04 Hz, 1H), 7.90 (dd, 7.9 and 7.7 Hz, 1H), 8.05 (d, 9.8 Hz, 1H), 8.13 (d, 7.9 Hz, 1H), 8.32 (d, 7.7 Hz, 1H), 8.42 (d, 9 Hz, 1H) ppm (NMR spectra Figures S18 and S19 in the Supporting Information).^[27] Its GC/MS spectrum presents a peak at m/z 254 (Figure S20 in the Supporting Information) and fragment ions at 226 ($M^+ - 28$) and 198 ($M^+ - 56$), which might be attributed to a polycyclic, unsaturated lactone (loss of m/z 56, corresponding to C_2O_2). This is in accordance with the absorption peak at 1715.2 cm^{-1} in its IR spectrum. Its HMRS presented a m/z for $[M+H]^+$ of 255.0208, which agrees with a $\text{C}_{15}\text{H}_9\text{O}_2\text{Cl}$ molecular formula. Data suggested formation of the 3-chloro-5H-naphtho[8,1,2-cde]chromen-5-one structure.

Control experiments showed that compound VI was not generated in the irradiation of aerated chloroform solutions of 1-chloropyrene. However, formation of 4-oxapyrene-5-one has been proposed in the photocatalytic reaction of pyrene at $\text{TiO}_2/\text{water}$ interfaces,^[28] in the electrochemical oxidation of pyrene,^[29] and in the reaction of gas phase O_3 with pyrene adsorbed on silica particles.^[30] The evolution of the fluorescence spectra of the pyrene photolysate as a function of the irradiation time (Figure S7 in the Supporting Information) showed that compound VI appeared after a considerable irradiation time and that it could originate from compound V. This was

confirmed by irradiation of compound V for a short period of time (not shown).

Figure 7e,f show the absorption and emission spectra of a mixture of the pyrenecarbaldehydes, which exhibit a broad emission at λ_{max} of ca. 430 nm and their longest wavelength absorption is in the 320–420 nm region (NMR spectrum S21 in the Supporting Information).^[31] These compounds were by far the most abundant photoproducts.

In addition, we isolated a photoproduct whose GC/MS spectrum presented a peak at m/z 302 for the molecular ion and fragment ions at 285 ($M^+ - 10$) and 202 ($M^+ - 100$), which represented the probable loss of OH and CHCl_2 (Figure S22 in the Supporting Information). Its HMRS did not show the m/z for M^+ but a m/z of 285.0027, which agrees with the molecular formula of the fragment $\text{C}_{17}\text{H}_{11}\text{Cl}_2$. This compound was not even detected in the GC/MS spectrum of the photolysate, which indicates it is obtained in a very low yield. Its ^1H NMR spectrum showed signals at 4.02 (dd, 6.4 and 2.3 Hz, 1H), 5.53 (d, 2.3 Hz, 1H), 5.81 (d, 6.6 Hz, 1H), 7.59–7.65 (m, 3H), 7.81 (bs, 2H), 7.88–7.91 ppm (m, 2H) (Figure S23 in the Supporting Information). These data suggest the attachment of hydroxyl and dichloromethyl moieties to the 4- and 5-position of pyrene, and therefore the formation of 5-dichloromethyl-4,5-dihydroxy-1-pyrene (compound VII, Scheme 2). Moreover, we succeeded in isolating the other photoproduct detected in the pyrene photolysate whose GC/MS spectrum presented a peak at m/z 252 for the molecular ion (compound II, spectrum in Figure S24 in the Supporting Information). Fragment ions at 223 ($M^+ - 29$) and 207 ($M^+ - 45$) represented the probable loss of an ethoxy group. Its structure was established by HRMS, IR, and ^1H NMR (in comparison with published data of phenalene-9-formylphenalene). Its UV-absorption spectrum (Figure 8) resembles that of phenalene.^[32,33] Its HMRS showed the m/z for MH^+ at 253.0862, which agrees with the $\text{C}_{16}\text{H}_{13}\text{O}_3$ molecular formula. These data together with those from the NMR measurements (Figures S25–S28 in the Supporting Information) suggest formation of ethyl 1-oxo-1H-phenalene-9-carboxylate. Control experiments showed that this compound was not generated during irradiation of aerated chloroform solutions of 1-chloropyrene. However, this compound was detected (CG/MS) when the solvent of chloroform solutions of 1-pyrenol were eliminated under mild heating.

Steady-state irradiation of $\text{Py-L}_2\text{-OH}$ was also performed in aerated chloroform solutions ($3.5 \times 10^{-4}\text{ M}$) for 30 h to obtain information on the photoproducts structure. Remarkably, NMR spectra of the photolysate revealed the presence of mainly 1-pyrenecarbaldehyde, while the GC/MS analysis showed peaks at m/z 236 (35%), 230 (70%), 244 (15%), and $\text{Py-L}_2\text{-OH}$ (9.5%). The peak at m/z 230 fits well with that of 1-pyrenecarbaldehyde. The peak at m/z 236 is 1-chloropyrene, and that at m/z 244 can be assigned to 1-(pyrene-1-yl)ethanone. These results suggest that the phototransformation of the 1-alkylpyrene involves detachment of the alkyl chain from the aromatic ring as well as oxidation of the alkyl chain at the benzylic position.

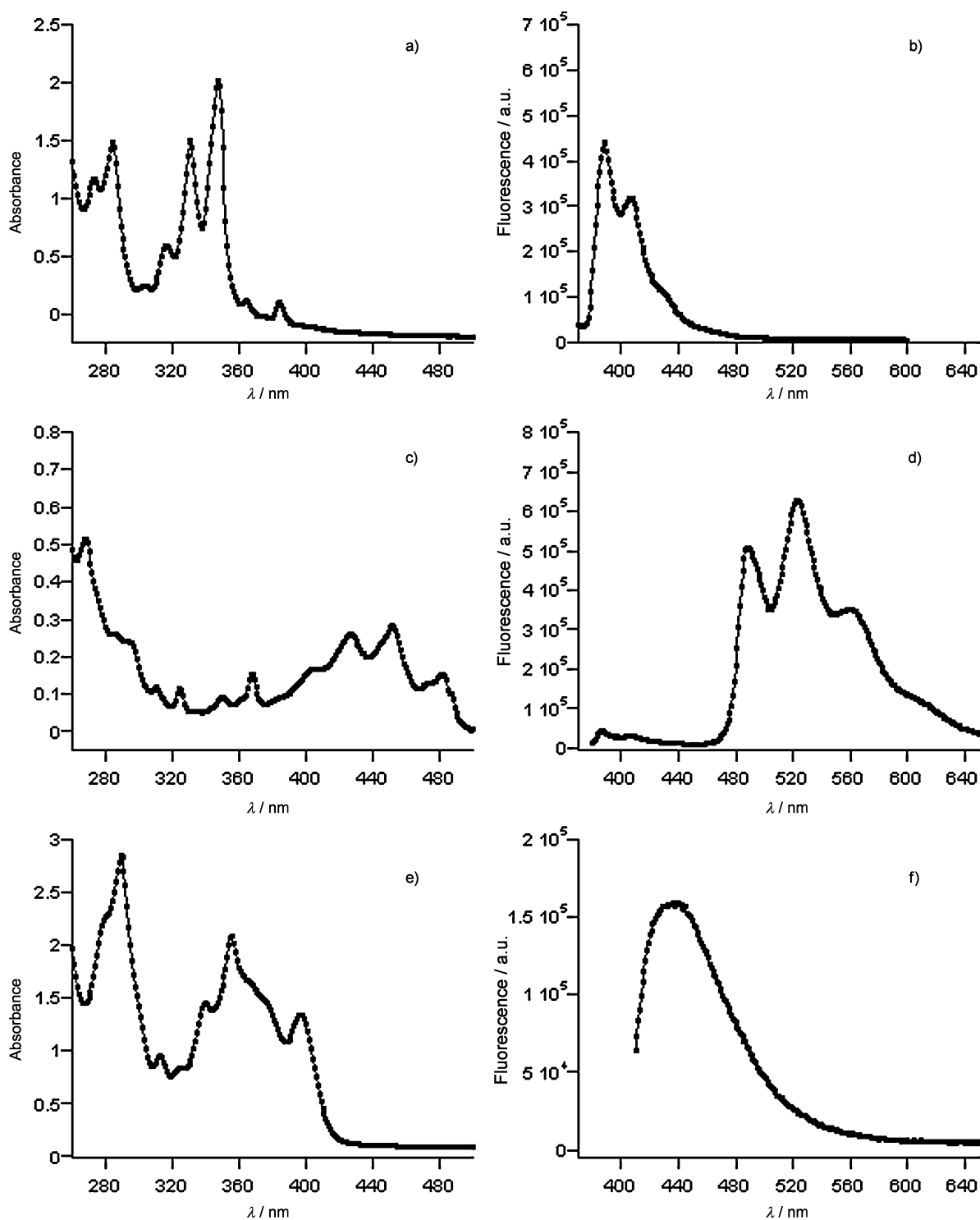


Figure 7. Absorption and emission spectrum ($\lambda_{\text{ex}}=355$ nm) of compounds V (a,b); VI (c,d), and VII (e,f).

2.5. Mechanistic Proposal of the Photodegradation of the Pyrene Systems

Plausible explanations for the phototransformation of the pyrene systems under UV-A illumination are depicted in Scheme 3 and Scheme 4. Electron transfer from the pyrene excited state to the halogenated solvents (chloroform and dichloromethane) would lead to the haloalkane radical anion as

well as the radical cation of the aromatic molecule. The pyrene radical cation was detected by laser flash photolysis technique in both halogenated solvents (the rapid dissociation of the haloalkane radical anion into products impedes rapid back-electron transfer to the pyrene radical cation).

The higher photostability of pyrene in dichloromethane together with the fact that pyrenecarbaldehydes were the main

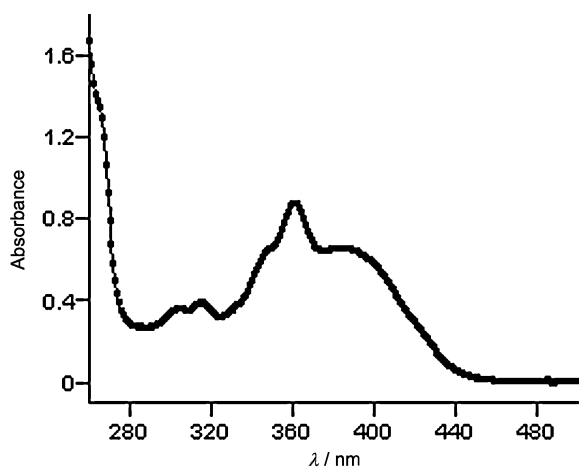
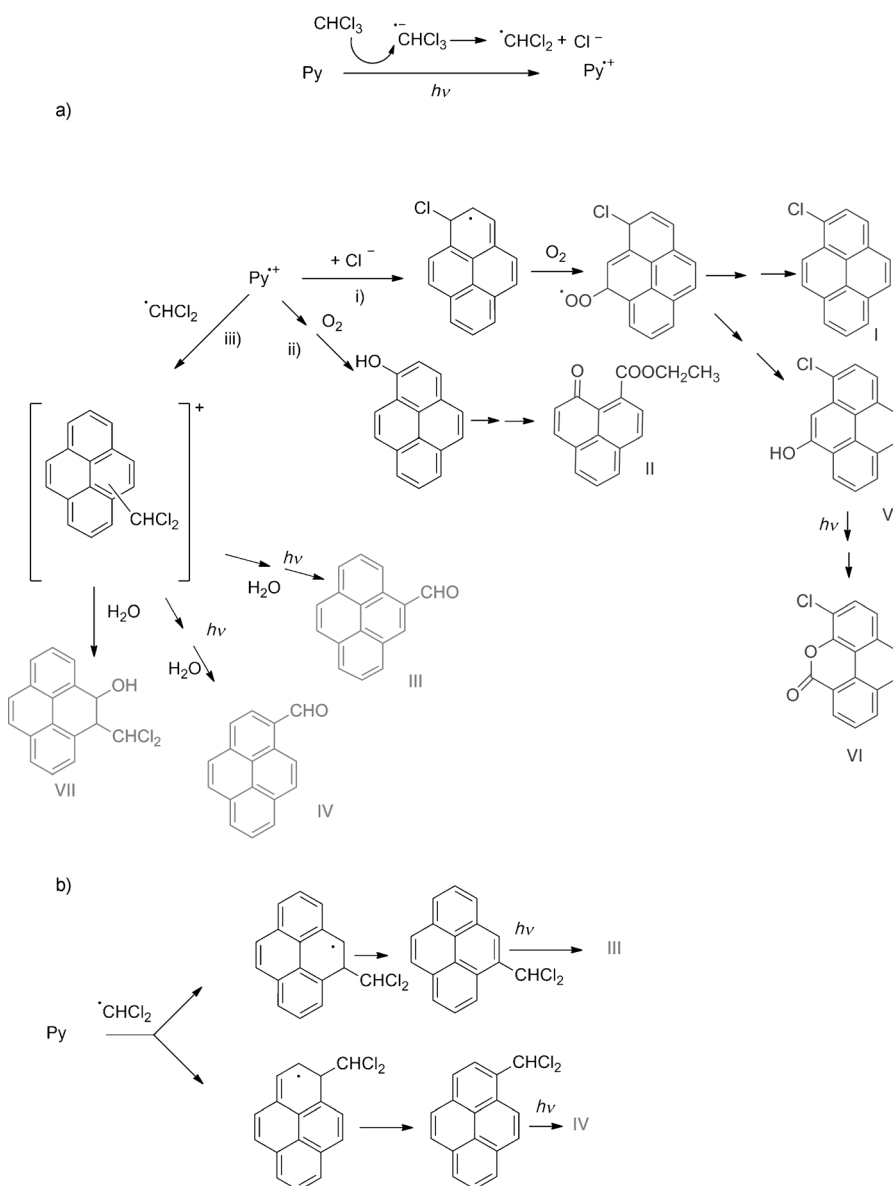


Figure 8. Absorption spectrum of compound II.



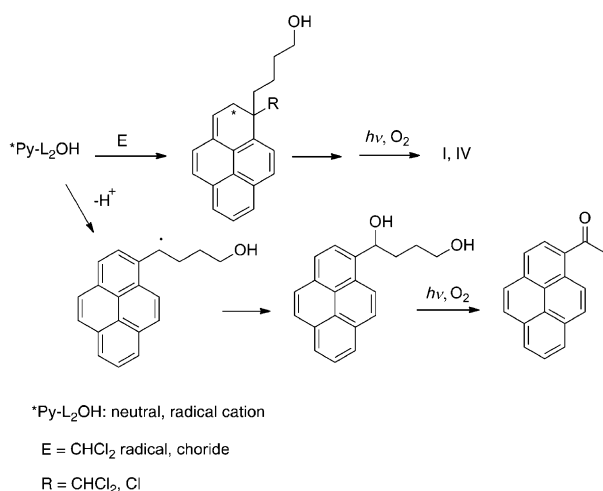
photoproducts in the degradation of pyrene in chloroform, suggests that the haloalkane radical, and not the chloride anion, is the main solvent species responsible for the transformation of pyrene. Indeed, pyrene photodegraded faster in distilled chloroform.

Therefore, the high stability of the pyrene systems in dichloromethane should be attributed to the lower reactivity of $\text{CH}_2\text{Cl}^\bullet$ radicals towards pyrene, together with their higher reactivity towards oxygen, compared to CHCl_2^\bullet radicals.^[34]

In the case of chloroform, the halomethyl radicals could react with $\text{Py}^{+\bullet}$ (Scheme 3a,iii). Alternatively, the addition of the haloradicals to Py could be a competitive reaction (Scheme 3b). It is known that polycyclic aromatic compounds generate radicals that are incapable of continuing the chain. So, pyrene is considerably more reactive (>1000 times) than benzene towards the addition of CCl_3^\bullet radicals, though four times less reactive than anthracene, for which a quantum efficiency of 0.4 has been reported for the UV-light induced reaction with CCl_4 .^[35]

Pyrene has five chemically distinct carbons and, in principle, five CHCl_2 -adduct radicals could be generated. It has been demonstrated that H(muonium^[36]) addition to pyrene mainly gives rise to two hydroperenyl radicals (1-Mu-pyrenyl and 4-Mu-pyrenyl, the first being the main product).^[37] Other studies have also shown that ground state pyrene is more easily attacked by radicals at the 1-position.^[38] In addition, selective attachment of alkyl radicals to the 1-position of pyrene upon irradiation at $\lambda > 300$ nm in solid n-alkane matrices has also been reported.^[39] These data are in agreement with the formation of 1-, and 4-pyrenecarbaldehydes in a 1.5/1.0 molar ratio.^[40]

A barely competitive process was the addition of chloride ions to pyrene radical cations leading to 1-chloropyrene and 1-chloropyren-2-ol (Scheme 3a,i). Some 1-chloropyrene has shown to be formed without photoexcitation of pyrene.^[11] Taking the control experiments into account, lactone VI and compound II could derive from 6-chloropyren-4-ol and 1-pyrenol, respectively, which are compounds generated through the pyrene radical cation (Scheme 3a,i and ii).



Scheme 4. Mechanistic proposal for the photodegradation of Py-L₂-OH

Oxygen radical anions, arising through electron transfer from the pyrene singlet excited state to molecular oxygen,^[41,42] could subsequently act as oxidant species.

On the other hand, the formation of 1-pyrene-carbaldehyde in the photolysis of 4-(1-pyrenyl)butanol in chloroform requires the ipso substitution of the alkyl chain by CHCl₂ radicals (Scheme 4). The addition of solvent species to pyrene or the pyrene radical cation, followed by β-scission of the aryl-alkyl C–C bond could be responsible for the chain detachment. The radical mechanism has been suggested in the pyrolyses of 1-alkylpyrene.^[43] A less competitive process would be the addition of the chloride anion to pyrene radical cations and the subsequent alkyl chain detachment.

In addition, the alkyl chain oxidation could arise from loss of a proton from the Py-L₂-OH radical cation, followed by the reaction with oxygen. Further oxidation of the benzylic-like alcohol would lead to the corresponding ketone, whose Norrish II photocleavage would produce 1-acetylpyrene.

As a consequence, the high stability of the pyrene systems in dichloromethane should be attributed to the low reactivity of CH₂Cl radicals towards the aromatic ring together with their higher reactivity towards oxygen.^[34,44]

Finally, it is worth mentioning that pyrene systems proved to be as photo-unstable in other non-halogenated solvents, such as THF (high pyrene photodegradation after 30 min of UV-A irradiation, spectrum not shown), as in chloroform.

3. Conclusions

In summary, pyrene fluorophores are widely applied, in relation with its fluorescent properties, for designing many molecular, as well as macro- and supra-molecular functional devices. Such studies are frequently performed in chloroform, due to the good solubility properties of this solvent.

However, we demonstrated that chloroform combined with illumination causes a considerable photodegradation of different types of pyrene systems, and that dichloromethyl radicals play a key role in such processes.

Interestingly, we showed that dichloromethane can be a suitable alternative to chloroform in those applications of pyrene systems requiring the use of light. Surprisingly, chloromethyl radicals hardly react with pyrene structures, and furthermore they protect the chromophore from photooxidation. These findings will be useful for a wide variety of aromatic dyes and fluorophores,^[45] since they may well undergo electron transfer to haloalkanes under light illumination.

Experimental Section

Materials: All reagents were commercially available and used as received. The 11-mercaptoundecanol (MU), and 1-pyrenebutanol were purchased from Sigma–Aldrich. Solvents for chromatography (ethyl acetate and hexane) were reagent grade and used without further purification.

Characterization: UV/Vis spectra of the samples were recorded using a quartz cuvette spectrometer in a UV/Visible spectrophotometer Agilent 8453E. The average diameter value of the nanoparticles was estimated following the Peng et al.^[46] procedure.

Steady-state fluorescence spectra (LPS-220B, motor driver (MD-5020), Brytebox PTI) were measured on a spectrofluorometer PTI, equipped with a lamp power supply and working at room temperature. The Felix 32 Analysis software was used to register the data. The fluorescence quantum yield was calculated by following the procedure of Resch–Genger et al.^[47]

Laser flash photolysis (LFP) studies were performed on a pulsed Nd:YAG laser, using 355 nm as excitation source. The pulses width was ca. 10 ns, and the energy was ca. 15 mJ pulse⁻¹. A xenon lamp was employed as the detecting light source. The apparatus consisted of a pulsed laser, a Xe lamp, a monochromator, and a photomultiplier (PMT) system. The output signal from the oscilloscope was transferred to a personal computer. Samples were prepared such that they absorbed ca. 0.3 at 355 nm and they were bubbled with nitrogen for 10 min.

Images from the QDs were obtained by high resolution transmission electron microscopy (HRTEM, FEI Tecnai G2 F20) at an accelerating voltage of 200 kV. Samples were prepared by dropping the colloidal solution on a Lacey Formvar/carbon-coated copper grid. The digital analysis of the HRTEM micrographs was done using digital Micrograph™ 1.80.70 for GMS by Gatan.

TLC was performed on Merck Silica Gel 60 F254 aluminum sheets and developed by UV light and ethanolic sulfuric acid (5% v/v). Flash column chromatography was performed on Merck Silica Gel (230–400 mesh, ASTM).

Mass spectra were obtained by electron impact (EI) at 70 eV or chemical ionization (CI). High resolution mass spectra were recorded on an AB SCIEX TripleTOF 5600 instrument.

¹H-, ¹³C-, and 2D-NMR (COSY, HMQC and HMBC) spectra were recorded on Bruker Avance DPX300, 400, and 500. Standard Bruker software was used for acquisition and processing routines. Chemical shifts are given in ppm and *J* values are given in Hz. Carbon substitution degrees were established by DEPT pulse sequences. COSY, HMQC, and HMBC experiments were utilized to obtain additional information. IR spectra were measured using a FT-IR Nicolet IS10 instrument.

Synthesis of 4-(pyren-4-yl) butyl-11-mercaptoundecanoate (Py-L1-SH)^[18]: The Py-SH ligand was prepared following an esterification method described in the literature. In brief, 4-(1-pyrenyl)butanol (722 mg, 2.6 mmol) and 11-mercaptoundecanoic acid (574 mg, 2.6 mmol) were dissolved in anhydride toluene (30 mL). A complex

of hafnium/THF (2 mg) was added and the mixture was heated for 48 h under azeotropic reflux conditions to remove water through a Soxhlet thimble with 3 Å molecular sieves. In order to quench the reaction, 1 mL of water was added. After solvent removal, the product was purified by column chromatography using hexane:ethyl acetate solvents (9:1). The compound was obtained in a 89% yield.

¹H NMR (300 MHz, CDCl₃): δ = 1.07–1.20 (m, 12H), 1.23 (t, *J* = 7.7 Hz; 1H), 1.43–1.57 (m, 4H), 1.68–1.93 (m, 4H), 2.21 (t, *J* = 7.7 Hz; 2H), 2.41 (q, *J* = 7.0 Hz; 2H), 3.30 (t, *J* = 7.8 Hz; 2H), 4.08 (t, *J* = 6.3 Hz; 2H), 7.76–7.81 (d, *J* = 7.8 Hz; 1H), 7.88–7.96 (m, 3H), 8.00–8.11 (m, 4H), 8.16–8.21 ppm (d, *J* = 9.3 Hz; 1H).

Synthesis of QD@Py: A chloroform solution (25 mL) of QD@TOPO (2.85 × 10⁻⁷ mol) Py-L1-SH (9.62 × 10⁻⁴ mol, [thiol]/[QD] = 3375 molar ratio) was heated to reflux under nitrogen atmosphere for 48 h. After almost total solvent evaporation (2 mL remaining) and the addition of methanol (30 mL), the samples were centrifuged at 8000 rpm for 20 min at 25 °C and the supernatant was decanted. The nanoparticles (QD@Py) were dissolved in toluene (2 mL) and the purification process was repeated five times in order to eliminate the unreacted ligand.

Steady-state irradiations were performed with a LuzChem photo-reactor, using ten lamps emitting at 316 < λ < 400 nm, λ_{max} at 351 nm, 53 W m⁻².

Acknowledgements

We thank MEC (Project CTQ2008-06777-CO2-01, contract granted to J.A.-S., and RyC contract granted to R.E.G.), GVA (Project ACOMP/2009/334), and UVEG (Project UV-AE-09-5805) for their support.

Keywords: fluorescence · halogenated solvents · laser spectroscopy · pyrenes · steady-state photolysis

- [1] a) C. Bohne, E. B. Abuin, J. C. Scaiano, *J. Am. Chem. Soc.* **1990**, *112*, 4226; b) S. L. Murov, I. Carmichael, G. L. Hug in *Handbook of Photochemistry*, 2nd ed., Marcel Dekker, New York, **1992**.
- [2] Y. Chen, C. J. Durning, N. J. Turro, *Macromolecules* **1999**, *32*, 4151.
- [3] N. Van Anh, F. Schlosser, M. M. Groeneveld, I. H. M. Stokkum, F. Würthner, R. M. Williams, *J. Phys. Chem. C* **2009**, *113*, 18358.
- [4] A. B. Patel, P. Khumsupan, V. Narayanaswani, *Biochemistry* **2010**, *49*, 1766.
- [5] B. Srinivas, C. J. Durning, N. J. Turro, *Macromolecules* **1996**, *29*, 5505.
- [6] a) B. Schazmann, N. Alhashimy, D. Diamond, *J. Am. Chem. Soc.* **2006**, *128*, 8607; b) S. H. Lee, S. H. Kim, S. K. Kim, J. H. Jung, J. S. Kim, *J. Org. Chem.* **2005**, *70*, 9288; c) K.-S. Focsaneanu, J. C. Scaiano, *Photochem. Photobiol. Sci.* **2005**, *4*, 817.
- [7] A. S. Oliveira, L. F. Vieira Ferreira, J. P. Da Silva, J. C. Moreira, *Int. J. Photoenergy* **2004**, *6*, 205.
- [8] Y.-P. Sun, B. Ma, G. E. Lawson, C. E. Bunker, H. W. Rollins, *Anal. Chim. Acta* **1996**, *319*, 379.
- [9] P. Kubát, S. Civiš, A. Muck, J. Barek, J. Zima, *J. Photochem. Photobiol. A* **2000**, *132*, 33.
- [10] C. A. Reyes, M. Medina, C. Crespo-Hernandez, M. Z. Cedeno, R. Arce, O. Rosario, D. M. Steffenson, I. N. Ivanov, M. E. Sigman, R. Dabestani, *Environ. Sci. Technol.* **2000**, *34*, 415.
- [11] S. Yamada, H. Kuroki, M. Maeda, M. Takagi, T. Yamashita, *Microchem. J.* **1994**, *49*, 117.
- [12] M. Amelia, A. Lavie-Cambot, N. D. McClenaghan, A. Credi, *Chem. Commun.* **2011**, *47*, 325.

- [13] S. A. Tucker, L. E. Cretella, R. Waris, K. W. Street, Jr., W. E. Acree, Jr., J. C. Fetzer, *Appl. Spectrosc.* **1990**, *44*, 269.
- [14] J. Shirdel, A. Penzkofer, R. Procházka, Z. Shen, J. Strauss, J. Daub, *Chem. Phys.* **2007**, *331*, 427.
- [15] M. Sigman, P. Schuler, M. Ghosh, R. T. Dabestani, *Environ. Sci. Technol.* **1998**, *32*, 3980.
- [16] M. Montali, L. Prodi, N. Zaccheroni, R. Baxter, G. Teobaldi, F. Zerbetto, *Langmuir* **2003**, *19*, 5172.
- [17] S. F. Wuister, C. de Mello Donegá, A. Meijerink, *J. Phys. Chem. B* **2004**, *108*, 17393.
- [18] The Φ_f of pyrene in chloroform changes from 0.52 in deaerated to 0.04 in aerated solutions: J. Kollár, P. Hrdlovic, S. Chmela, *J. Photochem. Photobiol. A* **2010**, *214*, 33.
- [19] Pyrene excimer decays by fluorescing, dissociating to the excited singlet state, and decaying to the triplet monomer and the ground state.
- [20] T. Medinger, F. Wilkinson, *Trans. Faraday Soc.* **1966**, *62*, 1785.
- [21] These values are close to those reported for pyrene and 1-methylpyrene radical cations in dichloromethane (see ref. [14]).
- [22] A triplet quantum yield of 0.7 has been previously reported for N-acetyl-1-pyrenylmethylamine in dichloromethane, see: M. González-Béjar, A. Bentama, M. A. Miranda, S. E. Sitiba, J. Pérez-Prieto, *J. Org. Lett.* **2007**, *9*, 2067.
- [23] W. L. F. Amarego, C. L. L. Chai, *Purification of Laboratory Chemicals*, 5th ed., Elsevier, Amsterdam, **2003**.
- [24] T. Ohura, A. Kitazawa, T. Amagai, *Chemosphere* **2004**, *57*, 831.
- [25] R. G. Harvey, M. Konieczny, J. Pataki, *J. Org. Chem.* **1983**, *48*, 2930.
- [26] A solution of pyrene was irradiated for two hours and the photolysate was analyzed by GC/MS using an internal standard, the result of which is: pyrene (87.0%), I (2.6%), II (0.006%), III (2.8%), IV (6.1%), V (1.9%).
- [27] The small amount of this compound and its instability in solution under ambient light made it impossible to obtain an adequate ¹³C NMR spectrum.
- [28] S. Wen, J. Zhao, G. Sheng, J. Fu, P. Peng, *Chemosphere* **2003**, *50*, 111.
- [29] D. S. Cordeiro, P. Corio, *J. Braz. Chem. Soc.* **2009**, *20*, 80.
- [30] K. Miet, K. L. Menach, P. M. Flaud, H. Budzinski, E. Villenave, *Atmos. Environ.* **2009**, *43*, 3699.
- [31] D. Bhattacharjee, K. Mukherjee, T. N. Misra, *J. Phys. Chem. Solids* **2000**, *61*, 751.
- [32] C. Flors, S. Nonell, *Helv. Chim. Acta* **2001**, *84*, 2533.
- [33] The phenalenone chromophore usually shows a quantum yield for triplet formation close to one.
- [34] V. D. Knyazev, I. R. Slagle, *J. Phys. Chem. A* **1998**, *102*, 1770.
- [35] E. J. Bowen, K. K. Rohatgi, *Discuss. Faraday Soc.* **1953**, *14*, 146.
- [36] Muonium is the single-electron atom with a positive muon as nucleus and can be considered as a light isotope of hydrogen.
- [37] P. W. Percival, B. Addison-Jones, J. C. Brodovitch, K. Ghandi, J. Schüth, *Can. J. Chem.* **1999**, *77*, 326.
- [38] R. H. Mitchell, Y. H. Lai, R. V. Williams, *J. Org. Chem.* **1979**, *44*, 4733.
- [39] O. E. Zimmerman, R. G. Weiss, *J. Phys. Chem. A* **1999**, *103*, 9794.
- [40] Traces of the potential 2-pyrenecarbaldehyde were also detected.
- [41] T. Ogawa, Y. Tenkyuu, K. Nakashima, *Anal. Sci.* **2000**, *16*, 913.
- [42] It has been demonstrated that singlet oxygen is not involved in the photochemical transformation of pyrene: see ref. [15] and M. Mazur, G. J. Blanchard, *J. Phys. Chem. B* **2004**, *108*, 1038.
- [43] C. M. Smith, P. E. Savage, *Energy Fuels* **1992**, *6*, 195.
- [44] S. I. Stoliarov, A. Bencsura, E. Shafir, V. D. Knyazev, I. R. Stagle, *J. Phys. Chem. A* **2001**, *105*, 76.
- [45] a) J. Shirdel, A. Penzkofer, R. Procházka, J. Daub, E. Hochmuth, R. Deutzmann, *Chem. Phys.* **2006**, *326*, 489; b) M. P. Joshi, S. Raj Mohan, T. S. Dhami, B. Jain, H. Ghosh, T. Shripathi, U. P. Deshpande, *Appl. Phys. A* **2008**, *90*, 351; c) K. Iwata, *J. Raman Spectrosc.* **2008**, *39*, 1512; d) A. El-Agamey, M. Burke, R. Edge, E. J. Land, D. J. McGarvey, T. G. Truscott, *Rad. Phys. Chem.* **2005**, *72*, 341.
- [46] W. W. Yu, L. Qu, W. Guo, X. Peng, *Chem. Mater.* **2003**, *15*, 2854.
- [47] M. Grabolle, M. Spieles, V. Lesnyak, N. Gaponik, A. Eychmüller, U. Resch-Genger, *Anal. Chem.* **2009**, *81*, 6285.

Received: October 25, 2011

Published online on January 24, 2012

CHEMPHYSICHEM

Supporting Information

© Copyright Wiley-VCH Verlag GmbH & Co. KGaA, 69451 Weinheim, 2012

Further Insight into the Photostability of the Pyrene Fluorophore in Halogenated Solvents

Jordi Aguilera-Sigalat,^[a] Jaime Sanchez-SanMartín,^[a] Carlos E. Agudelo-Morales,^[a]
Elena Zaballos,^[b] Raquel E. Galian,^{*,[a, c]} and Julia Pérez-Prieto^{*,[a]}

cphc_201100843_sm_miscellaneous_information.pdf

Supporting Information

TABLE OF CONTENTS

Title	page
Figure S1: Absorption spectra of QD@Py and Py in toluene.	S3
Figure S2: HRTEM image of QD@Py	S4
Figure S3: ¹ H-NMR spectrum of Py-L ₂ -SH in Cl ₃ CD and QD@Py in Cl ₃ CD	S5
Figure S4: Fluorescence spectra (λ_{ex} 450 nm) of QD@TOPO and QD@Py in toluene	S6
Figure S5. A: Absorption spectra of chloroform solutions of Py-L ₂ -OH before and after UVA-lamp irradiation for up to 45 min. B: Difference spectrum showing the disappearance of the pyrene absorbance after 45 min of irradiation and the formation of the photoproducts	S7
Figure S6. A: Absorption spectra of chloroform solutions of QD@Py before and after UVA-lamp irradiation for up to 45 min. B: Difference spectrum showing the disappearance of the pyrene absorbance and the QD exciton peak after 45 min of irradiation and the formation of the photoproducts	S8
Figure S7 Evolution of the emission spectra of Py in aerated chloroform with the irradiation time (up to 750 min); the spectra were recorded at λ_{ex} 355 nm (A), 400 nm (B), and 450 nm (C).	S9
Figure S8. Evolution of the emission spectra of Py-L ₂ -OH in aerated chloroform with the irradiation time (up to 45 min); the spectra were recorded at λ_{ex} 355 nm (A), 400 nm (B), and 450 nm (C).	S10
Figure S9. Evolution of the emission spectra of QD@Py in aerated chloroform with the irradiation time (up to 45 min); the spectra were recorded at λ_{ex} 355 nm (A), 400 nm (B), and 450 nm (C).	S11
Figure S10. Fluorescence excitation spectra of Py-L ₂ -OH inside the cell	S1

compartment of the spectrofluorometer monitored at 480 nm, taken before and after excitation at 355 nm for 200 scans	S12
Figure S11. Absorption spectra of QD@Py (A), Py-L ₂ -OH (B), and Py (C) in amylene-free dichloromethane before and after 50 minutes UVA-lamp illumination in the presence of air.	S13
Figure S12. ¹ H-NMR spectrum of the photolysate of pyrene	S14
Figure S13. GC/MS spectrum of compound V	S14
Figure S14. ¹ H-NMR spectrum of compound V	S15
Figure S15. ¹³ C-NMR spectrum of compound V	S15
Figure S16. COSY-NMR spectrum of compound V	S16
Figure S17. HSQC-NMR spectrum of compound V	S16
Figure S18. ¹ H-NMR spectrum of compound VI	S17
Figure S19. COSY-NMR spectrum of compound VI	S17
Figure S20. GC/MS spectrum of compound VI	S18
Figure S21. ¹ H-NMR spectrum of a mixture of 1- and 4-pyrenecarbaldehyde	S18
Figure S22. GC/MS spectrum of compound VII	S19
Figure S23. ¹ H-NMR spectrum of compound VII	S20
Figure S24. GC/MS spectrum of compound II	S21
Figure S25. ¹ H-NMR spectrum of compound II	S21
Figure S26. ¹³ C-NMR spectrum of compound II	S22
Figure S27. HSQC-NMR spectrum of compound II	S22
Figure S28 – COSY-NMR spectrum of compound II	S23

Synthesis and characterization of QD@TOPO nanoparticles. CdSe core QDs capped with TOPO/TOP ligands (QD@TOPO) were synthesised according to the methodology reported by Peng et al.^[1] The size of the nanoparticles was estimated using the maximum of the first exciton peak in the UV-visible spectrum^[2]; the maximum at 530 nm was indicative of a diameter of 2.7 nm. The emission peak was at 541 nm and the full width at half maximum (fwhm) of 30 nm indicated a narrow-size distribution of the QDs. High resolution transmission electron microscopy (HRTEM) images confirmed the size of the nanoparticles as well as the crystalline properties and monodispersity of QD@TOPO (size 2.6 ± 0.3 nm).

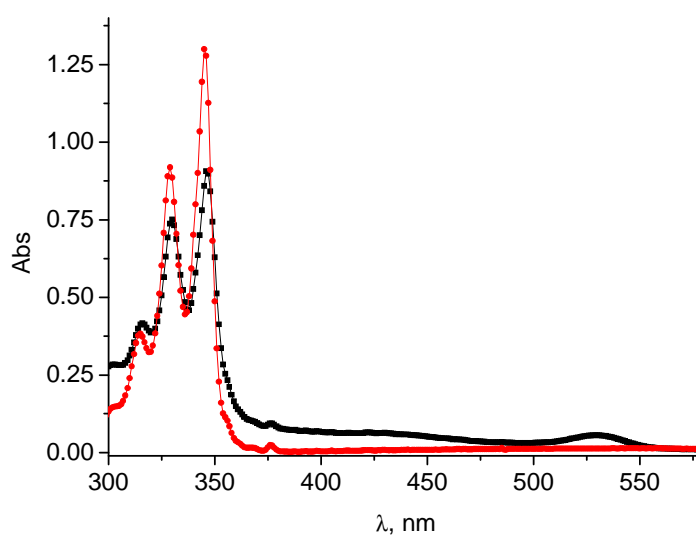


Figure S1 : Absorption spectra of QD@Py (1.3×10^{-7} M) and Py (1.65×10^{-4} M) in toluene.

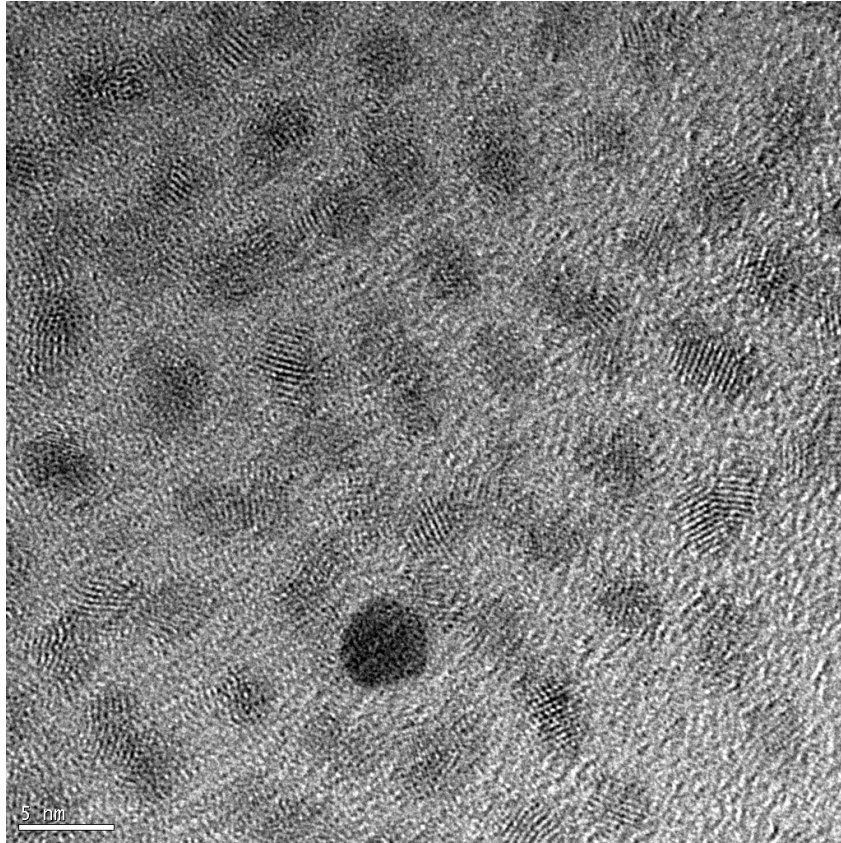


Figure S2: HRTEM image of QD@Py

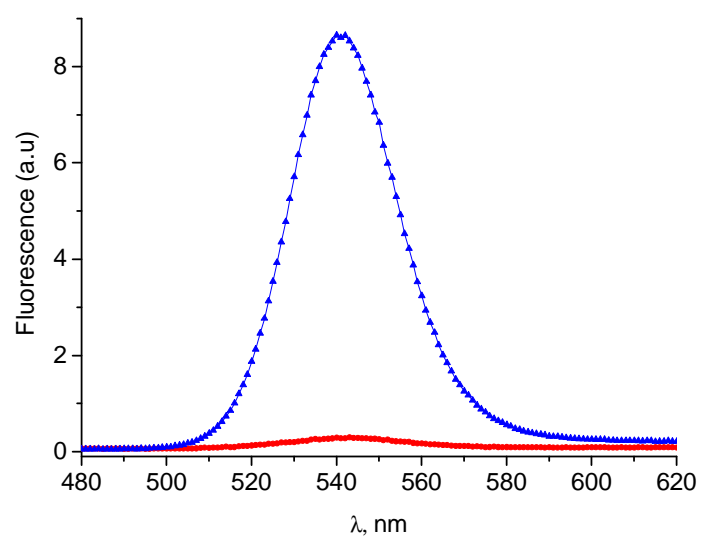


Figure S4 : Fluorescence spectrum (λ_{ex} 450 nm) of QD@TOPO (▲) and QD@Py (■) in toluene.

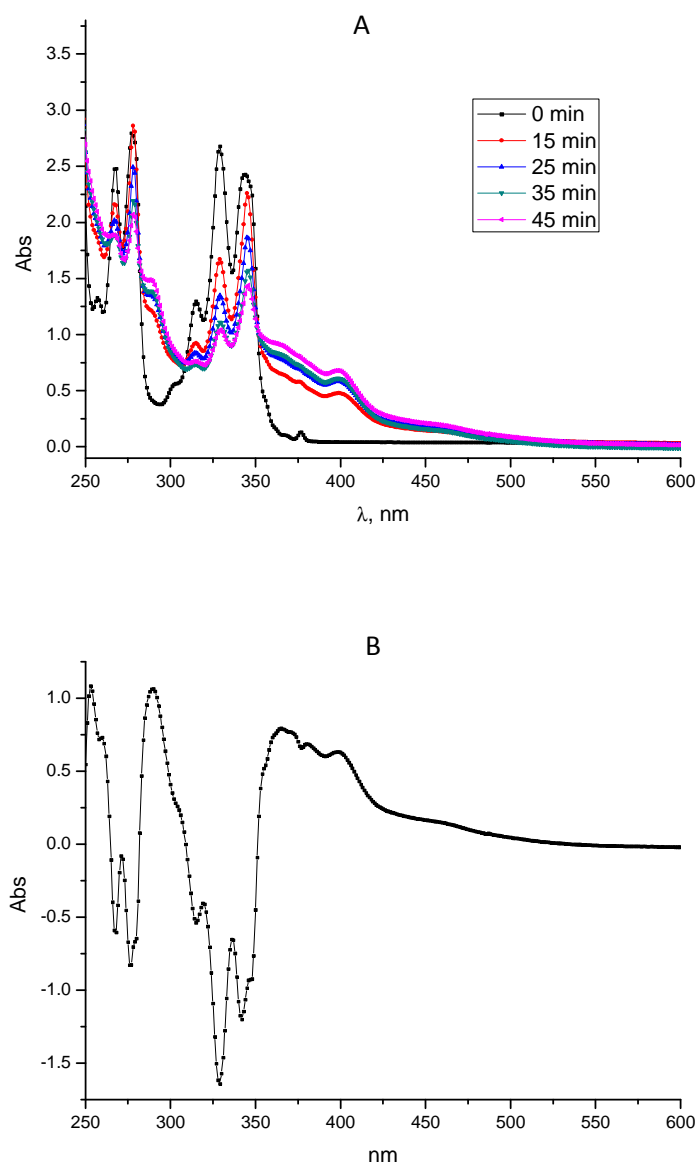


Figure S5 A: Absorption spectra of chloroform solutions of Py-L₂-OH before and after UVA-lamp irradiation for up to 45 min. **B:** Difference spectrum showing the disappearance of the pyrene after 45 min of irradiation and the formation of the photoproducts.

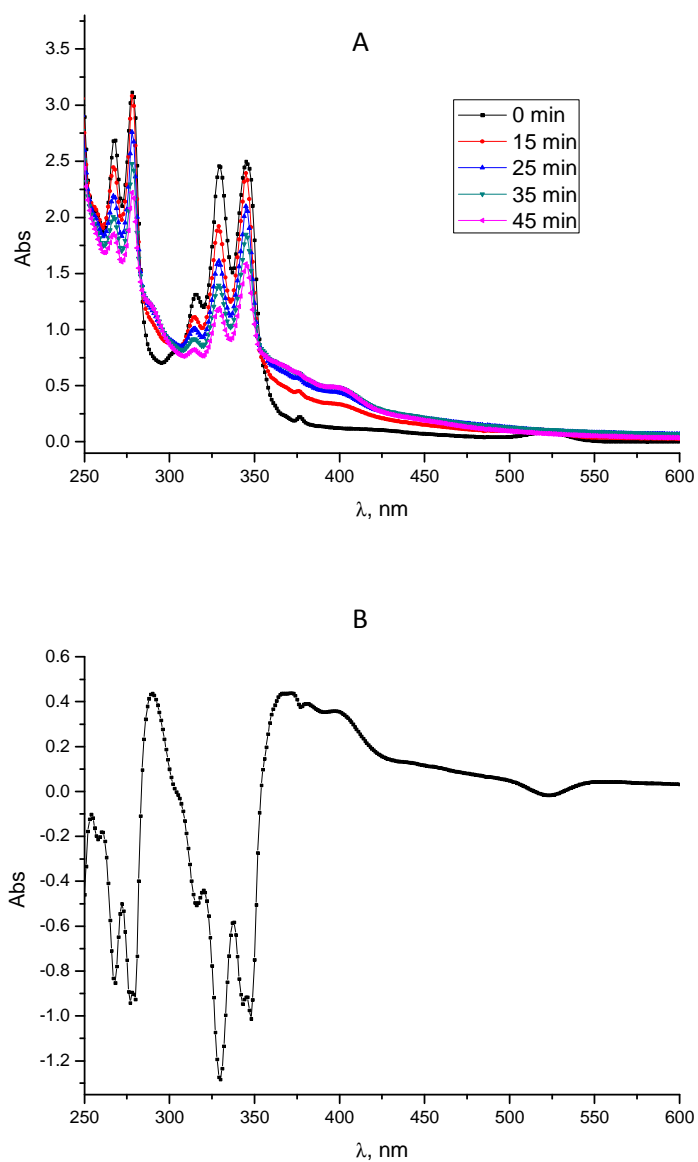


Figure S6 A: Absorption spectra of chloroform solutions of QD@Py before and after UVA-lamp irradiation for up to 45 min. **B:** Difference spectrum showing the disappearance of the pyrene and the QD excitation peak after 45 min of irradiation and the formation of the photoproducts.

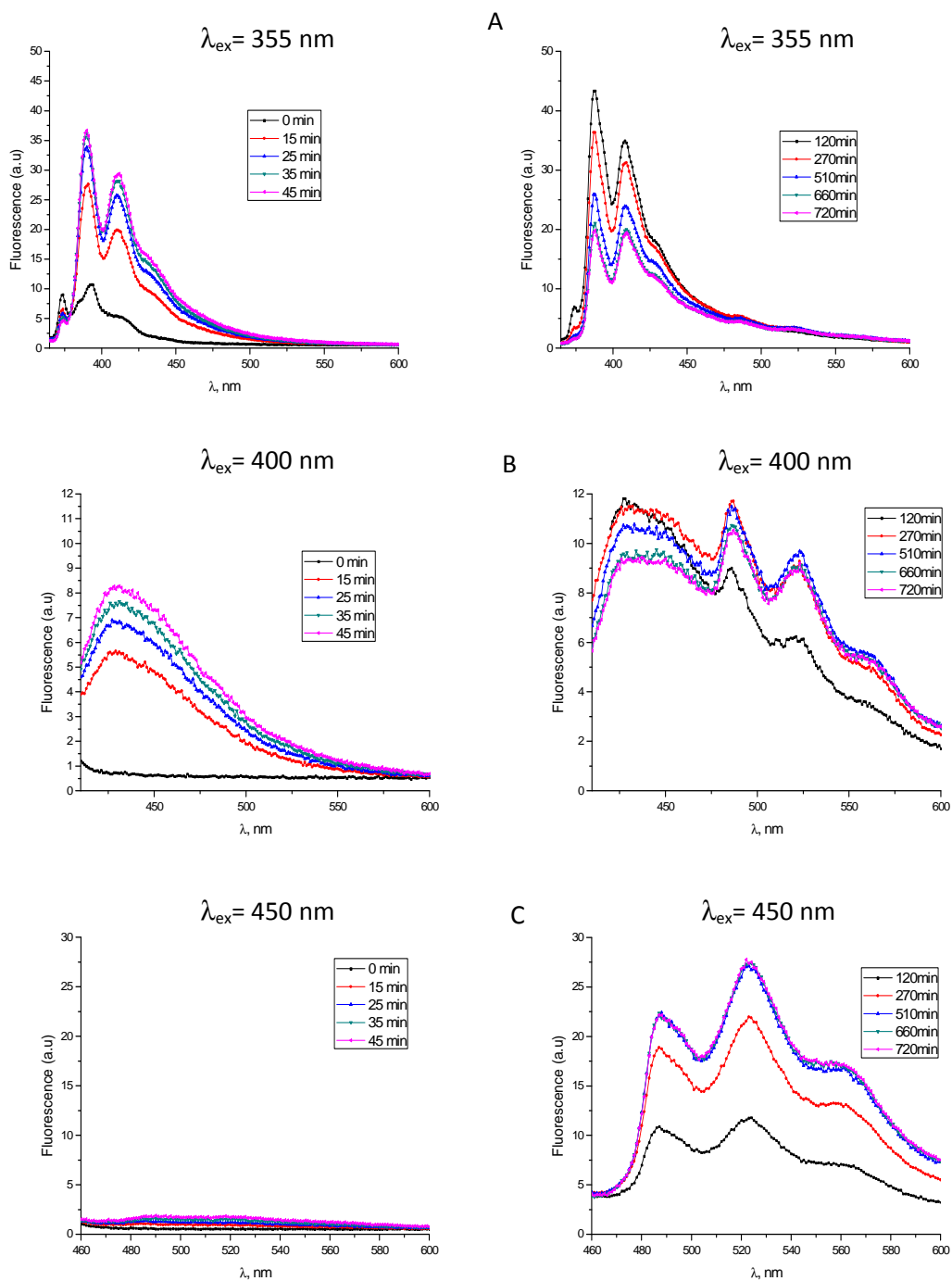


Figure S7. Evolution of the emission spectra of Py (3.3×10^{-4} M) in aerated chloroform with the irradiation time (up to 750 min); the spectra were recorded at λ_{ex} 355 nm (A), 400 nm (B), and 450 nm (C).

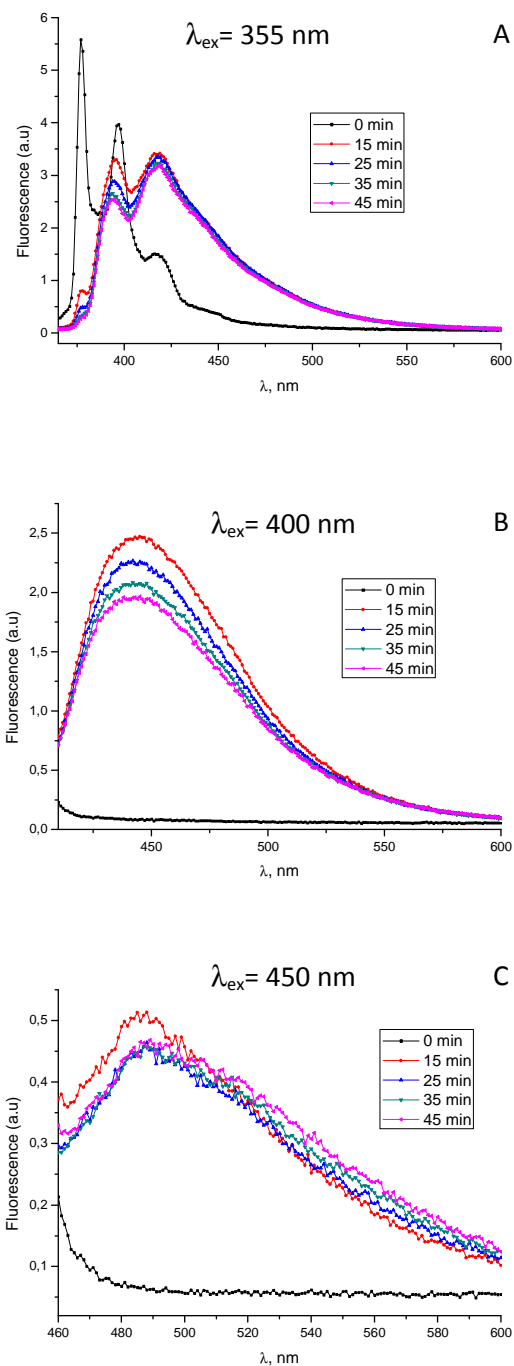


Figure S8. Evolution of the emission spectra of Py-L₂-OH (2.4 × 10⁻⁴ M) in aerated chloroform with the irradiation time (up to 45 min); the spectra were recorded at λ_{ex} 355 nm (A), 400 nm (B), and 450 nm (C).

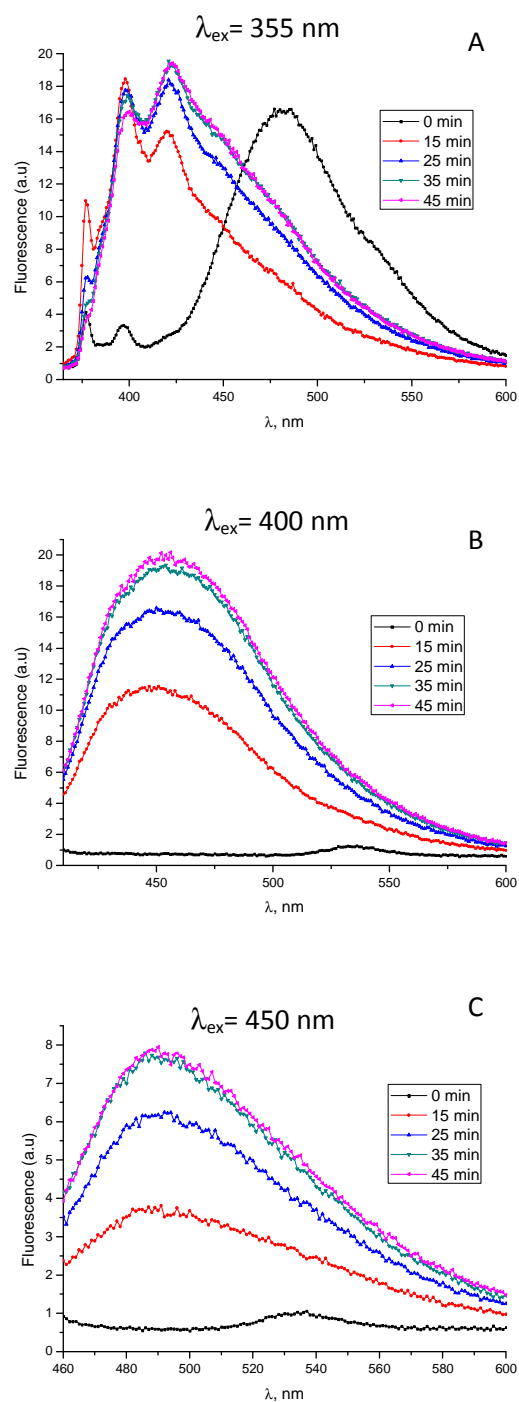


Figure S9. Evolution of the emission spectra of QD@Py (1.3×10^{-7} M) in aerated chloroform with the irradiation time (up to 45 min); the spectra were recorded at λ_{ex} 355 nm (A), 400 nm (B), and 450 nm (C).

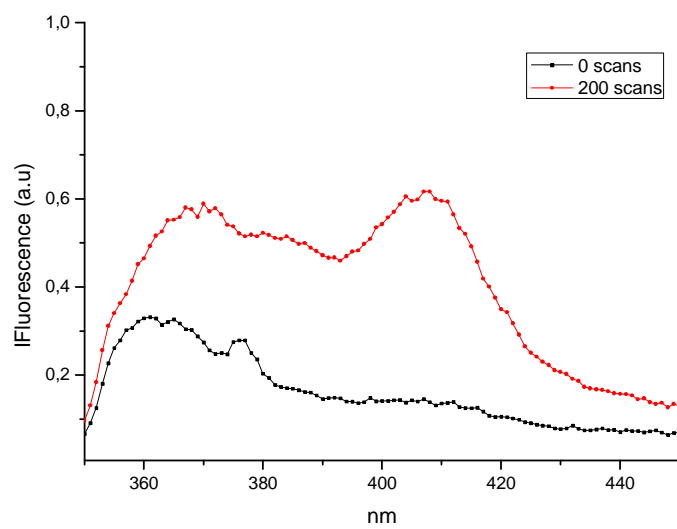


Figure S10. Fluorescence excitation spectra of Py-L₂-OH at 480 nm, taken before (●) and after (●) excitation at 355 nm inside the cell compartment of the spectrofluorometer for 200 scans.

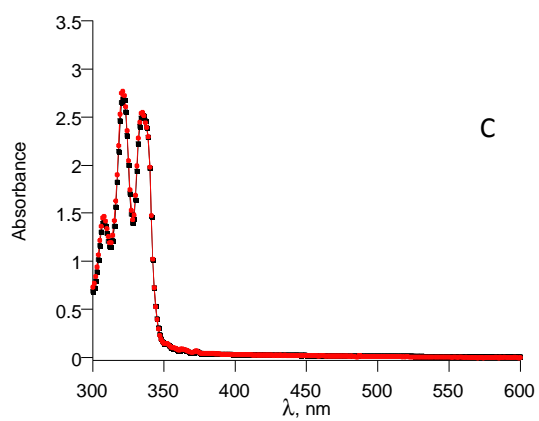
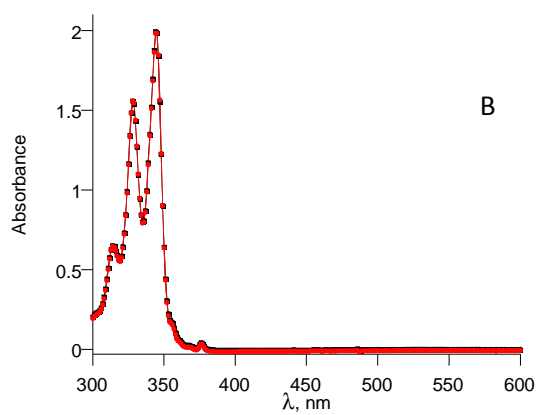
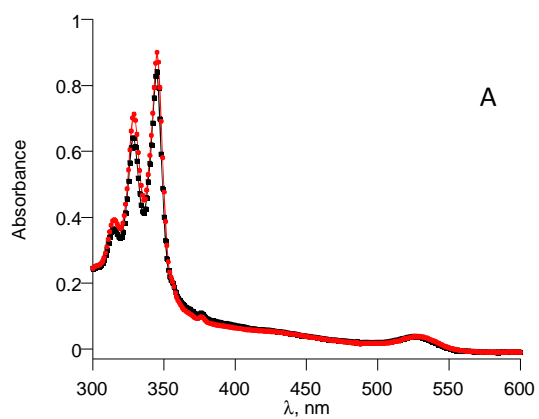


Figure S11. Absorption spectra of QD@Py (A), Py-L₂-OH (B), and Py (C) in amylene-free dichloromethane before (■) and after 50 minutes (●) UVA-lamp illumination in the presence of air.

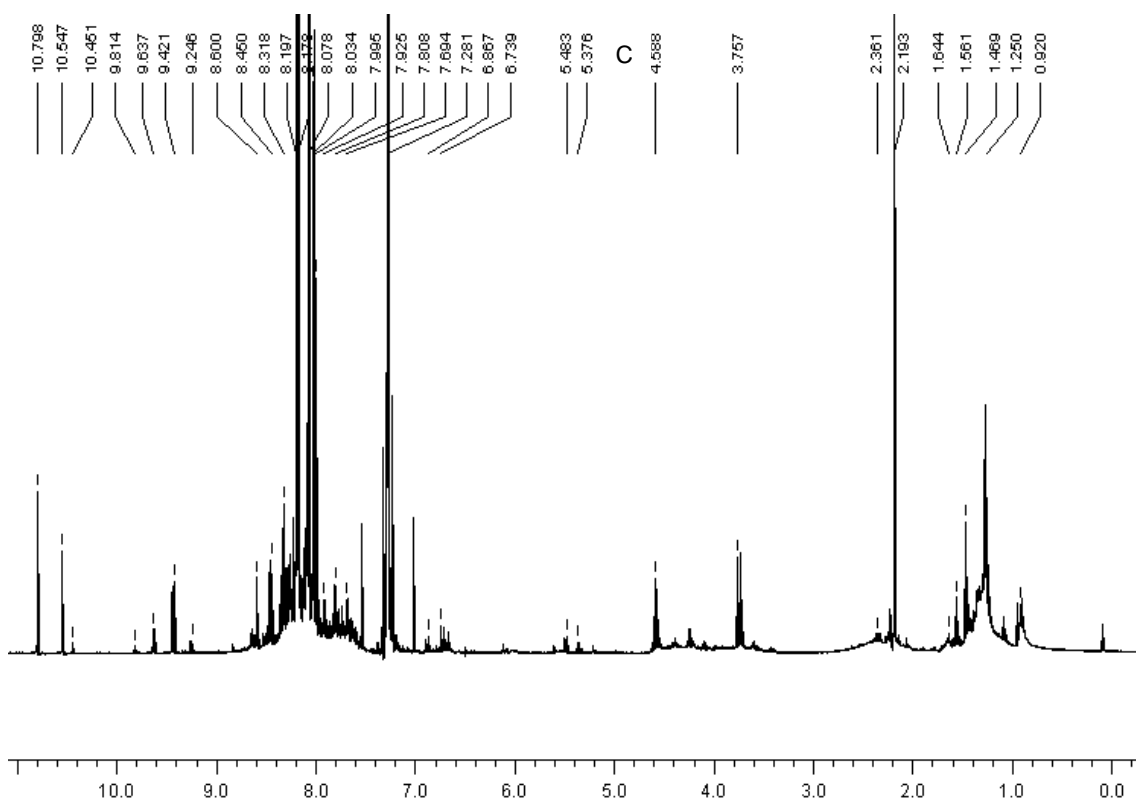


Figure S12. ^1H -NMR spectrum of the photolysate of pyrene (UVA irradiation for 12 h).

GC/MS and NMR spectra of compound V (Figures S13-S17)

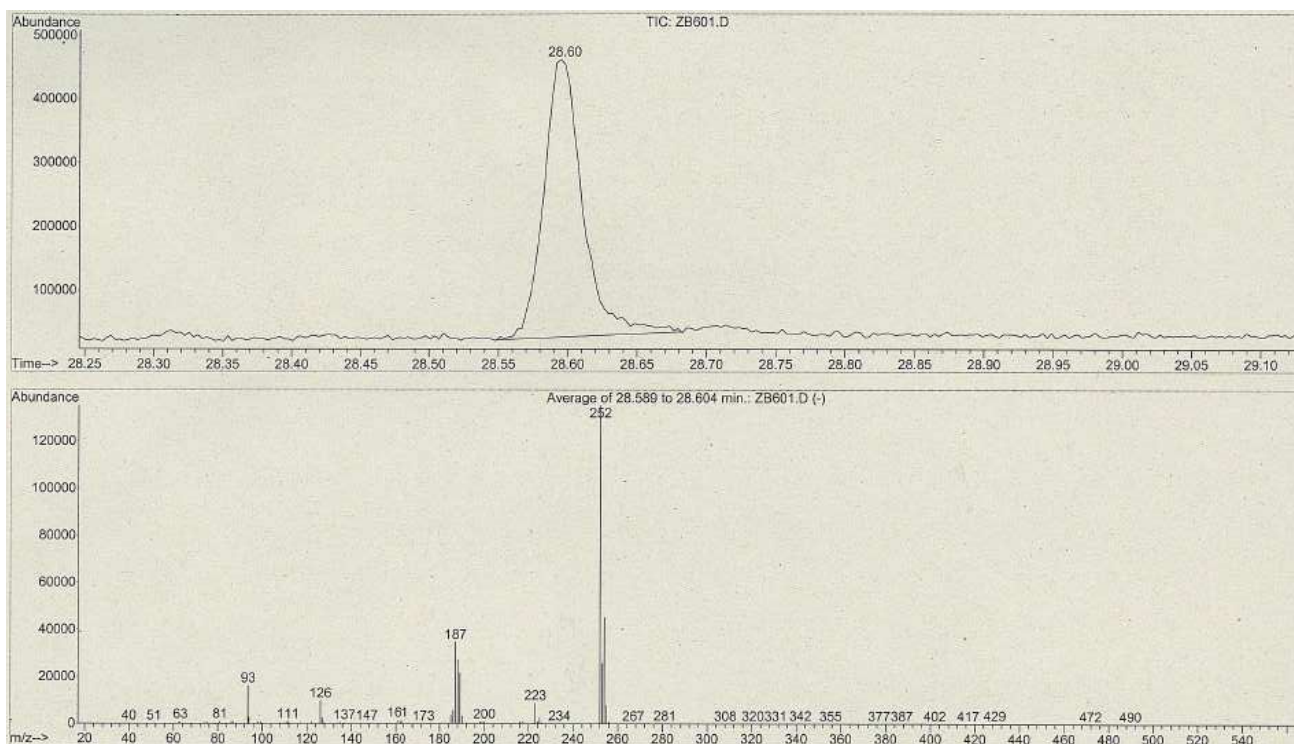


Figure S13. GC/MS spectrum of compound V

$^1\text{H-NMR}$ spectrum of compound V showed signals at 6.03 (s, 1H, proton exchangeable with D_2O), 7.77 (s, 1H), 7.88 (d, 9.2 Hz, 1H), 7.91 (d, 7.5 Hz, 1H), 7.98 (d, 9.2 Hz, 1H), 8.10-8.16 (m, 3H), and 8.27 (d, 9.2 Hz, 1H) ppm (Figures S14-S17). HSQC (Heteronuclear Single Quantum Coherence) experiment correlated the proton at 7.77 ppm (s) with the carbon at 111.98 ppm.

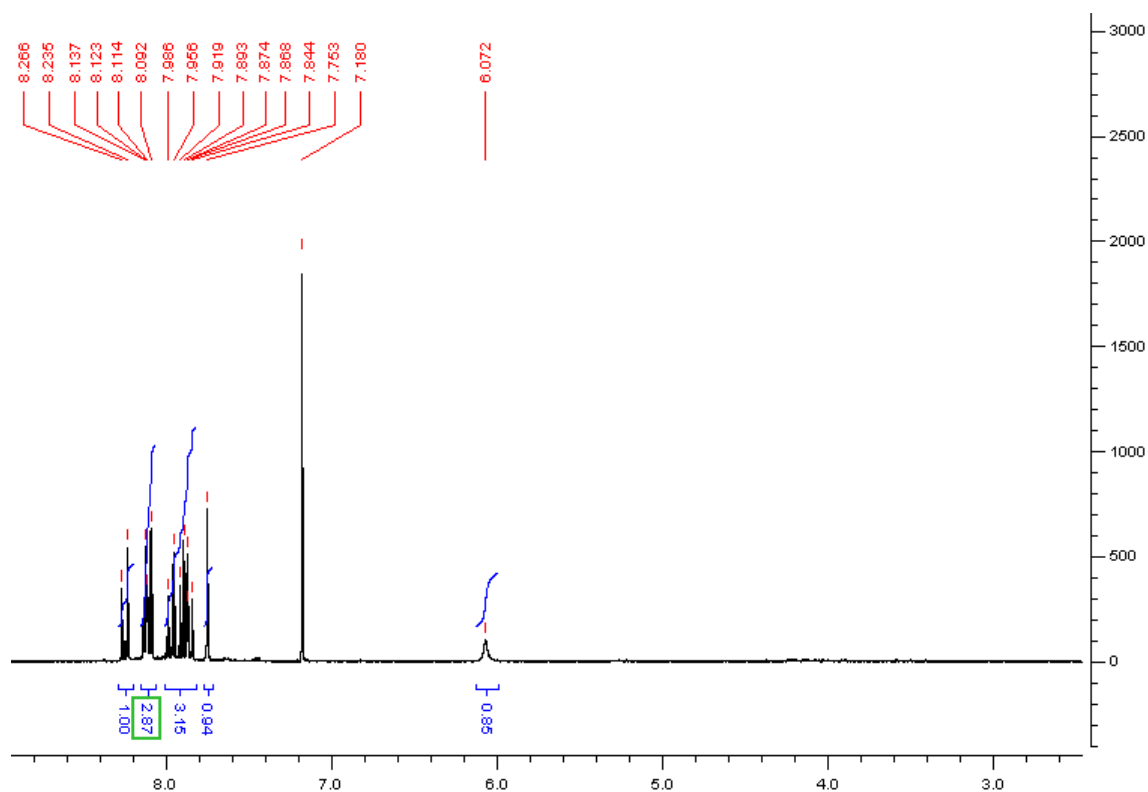


Figure S14. $^1\text{H-NMR}$ spectrum of compound V

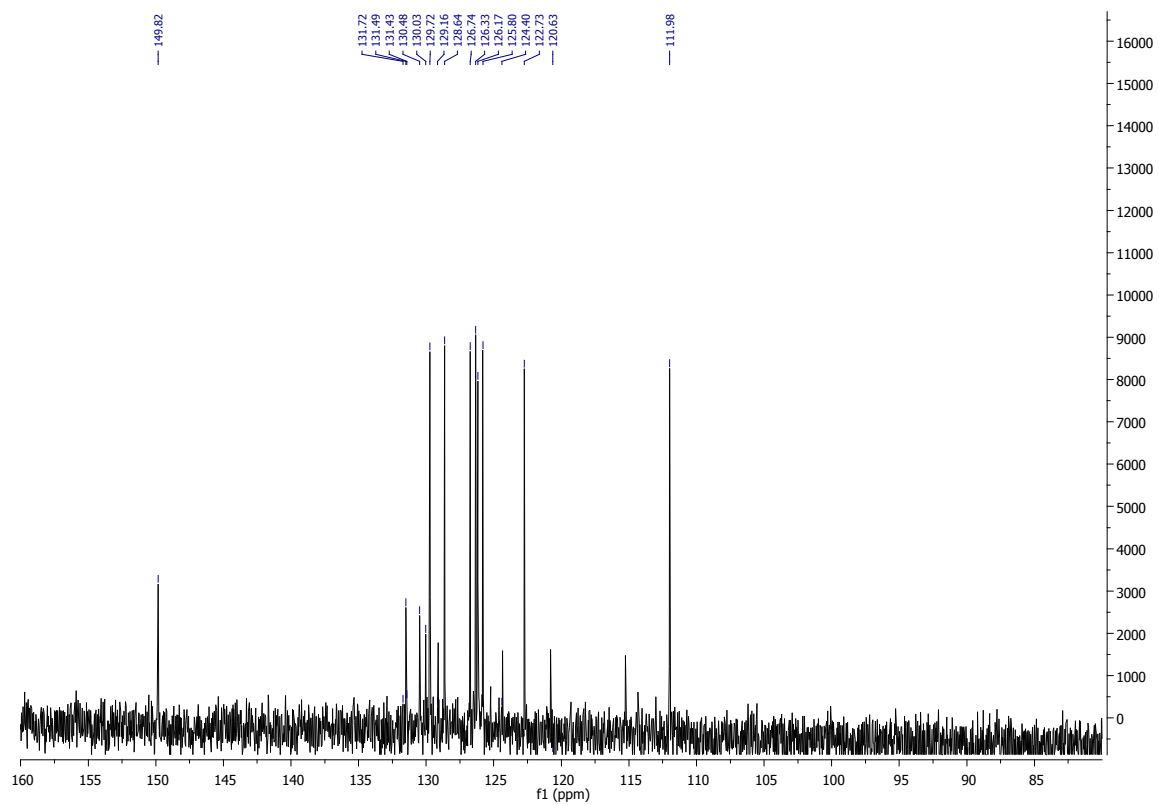


Figure S15. ^{13}C -NMR spectrum of compound V

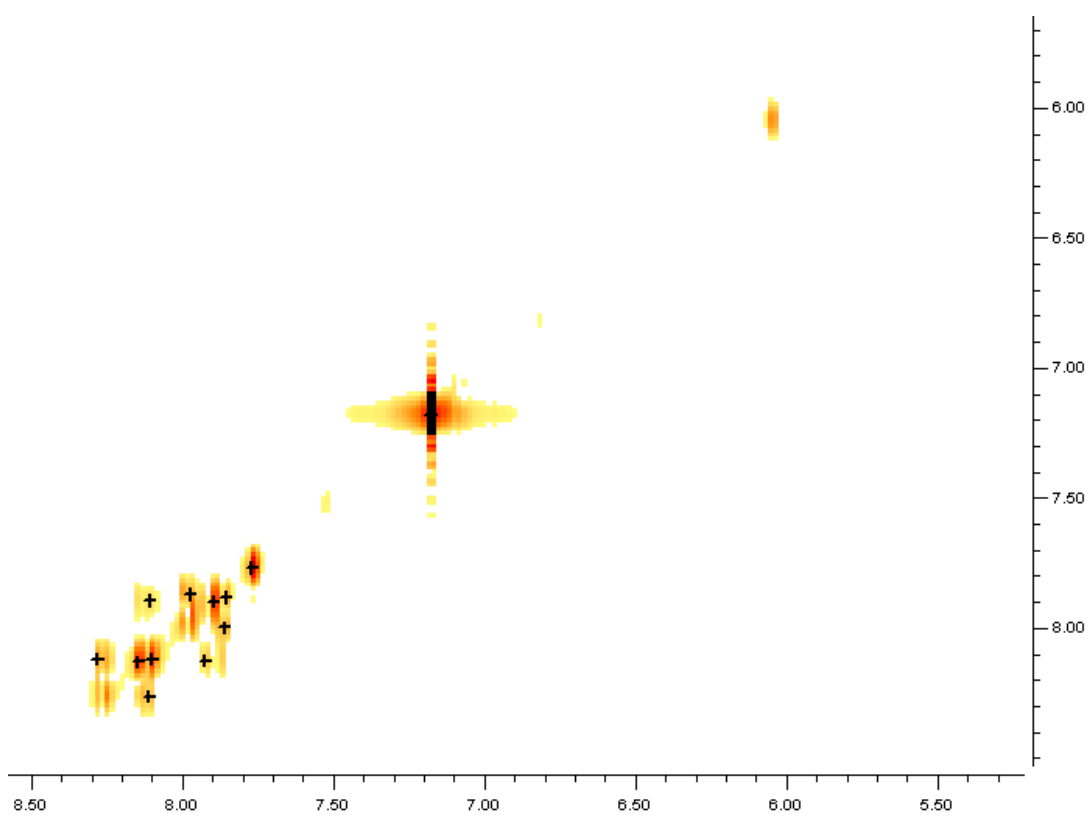


Figure S16. COSY-NMR spectrum of compound V

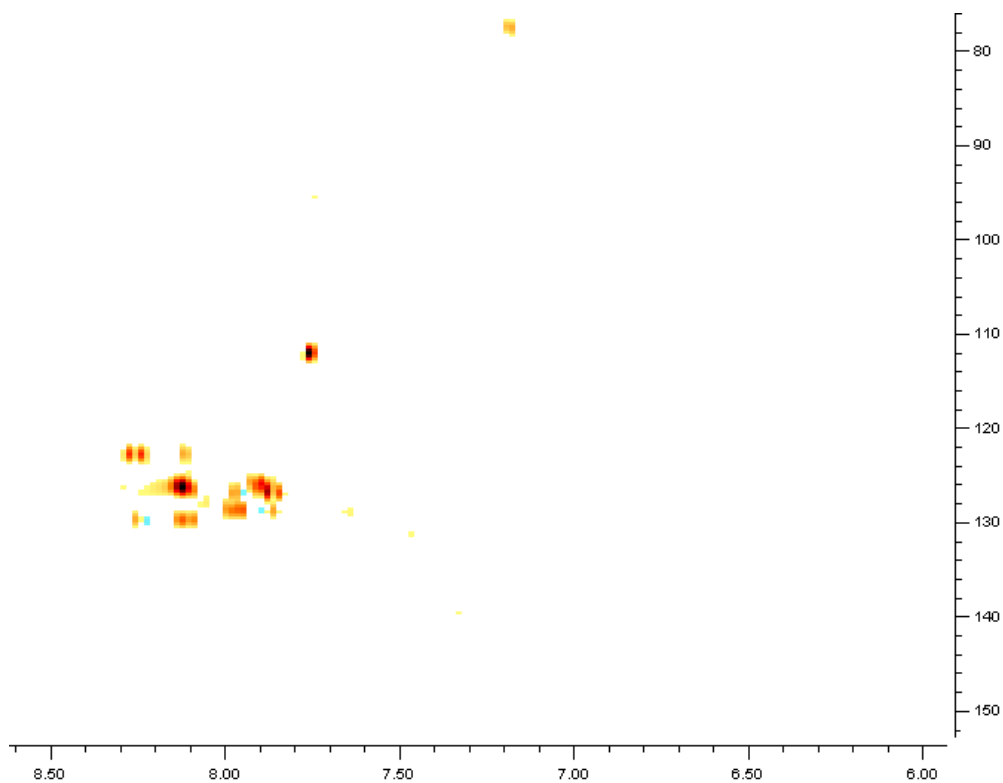


Figure S17. HSQC-NMR spectrum of compound V

NMR and GC/MS spectra of compound VI (Figures 18-20)

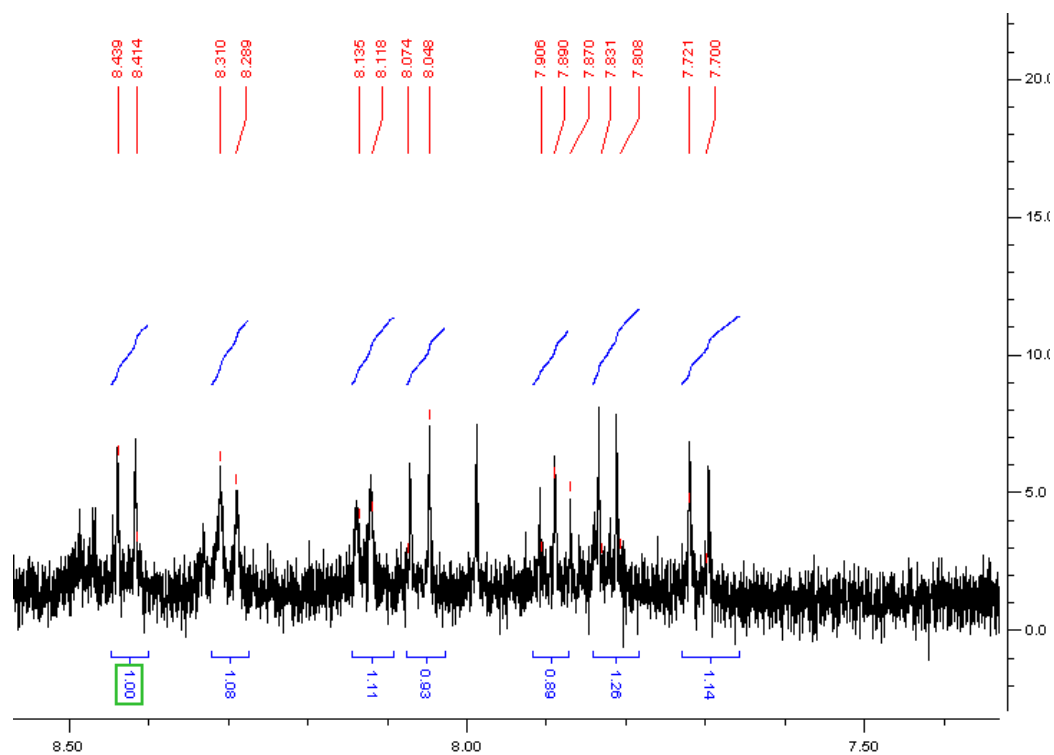


Figure S18. ¹H-NMR spectrum of compound VI

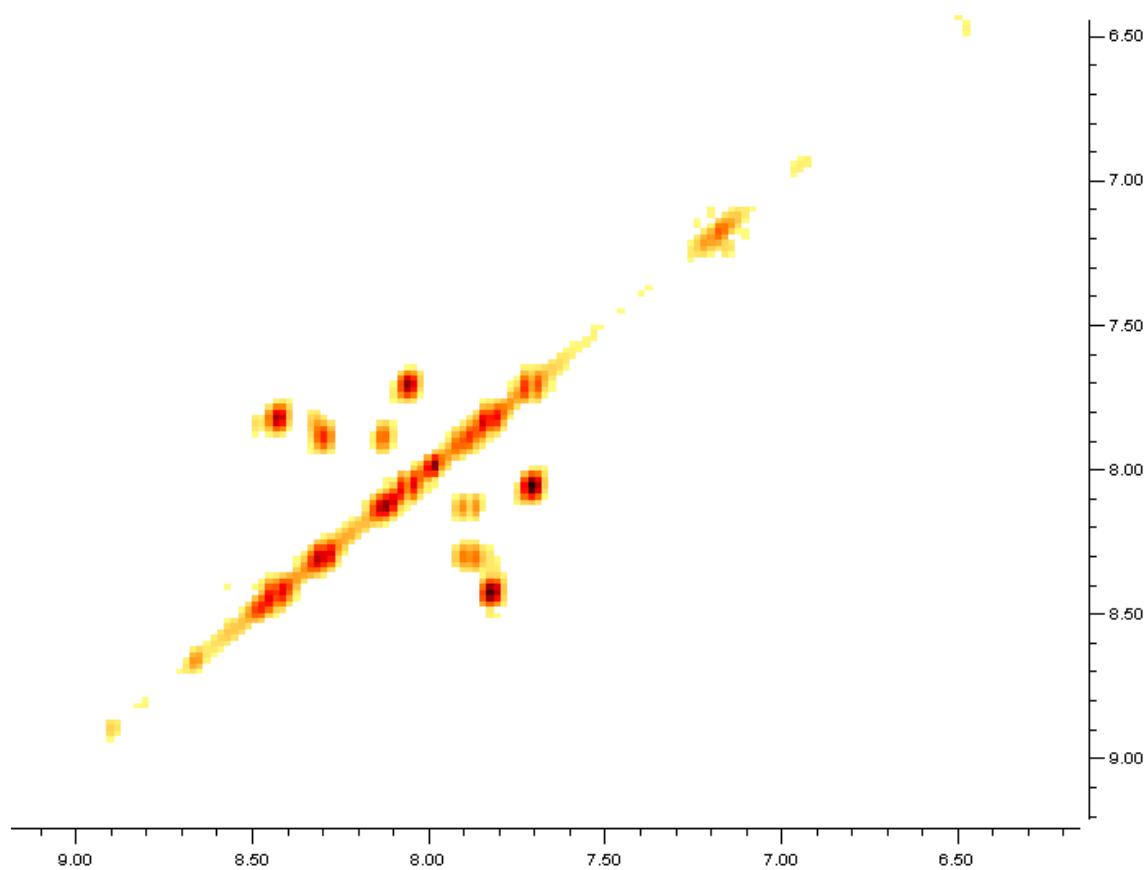


Figure S19. COSY-NMR spectrum of compound VI

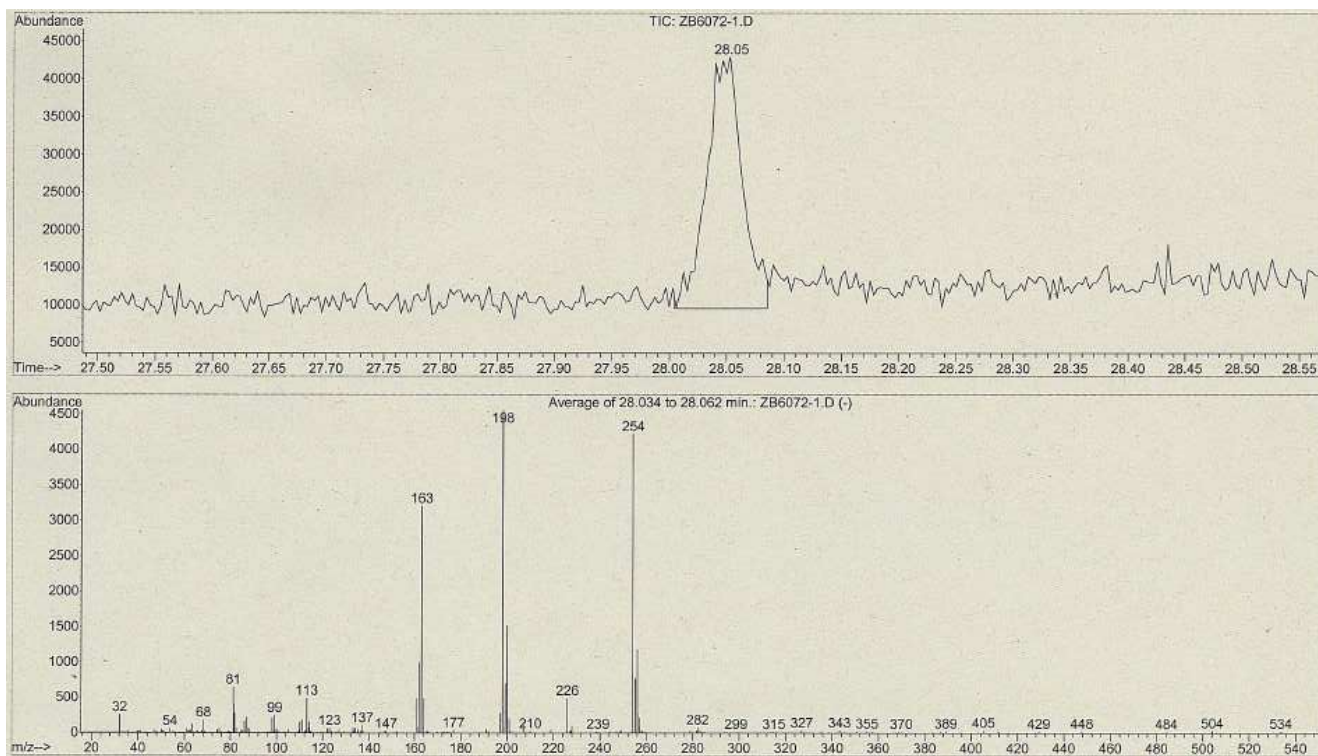


Figura S20. GC/MS spectrum of compound VI

¹H NMR spectra of a mixture of pyrenecarbaldehydes

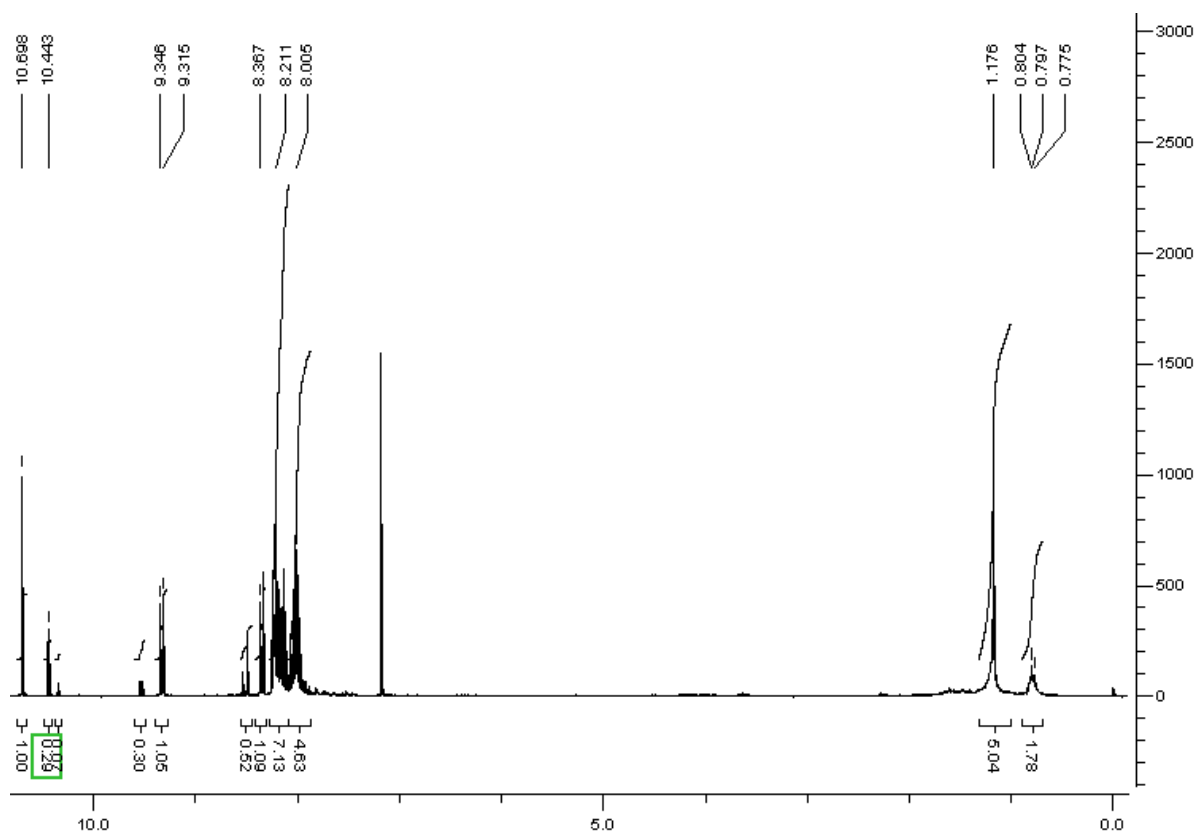


Figure S21. ¹H-NMR spectrum of a mixture of 1- and 4-pyrenecarbaldehyde

GC/MS and NMR spectra of compound VII (Figures 22 and 23)

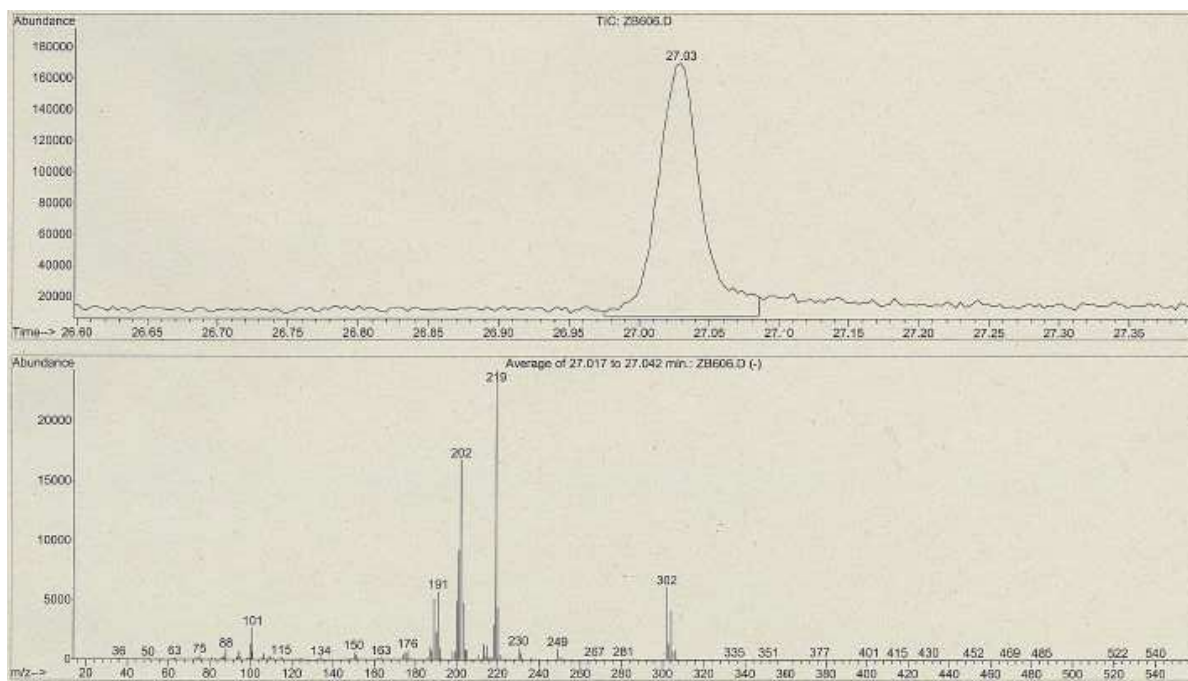


Figure S22. GC/MS spectrum of compound VII

GC/MS and NMR spectra of compound II (Figures 24-28)

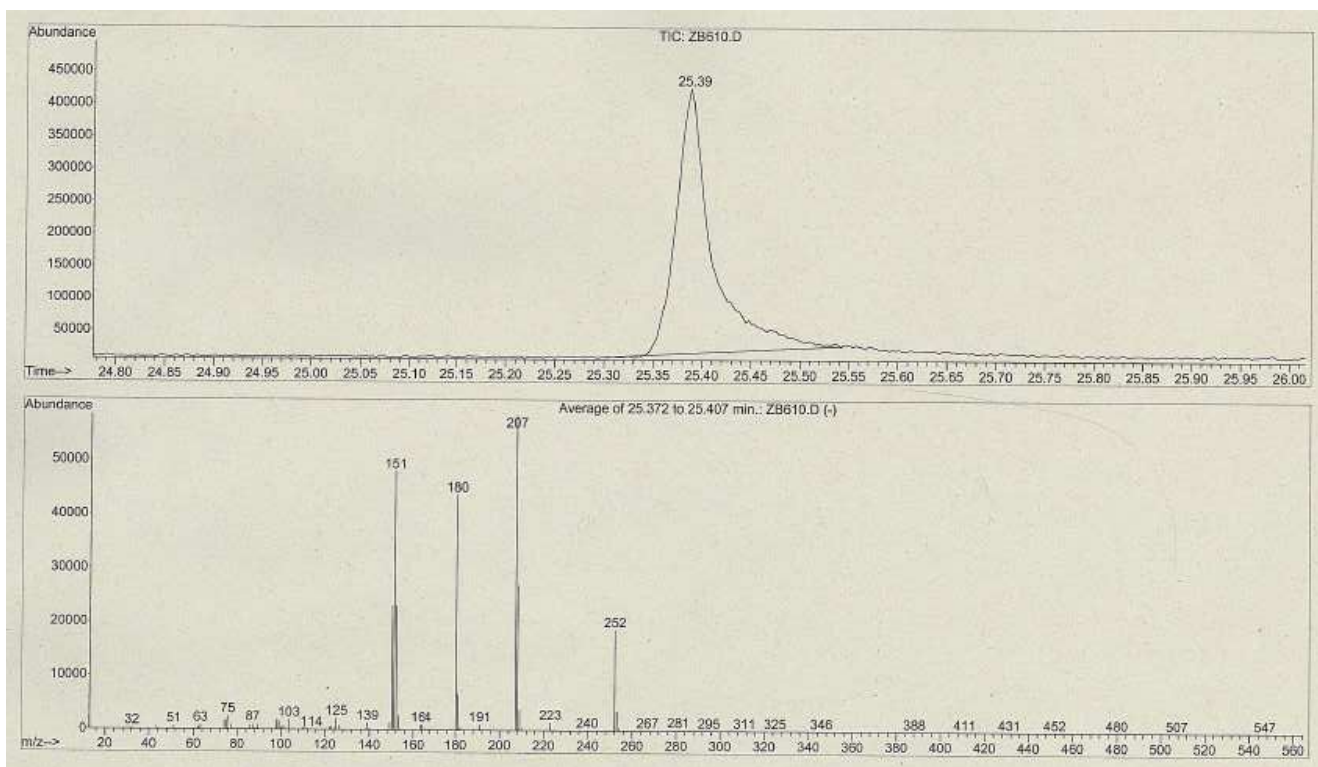


Figure S24. GC/MS spectrum of compound II

The $^1\text{H-NMR}$ spectrum of compound II showed signals at 1.36 (c, 7Hz, 3H), 4.47 (d, 7Hz, 2H), 6.61 (d, 10Hz, 1H), 7.55 (dd, 8.1 and 6.4, 1H), 7.58 (d, 8.3Hz), 1H), 7.68 (d, 10Hz, 1H), 7.73 (dd, 6.4 and 1.2Hz, 1H), 7.95 (dd, 8.2 y 1.1Hz, 1H), 8.15 (d, 8.2Hz, 1H). In addition, its $^{13}\text{C-NMR}$ presented signals at 14.00 (q), 62.16 (t), 125.57 (d), 126.14 (s), 127.66 (s), 127.71 (s), 128.64 (d), 129.32 (d), 132.02 (d), 132.5 (d), 132.71 (s), 135.03 (d), 137.35 (s), 141.91 (d), 170.72 (s), 184.69 (s) ppm.

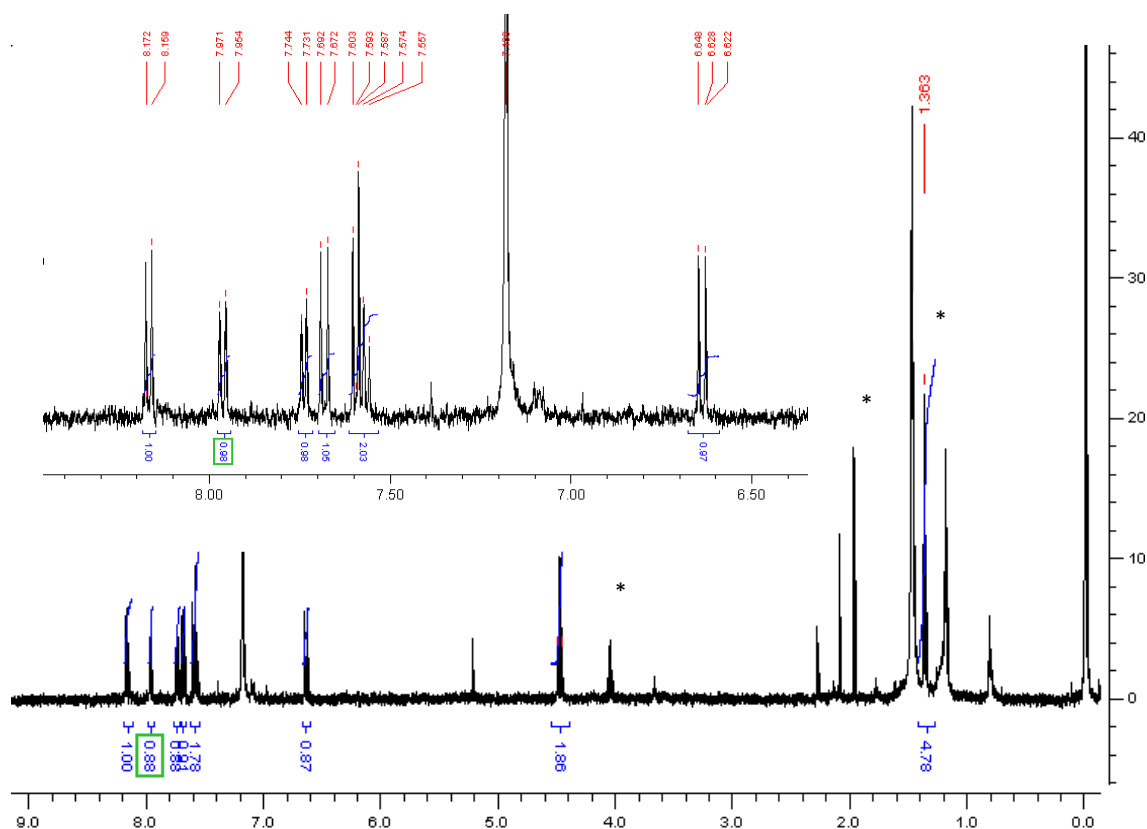


Figure S25. $^1\text{H-NMR}$ spectrum of compound II, * corresponds to the ethyl acetate used as eluent

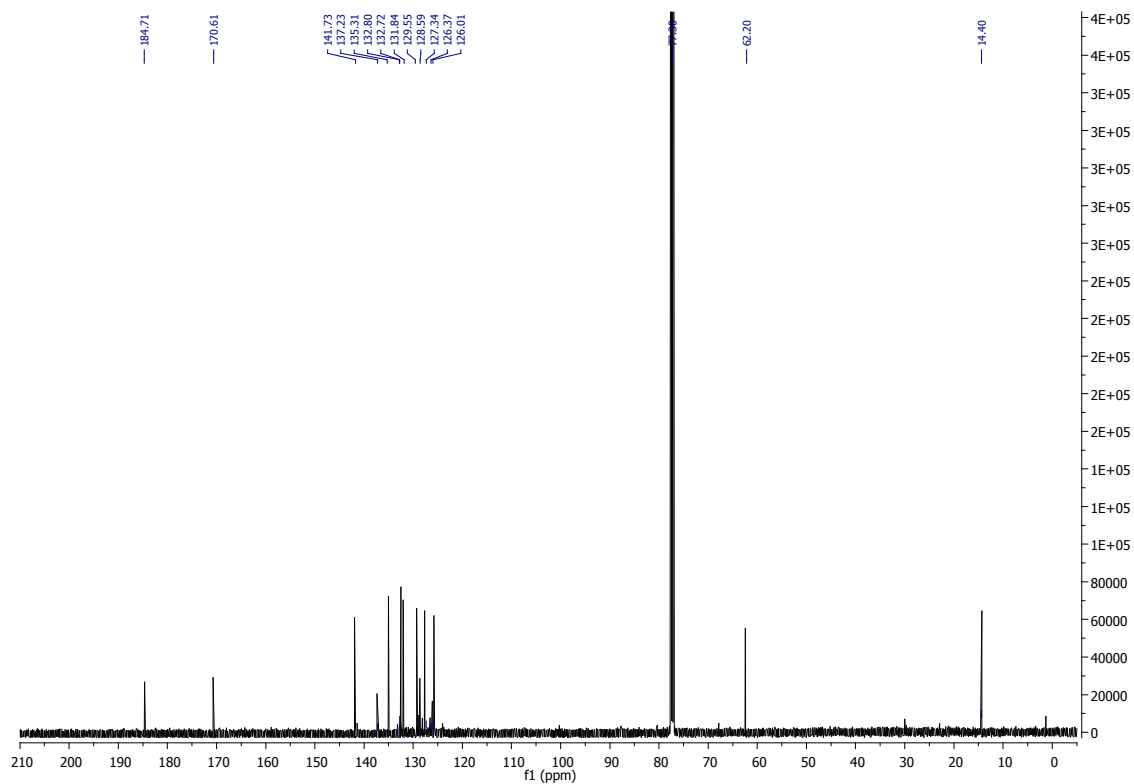


Figure S26. ^{13}C -NMR spectrum of compound II

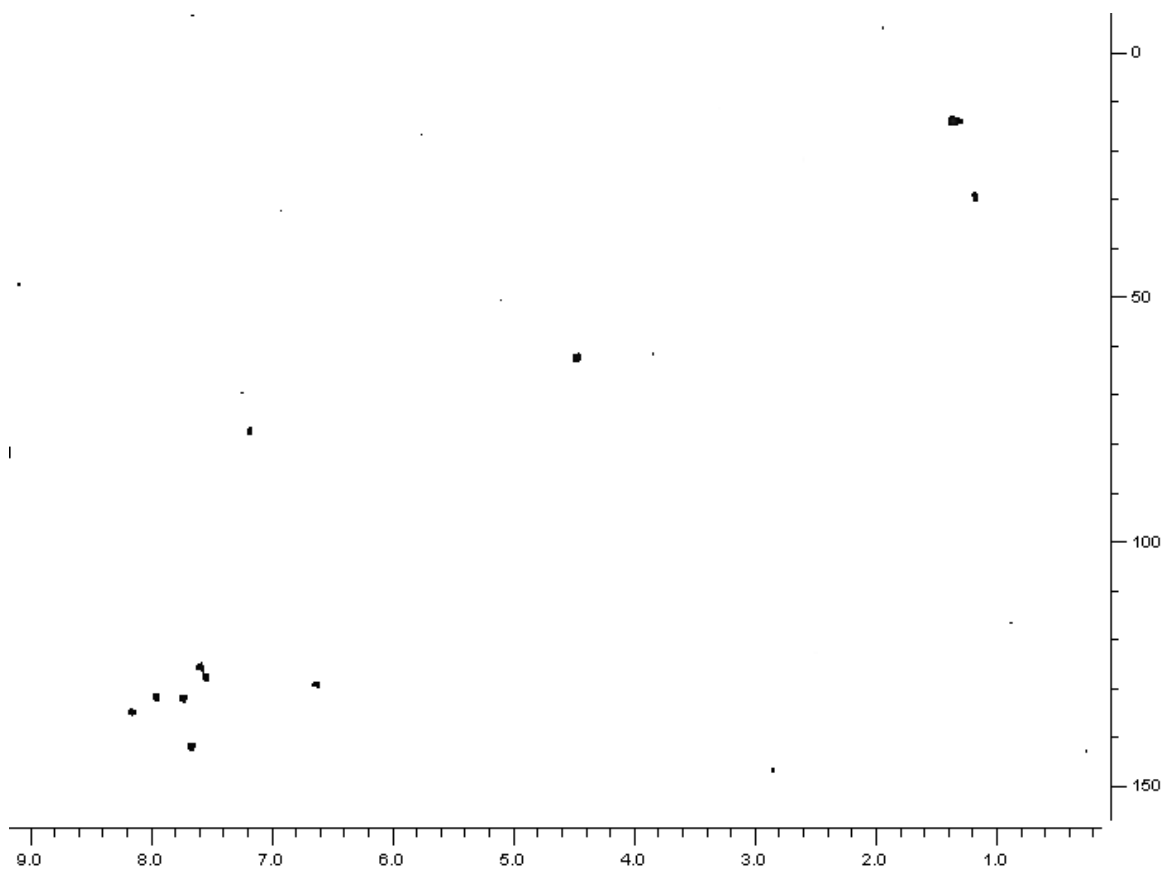


Figure S27. HSQC-NMR spectrum of compound II

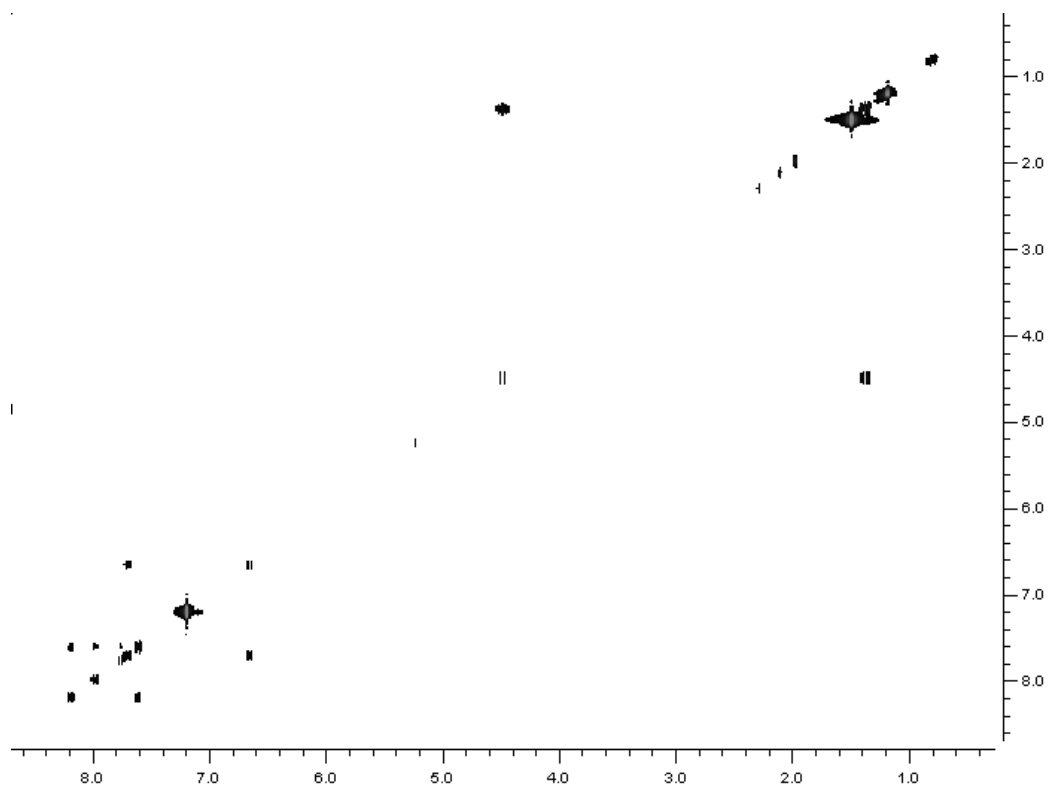


Figure S28 – COSY-NMR spectrum of compound II

¹ Z. A. Peng, X. Peng, *J. Am. Chem. Soc.* **2001**, *123*, 183

² W.W. Yu, L.Qu, W.Guo, X. Peng, *Chem. Mat.* **2003**, *15*, 2854.

Photoluminescence Enhancement of CdSe Quantum Dots: A Case of Organogel–Nanoparticle Symbiosis

Prashant D. Wadhavane,[†] Raquel E. Galian,^{‡,⊥} M. Angeles Izquierdo,^{*,†} Jordi Aguilera-Sigalat,[‡] Francisco Galindo,[†] Luciana Schmidt,^{‡,§} M. Isabel Burguete,[†] Julia Pérez-Prieto,^{*,‡} and Santiago V. Luis^{*,†}

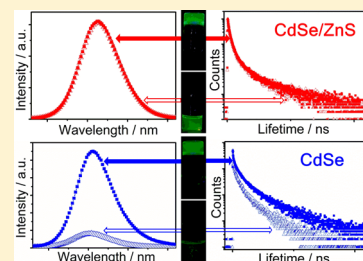
[†]Universitat Jaume I, Departamento de Química Inorgánica y Orgánica, Av. Sos Baynat, s/n, E-12071 Castellón, Spain

[‡]Instituto de Ciencia Molecular, Universidad de Valencia, c/Catedrático José Beltrán 2, Paterna, 46980 Valencia, Spain

[⊥]Departamento de Química Analítica, Edificio de Investigación, Universidad de Valencia, Dr. Moliner 50, 46100 Burjassot, Valencia, Spain

Supporting Information

ABSTRACT: Highly fluorescent organogels (QD–organogel), prepared by combining a pseudopeptidic macrocycle and different types of CdSe quantum dots (QDs), have been characterized using a battery of optical and microscopic techniques. The results indicate that the presence of the QDs not only does not disrupt the supramolecular organization of the internal fibrillar network of the organogel to a significant extent, but it also decreases the critical concentration of gelator needed to form stable and thermoreversible organogels. Regarding the photophysical properties of the QDs, different trends were observed depending on the presence of a ZnS inorganic shell around the CdSe core. Thus, while the core–shell QDs preserve their photophysical properties in the organogel medium, a high to moderate increase of the fluorescence intensity (up to 528%) and the average lifetime (up to 1.7), respectively, was observed for the core QDs embedded in the organogel. The results are relevant for the development of luminescent organogels based on quantum dots, which have potential applications as advanced hybrid materials in different fields.



1. INTRODUCTION

The development of hybrid materials is an area of research of increasing interest due to symbiotic effects which can yield novel properties and potential applications upon combination of inorganic nanoparticles with organic scaffolds such as peptides, carbon nanotubes, polymers, or gels.¹ In particular, low molecular weight gelators are well studied functional organic molecules for the development of hybrid materials because they are known to self-assemble via noncovalent interactions to yield well ordered supramolecular structures (organogels) under favorable experimental conditions.² Such systems constitute a supporting environment for metallic nanoparticles of different nature, providing both stability and spatial organization to the inorganic components.³ Thus, a broad variety of nanoparticle doped organogels based mainly on the interaction of gold⁴ and silver⁵ nanoparticles with self-assembled fibrillar networks have been described. Studies on the chemical structure of the gelators, and the nanoparticles have allowed a better understanding of the structural parameters determining the final properties of such systems.

Due to their intrinsic photophysical properties, emissive semiconductor nanocrystals (quantum dots, QDs) can be used in the development of fluorescent organogels, which are of great interest due to their potential applications in the preparation of optoelectronic devices and sensors.⁶ It must be noted that gold nanoparticles in combination with organic fluorophores have been previously used to prepare fluorescent

hybrid organogels.^{4b} However, gold nanoparticles often quench the fluorescence of organic chromophores,^{4a–c} and therefore, QDs appear to be very promising nanoparticles in the development of fluorescent hybrid organogels.

QDs are composed of a fluorescent core, usually CdSe or CdTe, which can be covered by an inorganic shell of a higher band gap material (ZnS, ZnSe, CdS) to yield core–shell (CS) QDs, which exhibit higher fluorescence quantum yields (Φ_F) than the core QDs in most cases.⁷ Inorganic nanoparticles also need to be capped by organic ligands, which provide them with colloidal stability and determine the solubility of the nanoparticles in different media. Trioctylphosphine and trioctylphosphine oxide (T) are the most common organic ligands used in the synthesis of hydrophobic quantum dots.⁸ Alternatively, amines with a long alkyl chain have also been used to stabilize different types of quantum dots.⁹ Compared to organic fluorophores, QDs exhibit exceptional features, such as broad excitation bands along with narrow and size-dependent emission spectra.¹⁰ The synthesis and characterization of these nanoparticles have been the object of many studies,^{7b,8a,11} and different biological^{10c,12} and analytical^{12b,c,13} applications have been described for them. However, very few examples deal with the incorporation of quantum dots into supramolecular materials such as organogels. For instance, the groups of

Received: October 24, 2012

Stupp,¹⁴ McPherson,¹⁵ and Banerjee¹⁶ incorporated CdS nanoparticles into self-assembled structures obtained from organogel and hydrogel-based systems. Li and co-workers described the preparation of hybrid organogels by mixing CdSeS nanocrystals with a dipeptide molecule in a gelling solution.¹⁷ Bardelang and co-workers prepared CdSe/ZnS QD-peptide nanocomposites¹⁸ using ultrasonic treatment and suggested the size reduction of the QDs by a peptidic amyloid supergelator, based on the blue shift of the photoluminescence emission.^{18b} Very recently, the groups of Zhou and You reported the rational design of a hyperbranched molecule to prepare fluorescent CdSe and CdSe/ZnS based hybrid materials by sonication.¹⁹ In addition, the potential application of QD-doped organogels as chemical sensors of gases has been recently demonstrated.^{18a,20}

Although these pioneering works set the basis for the development of QD-doped organogels, a number of fundamental aspects, such as (i) the influence of the QD composition on the QD/organogel mutual interaction and (ii) the potential synergic effects between the QDs and the organogel to improve the (photo)physical properties of the hybrid system, remain unexplored. In the present work we used the pseudo-peptidic macrocyclic compound **1** (Figure 1A) as

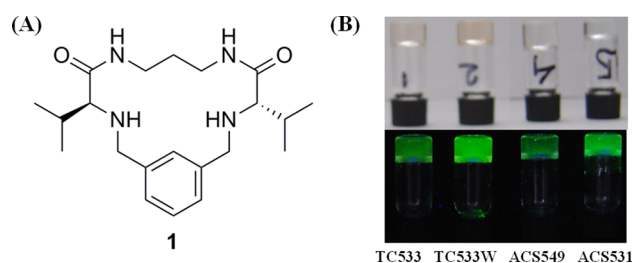


Figure 1. (A) Chemical structure of organogelator **1**. (B) Photographs of representative samples of hybrid organogels containing different types of core and core-shell QDs under room (top) and UV (bottom) light, showing the luminescence of the QDs in organogel media.

the organogelator along with different types of QDs, such as the CdSe core and the CdSe/ZnS core-shell capped with trioctylphosphine oxide and octadecylamine (ODA), as organic ligands. Our results indicate that the formation of the organogel is favored in the presence of the QDs because it is possible to reduce the concentration of gelator to form stable and thermoreversible QD-organogels. The analysis of the photo-physical properties of the QDs reveals that the core-shell QDs preserve their emission intensity and fluorescence lifetime under the experimental conditions used to prepare the organogels. The fluorescence lifetimes and their corresponding contributions to the fluorescence signal follow the same pattern for each set of core-shell QDs regardless of the presence of organogelator **1**. Very importantly, the optical properties of the core QDs used in this study are in fact significantly improved in the organogel media. Thus, a high increase in the luminescence intensity, combined with a moderate increase of the average luminescence lifetime, is observed for the core QDs embedded in the organogel. Our data are in accordance with a gel-induced increase of the radiative rate constant as the main contributing factor for the fluorescence enhancement.

2. EXPERIMENTAL SECTION

2.1. Materials. All reagents were used as received without further purification. Toluene (spectroscopy grade), hexanes (spectroscopy grade), methanol (spectroscopy grade), and acetone (spectroscopy grade) were purchased from Scharlab. Cadmium oxide (CdO, >99.9%, powder), selenium (Se, 99.99%, powder, 100 mesh), trioctylphosphine oxide (T, 99%), trioctylphosphine (90%), diethylzinc solution (ZnEt₂), bis(trimethylsilyl) sulphide (TMS)₂S, 1-octadecene (ODE, 90%), oleic acid (OA, 90%), and octadecylamine (ODA, 97%) were purchased from Sigma-Aldrich. Tetradecylphosphonic acid (TDPA, 98%) was purchased from Alfa Aesar). Cyclophane **1** was synthesized according to the described experimental procedure.²¹ The spectral characterization of the prepared compound **1** coincided with the reported data.

2.2. Synthesis of Quantum Dots. **2.2.1. Synthesis of Core QDs.** The CdSe QDs were synthesized following the methodology of Peng et al. with some modifications.^{8a,22}

Synthesis of TC533 QDs. Briefly, the mixture of CdO (51 mg), TDPA (223 mg), and trioctylphosphine oxide (3.776 g) was heated at 300 °C under Ar until a clear solution was obtained. Then, the temperature was lowered to 270 °C and a solution of Se in trioctylphosphine (41 mg in 2.4 mL) was added and maintained during 1.5 min. The nanoparticles were precipitated in cold methanol, centrifuged three times (8000 rpm), and redissolved in toluene to yield TC533 QDs ($\Phi_F = 8\%$).

Synthesis of TC533W QDs. In order to eliminate part of the organic ligands from the TC533 inorganic surface, the nanoparticles were washed 6 times with methanol and redissolved in toluene to yield TC533W QDs ($\Phi_F = 3\%$).

Synthesis of ACS527 QDs. The TC533 QDs were used to obtain CdSe QDs covered with ODA. The ligand exchange reaction was made in toluene under nitrogen atmosphere, using an amine/QD ratio of 5000:1, for 48 h. The resulting nanoparticles were precipitated, and washed with methanol and redissolved in toluene to yield ACS527 QDs ($\Phi_F = 4.2\%$).

2.2.2. Synthesis of Core-Shell QDs. **Synthesis of TC5572 QDs.** In the case of CdSe/ZnS QDs capped with trioctylphosphine oxide as ligand, a one-pot Raymo et al. procedure was used.²³ In this case, the temperature of addition of Se to the trioctylphosphine solution was 220 °C and the mixture was maintained at 200 °C for 40 min. Then, the temperature was lowered to 120 °C and a solution of ZnEt₂ (197 mg) and (TMS)₂S (250 mg) in trioctylphosphine (5 mL) was added dropwise. After addition, the mixture was maintained at 70 °C for 24 h. After cooling to ambient temperature, MeOH was added and the resulting precipitate was filtered and dissolved in hexane to yield TC5572 QDs ($\Phi_F = 35\%$).

Synthesis of ACS531 QDs. The above-mentioned methodology (one pot synthesis) with some modifications was used for the synthesis²³ but using OA and ODE instead of phosphines. Briefly, CdO (51 mg), oleic acid (339 mg), and ODE (9.8 mL) were heated in a flask to 300 °C under nitrogen atmosphere. The temperature was then lowered to 220 °C and a solution of Se (39 mg) in ODE (2.5 mL) and ODA (previously heated to 220 °C for 3 h) was added. Then, the temperature was lowered to 200 °C and maintained for 10–40 min depending on the nanoparticle size desired. Subsequently, the temperature was lowered to 120 °C, a mixture of ZnEt₂ and (TMS)₂S dissolved in ODE was added, and the temperature was maintained at 70 °C overnight. The QDs were precipitated in acetone and dissolved in hexane or toluene to yield ACS531 QDs ($\Phi_F = 18\%$).

Synthesis of ACS549 QDs. A standard procedure was applied to the ligand exchange of CdSe/ZnS QDs covered with trioctylphosphine oxide by octadecylamine to yield ACS549 QDs ($\Phi_F = 41\%$).

2.3. Photophysical Characterization. UV-visible absorption measurements were made using a Hewlett-Packard 8453 spectrophotometer. Steady-state fluorescence spectra were recorded in a Spex Fluorog 3-11 equipped with a 450 W xenon lamp. Fluorescence spectra were recorded in the front face mode. Time-resolved fluorescence measurements were done with the technique of time correlated single photon counting (TCSPC) in an IBH-5000U.

Table 1. Description of Core and Core–Shell QDs Used in This Study

sample	core	shell	ligand	D (nm)	λ_{abs} (nm)	λ_{em}^a (nm)	fwhm ^b (nm)	Φ_{F}
TC533	CdSe		trioctylphosphine oxide	2.63 (2.5) ^c	525	533	22	0.08 ^d
TC533W	CdSe		trioctylphosphine oxide	2.63 (2.5) ^c	525	533	22	0.03 ^d
ACS27	CdSe		octadecylamine	2.63 (2.5) ^c	520	526	24	0.04 ^d
TCS572	CdSe	ZnS	trioctylphosphine oxide	3.33 (3.5) ^c	565	572	23	0.35 ^e
ACS531	CdSe	ZnS	octadecylamine	2.50 (3.2) ^c	516	531	25	0.18 ^d
ACS549	CdSe	ZnS	octadecylamine	2.8 (3.8) ^c	540	549	25	0.41 ^d

^a $\lambda_{\text{exc}} = 465$ nm. ^bfwhm = full width at half-maximum. ^cCalculated based on TEM images. ^dFluorescein in NaOH (0.1 M) was used as reference ($\Phi_{\text{ref}} = 0.87$). ^eRhodamine 6G in EtOH was used as reference ($\Phi_{\text{ref}} = 0.95$).

Samples were excited with an IBH 464 nm NanoLED with a fwhm of 1.4 ns and a repetition rate of 100 kHz. Data were fitted to the appropriate exponential model after deconvolution of the instrument response function by an iterative deconvolution technique, using the IBH DAS6 fluorescence decay analysis software, where reduced χ^2 and weighted residuals serve as parameters for goodness of the fit. All the samples were measured in aerated conditions, except when otherwise stated.

2.4. ¹H NMR and ³¹P NMR Spectroscopy. ¹H and ³¹P NMR spectra were recorded on Bruker Avance DPX300 and 400. Standard Bruker software was used for acquisition and processing routines. The NMR samples containing organogelator **1** were prepared by heating the compound (2.5 mg) in deuterated toluene (2.5 mL) to 80 °C. The resulting homogeneous mixture (0.7 mL) was transferred into a NMR tube. The samples were allowed to cool to room temperature before the measurements. The NMR samples containing the nanoparticles were prepared by dissolving TC533 QDs (7.2×10^{-4} M) or TC533W QDs (6.8×10^{-4} M) in 0.7 mL of deuterated toluene. The NMR samples containing the QDs/organogelator **1** mixture were prepared by adding TC533 or TC533W QDs to a vial containing organogelator **1** in deuterated toluene at 80 °C (gelator: 2.67×10^{-3} M in 1.4 mL of toluene, 1/QD ratio of 3.7/1 and 3.9/1 for TC533 and TC533W, respectively). The resulting homogeneous mixture (0.7 mL) was transferred into a NMR tube. The samples were allowed to cool to room temperature before the measurements.

2.5. IR Spectroscopy. Infrared measurements were performed on a Fourier transform-infrared spectrometer NICOLET 5700 (Thermo Electron Corporation). The samples were prepared as follows: organogelator **1** (5 mg) was dissolved in toluene (1 mL) by heating to 80 °C. After complete solubilization of **1**, 0.5 mL of the solution was transferred into a vial containing 0.2 mL of TC533 (organogelator/QDs was 50/1 in molar ratio). Both samples, the 4.5 remaining milliliters of organogelator **1** and the nanoparticle/**1** mixture, were cooled to room temperature. After gelation, a small amount of each sample was triturated with KBr in order to prepare the pellet for IR measurements. The TC533 QDs sample was prepared by slow evaporation of the solvent (toluene) in a mortar followed by the subsequent addition of KBr. A similar procedure was followed when using an organogelator concentration lower than that needed to obtain gelation.

2.6. Transmission Electron Microscopy. Samples for transmission electron microscopy (TEM) were prepared by dissolving macrocycle **1** (6 mg/mL) in hot toluene, followed by addition of QDs to the samples at the suitable concentration to visualize the individual nanoparticles. A drop of the solution was deposited onto a holey carbon coated 300 mesh TEM copper grid and was dried under air. The dried grid was loaded into a single-tilt sample holder. The TEM samples were examined on a JEOL 2100 TEM equipped with a high resolution Gatan CCD camera (11 Mpixels). The TEM equipment was operated at 120 kV and 62 μ A.

2.7. Atomic Force Microscopy. Atomic force microscopy (AFM) images were recorded under ambient conditions using a JEOL SPM-5200 operating in the tapping mode regime. Microsilicon cantilever tips (μ m-mash NSC35/ALBS) with a resonance frequency of approximately 275 kHz, a tip radius curvature smaller than 10 nm, a cone angle smaller than 30°, and a spring constant of about 15 N/m were used. Height and amplitude images were measured simulta-

neously. The atomic force microscope samples were prepared by dissolving macrocycle **1** in hot toluene followed by addition of QDs. The clear solutions were drop cast on freshly cleaved muscovite mica and allowed to evaporate for 20 h at room temperature.

2.8. Formation of the Nanoparticle Doped Organogels. A certain amount of cyclophane **1** was placed in open vials and dissolved in toluene at 80 °C. The transparent solutions were transferred to preheated 1 cm \times 1 cm \times 4 cm fluorescence cuvettes (quartz) immersed in a water bath at 80 °C. Then, the different types of QDs dissolved in toluene were added at the appropriate concentrations for the photophysical measurements (typically, absorbance <0.1 at the excitation wavelength for the fluorescence experiments). The samples were allowed to cool to room temperature in the fluorescence cuvettes in the dark for 30 min.²⁴ The transparent nature of the gels made recording of the pertinent spectroscopic data possible.

3. RESULTS AND DISCUSSION

3.1. Selection of Quantum Dots and Organogelator.

Several factors need to be considered when selecting the components to prepare hybrid organogels with suitable optical properties: (i) the inorganic nanoparticles and the gelator need to be dispersed in a compatible solvent in order to obtain a homogeneous solution of the system, (ii) the components must be stable under the experimental conditions, and (iii) the resulting QD–organogel must exhibit excellent transparency for the optical characterization. Pseudopeptidic macrocycle **1** was selected because of its ability to self-assemble in a number of solvents to yield organogels with excellent optical transparency,²⁵ suitable to study photochemical and photophysical processes.^{24,26} In a preliminary work, compound **1** in combination with commercial CdSe/ZnS QDs emitting at 480 nm were used to prepare emissive hybrid organogels demonstrating that the important photophysical properties of the QDs, such as the position of the first exciton and the emission maxima, the emission intensity, and the fluorescence lifetimes, were preserved in the organogel medium.²⁰ The interest of the results and the simplicity of the methodology used to prepare the transparent QD–organogels encouraged us to study the use of different types of noncommercial core and core–shell quantum dots to investigate the potential symbiotic effects between the QDs and the organogel that could lead to an improvement of the (photo)physical properties of the hybrid system. The QDs used in this work were synthesized in our lab following reported methodologies with some modifications.^{8a,22,23}

As stated above, the photophysical properties of quantum dots and their potential applications depend on their chemical composition. In this study, we selected quantum dots based on CdSe core because many synthetic protocols are available to prepare this type of semiconductor nanocrystals soluble in toluene,²⁷ where cyclophane **1** forms transparent and stable organogels. We focused on the preparation of core and core–

shell QDs, the latter having a ZnS inorganic shell which produces nanocrystals with improved fluorescence and higher stability.⁷ In addition, two different types of capping ligands often used in the preparation of QDs were introduced in order to determine their possible effect on the photophysical properties of the QD–organogel system. Table 1 summarizes the chemical composition and main characteristics of the quantum dots used in this study. Herein, the nanocrystals are labeled with a letter to denote the organic ligand on the surface (T for trioctylphosphine oxide, A for the amine derivatives), one or two letters to indicate the absence or the presence of the ZnS inorganic shell (C for core, CS for core–shell), and a three digit number which corresponds to the position of the maximum emission wavelength for each sample. The letter W denotes that this type of QDs was washed more times than the parent QDs, as indicated in the Experimental Section. The sizes of the QDs were between 2.5 and 3.3 nm, as calculated using the maximum in absorption UV–visible spectra^{10d} and checked by transmission electron microscopy (TEM). The fluorescence quantum yield of the QDs is in the range of 0.18–0.41 for the CdSe/ZnS QDs and 0.03–0.08 for the CdSe QDs (Table 1). In addition, the small full width at half-maximum (fwhm) in the fluorescence spectra indicates a narrow size distribution of the QDs. This fact together with the absence of a surface trap emission band at longer wavelength shows the good quality of the QDs.

3.2. Preparation of the Nanoparticle Doped Organogels. QD–organogels can be formed by using different methods, such as ultrasound treatment,^{18,19} mixing of polar and apolar solvents in different proportions,¹⁷ or, more recently, heating of the gelator in a suitable solvent to obtain a homogeneous solution followed by cooling.²⁰ As demonstrated by our research group, the heating method allows direct formation of the QD–organogel after cooling at room temperature inside the fluorescence cuvettes, which is very advantageous for their complete photophysical characterization and has been used to prepare a number of organogels derived from macrocycle **1**.^{20,24–26} In this case, toluene was chosen as solvent because the QDs are readily obtained in toluene and macrocycle **1** forms very transparent and stable organogels. Thus, a certain amount of cyclophane **1** was placed in a vial with toluene and heated to the boiling temperature of the solvent to completely dissolve the gelator **1**. The transparent solutions were transferred to preheated fluorescence cuvettes, and then, different toluene solutions of QDs were mixed with the clear solutions of **1** and allowed to cool down at room temperature. Stable, very transparent, and slightly red or yellow colored organogels were obtained after 30 min. They emitted green or orange luminescence upon irradiation with UV light, as shown in Figure 1B for representative examples of green emitting organogels. It must be noted that the QD–organogels obtained by addition of the QDs after complete solubilization of **1** were found to preserve the QDs photophysical properties better than if the QD-doped organogels were obtained by directly mixing **1** with the QDs and toluene, followed by heating the solution to dissolve **1**. This is because the properties of QDs are known to be sensitive to temperature and oxygen.²⁸ Thus, prolonged heating of the QDs in the presence of the gelator should be avoided to obtain homogeneous luminescent samples.

The presence of the semiconductor nanocrystals did not appear to have a negative effect on the stability of the as-prepared hybrid gels. In order to confirm that the nanoparticles

do not destabilize the supramolecular system, the gel-to-liquid transition temperatures of the different gels were measured by the inversion vial method. The control sample without QDs was prepared in parallel to the hybrid organogels in order to obtain comparable data. Typically, the melting temperatures were 3–12 °C higher for the hybrid organogels than for the control organogel, indicating a slightly better stability of the gel in the presence of the QDs. Preliminary studies to determine the critical concentration of gelator (*c_{cg}*) in the presence of the QDs indicated that it is possible to form stable organogels by using a lower concentration of the gelator **1** (1.2 mg/mL; 3.2 mg/mL of gelator was needed in the absence of the QDs). Such effects are in agreement with studies for other hybrid organogels doped with different types of nanoparticles^{3a,f,4a,b,29} and confirm that the presence of the luminescent semiconductor nanocrystals does not disrupt the supramolecular organization of the organogel under the experimental conditions used in this study but enhance the formation of the organogel state. The complete rheological characterization of the materials was out of the scope of this article.

3.3. Photophysical Characterization of the QDs in the Different Sets of Samples. With the view to establishing the influence of the organogel media on the optical properties of the QDs, we compared them with those of related QD samples in toluene solution under the same experimental conditions. The main absorption and emission features are provided in Table 2. Overall, our results indicate that both CdSe and CdSe/

Table 2. Absorption and Emission Properties of Core and Core–Shell QDs in the Different Types of Samples

sample	gelator (mg/mL)	λ_{abs} (nm)	λ_{em}^a (nm)	fwhm (nm)	ΔF^b (%)
TCS533		525	533	22	
TCS533	3.2	525	533	23	268
TCS533W		525	533	23	
TCS533W	3.2	525	533	23	485
ACS27		518	527	24	
ACS27	3.2	519	529	24	528
TCS572		565	572	22	
TCS572	3.2	565	572	22	11
ACS531		516	531	25	
ACS531	3.2	516	531	25	1
ACS549	-	540	549	25	
ACS549	3.2	541	549	25	-15

^a $\lambda_{\text{exc}} = 465$ nm. ^b $\Delta F(\%) = (F - F_{\text{gel}})/F_{\text{sol}}$, where F_{gel} is the emission intensity of the QDs in the QD–organogel and F_{sol} is the emission intensity of the QDs in toluene.

ZnS QDs can be used to prepare luminescent hybrid organogels. However, different trends were observed for the core and core–shell QDs, as will be discussed below.

UV–visible absorption measurements reveal that the only appreciable difference in the absorption spectra of the QD–organogels was the increased baseline as a consequence of light scattering, a typical phenomenon observed in gels (Figure S1 of the Supporting Information).^{26,30} In order to better compare the shape of the absorption spectra and the position of the first exciton, the corrected and normalized absorption spectra were represented and can be seen in Figure 2 for representative samples (for all the samples see Figure S2 in the Supporting Information). The first exciton peak wavelength depended on

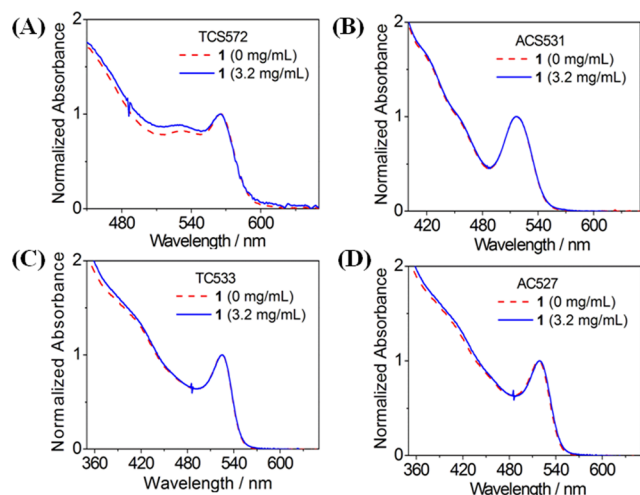


Figure 2. Corrected and normalized absorption spectra of samples prepared in toluene containing different types of QDs with and without organogelator 1. The samples contain the following: (A) TCS572 (0.2 μM); (B) ACS531 (1.4 μM); (C) TC533 (1.8 μM); (D) ACS27 (2.0 μM).

the QD diameter and did not change for most of the samples tested. Only in the case of the ACS27 was a slight red shift of 1 nm observed in the organogel media.

The emission spectra are related to the quality and monodispersity of the QDs, and Figure 3 shows them for

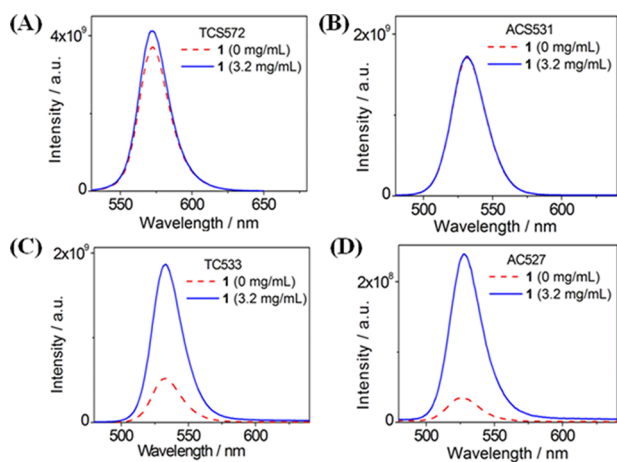


Figure 3. Emission spectra of samples prepared in toluene containing QDs with and without organogelator 1 ($\lambda_{\text{exc}} = 465 \text{ nm}$). The samples contain the following: (A) TCS572 (0.2 μM); (B) ACS531 (1.4 μM); (C) TC533 (1.8 μM); (D) ACS27 (2.0 μM).

representative samples of QDs in the presence and in the absence of the gelator 1 (for all the samples, see Figure S3 in the Supporting Information). The position of the emission maximum and the fwhm remained unchanged for most of the samples, regardless of the presence or absence of 1. Only in the case of ACS27 was a slight red shift of 2 nm observed in the organogel media. Consequently, the nanoparticles were very stable under the experimental conditions used to prepare the organogel and did not aggregate or oxidize, which would result in a red or blue shift, respectively, of the emission maximum, along with broadening of the emission band.

Regarding the emission intensity, two main trends were observed depending on the type of the QDs used to prepare

the QD–organogels. Their different behavior was significantly marked for the presence of the ZnS inorganic shell around the CdSe core of the QDs. Thus, TCS572, ACS531, and ACS549 core–shell QDs exhibited stable emission intensity, and the gelator hardly affected that property. The low sensitivity of the core–shell QDs to organic ligands and radicals has been attributed to the efficient passivation of the CdSe surface defects by the ZnS inorganic shell,³¹ which reduces significantly the effect of the gelator on the photophysical properties of the QDs.

Remarkably, in the case of the core QDs (TC533, TC533W, and ACS27), a dramatic enhanced emission was observed for all of them in the hybrid organogels as compared to the QD emission in toluene under the otherwise same experimental conditions. Thus, the emission intensity of the core QDs was enhanced up to 528% in the QD–organogel system. In principle, the enhanced core-QD fluorescence in the hybrid organogels could be attributed to passivation of the QD surface defects. In fact, the relative effect of the different types of core QDs depends on the post-treatment used in the purification of the QDs. The TC533W and ACS27 QDs, which required more washing steps in their preparation, as indicated in the experimental protocol, showed higher fluorescence enhancement, and this could be attributed, in part, to the presence of a higher number of defects generated in the synthetic protocol. However, as we will discuss further on in this report, this does not appear to be the main contributing factor for the impressive increase of the QD fluorescence when it is within the organogel.

It has been reported that a stabilization period may be required to obtain a stable fluorescence signal for the QDs in the presence of organic ligands.^{31a} Therefore, the emission spectra of the QDs were recorded for 5 h in order to evaluate completely the effect of gelator 1 on the luminescence of the QDs (see Supporting Information Figure S4). In most cases, a stable photoluminescence signal was obtained after 1 h, which remained constant for several hours, indicating the absence of deleterious processes, which would destroy the photoluminescence of the QDs in the hybrid materials, at least for the time scale of our experiments.

The thermoreversibility of the formation and emissive properties of the gel is another important characteristic, which must be taken into account in the development of luminescent supramolecular materials. Thus, the QD–organogels were submitted to several thermal cycles by heating the cuvette up to 80 °C to obtain a clear solution and cooling to room temperature. After stabilization of the samples, the emission spectra of the QD–organogels were recorded. The cycles could be repeated in the same cuvette up to six times without any sign of fatigue or significant changes in the position, intensity, and fwhm of the emission spectra, as can be seen in Figure 4 for a representative example. These results indicate a good compatibility between the QDs and gelator 1, in agreement with previous results obtained for other QD–organogel systems.^{19,20} They are particularly interesting in the case of the core QDs because they indicate that the enhancement of the emission intensity in the presence of macrocycle 1 is preserved after several heating/cooling cycles, supporting the stabilizing role of organogelator 1 on the QD emissive properties.

Time-resolved fluorescence spectroscopy has been used to study dynamic quenching processes and to probe different heterogeneous systems.^{26,32} However, to the best of our

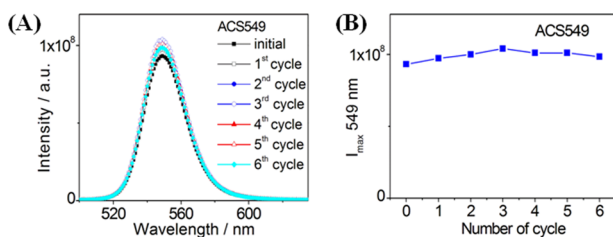


Figure 4. (A) Emission spectra of samples prepared in toluene containing QDs and organogelator **1** ($\lambda_{\text{exc}} = 465$ nm). (B) Plots of the emission intensity at the maximum emission wavelength after each cycle of melting–gelation. The samples contain organogelator **1** (3.2 mg/mL) and ACS549 (1.0 μM).

knowledge, this technique has only been used previously by our research group to characterize commercial core–shell QDs in the organogel medium, making it possible to study the effect of the gelator concentration on the QDs lifetime.²⁰ Thus, in order to characterize the new hybrid supramolecular soft-materials thoroughly, time correlated single photon counting (TCSPC) studies were carried out. Fluorescent decay traces of the QDs in toluene solutions and in gelled toluene were recorded exciting at 464 nm. The emission lifetimes of the QDs are a subject of study, but the occurrence of multiphotonic processes leading to different decay processes is generally accepted.³³ Thus, the decays were fitted to a multiexponential model following eq 1, as is commonly done in the case of QDs in solution.³³ In this expression, τ_i refers to the decay times and α_i represents the amplitudes of the components.

$$I(t) = \sum_i \alpha_i \exp\left(-\frac{t}{\tau_i}\right) \quad (1)$$

The emission decay traces can be seen in Figure 5 (see all data in Supporting Information Figure S5); the emission lifetimes and their corresponding contributions to the total signal are shown in Table 3 for each set of QDs. In order to reach low χ^2 values and random distributions of the weighted residuals, the decays were fitted to a sum of three or four exponential

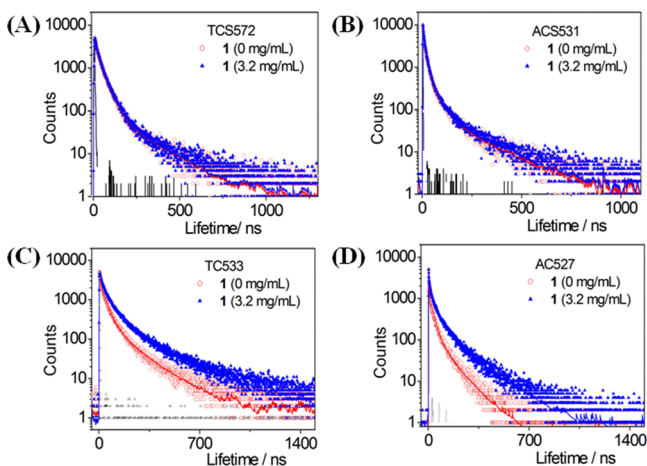


Figure 5. Fluorescence decay curves of QDs in toluene and toluene organogel containing cyclophane **1** ($\lambda_{\text{exc}} = 464$ nm, $\lambda_{\text{em}} = 575$ nm for A, $\lambda_{\text{em}} = 530$ nm for B–D). The incident light pulse is also shown (black solid line). The samples contain the following: (A) TCS572 (0.2 μM); (B) ACS531 (1.4 μM); (C) TCS33 (1.8 μM); (D) ACS27 (2.0 μM).

functions. The complex multiexponential decays have been attributed to a combination of surface chemistry effects and to the differences between the individual QDs present in the same nanoparticle sample.^{33d,f,34} In this case, the lifetimes and pre-exponential factors differ for the sets of QDs due to the intrinsic different chemical composition of each type of QDs. However, the analysis of each type of QDs in solution and in the organogel reveals two main trends, which depend on the presence of the inorganic shell of ZnS around the CdSe core. On the one hand, the fluorescence lifetimes and their corresponding contributions to the fluorescence signal follow the same pattern for each set of core–shell QDs regardless of the presence of organogelator **1**. On the other hand, an increase in the fluorescence lifetime was observed in the case of the core QDs in the organogel medium. In order to better compare the emission lifetimes of the QDs in the presence of gelator **1**, their average lifetimes (τ_{av}) were calculated using eq 2, and the results are provided in Table 3. The average lifetime was increased by a 1.5–1.7 factor in the gels for the core QDs, while the average lifetime of the core–shell QDs was not significantly affected by the presence of the organogel structure.

$$\tau(\text{av}) = \frac{\sum \alpha_i \tau_i^2}{\sum \alpha_i \tau_i} \quad (2)$$

Our results demonstrate that the dynamic properties of the core–shell QDs at the nanosecond time scale are preserved in the gel state under the experimental conditions used to prepare the organogels. The fluorescence lifetimes and their corresponding contributions to the fluorescence signal follow the same pattern for each set of core–shell QDs regardless of the presence of organogelator **1**. This could be of interest for a number of potential applications of hybrid soft supramolecular materials, such as the development of sensors based on the changes in the fluorescence lifetime of the nanoparticles as has been recently demonstrated for QDs in solution.^{33e}

The emission spectra and the fluorescence lifetime of the TCS33W QDs were recorded in the presence of different concentrations of the gelator to further investigate the effect of **1** on the photophysical properties of the core QDs. The relative change in the emission intensity and the average lifetime of the TCS33W QDs are represented in Figures 6A and S6 as a function of the concentration of **1**. The results reveal an enhancement in the emission intensity and the fluorescence lifetime even in the presence of low concentrations of **1**, when the sample exhibits a liquid-like physical appearance. The increase of the steady-state and time-resolved values follows the same trend for low concentrations (up to 4 mM) of **1**. Remarkably, the relative average lifetime did not increase further for higher concentrations (up to 8 mM) of **1**, while the emission intensity showed an upward dependence on the concentration of **1**, indicating that the formation of the gel state had a dramatic effect on the fluorescence intensity of the QDs but not on their lifetime.

Subsequently, we estimated the radiative rate constant (k_r) and the nonradiative rate constant (k_{nr}) of the QDs in the presence of different concentrations of the macrocycle, by using eqs 3 and 4, where Φ refers to the quantum yield and τ_f refers to the lifetime (τ_{av} in this case), and we calculated the relative change in the radiative and nonradiative rate constants (Figure 6B). Data in Figure 6 reveal that the increase of the QDs fluorescence quantum yield in the presence of the gelator is mainly due to an increase in the radiative rate constant, while

Table 3. Fluorescence Lifetimes of Core and Core–Shell QDs in the Different Types of Samples

sample	gelator 1 (mg/mL)	τ_1^a (ns)	B_1 (%)	τ_2^a (ns)	B_2 (%)	τ_3^a (ns)	B_3 (%)	τ_4^a (ns)	B_4 (%)	τ_{av} (ns)
TCS533 ^b		2.7	13	19.3	61	79.3	26			56.9
TCS533 ^b	3.2	6.5	14	30.9	59	129.2	27			93.9
TCS33W ^b		1.3	14	15.3	58	65.4	28			48.7
TCS33W ^b	3.2	4.3	13	25.4	61	106.1	26			76.1
ACS27 ^b		1.9	24	29.5	54	115.1	22			81.2
ACS27 ^b	3.2	4.5	14	41.2	53	161.3	33			125.3
TCS572 ^c		6.2	13	35.2	74	153.5	13			84.4
TCS572 ^c	3.2	7.0	13	35.4	74	150.1	13			82.5
ACS531 ^b		1.8	16	12.3	53	45.3	22	192.4	9	112.9
ACS531 ^b	3.2	1.4	15	10.6	46	35.3	28	182.8	11	114.4
ACS549 ^b		0.5	24	5.4	33	15.8	36	78.0	7	41.2
ACS549 ^b	3.2	0.6	22	5.3	35	16.5	36	82.4	7	43.1

^a $\lambda_{exc} = 464$ nm. ^b $\lambda_{em} = 530$ nm. ^c $\lambda_{em} = 575$ nm.

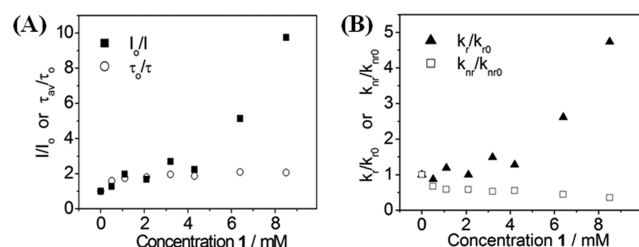


Figure 6. (A) Relative change in the emission intensities and the average lifetimes of the TCS33W QDs vs concentration of 1. (B) Relative change in the radiative rate constants and the nonradiative rate constants of the TCS33W QDs vs the concentration of 1.

the decrease of the k_{nr} , related to the reduction of surface defects that otherwise would trap excited electrons and decrease the emissive properties of the QDs, plays a minor role (Figure 6B). In the literature there are few reports that study the influence of surface ligands on the radiative rate constant of CdSe and CdSe/ZnS QDs. The mechanism for this phenomenon is not clear, but it has been suggested that the ligand induces shifts in energies of exciton states.³⁵ Photoluminescence excitation (PLE) spectroscopy has been used by Bawendi and co-workers³⁶ for mapping the electronic states of CdSe QDs. We performed preliminary PLE studies aimed to determine the effect of the gelator 1 and the gelation on the energy of the QD excited states. Figure S7 shows negligible changes between the PLE spectra. Alternatively, the boost in the k_r value of the CdSe QDs at high gelator concentration could also be due to the expected increase in the refractive index of the medium after formation of the highly entangled fibrillar network.³⁷ Further research is ongoing in order to clarify the effect of the macrocycle 1 on the radiative rate constants of the QDs in the gel state.

$$\Phi = \frac{k_r}{(k_r + k_{nr})} = \tau_f k_r \quad (3)$$

$$\tau_f = \frac{1}{(k_r + k_{nr})} \quad (4)$$

Organic compounds exhibiting different functional groups are known to modify the photophysical properties of QDs.³⁸ Pseudopeptidic macrocycle 1 contains amide and amine groups, as well as hydrophobic domains, in its chemical structure. Amide groups have been described to have no significant effects.³⁹ However, their role in the stabilization of the

inorganic core of QDs cannot be completely ruled out, as described for the interaction of peptides exposed to semiconductor precursors.⁴⁰ On the other hand, amines can have important effects on the final properties of nanoparticles.^{9a,31a,41} Therefore, the luminescent properties of the different QDs in organogel media can be understood by taking into account that gelator 1 is a multifunctional organic compound, which could also undergo ligand interdigitation with the QDs. This effect should be particularly favored by gelation, eventually influencing the QDs properties and generating organogels with improved properties and functionalities (symbiotic effect). Therefore, NMR and IR experiments were performed to get insight into the interaction of the macrocycle with the QDs.

3.4. NMR and IR Studies of the QD–Organogelator 1 System. The ¹H NMR spectrum of the organogelator 1 in deuterated toluene was registered in the presence of TCS33 QDs, using an organogelator concentration lower than the critical concentration needed to form a stable organogel. Figure 7 shows the comparison between the representative signals of the macrocycle in the presence and the absence of the QDs, and it also shows the signals in the presence of trioctylphosphine oxide. A broadening of the signals was detected in the case of the QDs/1 sample, which suggests the occurrence of an interaction between the organogelator 1 and

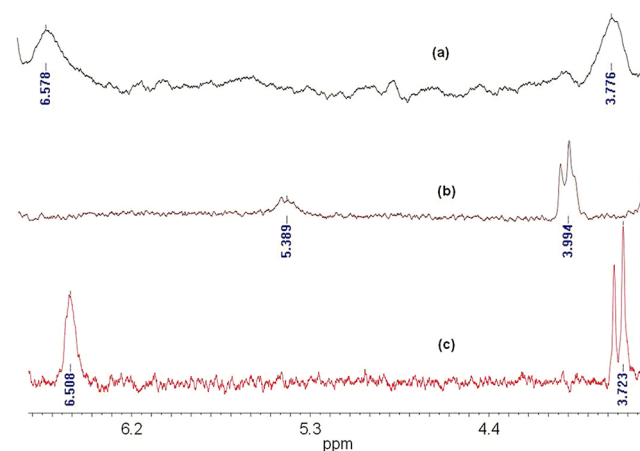


Figure 7. Bottom to top: Amplification between 3.6 ppm and 6.7 ppm of the ¹H NMR spectrum of the organogelator 1 (2.67×10^{-3} M, c) in deuterated toluene compared with those of 1 in the presence of trioctylphosphine oxide (1/phosphine oxide molar ratio of 1000/1, b) and in the presence of TCS33 QDs (7.20×10^{-4} M, a).

the QDs even before the organogel is formed. Moreover, it should be noted that signals for the macrocycle underwent considerable displacement in the presence of TOPO; however, this was not the case in the presence of the QDs. It seems logical to suppose that the macrocycle cannot interact with the TOPO oxygen when it is attached to the QDs surface.

The interactions between **1** and the QDs before gelation were corroborated by registering the ^{31}P NMR spectra of the deuterated toluene solutions of TC533 QDs and TC533 QDs/**1** (Supporting Information Figure S8). The spectrum of the QDs/**1** mixture showed the characteristic broadening of the phosphorus signal (centered at ca. 19 ppm), remarkably shifted to high field compared to those of trioctylphosphine oxide. The presence of the organogelator **1** provoked a considerable displacement of the broad band (centered at ca. 25 ppm) to low field. Moreover, the characteristic signals of trioctylphosphine oxide were not detected in the mixture (Figure S9), demonstrating that no significant macrocycle exchange with trioctylphosphine oxide occurred once the materials had been mixed together.

Additionally, the IR spectrum of the organogelator **1** was also registered in the presence of TC533 QDs, using an organogelator concentration lower than the critical gelation concentration. Figure 8A shows the comparison between the N–H

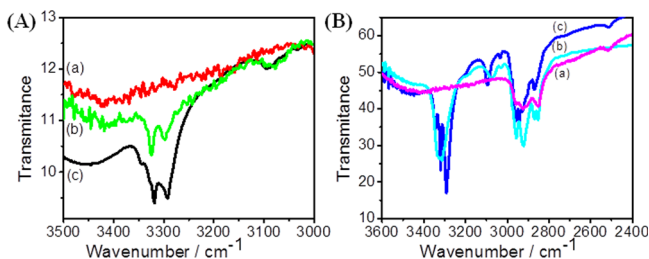


Figure 8. Comparative IR spectra of TC533 QDs (a), **1**/TC533 mixture (b, 50/1 molar ratio), and organogelator **1** (c), using KBr. (A) Compound **1** (1 mg) was dissolved in toluene (1 mL); (B) compound **1** (5 mg) was dissolved in toluene (1 mL).

bands of the macrocycle (at ca. 3300 cm^{-1}) and those in the QDs/**1** mixture, evidencing a slight increase of the N–H bond strength, indicative of a weakening of hydrogen bonding interactions. By contrast, the C–H of the aromatic bonds (at ca. 3100 cm^{-1}) shifted to lower frequencies. Similar observations were obtained for TC533W QDs. All these facts are indicative of the presence of considerable interactions between the QDs and the macrocycle **1** even before the formation of the organogel, where these interactions should be enhanced. In fact, this was corroborated by registering the IR spectrum of the hybrid organogel formed from TC533 QDs (Figures 8B and S10).

3.5. Microscopic Characterization of the QD–Organogelator **1.** To get further insight into the morphological features of the hybrid systems, microscopy experiments were carried out with representative samples of xerogels containing QDs. Homogeneous toluene solutions containing different gelator concentrations were drop cast onto freshly cleaved mica and allowed to evaporate. At higher gelator concentrations, AFM images revealed the formation of a highly entangled fibrillar network distributed across the mica surface (Figure 9A, B). The samples with lower gelator concentrations made visualization of isolated fibers possible (Supporting Information Figure S11). The cross-sectional analysis revealed formation of

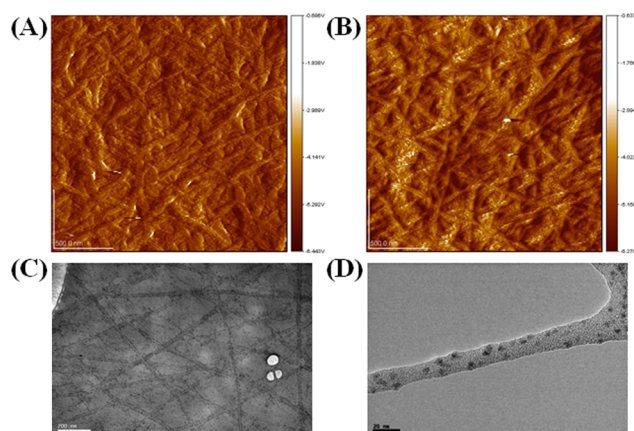


Figure 9. (A, B) AFM amplitude micrographs of xerogels prepared from solutions containing the same initial concentration of organogelator **1**. (A) Control xerogel without QDs. (B) Xerogel containing TC533 QDs. Scan area: $5.5\ \mu\text{m} \times 5.5\ \mu\text{m}$. (C, D) TEM micrographs of the fibrillar structure of cyclophane **1** xerogel containing ACS531 QDs. Scalebar: (C) 200 nm; (D) 20 nm.

long fibers with a height of around 7 nm and a width of around 111 nm for the smallest isolated fibers observed. Control experiments performed with a xerogel with the same gelator concentration but without QDs showed the formation of similar fibers with a width of 98 nm and a height of 8 nm. Overall, the AFM results indicate that the morphology of the fibrillar network formed by **1** is preserved in the presence of the QDs.

The semiconductor nanocrystals could not be visualized in the AFM micrographs because of their small size (2.2–3 nm), which was below the sensitivity of the microsilicon cantilever tips used in our experiments. Therefore, the QD-doped xerogel samples were analyzed by transmission electron microscopy (TEM). A certain volume of the different types of QDs was added to a hot solution of organogelator **1** in toluene to obtain a homogeneous sample. A drop of the transparent solution was deposited onto the holey carbon coated copper grid and dried under air overnight to prepare the corresponding xerogel. The amounts of both the organic and the inorganic components were adjusted in order to obtain a xerogel exhibiting a suitable contrast to observe both the fibrillar network and the nanoparticles. Each sample was imaged in different areas, and representative micrographs of the QD-xerogels are shown in Figure 9C, D (and Supporting Information Figures S12–S16).

Due to the holey nature of the carbon coated copper grid, the hybrid xerogel was formed both on the surface of the carbon coating and within the holes left within the amorphous material. Figure 9C shows a representative image of the xerogel formed on top of the amorphous material; the highest density of QDs is located at the edges of the fibers, suggesting that the QDs could interact preferentially with the fibers in the xerogel state. However, the fibrillar network of the gelator **1** does not always exhibit enough contrast when formed on top of the amorphous carbon material. Thus, in order to characterize the hybrid nanocomposites better, micrographs of the xerogel formed within the holes of the carbon coated copper grid were also taken (Figure 9D and Supporting Information). In all the cases, the fibrillar network of the organogel containing well dispersed QDs was obtained. The QDs exhibit the highest contrast in all TEM micrographs due to the highest electron density of the inorganic material. The individual QDs with a

regular shape are uniformly attached to the cross-linking gel fibers, and no QD aggregates were observed under the used experimental conditions.

TEM and AFM data show that the presence of the QDs does not disrupt the fibrillar network in the xerogel to a significant extent. These results together with those mentioned above indicate that core and core-shell QDs stabilize the fibrillar network formed by the pseudo-peptidic macrocycle **1**, a role previously assigned to metallic nanoparticles on peptidic fibers. It must be taken into account that organogels have been described as supramolecular systems composed of a series of *pools of solvent* in which the mobility of the molecules is identical to the solution, but this could hardly explain the drastic changes of the emissive features of the CdSe QDs in the organogel. Indeed, the interaction of the QDs with the macrocycle starts well before the fibrillar network is formed. Therefore, the fact that the *c_{cg}* for mixtures of QDs in organogel is lower than the *c_{cg}* for the gelator **1** alone is a consequence of the QD acting as a nucleation site of the gelator. This could increase the local concentration of the gelator and favor the gelation. The synergistic stabilizing effect of the organogelator/QD combination is attributed to interdigitation of the gelator **1** and the QDs organic ligand, which is in good agreement with the spectroscopic results.^{4b,c,18a,42} Further research is ongoing to understand the interaction of the QDs with the fibrillar network.

4. CONCLUSIONS

We have shown the symbiosis between CdSe (core and core-shell) and an organogel arising from a pseudo-peptidic macrocycle in toluene. The organogel benefits from a decreased critical concentration needed to be generated in the presence of the QDs. Regarding the profits for the QDs, the most remarkable is the enhanced luminescence of the core QDs. This cooperative effect has led to highly transparent, stable, and fluorescent QD-organogels, which can be easily prepared by heating the gelator in a suitable solvent, followed by cooling at room temperature in the presence of the nanoparticles. Future studies of these materials would be addressed to investigate the use of different types of gelators to form hybrid materials doped with QDs and to study in more detail the interaction of the nanoparticles with the gelator molecules.

■ ASSOCIATED CONTENT

Supporting Information

Photophysical properties of TC533W QDs in the presence of different concentrations of gelator (Table S1), complementary spectroscopic information (Figures S1–S10), and complementary AFM and TEM micrographs of the fibrillar structure of the hybrid organogels (Figures S11–S16). This material is available free of charge via the Internet at <http://pubs.acs.org>.

■ AUTHOR INFORMATION

Corresponding Author

*mizquier@uji.es; julia.perez@uv.es; luiss@uji.es

Present Address

[§]Universidad Nacional de Córdoba, Departamento de Química Orgánica, Haya de la Torre y Medina Allende, s/n, 5000 Córdoba, Argentina.

Notes

The authors declare no competing financial interest.

■ ACKNOWLEDGMENTS

Financial support from the Spanish MICINN (CTQ2008-02907-E, CTQ2009-09953 and CTQ2009-14366-C02-01), GV (ACOMP/2010/258, ACOMP/2010/282 and PROMETEO/2012/020) Fundació Caixa Castelló-UJI (project P1-1B-2009-59, P1-1B2009-58) is acknowledged. P.D.W. thanks the financial support from GV (Grisolia Fellowship). We also thank MEC for the financial support (Project CTQ2011-27758), postdoctoral fellowship (L.C.S), Ramón y Cajal contract (R.E.G) and student contract (J. A-S); GVA (Project ACOMP/2009/334), and UVEG (Project UV-AE-09-5805). M. Carmen Peiro (SCIC) for technical assistance in TEM measurements and P. Clement (SCIC) for technical assistance in AFM measurements. This article is dedicated to Professor M. A. Miranda on the occasion of his 60th birthday.

■ REFERENCES

- (1) (a) Descalzo, A. B.; Martínez-Mañez, R.; Sancenón, R.; Hoffmann, K.; Rurack, K. *Angew. Chem., Int. Ed.* **2006**, *45*, 5924–5948. (b) Aili, D.; Stevens, M. M. *Chem. Soc. Rev.* **2010**, *39*, 3358–3370. (c) Fabregat, V.; Izquierdo, M. A.; Burguete, M. I.; Galindo, F.; Luis, S. V. *Inorg. Chem. Acta* **2012**, *381*, 212–217. (d) Yang, Y. H.; Wen, Z. K.; Dong, Y. P.; Gao, M. Y. *Small* **2006**, *2*, 898–901. (e) Li, J.; Hong, X.; Liu, Y.; Li, D.; Wang, Y. W.; Li, J. H.; Bai, Y. B.; Li, T. J. *Adv. Mater.* **2005**, *17*, 163–166. (f) Wang, Y.-Q.; Zhang, Y.-Y.; Zhang, F.; Li, W.-Y. *J. Mater. Chem.* **2011**, *21*, 6556. (g) Sheng, W.; Kim, S.; Lee, J.; Kim, S.-W.; Jensen, K.; Bawendi, M. G. *Langmuir* **2006**, *22*, 3782–3790. (h) Yan, X. H.; Zhu, P. L.; Li, J. B. *Chem. Soc. Rev.* **2010**, *39*, 1877–1890.
- (2) (a) Sangeetha, N. M.; Maitra, U. *Chem. Soc. Rev.* **2005**, *34*, 821–836. (b) George, M.; Weiss, R. G. *Acc. Chem. Res.* **2006**, *39*, 489–497. (c) Piepenbrock, M. O. M.; Lloyd, G. O.; Clarke, N.; Steed, J. W. *Chem. Rev.* **2010**, *110*, 1960–2004. (d) Hirst, A. R.; Escuder, B.; Miravet, J. F.; Smith, D. K. *Angew. Chem., Int. Ed.* **2008**, *47*, 8002–8018. (e) Dawn, A.; Shiraki, T.; Haraguchi, S.; Tamaru, S. I.; Shinkai, S. *Chem. Asian J.* **2011**, *6*, 266–282. (f) Zhu, P. L.; Yan, X. H.; Su, Y.; Yang, Y.; Li, J. B. *Chem.—Eur. J.* **2010**, *16*, 3176–3183.
- (3) (a) Wu, J.; Tian, Q.; Hu, H.; Xia, Q.; Zou, Y.; Li, F.; Yi, T.; Huang, C. *Chem. Commun.* **2009**, 4100–4102. (b) Love, C. S.; Chechik, V.; Smith, D. K.; Wilson, K.; Ashworth, I.; Brennan, C. *Chem. Commun.* **2005**, 1971–1973. (c) Kar, T.; Dutta, S.; Das, P. K. *Soft Matter* **2010**, *6*, 4777–4787. (d) Ray, S.; Das, A. K.; Banerjee, A. *Chem. Commun.* **2006**, 2816–2818. (e) Amabilino, D. B.; Puigmartí-Luis, J. *Soft Matter* **2010**, *6*, 1605–1612. (f) Das, D.; Kar, T.; Das, P. K. *Soft Matter* **2012**, *8*, 2348–2365.
- (4) (a) van Herrikhuyzen, J.; George, S. J.; Vos, M. R. J.; Sommerdijk, N.; Ajayaghosh, A.; Meskers, S. C. J.; Schenning, A. *Angew. Chem., Int. Ed.* **2007**, *46*, 1825–1828. (b) Sangeetha, N. M.; Bhat, S.; Raffy, G.; Belin, C.; Loppinet-Serani, A.; Aymonier, C.; Terech, P.; Maitra, U.; Desvergne, J. P.; Del Guerso, A. *Chem. Mater.* **2009**, *21*, 3424–3432. (c) Kumar, V. R. R.; Sajini, V.; Sreeprasad, T. S.; Praveen, V. K.; Ajayaghosh, A.; Pradeep, T. *Chem. Asian J.* **2009**, *4*, 840–848. (d) Bhat, S.; Maitra, U. *Chem. Mater.* **2006**, *18*, 4224–4226. (e) Bhattacharya, S.; Srivastava, A.; Pal, A. *Angew. Chem., Int. Ed.* **2006**, *45*, 2934–2937. (f) Puigmartí-Luis, J.; Del Pino, A. P.; Laukhina, E.; Esquena, J.; Laukhin, V.; Rovira, C.; Vidal-Gancedo, J.; Kanaras, A. G.; Nichols, R. J.; Brust, M.; Amabilino, D. B. *Angew. Chem., Int. Ed.* **2008**, *47*, 1861–1865. (g) Coates, I. A.; Smith, D. K. *J. Mater. Chem.* **2010**, *20*, 6696–6702. (h) Kimura, M.; Kobayashi, S.; Kuroda, T.; Hanabusa, K.; Shirai, H. *Adv. Mater.* **2004**, *16*, 335–338.
- (5) (a) Manton, A.; Guex, A. G.; Foelske, A.; Mirolo, L.; Fromm, K. M.; Painsi, M.; Taubert, A. *Soft Matter* **2008**, *4*, 606–617. (b) Li, Y.; Liu, M. *Chem. Commun.* **2008**, 5571–5573.
- (6) (a) Sagawa, T.; Fukugawa, S.; Yamada, T.; Ihara, H. *Langmuir* **2002**, *18*, 7223–7228. (b) Ajayaghosh, A.; Praveen, V. K. *Acc. Chem. Res.* **2007**, *40*, 644–656. (c) Ikeda, M.; Ochi, R.; Hamachi, I. *Lab Chip* **2010**, *10*, 3325–3334.

- (7) (a) Hines, M.; Guyot-Sionnest, P. *J. Phys. Chem.* **1996**, *100*, 468–471. (b) Dabbousi, B. O.; RodriguezViejo, J.; Mikulec, F. V.; Heine, J. R.; Mattoussi, H.; Ober, R.; Jensen, K. F.; Bawendi, M. G. *J. Phys. Chem. B* **1997**, *101*, 9463–9475.
- (8) (a) Peng, Z. A.; Peng, X. G. *J. Am. Chem. Soc.* **2001**, *123*, 183–184. (b) Murray, C.; Norris, D.; Bawendi, M. G. *J. Am. Chem. Soc.* **1993**, *115*, 8706–8715.
- (9) (a) Talapin, D. V.; Rogach, A. L.; Kornowski, A.; Haase, M.; Weller, H. *Nano Lett.* **2001**, *1*, 207–211. (b) Yuan, C. T.; Chou, W. C.; Chen, Y. N.; Chou, J. W.; Chuu, D. S.; Lin, C. A. J.; Li, J. K.; Chang, W. H.; Shen, J. L. *J. Phys. Chem. C* **2007**, *111*, 15166–15172. (c) Shen, H.; Wang, H.; Tang, Z.; Niu, J. Z.; Lou, S.; Du, Z.; Li, L. S. *CrystEngComm* **2009**, *11*, 1733.
- (10) (a) Resch-Genger, U.; Grabolle, M.; Cavaliere-Jaricot, S.; Nitschke, R.; Nann, T. *Nat. Methods* **2008**, *5*, 763–775. (b) Murray, C. B.; Kagan, C. R.; Bawendi, M. G. *Annu. Rev. Mater. Sci.* **2000**, *30*, 545–610. (c) Chan, W. C. W.; Nie, S. M. *Science* **1998**, *281*, 2016–2018. (d) Yu, W. W.; Qu, L. H.; Guo, W. Z.; Peng, X. G. *Chem. Mater.* **2003**, *15*, 2854–2860.
- (11) (a) Cozzoli, P. D.; Pellegrino, T.; Manna, L. *Chem. Soc. Rev.* **2006**, *35*, 1195–1208. (b) Burda, C.; Chen, X. B.; Narayanan, R.; El-Sayed, M. A. *Chem. Rev.* **2005**, *105*, 1025–1102.
- (12) (a) Bruchez, M.; Moronne, M.; Gin, P.; Weiss, S.; Alivisatos, A. P. *Science* **1998**, *281*, 2013–2016. (b) Lin, C. A. J.; Liedl, T.; Sperling, R. A.; Fernandez-Arguelles, M. T.; Costa-Fernandez, J. M.; Pereiro, R.; Sanz-Medel, A.; Chang, W. H.; Parak, W. J. *J. Mater. Chem.* **2007**, *17*, 1343–1346. (c) Smith, A. M.; Nie, S. M. *Analyst* **2004**, *129*, 672–677.
- (13) (a) Zhang, F.; Ali, Z.; Amin, F.; Riedinger, A.; Parak, W. J. *Anal. Bioanal. Chem.* **2010**, *397*, 935–942. (b) Callan, J. F.; De Silva, A. P.; Mulrooney, R. C.; Mc Caughan, B. *J. Inclusion Phenom. Macrocycl. Chem.* **2007**, *58*, 257–262. (c) Martinez-Mañez, R.; Sancenon, F.; Hecht, M.; Biyikal, M.; Rurack, K. *Anal. Bioanal. Chem.* **2011**, *399*, 55–74. (d) Baù, L.; Tecilla, P.; Mancini, F. *Nanoscale* **2011**, *3*, 121–133.
- (14) Sone, E. D.; Zubarev, E. R.; Stupp, S. I. *Angew. Chem., Int. Ed.* **2002**, *41*, 1705–1709.
- (15) Simmons, B.; Li, S. C.; John, V. T.; McPherson, G. L.; Taylor, C.; Schwartz, D. K.; Maskos, K. *Nano Lett.* **2002**, *2*, 1037–1042.
- (16) Palui, G.; Nanda, J.; Ray, S.; Banerjee, A. *Chem.—Eur. J.* **2009**, *15*, 6902–6909.
- (17) Yan, X. H.; Cui, Y.; He, Q.; Wang, K. W.; Li, J. B. *Chem. Mater.* **2008**, *20*, 1522–1526.
- (18) (a) Bardelang, D.; Zaman, M. B.; Moudrakovski, I. L.; Pawsey, S.; Margeson, J. C.; Wang, D. S.; Wu, X. H.; Ripmeester, J. A.; Ratcliffe, C. I.; Yu, K. *Adv. Mater.* **2008**, *20*, 4517–4520. (b) Zaman, M. B.; Bardelang, D.; Prakesch, M.; Leek, D. M.; Naubron, J. V.; Chan, G.; Wu, X.; Ripmeester, J. A.; Ratcliffe, C. I.; Yu, K. *ACS Appl. Mater. Interfaces* **2012**, *4*, 1178–1181.
- (19) Yan, J. J.; Wang, H.; Zhou, Q. H.; You, Y. Z. *Macromolecules* **2011**, *44*, 4306–4312.
- (20) Wadhavane, P. D.; Izquierdo, M. A.; Galindo, F.; Burguete, M. I.; Luis, S. V. *Soft Matter* **2012**, *8*, 4373–4381.
- (21) Becerril, J.; Bolte, M.; Burguete, M. I.; Galindo, F.; Garcia-Espana, E.; Luis, S. V.; Miravet, J. F. *J. Am. Chem. Soc.* **2003**, *125*, 6677–6686.
- (22) Aguilera-Sigalat, J.; Rocton, S.; Sanchez-Royo, J. F.; Galian, R. E.; Perez-Prieto, J. *RSC Adv.* **2012**, *2*, 1632–1638.
- (23) Tomasulo, M.; Yildiz, I.; Kaanumalle, S. L.; Raymo, F. M. *Langmuir* **2006**, *22*, 10284–10290.
- (24) Galindo, F.; Burguete, M. I.; Gavara, R.; Luis, S. V. *J. Photochem. Photobiol., A* **2006**, *178*, 57–61.
- (25) (a) Becerril, J.; Burguete, M. I.; Escuder, B.; Luis, S. V.; Miravet, J. F.; Querol, M. *Chem. Commun.* **2002**, 738–739. (b) Becerril, J.; Burguete, M. I.; Escuder, B.; Galindo, F.; Gavara, R.; Miravet, J. F.; Luis, S. V.; Peris, G. *Chem.—Eur. J.* **2004**, *10*, 3879–3890. (c) Becerril, J.; Escuder, B.; Miravet, J. F.; Gavara, R.; Luis, S. V. *Eur. J. Org. Chem.* **2005**, 481–485.
- (26) Burguete, M. I.; Izquierdo, M. A.; Galindo, F.; Luis, S. V. *Chem. Phys. Lett.* **2008**, *460*, 503–506.
- (27) (a) Park, J.; Joo, J.; Soon, G. K.; Jang, Y.; Hyeon, T. *Angew. Chem., Int. Ed.* **2007**, *46*, 4630–4660. (b) De Mello Donegá, C.; Liljeroth, P.; Vanmaekelbergh, D. *Small* **2005**, *1*, 1152–1162.
- (28) (a) Katari, J. E. B.; Colvin, V. L.; Alivisatos, A. P. *J. Phys. Chem.* **1994**, *98*, 4109–4117. (b) Lee, W. Z.; Shu, G. W.; Wang, J. S.; Shen, J. L.; Lin, C. A.; Chang, W. H.; Ruaan, R. C.; Chou, W. C.; Lu, C. H.; Lee, Y. C. *Nanotechnology* **2005**, *16*, 1517–1521. (c) Borkovska, L. V.; Stara, T. R.; Korsunskaya, N. O.; Pecherška, K. Y.; Germash, L. P.; Bondarenko, V. O. *Semicond. Phys. Quantum Electron. Optoelectron.* **2010**, *13*, 202–208.
- (29) (a) Srinivasan, S.; Babu, S. S.; Praveen, V. K.; Ajayaghosh, A. *Angew. Chem., Int. Ed.* **2008**, *47*, 5746–5749. (b) Taboada, E.; Feldborg, L. N.; Pérez Del Pino, Á.; Roig, A.; Amabilino, D. B.; Puigmartí-Luis, J. *Soft Matter* **2011**, *7*, 2755–2761. (c) Das, R. K.; Bhat, S.; Banerjee, S.; Aymonier, C.; Loppinet-Serani, A.; Terech, P.; Maitra, U.; Raffy, G.; Desvergne, J. P.; Del Guerso, A. *J. Mater. Chem.* **2011**, *21*, 2740–2750.
- (30) Murata, K.; Aoki, M.; Suzuki, T.; Harada, T.; Kawabata, H.; Komori, T.; Ohseto, F.; Ueda, K.; Shinkai, S. *J. Am. Chem. Soc.* **1994**, *116*, 6664–6676.
- (31) (a) Galian, R. E.; Scaiano, J. C. *Photochem. Photobiol. Sci.* **2009**, *8*, 70–74. (b) Heafey, E.; Laferriere, M.; Scaiano, J. C. *Photochem. Photobiol. Sci.* **2007**, *6*, 580–584.
- (32) Burguete, M. I.; Galindo, F.; Gavara, R.; Izquierdo, M. A.; Lima, J. C.; Luis, S. V.; Parola, A. J.; Pina, F. *Langmuir* **2008**, *24*, 9795–9803.
- (33) (a) Wang, X. Y.; Qu, L. H.; Zhang, J. Y.; Peng, X. G.; Xiao, M. *Nano Lett.* **2003**, *3*, 1103–1106. (b) de Mello, D.; Aacute, C.; Bode, M.; Meijerink, A. *Phys. Rev. B* **2006**, *74*, 085320. (c) Zhang, J. M.; Zhang, X. K.; Zhang, J. Y. *J. Phys. Chem. C* **2009**, *113*, 9512–9515. (d) Kloepper, J. A.; Bradforth, S. E.; Nadeau, J. L. *J. Phys. Chem. B* **2005**, *109*, 9996–10003. (e) Ruedas-Rama, M. J.; Orte, A.; Hall, E. A. H.; Alvarez-Pez, J. M.; Talavera, E. M. *Chem. Phys. Chem.* **2011**, *12*, 919–929. (f) Jones, M.; Nedeljkovic, J.; Ellingson, R. J.; Nozik, A. J.; Rumbles, G. *J. Phys. Chem. B* **2003**, *107*, 11346–11352. (g) Rubio, J.; Izquierdo, M. A.; Burguete, M. I.; Galindo, F.; Luis, S. V. *Nanoscale* **2011**, *3*, 3613–3615.
- (34) (a) Bawendi, M. G.; Carroll, P. J.; Wilson, W. L.; Brus, L. E. *J. Chem. Phys.* **1992**, *96*, 946–954. (b) Wang, X.; Qu, L.; Zhang, J.; Peng, X.; Xiao, M. *Nano Lett.* **2003**, *3*, 1103–1106. (c) Neuhauser, R. G.; Shimizu, K. T.; Woo, W. K.; Empedocles, S. A.; Bawendi, M. G. *Phys. Rev. Lett.* **2000**, *85*, 3301–3304. (d) Fisher, B. R.; Eisler, H. J.; Stott, N. E.; Bawendi, M. G. *J. Phys. Chem. B* **2004**, *108*, 143–148.
- (35) Fomenko, V.; Nesbitt, D. J. *Nano Lett.* **2008**, *8*, 287–293.
- (36) Norris, D. J.; Bawendi, M. G. *Phys. Rev. B* **1996**, *53*, 16338–16346.
- (37) (a) Brokmann, X.; Coolen, L.; Dahan, M.; Hermier, J. P. *Phys. Rev. Lett.* **2004**, *93*. (b) Vidyasagar, A.; Handore, K.; Sureshan, K. M. *Angew. Chem., Int. Ed.* **2011**, *50*, 8021–8024.
- (38) Galian, R. E.; de la Guardia, M. *Trends Anal. Chem.* **2009**, *28*, 279–291.
- (39) Bullen, C.; Mulvaney, P. *Langmuir* **2006**, *22*, 3007–3013.
- (40) Mao, C.; Flynn, C. E.; Hayhurst, A.; Sweeney, R.; Qi, J.; Georgiou, G.; Iverson, B.; Belcher, A. M. *Proc. Natl. Acad. Sci. U.S.A.* **2003**, *100*, 6946–6951.
- (41) (a) Landes, C.; Burda, C.; Braun, M.; El-Sayed, M. A. *J. Phys. Chem. B* **2001**, *105*, 2981–2986. (b) Dannhauser, T.; Oneil, M.; Johansson, K.; Whitten, D.; McLendon, G. *J. Phys. Chem.* **1986**, *90*, 6074–6076. (c) Cowderycorvan, J. R.; Whitten, D. G.; McLendon, G. L. *Chem. Phys.* **1993**, *176*, 377–386. (d) Landes, C. F.; Braun, M.; El-Sayed, M. A. *J. Phys. Chem. B* **2001**, *105*, 10554–10558. (e) Sharma, S. N.; Sharma, H.; Singh, G.; Shivaprasad, S. M. *Mater. Chem. Phys.* **2008**, *110*, 471–480. (f) Nose, K.; Fujita, H.; Omata, T.; Otsuka-Yao-Matsuo, S.; Nakamura, H.; Maeda, H. *J. Lumines.* **2007**, *126*, 21–26. (g) Liang, J. G.; Zhang, S. S.; Ai, X. P.; Ji, X. H.; He, Z. K. *Spectrochim. Acta, A: Mol. Biomol. Spectrosc.* **2005**, *61*, 2974–2978.
- (42) Bose, P. P.; Drew, M. G. B.; Banerjee, A. *Org. Lett.* **2007**, *9*, 2489–2492.

Photoluminescence Enhancement of CdSe Quantum Dots: A Case of Organogel-Nanoparticle Symbiosis

Prashant D. Wadhavane,[†] Raquel E. Galián,[‡] M. Angeles Izquierdo,^{ †} Jordi Aguilera-Sigalat,[‡]
Francisco Galindo,[†] Luciana C. Schmidt,^{‡,§} M. Isabel Burguete,[†] Julia Pérez-Prieto,^{* ‡} and Santiago V.
Luis^{* †}*

[†]Universitat Jaume I, Departamento de Química Inorgánica y Orgánica, Av. Sos Baynat, s/n, E-12071
Castellón (Spain)

[‡]Instituto de Ciencia Molecular, Universidad de Valencia, c/ Catedrático José Beltrán 2, Paterna, 46980,
Valencia (Spain)

[⊥]Departamento de Química Analítica, Edificio de Investigación, Universidad de Valencia, Dr. Moliner
50, 46100 Burjassot, Valencia (Spain)

[§]Present Address: Universidad Nacional de Córdoba, Departamento de Química Orgánica, Haya de la
Torre y Medina Allende s/n, 5000 Córdoba (Argentina)

Index	Page
Table S1.....	S3
Figure S1.....	S4
Figure S2.....	S5
Figure S3.....	S6
Figure S4.....	S7
Figure S5.....	S8
Figure S6.....	S9
Figure S7.....	S10
Figure S8.....	S11
Figure S9.....	S12
Figure S10.....	S13
Figure S11.....	S14
Figure S12.....	S15
Figure S13.....	S16
Figure S14.....	S17
Figure S15.....	S18
Figure S16.....	S19

Table S1. Photophysical properties of TC533W QDs in the presence of different concentrations of gelator **1**.

Concentration 1 (mM)	Φ_F^a	τ_{av} (ns)	k_r (s^{-1}) $\times 10^{-7}$	k_{nr} (s^{-1}) $\times 10^{-7}$
0	0.030	37.0	0.08	2.62
0.5	0.039	54.4	0.07	1.77
1.1	0.059	61.2	0.10	1.54
2.1	0.051	62.5	0.08	1.52
3.2	0.081	66.8	0.12	1.37
4.2	0.067	64.8	0.10	1.44
6.4	0.154	72.8	0.21	1.16
8.5	0.292	76.1	0.38	0.93

^a $\lambda_{exc} = 465$ nm, TC533W in toluene was used as reference ($\Phi_{ref} = 0.030$)

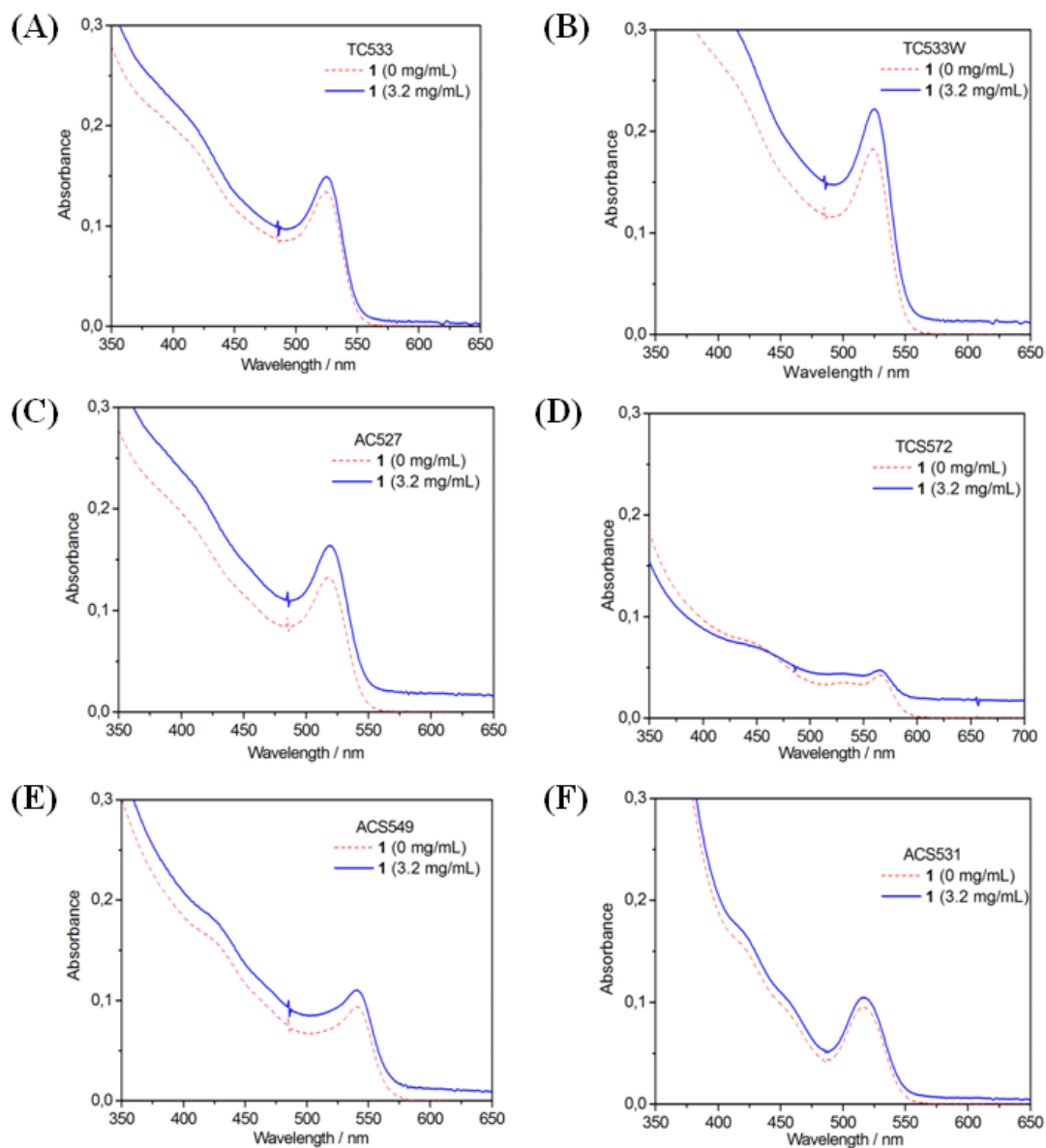


Figure S1. Absorption spectra of samples prepared in toluene containing different types of QDs with and without organogelator **1**. The samples contain: (A) TC533 (1.8 μM); (B) TC533W (2.5 μM); (C) AC527 (2.0 μM); (D) TCS572 (0.2 μM); (E) ACS549 (1.0 μM); (F) ACS531 (1.4 μM).

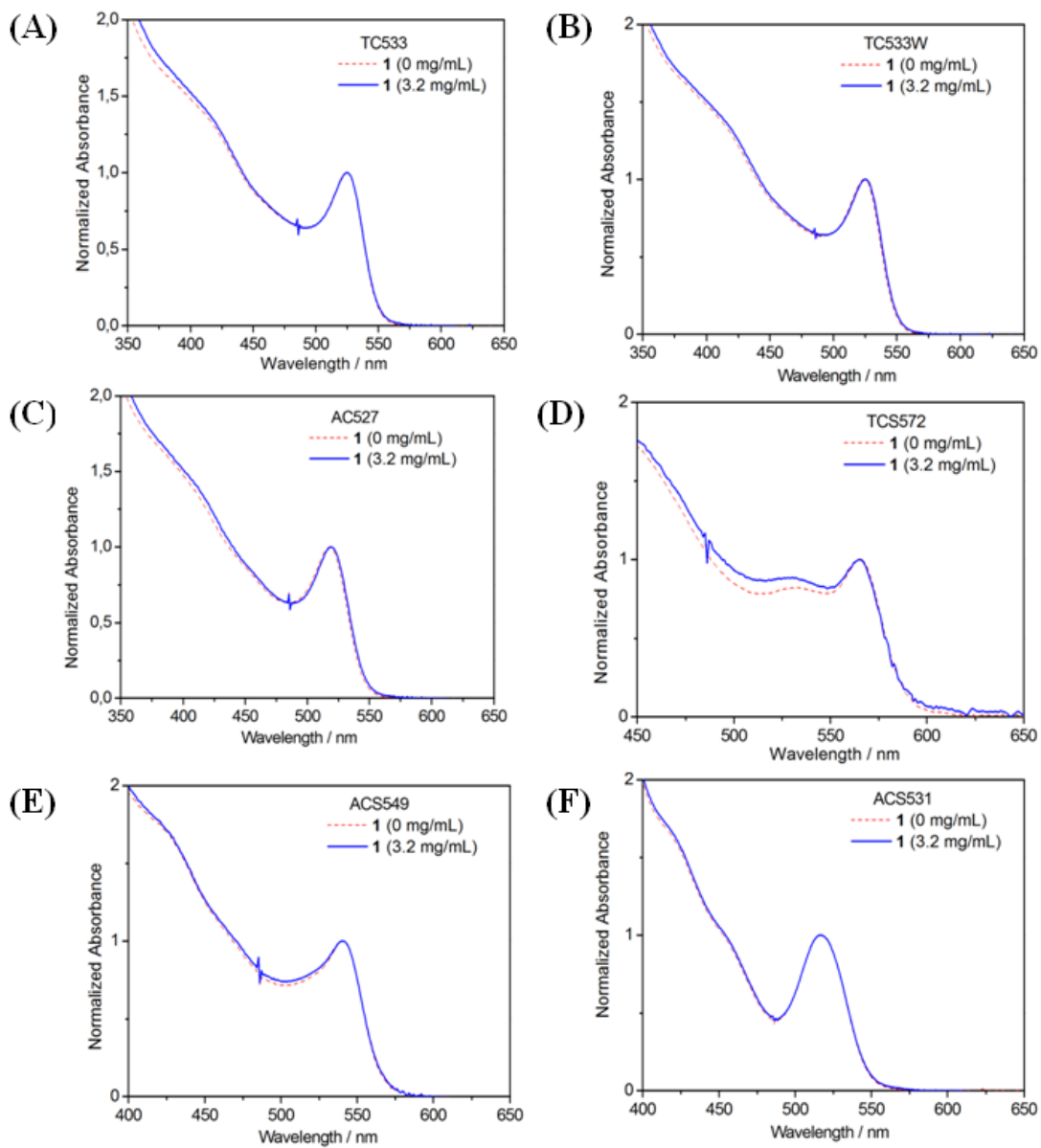


Figure S2. Corrected and normalized absorption spectra of samples prepared in toluene containing different types of QDs with and without organogelator **1**. The samples contain: (A) TC533 (1.8 μM); (B) TC533W (2.5 μM); (C) AC527 (2.0 μM); (D) TCS572 (0.2 μM); (E) ACS549 (1.0 μM); (F) ACS531 (1.4 μM);.

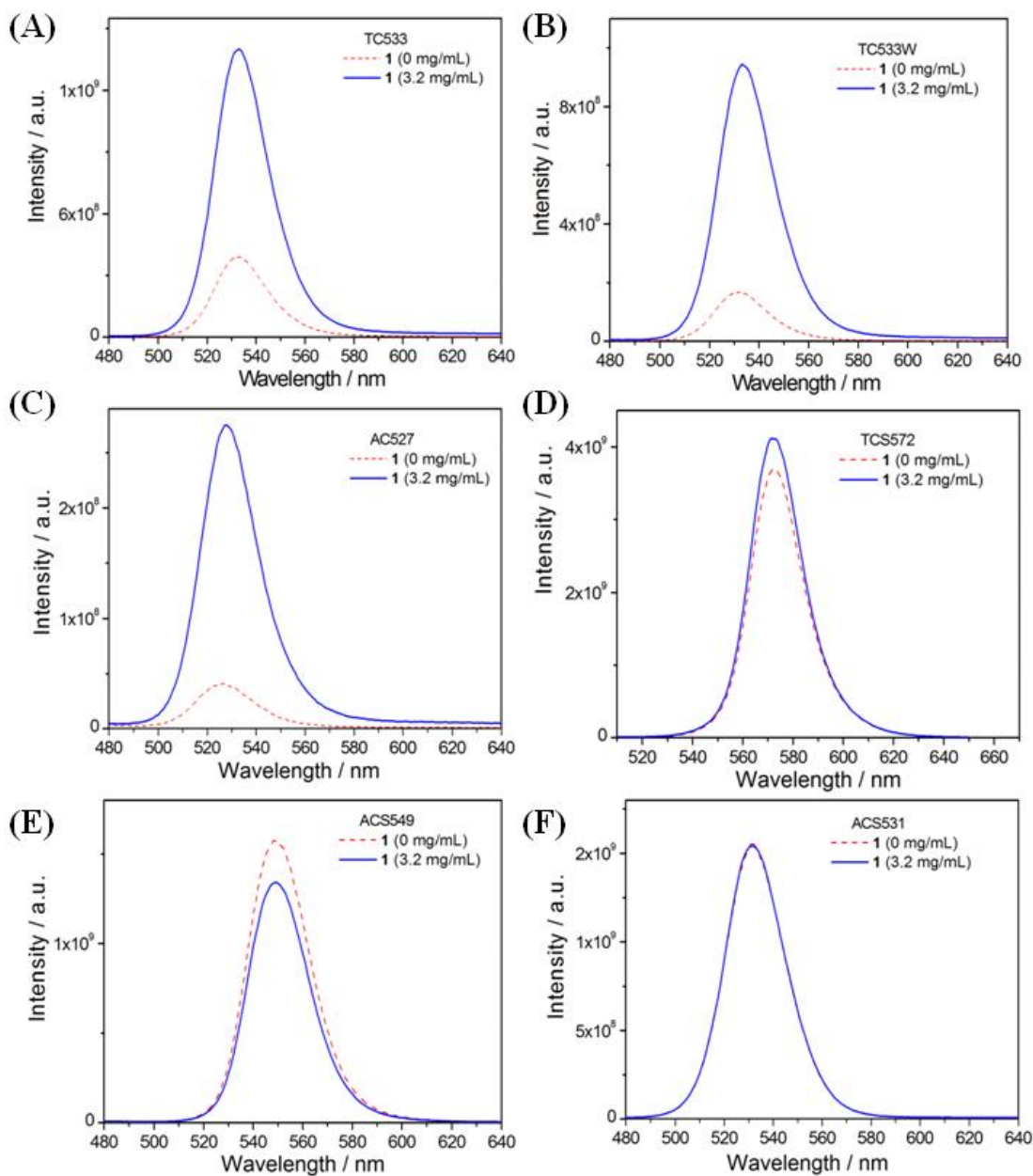


Figure S3. Emission spectra of samples prepared in toluene containing QDs and organogelator **1** ($\lambda_{\text{exc}} = 465 \text{ nm}$). The samples contain: (A) TC533 (1.8 μM); (B) TC533W (2.5 μM); (C) AC527 (2.0 μM); (D) TCS572 (0.2 μM); (E) ACS549 (1.0 μM); (F) ACS531 (1.4 μM).

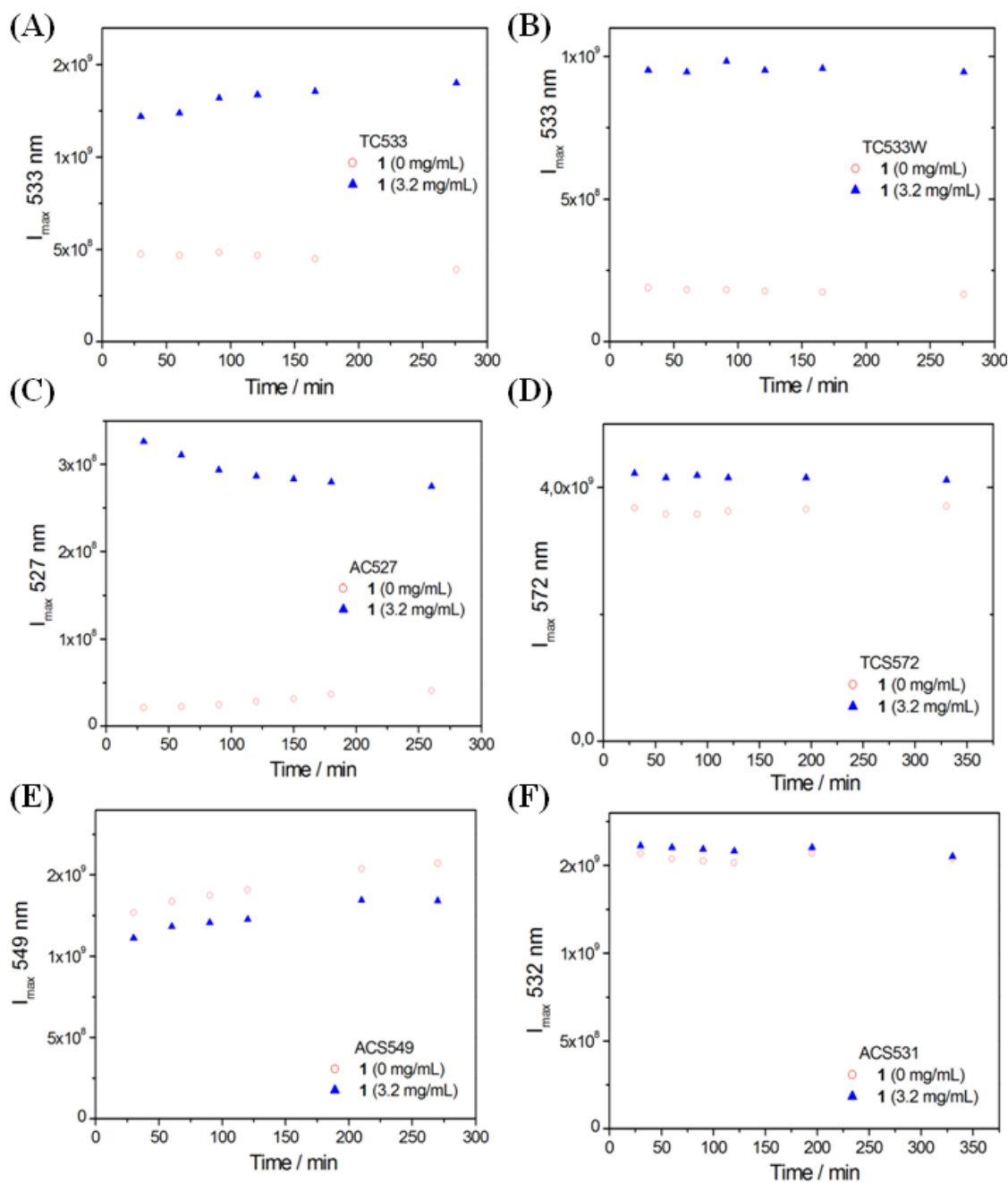


Figure S4. Evolution along the time of the emission intensity at the maximum emission wavelength of the samples prepared in toluene containing QDs with and without organogelator **1** ($\lambda_{\text{exc}} = 465$ nm). The samples contain: (A) TC533 (1.8 μM); (B) TC533W (2.5 μM); (C) AC527 (2.0 μM); (D) TCS572 (0.2 μM); (E) ACS549 (1.0 μM); (F) ACS531 (1.4 μM).

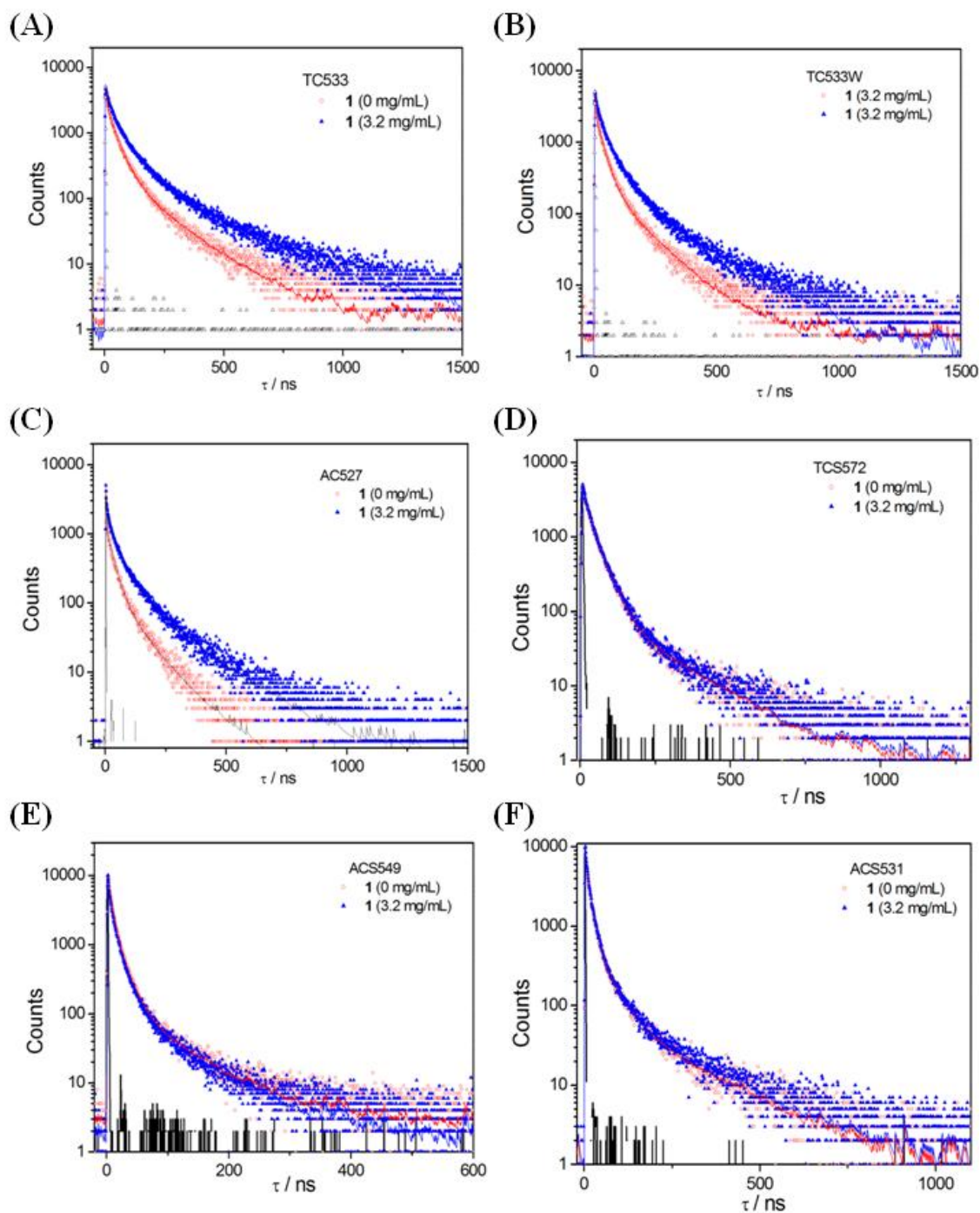


Figure S5. Fluorescence decay curves of QDs in toluene and toluene organogel containing cyclophane **1** ($\lambda_{\text{exc}} = 464 \text{ nm}$, $\lambda_{\text{em}} = 530 \text{ nm}$ for A, D-F, $\lambda_{\text{em}} = 575 \text{ nm}$ for B). The incident light pulse is also shown (black solid line). The samples contain: (A) TC533 ($1.8 \mu\text{M}$); (B) TC533W ($2.5 \mu\text{M}$); (C) ACS27 ($2.0 \mu\text{M}$); (D) TCS572 ($0.2 \mu\text{M}$); (E) ACS549 ($1.0 \mu\text{M}$) (F); ACS531 ($1.4 \mu\text{M}$).

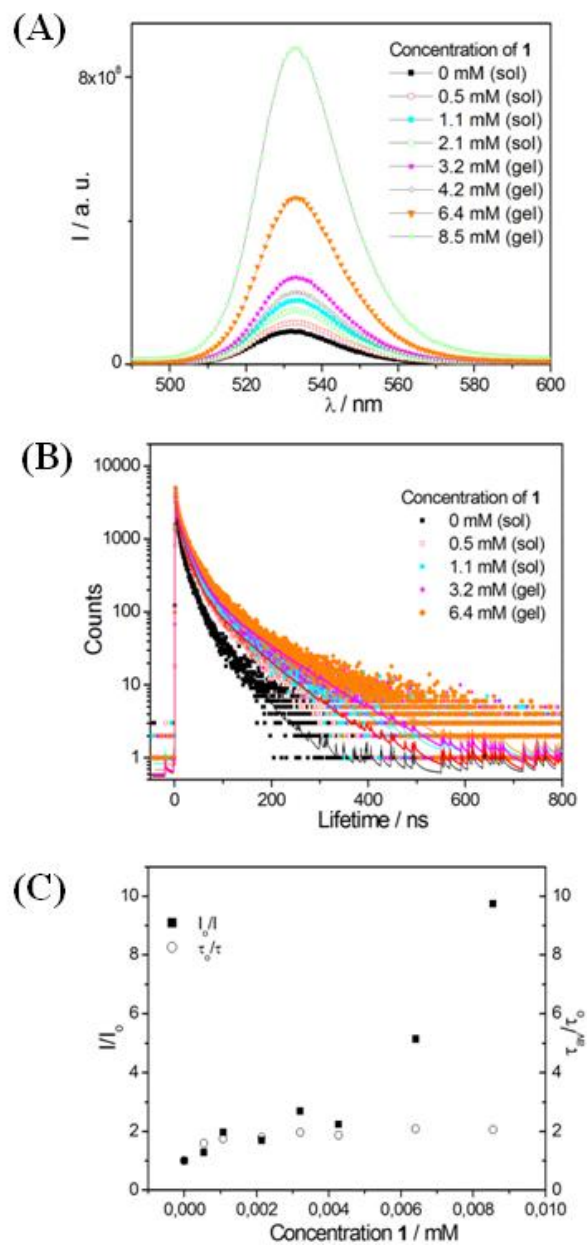


Figure S6. (A) Emission spectra of samples prepared in toluene containing TC533W QDs (2.5 μM) and different concentrations of organogelator **1** ($\lambda_{\text{exc}} = 465$ nm). (B) Decay traces of samples prepared in toluene containing TC533W QDs (2.5 μM) and different concentrations of organogelator **1** ($\lambda_{\text{exc}} = 465$ nm). (C) Relative change in the emission intensity and the average lifetime of the TC533W QDs as a function of the concentration of **1**.

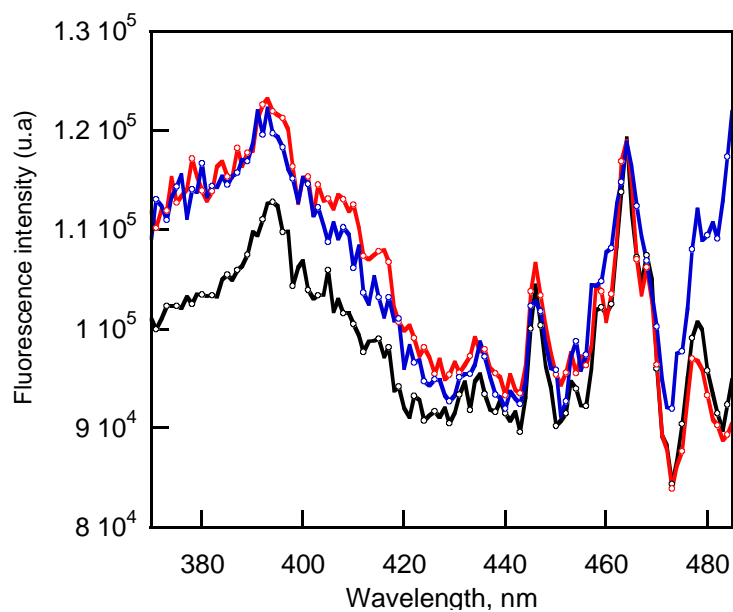


Figure S7. Normalized photoluminescence excitation scans ($\lambda_{em} = 499$ nm) for the CdSe TC533 QDs ($\lambda_{max} = 520$ nm, $[QD] = 7.20 \times 10^{-6}$ M) in the absence (—) and in the presence of organogelator **1** to form a fluid solution ($[1] = 2.67 \times 10^{-3}$ M, —) and a hybrid organogel ($[1] = 13.00 \times 10^{-3}$ M, —).

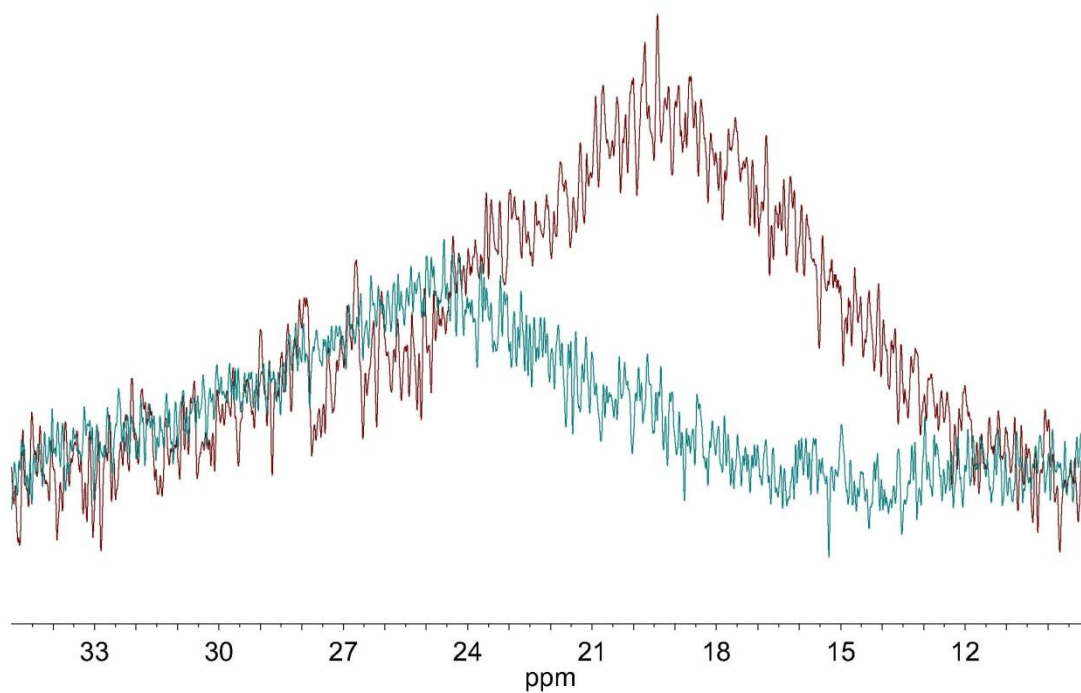


Figure S8. ³¹P-NMR spectra in deuterated toluene of TC533 QDs (7.20×10^{-6} M) in the absence (—) and in the presence of the organogelator **1** (2.67×10^{-3} M, —).

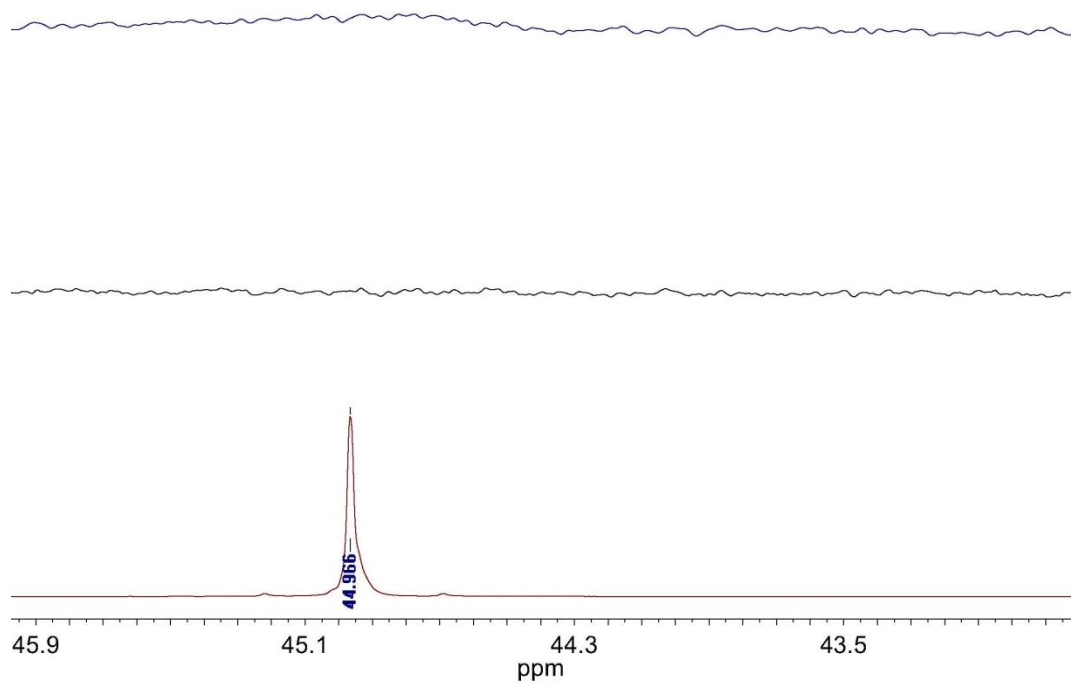


Figure S9. Bottom to top: Amplification between 42.8 and 46.0 ppm of the ^{31}P -NMR spectra in deuterated toluene of trioctylphosphine oxide (—), TC533 QDs in the absence (—) and in the presence of the organogelator (QD/**1** molar ratio of 1/3.7, —).

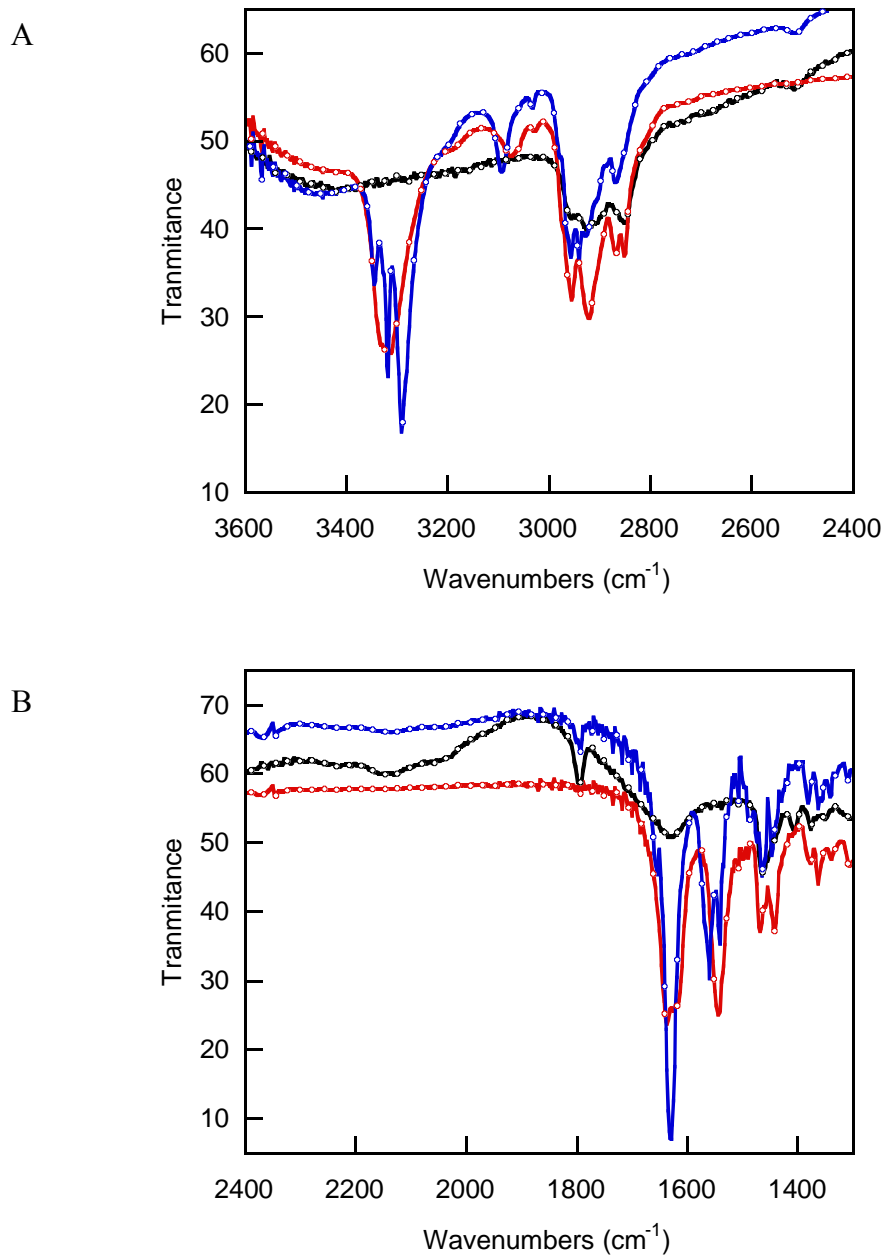


Figure S10. Comparative IR spectra of organogelator **1** (—), TC533 QDs (—), and **1**/TC533 QDs mixture (—, 50/1 molar ratio) using KBr. A: region from 3600 to 2400 cm⁻¹ and B: region from 1850 to 1300 cm⁻¹. Compound **1** (5 mg) was dissolved in toluene (1 mL). Significant changes were detected in the hybrid system, such as the strength of the N-H, C-H_{aromatic}, and C=O bonds of the macrocycle **1**.

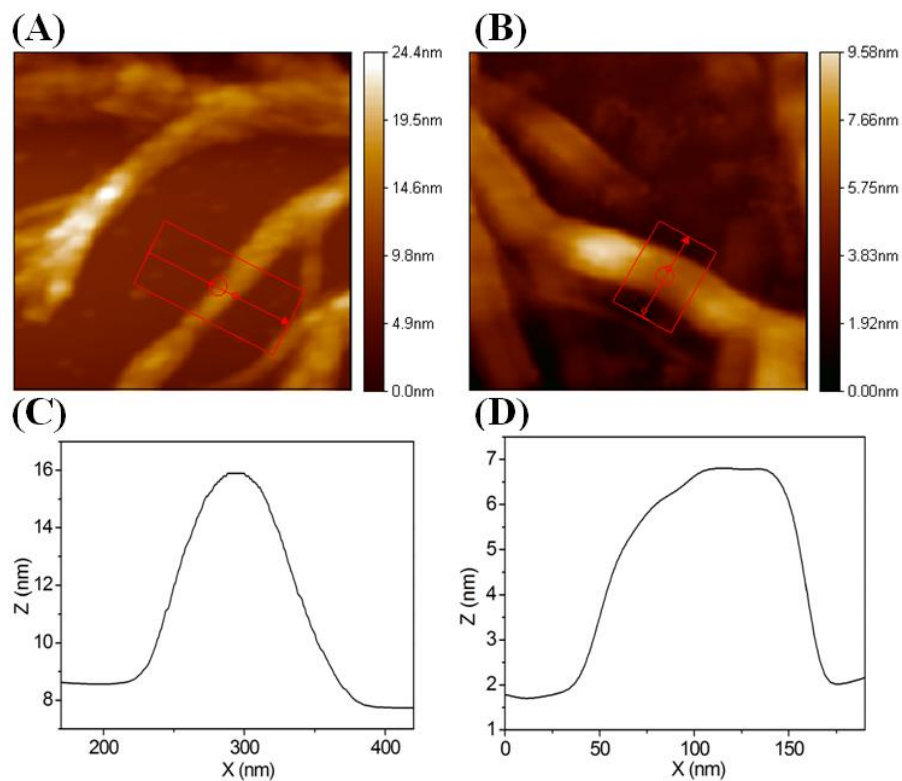


Figure S11. AFM height micrographs of xerogels prepared from solutions containing the same initial concentration of organogelator **1**. (A, C) Control xerogel without QDs. (B, D) Xerogel containing ACS531 QDs. The height profiles shown in Figures C and D have been corrected with respect to the baseline for a better comparison of the results.

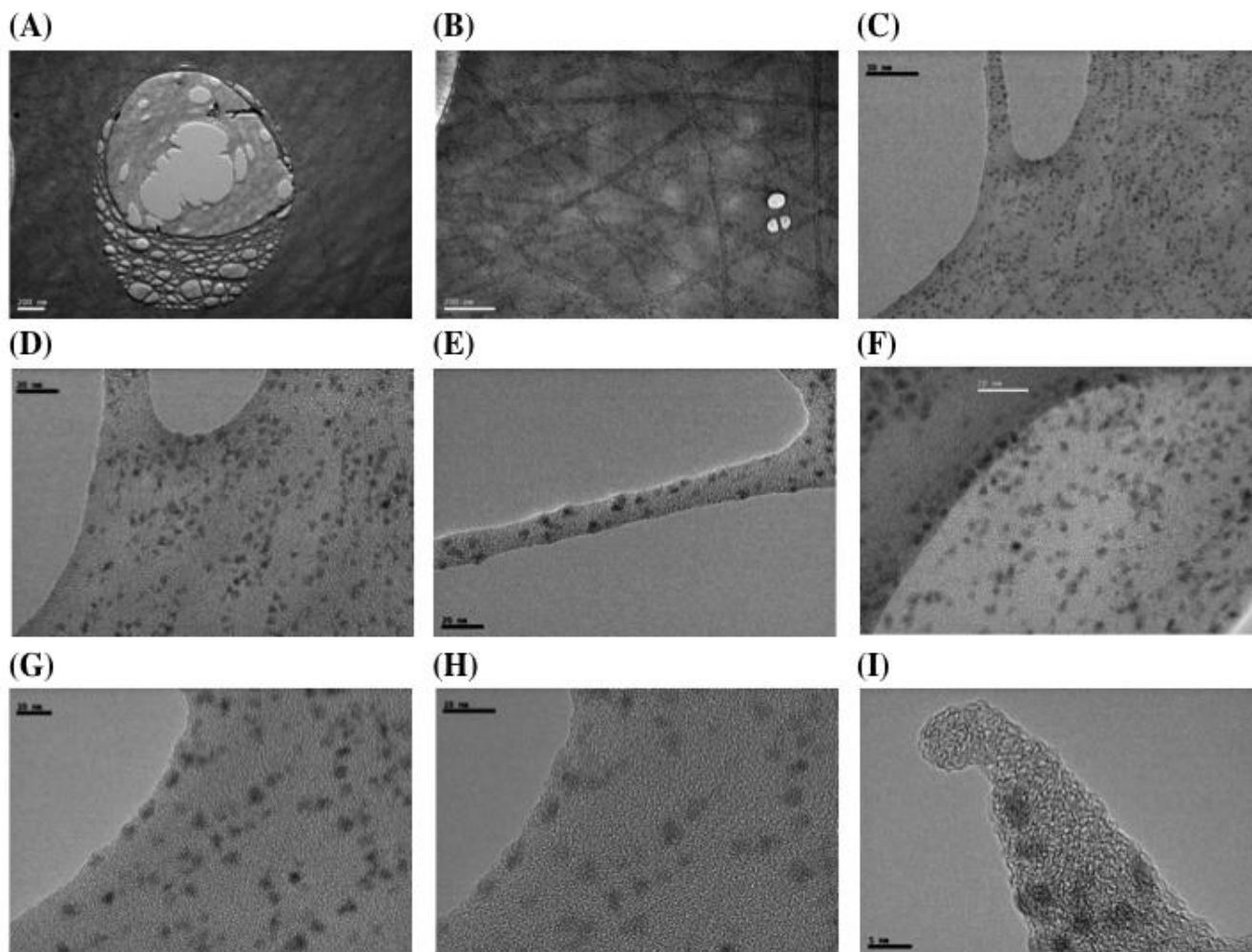


Figure S12. TEM micrographs of the fibrillar structure of cyclophane **1** xerogel containing ACS531 QDs. Scalebar is: A) 200 nm, B) 200 nm, C) 50 nm, D) 20 nm, E) 20 nm, F) 20 nm, G) 20 nm, H) 20 nm, I) 5 nm.

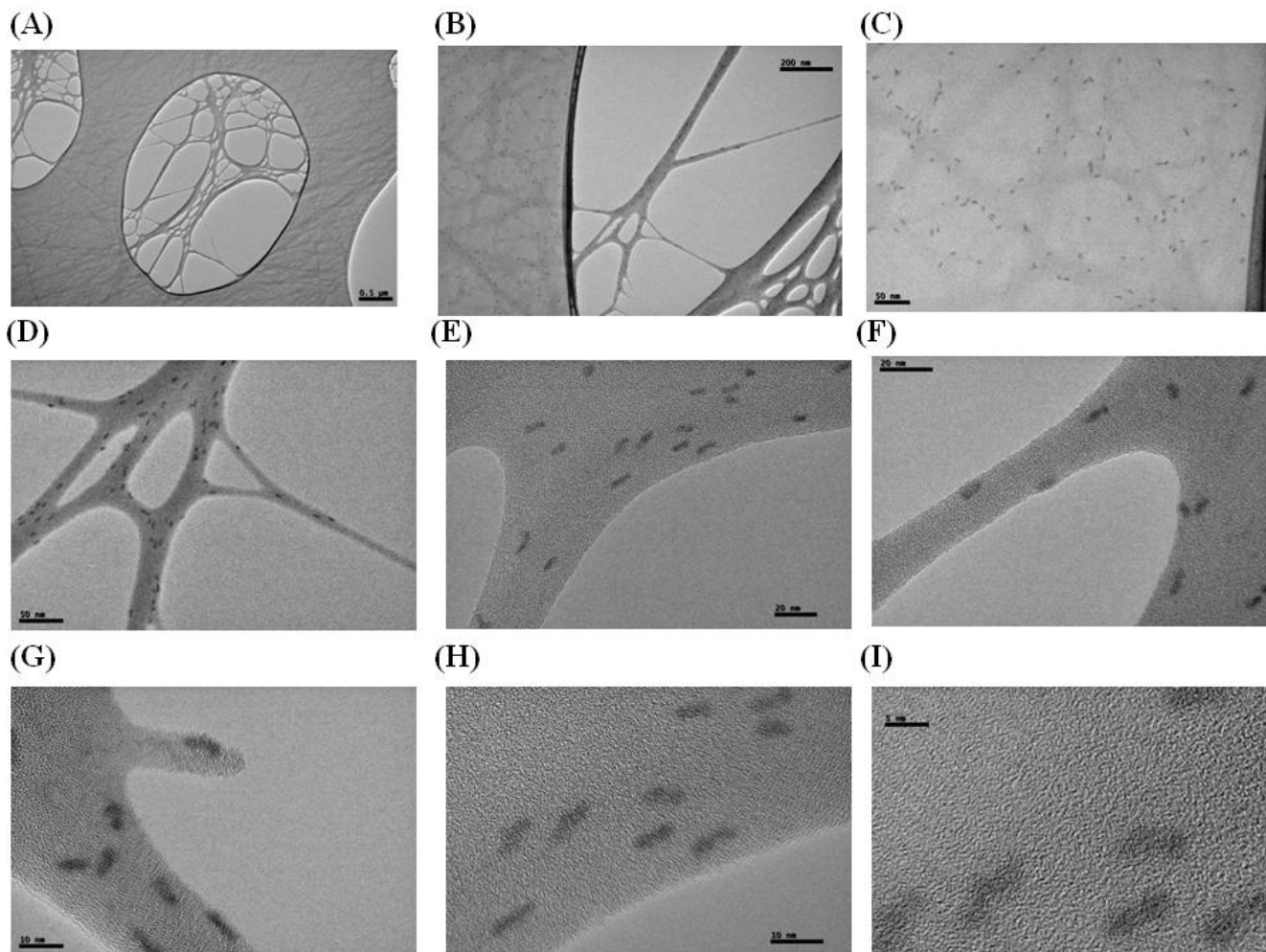


Figure S13. TEM micrographs of the fibrillar structure of cyclophane 1 xerogel containing TCS572 QDs. Scalebar is: A) 500 nm, B) 200 nm, C) 50 nm, D) 50 nm, E) 50 nm, F) 20 nm, G) 10 nm, H) 10 nm, I) 5 nm.

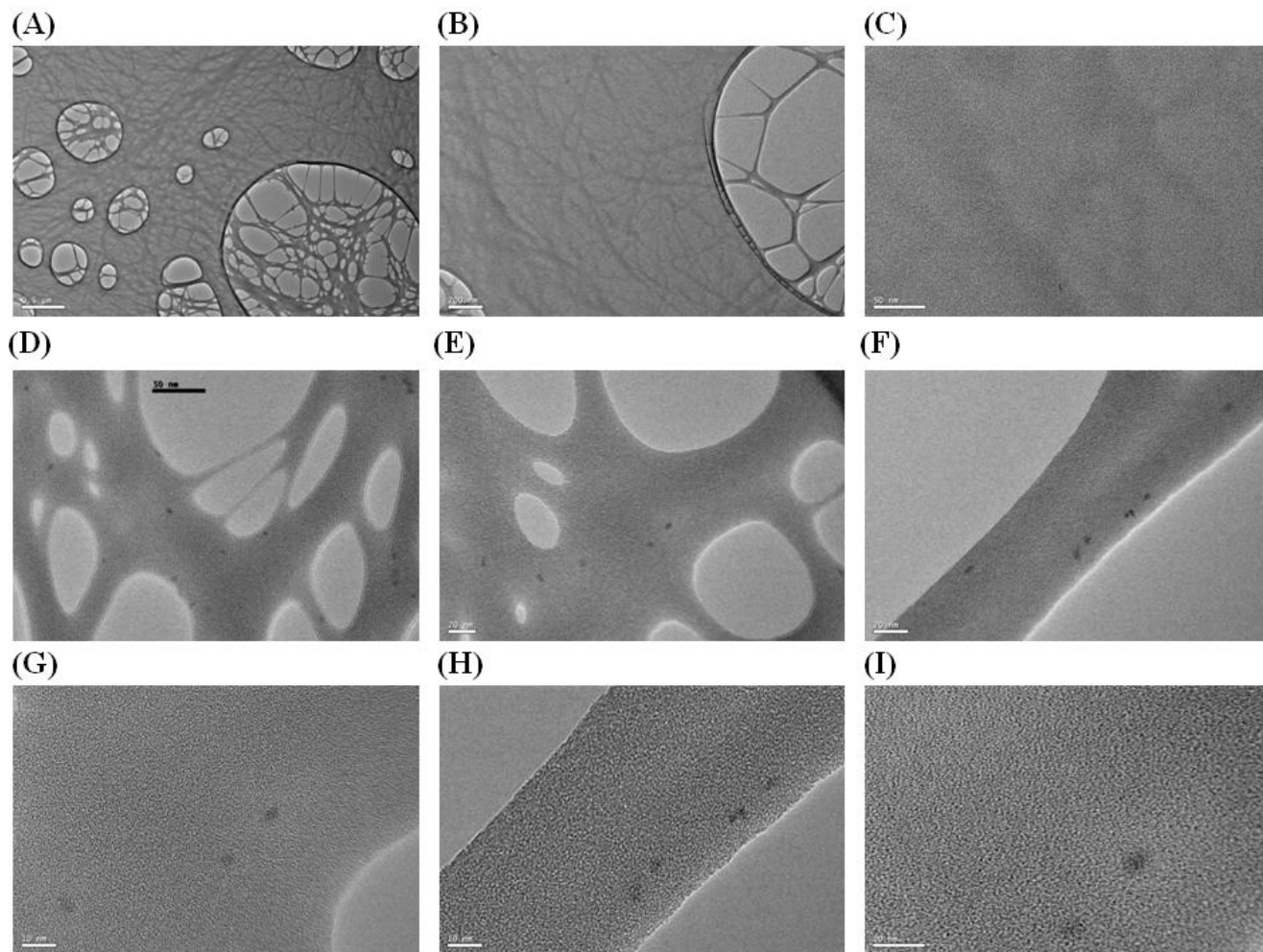


Figure S14. TEM micrographs of the fibrillar structure of cyclophane **1** xerogel containing ACS549 QDs. Scalebar is: A) 500 nm, B) 200 nm, C) 50 nm, D) 50 nm, E) 20 nm, F) 20 nm, G) 10 nm, H) 10 nm, I) 10 nm.

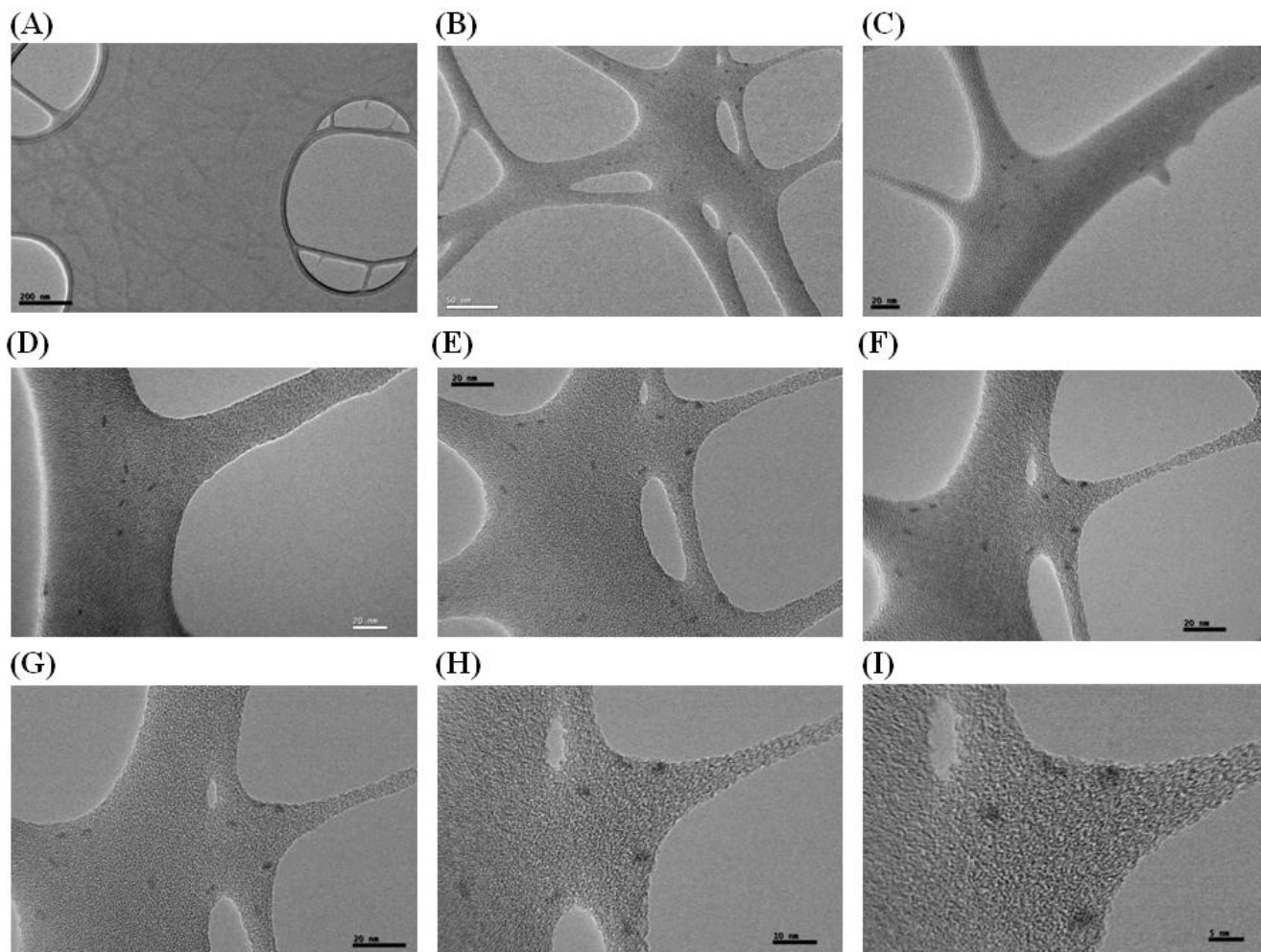


Figure S15. TEM micrographs of the fibrillar structure of cyclophane **1** xerogel containing TC533 QDs. Scalebar is: A) 200 nm, B) 50 nm, C) 20 nm, D) 20 nm, E) 20 nm, F) 20 nm, G) 20 nm, H) 10 nm, I) 5 nm.

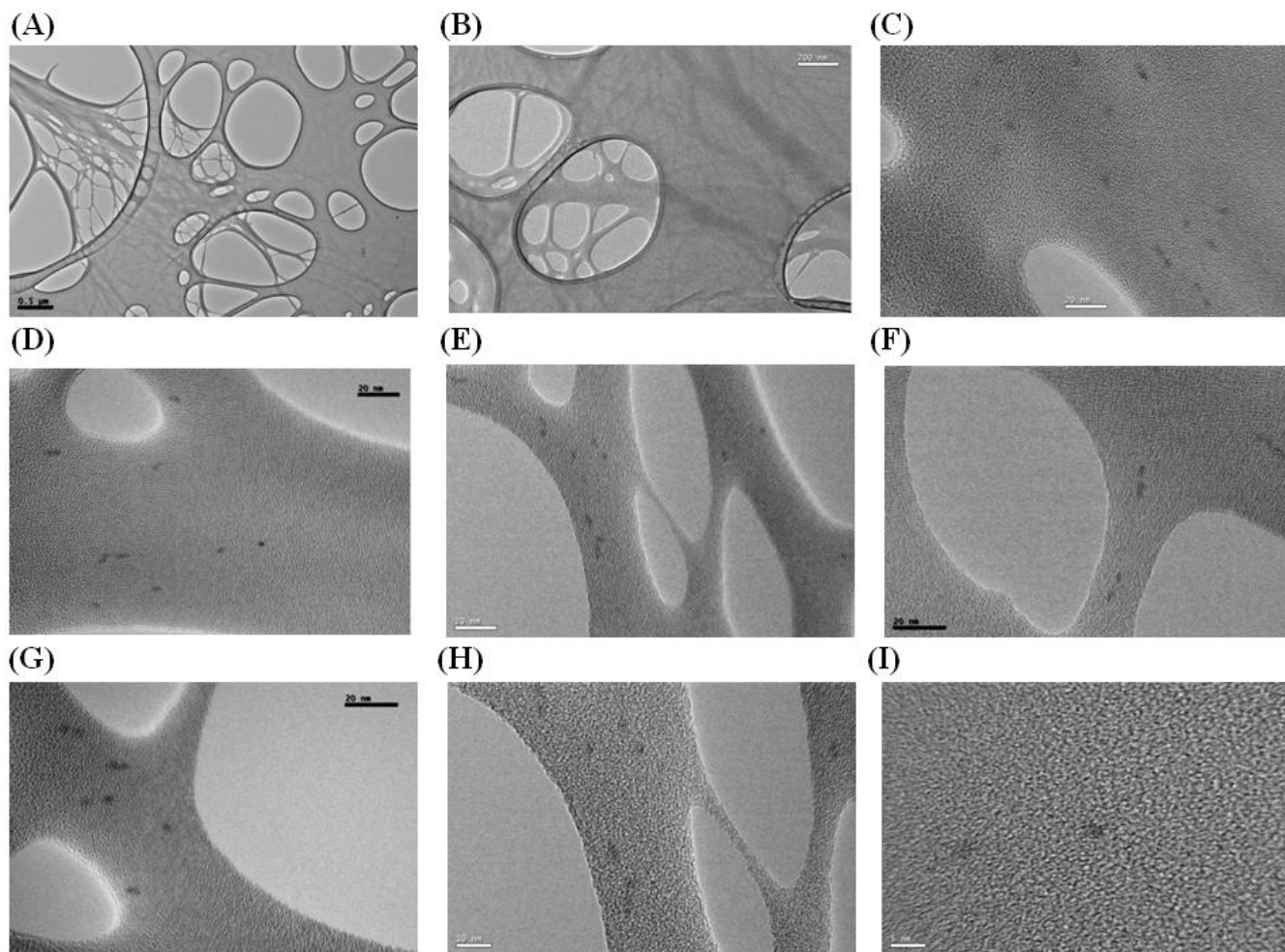


Figure S16. TEM micrographs of the fibrillar structure of cyclophane **1** xerogel containing TC533W QDs. Scalebar is: A) 500 nm, B) 200 nm, C) 20 nm, D) 20 nm, E) 20 nm, F) 20 nm, G) 20 nm, H) 10 nm, I) 5 nm.

**10 – PUBLISHED ARTICLES NO RELATED WITH THE
THESIS**

Application of molecular topology to the prediction of mosquito repellents of a group of terpenoid compounds

R. García-Domenech · J. Aguilera · A. El Moncef · S. Pocovi · Jorge Gálvez

Received: 21 April 2009 / Accepted: 13 June 2009 / Published online: 4 July 2009
© Springer Science+Business Media B.V. 2009

Abstract A topological-mathematical model based on multilinear regression analysis has been built to search new terpenoid actives as mosquito repellents. The structural depiction was performed using topological indices, and a four-variable model for the prediction of corrected repellent ratio ($r^2 = 0.9672$, $Q^2 = 0.9435$) was selected. The model was checked by cross-validation, internal validation, and randomization test. The results confirm its capability to predict the property analyzed. After carrying out a virtual screening upon such a model, new structures with potential repellent activity against mosquitoes are proposed.

Keywords Molecular topology · QSAR · Mosquito repellents · Terpenoid · Multilinear regression · Virtual screening

Introduction

Several diseases are associated to the mosquito–human interaction. Mosquitoes are the carriers of severe and well-known illnesses such as malaria, arboviral encephalitis, dengue fever, Rift Valley fever, West Nile virus, and yellow fever. These diseases produce significant morbidity and mortality in humans and livestock around the world [1]. Due to that,

new repellents are necessary to provide personal protection against mosquito bites. One of the most common repellents is *N, N*-diethyl-*m*-toluamide (DEET) which was first reported in 1951 [2,3]. Since then, several attempts have been made to synthesize repellents better than DEET [4].

The prediction of biological properties of organic compounds is one of the main issues of the methods based on quantitative structure–activity relationships, QSAR. Many works about this topic have been published up to date using this method. One of the earliest is the one by Suryanarayana et al. [5] who prepared 40 amides of aromatic and cyclohexyl carboxylic acids and developed QSAR models using lipophilicity, vapor pressure, and molecular length as correlating variables. Later on, other studies were carried out with the same dataset [6,7].

It is well known that a key issue to ensure the success of a QSAR approach is the selection of the adequate molecular descriptors.

Basak et al. [4] classified these descriptors into four categories:

- (1) Topostructural indices (TS) quantify information regarding the connectivity, adjacency, and distances between atoms—or vertices according to graph theoretical nomenclature—ignoring their distinct chemical nature.
- (2) Topochemical indices (TC) which are sensitive to both the pattern of connectedness of the atoms and their chemical and bonding characteristics.
- (3) 3D or geometrical parameters (3D).
- (4) Quantum chemical descriptors (QC) which encode electronic aspects of chemical structure.

Today, it is known—and at some extent surprising—that topostructural and topochemical information can explain the main part of the predicted properties, and that the inclusion

R. García-Domenech (✉) · J. Gálvez
Dept. Química Física, Facultad de Farmacia, Universitat de Valencia, Avd. V.A. Estellés, s/n, 46100 Burjassot, Valencia, Spain
e-mail: ramon.garcia@uv.es

J. Aguilera · S. Pocovi
Instituto de Ciencia Molecular (ICMOL), Universitat de Valencia, Poligono La Coma, s/n, 46980 Paterna, Valencia, Spain

A. El Moncef
Dept. Química Orgánica, Facultad de Farmacia, Universitat de Valencia, Avd. V.A. Estellés, s/n, 46100 Burjassot, Valencia, Spain

of three-dimensional features results in slightly improved predictive models in many cases [8].

Among the methodologies usually employed in the development of predictive QSAR models stand the multilinear regression analysis (MLRA) [9], Ridge regression (RR) [10, 11] principal components regression (PCR) [12], and partial least squares (PLS) [13].

Topological indices (TIs) are non-empirical descriptors calculated from the representation of the molecules as mathematical graphs [14–18]. These descriptors are able to characterize the most important features of molecular structure: molecular size, binding, and branching. The computation of TIs is very swift, and they also have the advantage of being true structural invariants. TIs have been useful in the prediction of biological properties related to toxicity and insecticidal activity, even in groups of compounds showing considerable structural diversity [19–25].

The aim of this study is to obtain a topological model using only topological and topochemical descriptors. The study consists of the utilization of the MLRA to develop a topological-mathematical model capable of identifying the activity of the terpenoids as mosquito repellent, and apply the model to the search of new potentially active compounds through molecular screening.

Materials and methods

Analyzed compounds

A group of 20 compounds synthesized from α - and β - pinene was used to study the activity as repellent against *Aedes albopictus* mosquito. All the compounds are derivatives of a six-carbon ring scaffold with a substituent containing at least one oxygen (see Table 1).

Repellent ratio (RR) was determined by applying test compounds at a dose of 0.16 mg/cm² on the depilated abdomen of white mice as follows:

$$RR = \frac{(TN - TNB)}{TN} \times 100,$$

TN is the total number of female mosquitoes used in testing, while TNB is the total number of biting female mosquitoes. The repellent ratio of the control experiment (CERR) was calculated in the same way as RR. The corrected repellent ratio (CRR) was also calculated to evaluate the repellency more accurately.

$$CRR = \frac{(RR - CERR)}{(100 - CERR)} \times 100.$$

CRR values for each compound are shown in the Table 1. Details over synthesis and repellent assays have been obtained from reference [26].

Molecular descriptors

A set of well-known topological descriptors was input for correlation, namely, subgraph Randić–Kier–Hall-like indices up to the fourth order (${}^m\chi_t, {}^m\chi_t^v$) [27, 28], topological charge indices (TCI) up to the fifth order, (J_m, G_m, J_m^v, G_m^v) [29], quotients and differences between valence and non-valence connectivity indices (${}^mC_t = {}^m\chi_t / {}^m\chi_t^v$ and ${}^mD_t = {}^m\chi_t - {}^m\chi_t^v$) and some ad hoc indices [30]. Each compound was characterized by a set of 62 descriptors. Table 2 shows the notation, name, and definition of each descriptor. All descriptors used in this study were obtained with the aid of the Desmol11 program (available by e-mail request).

Multilinear regression analysis

The general purpose of multilinear regression analysis (MLRA) is to outline the relation between two or more independent variables and a dependent variable by fitting a linear equation to observed data. In prediction of repulsive activity against mosquitoes, the MLRA was used as statistical method. This calculation was performed using the software package Statistica version 8.0. [31]. Variable selection was carried out by means of the Furnival–Wilson algorithm and variable sets with the minimal Mallows' Cp were selected as the best to the regression equations [32].

The predictability quality and robustness of the developed model must be verified by using different types of validation criteria. Usually four strategies are adopted [33]: (a) internal validation or cross-validation with leave-one-out, LOO, and leave-some-out, LSO; (b) validation by dividing the dataset into training and test compounds; (c) true external validation by application of the model on external data; and (d) data randomization or Y-scrambling. In this article, given that our dataset was small, $n = 20$, we used the strategies (a, b, and d) as validation criteria.

Results and discussion

In order to obtain the CRR predictive topological model, the multilinear regression analysis was applied; a rigorous statistical analysis using the Statistica 8.0 software was performed. Topological indices were used as independent variables and the CRR values, in their logarithmic transformation (LogCRR), were input as dependent variables. Likewise, according to the number of cases ($N = 20$) and the selected group of variables, the obtained function is summarized in Table 3.

If we observe the column p-level in Table 3, we realize that all the present indices are statistically significant at above 99%. This indicates that all contain, at a significant rate, topological and structural information enough to

Table 1 CAS registry number, structure of chemicals, and Log CRR experimental and obtained values in the QSAR study for the training group

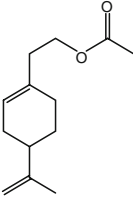
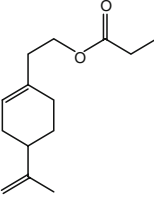
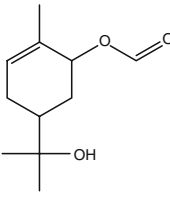
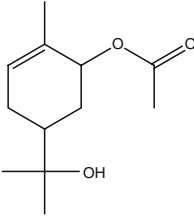
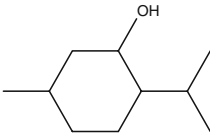
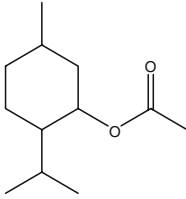
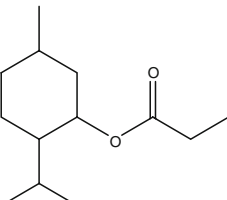
Compound	CAS	Structure	Log CRR _{exp} ^a	Log CRR _{calc} ^b	Log CRR _{calc} (cv) ^c
01	57782-95-3		1.767	1.791	1.806
02	1034449-20-1		1.803	1.797	1.795
03	902779-66-2		1.954	1.946	1.941
04	1081-64-7		1.908	1.915	1.924
05	1490-04-6		1.724	1.739	1.748
06	16409-45-3		1.588	1.577	1.570
07	–		1.607	1.586	1.577

Table 1 continued

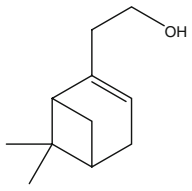
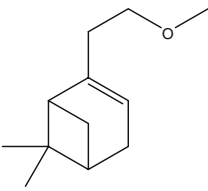
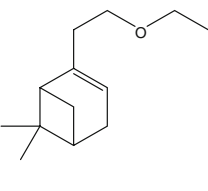
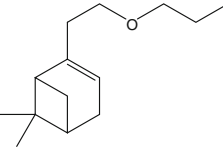
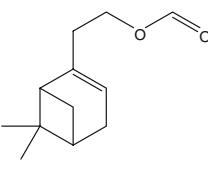
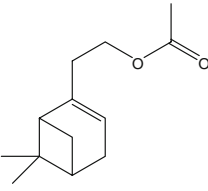
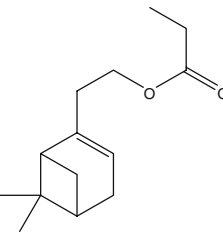
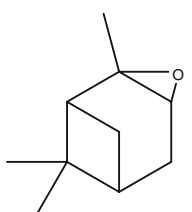
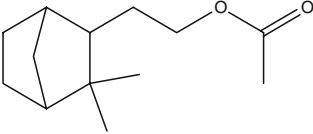
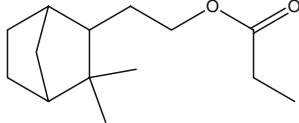
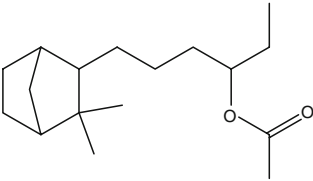
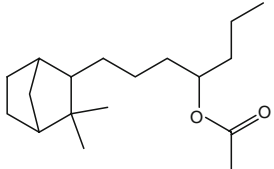
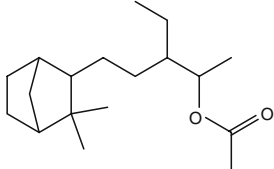
08	128-50-7		1.839	1.839	1.839
09	81991-72-2		1.717	1.753	1.761
10	–		1.794	1.799	1.800
11	259532-24-6		1.860	1.813	1.805
12	68310-60-1		1.749	1.738	1.735
13	128-51-8		1.784	1.785	1.785
14	259532-23-5		1.809	1.797	1.796
15	1686-14-2		1.577	1.589	1.599

Table 1 continued

16	94134-25-5		1.724	1.731	1.732
17	1037399-56-6		1.754	1.743	1.742
18	1037399-58-8		1.701	1.712	1.714
19	1037399-60-2		1.713	1.724	1.727
20	1037399-62-4		1.712	1.711	1.711

^a Values obtained from ref. [26]; ^b From selected equation; ^c From cross-validation study

quantify the property studied. In the selected equation, there are topological descriptors evaluating the topological docking of each compound, 2C and 4C_c , molecular branching, PR2, and the distributions of the intramolecular charge through the charge index J_1^v ; PR2 and 4C_c being the descriptors that contribute more to the value of r^2 (see column six in Table 3). Moreover, all the selected descriptors are only slightly intercorrelated ($r^2 < 0.56$).

The selected model is able to explain more than 96% of the variance of the property correlated ($r^2 = 0.9672$) with a standard estimation error below 6% of the range of the property ($SEE = 0.199$).

The summary of the linear regression for the dependent variable (LogCRR) applying the same statistical package provides a suitable correlation coefficient with a short standard error and a large Fisher factor.

Table 1 and Fig. 1 show the prediction values obtained for every compound of the group studied. Roughly 80% of the compounds exhibited residuals below ± 1 SEE, and only the compound n°11 shows a residual above ± 2 SEE.

The first validation test of the topological mathematical model arranged was a cross-validation type of LOO and LSO for $n \leq 5$. Table 1, column six, shows the predicted values for each compound in the LOO test. The coefficient of determination obtained, $Q^2 = 0.9435$, is similar to r^2 in the training set ($r^2 = 0.9672$), which stands for the statistical quality of the selected equation.

In the cross-validation of the type LSO, we work with values of $n = 2, 3, 4$, and 5 , which implies the elimination of 90%, 85%, 80%, and 75% of the compounds in the training set, respectively. The prediction coefficients were of similar order to those obtained with the complete group

Table 2 Descriptors used in this study

Symbol	Name	Definition
${}^k\chi_t$ $k = 0-4$ $t = \text{p,c,pc}$	Randić-like indices of order k and type path (p), cluster (c), and path cluster (pc)	${}^k\chi_t = \sum_{j=1}^{k_{n_t}} \left(\prod_{i \in S_j} \delta_i \right)^{-1/2}$ δ_i , number of bonds, σ or π , of the atom i to non-hydrogen atoms S_j , j th sub-structure of order k and type t
${}^k\chi_t^v$ $k = 0-4$ $t = \text{p,c,pc}$	Kier-Hall indices of order k and type path (p), cluster (c), and path cluster (pc)	${}^k\chi_t^v = \sum_{j=1}^{k_{n_t}} \left(\prod_{i \in S_j} \delta_i^v \right)^{-1/2}$ δ_i^v , Kier-Hall valence of the atom i S_j , j th sub-structure of order k and type t
G_k $k = 1-5$	Topological charge indices of order k	$G_k = \sum_{i=1}^{N-1} \sum_{j=i+1}^N M_{ij} - M_{ji} $ $\delta(k, \mathbf{D}_{ij}) \mathbf{M} = \mathbf{A}\mathbf{Q}$, product of the adjacency and inverse squared distance matrices for the hydrogen-depleted molecular graph \mathbf{D} , distance matrix δ , Kronecker delta
G_k^v $k = 1-5$	Valence topological charge indices of order k	$G_k^v = \sum_{i=1}^{N-1} \sum_{j=i+1}^N M_{ij}^v - M_{ji}^v \delta$ $(k, \mathbf{D}_{ij}) \mathbf{M}^v = \mathbf{A}^v \mathbf{Q}$, product of the electronegativity-modified adjacency and inverse squared distance matrices for the hydrogen-depleted molecular graph \mathbf{D} , distance matrix δ , Kronecker delta
J_k $k = 1-5$	Normalized topological charge indices of order k	$J_k = \frac{G_k}{N-1}$
J_k^v $k = 1-5$	Normalized valence topological charge indices of order k	$J_k^v = \frac{G_k^v}{N-1}$
kD_t $k = 0-4$ $t = \text{p,c,pc}$	Connectivity differences of order k and type path (p), cluster (c), and path cluster (pc)	${}^kD_t = {}^k\chi_t - {}^k\chi_t^v$
kC_t $k = 0-4$ $t = \text{p,c,pc}$	Connectivity quotients of order k and type path (p), cluster (c), and path cluster (pc)	${}^kC_t = \frac{{}^k\chi_t}{{}^k\chi_t^v}$
MW	Molecular weight	
R	Ramification	Number of single structural branches
PRk $k=0-3$	Pairs of ramifications at distance k	Number of pairs of single branches at distance k in terms of bonds.

$(Q_{n=2}^2 = 0.94348; Q_{n=3}^2 = 0.94342, Q_{n=4}^2 = 0.94316, \text{ and } Q_{n=5}^2 = 0.94316)$.

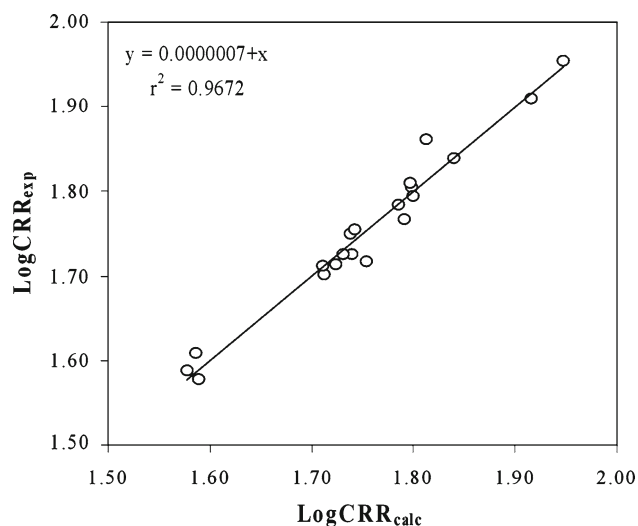
In a second stage, an internal validation was carried out by dividing the training set into five subsets (A–E), containing each 20% of the compounds analyzed: the first, sixth, eleventh, and sixteenth data points going into the subset A, the second, seventh, twelfth, and seventh into the second subset

B, and so forth. Four out of the five subsets (A, B, C, and D), (A, B, C, and E), (A, B, D, and E), (A, C, D, and E), and (B, C, D, and E) were used as the training set, whereas the remaining ones were left as test set. The regression equation obtained for each of the training sets containing the same descriptors was used to predict the values of the corresponding test sets. Table 4 shows the values of r^2 and r_{pred}^2 for each training and

Table 3 Statistical parameters of the four-variable equation in the QSAR study for the training set

	Coefficient	SE	<i>t</i> -stat.	<i>p</i> -level	Contribution to r^2
Intercept	1.387	0.091	15.27	0.0003	–
J_1^V	–0.535	0.059	–8.92	0.0001	0.1744
2C	0.666	0.090	7.39	0.0001	0.1197
4C_c	0.112	0.009	12.61	0.0002	0.3478
PR2	–0.076	0.005	–15.86	0.0001	0.5509

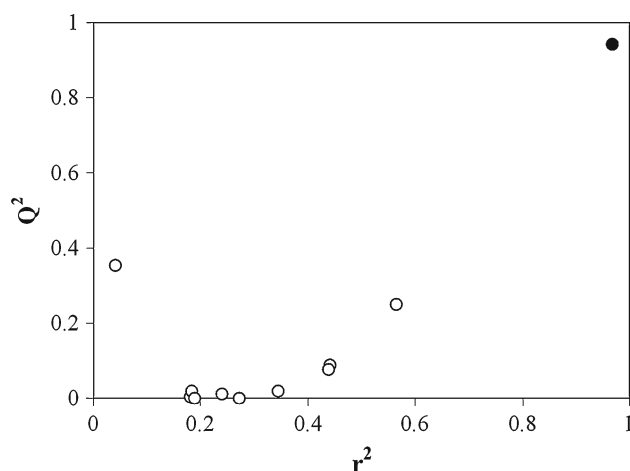
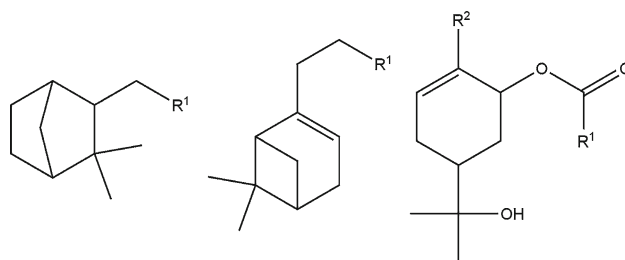
$N = 20$; $r^2 = 0.9672$; $SEE = 0.0199$; $Q^2 = 0.9435$; $F(4,15) = 110.6$; $p < 0.0001$

**Fig. 1** Graphic representation of Log CRR_{exp} versus Log CRR_{calc} from the topological model selected**Table 4** Internal validation of QSAR model

Training set	Test set	r^2 (training set)	r^2_{pred} (test set)
A, B, C, D and E	–	0.9672	–
B, C, D and E	A	0.9830	0.8864
A, C, D and E	B	0.9692	0.9996
A, B, D and E	C	0.9548	0.9986
A, B, C, and E	D	0.9724	0.9553
A, B, C, and D	E	0.9619	0.9941
Average		0.9725	0.9403

test set analyzed. The variability of r^2 and r^2_{pred} is low for each subset, and the average r^2 and r^2_{pred} ($r^2 = 0.9725$ and $r^2_{pred} = 0.9403$) is similar to that obtained with the selected model.

In a third stage, a randomization study was applied to the model to show that changes in the values of the property CRR among different molecules give rise to worse significance values as compared to the training system. Indeed, correlation coefficients (r^2 and Q^2) lower than 0.5 were observed, which makes obvious the conclusion of the non-randomness

**Fig. 2** Graphic representation of the prediction coefficient, Q^2 , versus correlation coefficient, r^2 , obtained by randomization study (black point: selected model)**Fig. 3** Chemical structures used in the virtual screening with Scifinder Scholar

of the selected equation, Fig. 2 (black point with the real values of each compound).

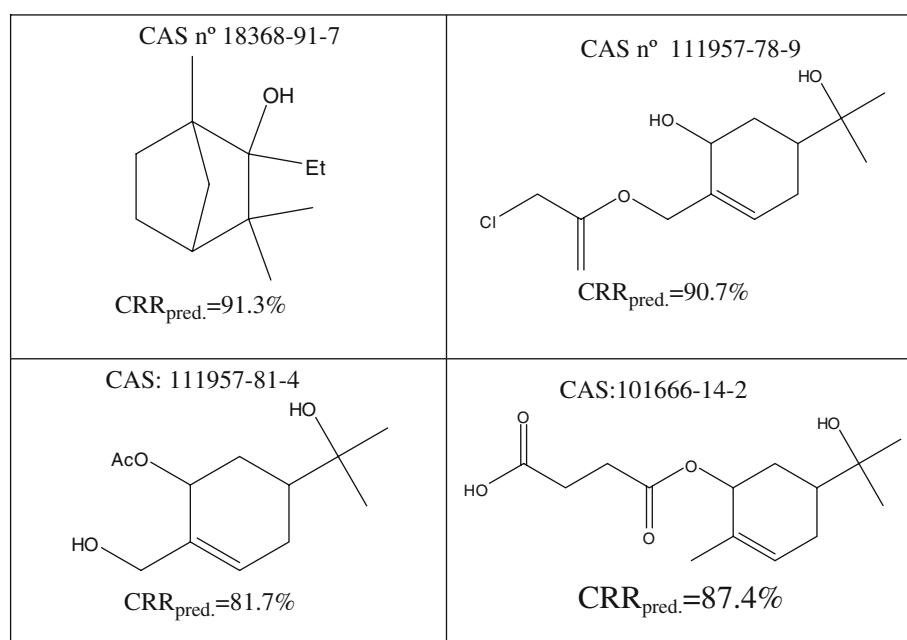
The results from the validation analysis stand for the robustness and stability of the regression model as well as its performance in predicting CCR for similar compounds (terpenoids).

As compared to the Wang et al.'s results [26], dealing with the same group of compounds and properties, one can see that those described here are better. For instance, for the four-variable equation, Wang's results are $r^2_{Wang} = 0.950$ and $SEE_{Wang} = 0.0250$ versus $r^2 = 0.967$ and $SEE = 0.0199$ obtained by us. Moreover, the only descriptors used in our models are topological indices, which are easy to calculate and are not affected by any experimental error. In the Wang model, parameters such as boiling point, dipole moment, molecular surface area, and charge are present; these parameters were experimentally measured and hence slower to determine and subject to experimental error.

Once validated the model for terpenic compounds, it was applied to the search of new terpenic compounds potentially showing mosquito repellent activity. Therefore, a virtual screening into the Scifinder Scholar database was carried out to find out new molecular candidates potentially active. Figure 3 illustrates the scaffolds used in the screening pro-

Table 5 Computational screening applied to terpenoid with a six-member-ring analogs obtained of Scifinder Scholar base and using the model selected by molecular topology

CAS n°	Log CRR _{pred.}	CRR _{pred.} (%)	CAS n°	Log CRR _{pred.}	CRR _{pred.} (%)
18368-91-7	1.960	91.3	127345-36-2	1.777	59.9
111957-78-9	1.958	90.7	18410-94-1	1.767	58.5
101666-14-2	1.942	87.4	22833-73-4	1.750	56.2
111957-81-4	1.912	81.7	66062-78-0	1.748	56.0
127345-32-8	1.871	74.2	648894-38-6	1.731	53.8
2226-14-4	1.852	71.1	22833-72-3	1.709	51.2
35836-73-8	1.839	69.1	85392-38-7	1.705	50.7
33885-51-7	1.830	67.6	474-10-2	1.697	49.8
7712-50-7	1.813	65.0	42370-07-0	1.691	49.1
124434-99-7	1.805	63.8	588708-10-5	1.678	47.7
68754-15-4	1.805	63.8	52557-97-8	1.598	39.7
33885-52-8	1.785	61.0			



cess. The structural fragments in the substituents R^1 and R^2 should only contain the atoms H, C, and O.

Table 5 depicts the predicted values for the CCR activity in the selected compounds. Among them, stand four candidates with repellent activity above 80%, namely, CAS: 18368-91-7 with CRR_{pred.} = 91.3%; CAS: 111957-78-9 with CRR_{pred.} = 90.7%; CAS: 101666-14-2 with CRR_{pred.} = 87.4%; and CAS: 111957-81-4 with CRR_{pred.} = 81.7%. Furthermore, according to the literature sources consulted, none of them has been yet described as mosquito repellent. Compound CAS: 101666-14-2 is known to show antipyretic activity [34] and could be a good candidate for experimental testing.

These suggestive results need to be confirmed by experimental tests. Should the test be positive, the model proposed would be validated and serve as a useful tool for the search of novel compounds with mosquito repellent activity.

Conclusions

Molecular topology has been successfully used to build up a QSAR model for predicting the mosquito repellent activity of a group of terpenoids comprised of six-membered ring compounds. All the molecular descriptors used in this study were graph-theoretical ones. The mathematical model

arranged here retains the main structural features involved in the correlated property, (corrected repellent ratio, CRR), and hence can be applied to the search of new active analogous compounds by virtual screening throughout databases. A virtual library of terpenoid derivatives was screened for seeking and optimizing the repellent activity against *Aedes albopictus* mosquitoes. The results demonstrate that new compounds potentially exhibiting activity have been obtained. The experimental results, whether positive, would strengthen the role of molecular topology in the prediction of mosquito repellent activity.

Acknowledgments The authors acknowledge financial aid from the Fondo de Investigación Sanitaria, Ministerio de Sanidad, Spain (project SAF2005-PI052128) and Master Interuniversitario en Química Sostenible of the Universitat of Valencia, Spain.

References

- Eldrige BF, Edman JD (2004) Medical entomology: a textbook of public health and veterinary problems caused by arthropods. 2nd ed. Kluwer Academic Publishers, Dordrecht
- Hayes WJJr (1982) Pesticides studied in man. Williams and Wilkins, Baltimore, MD
- US Environmental Protection Agency (1980) Office of pesticides and toxic substances. *N, N*-Diethyl-*m*-toluamide (DEET) pesticide registration standard
- Natarajan R, Basak SC, Mills D, Kraker JJ, Hawkins DM (2008) Quantitative structure-activity relationship modeling of mosquito repellents using calculated descriptors. *Croat Chem Acta* 81:333–340
- Suryanarayana MVS, Pandey KS, Prakash S et al (1991) Structure-activity relationship studies with mosquito repellent amides. *J Pharm Sci* 80:1055–1057
- Ma D, Bhattacharjee A, Gupta R, Karle J (1999) Predicting mosquito repellent potency of *N, N*-Diethyl-*m*-toluamide (DEET) analogs from molecular electronic properties. *Am J Trop Med Hyg* 60:1–6
- Katritzky AR, Dobchev DA, Tulp I, Karelson M, Carlson DA (2006) QSAR study of mosquito repellents using Codessa Pro. *Bioorg Med Chem Lett* 16:2306–2311
- Basak SC, Mills DR, Balaban AT, Gute BD (2001) Prediction of mutagenicity of aromatic and heteroaromatic amines from structure: A hierarchical QSAR approach. *J Chem Inf Comput Sci* 41:671–678
- Furnival GM, Wilson RW (2000) Regressions by leaps and bounds. *Technometrics* 42:69–79
- Hoerl AE, Kennard RW (1970) Ridge regression: biased estimation for nonorthogonal problems. *Technometrics* 12:55–67
- Hoerl AE, Kennard RW (2000) Ridge regression: biased estimation for nonorthogonal problems. *Technometrics* 42:80–86
- Massy WF (1965) Principal components regression in exploratory statistical research. *J Am Stat Assoc* 60:234–256
- Wold S (1993) Discussion: PLS in chemical practice. *Technometrics* 35:136–139
- Devillers J, Balaban AT (1999) Topological indices and related descriptors in QSAR and QSPR. Gordon and Breach Science Publishers, Singapore
- Ivanciuc O (2003) Topological indices. In: Gasteiger J (ed), Handbook of cheminformatics. Wiley-VCH, Weinheim
- Todeschini R, Consonni V (2000) Handbook of molecular descriptors. Wiley-VCH, Weinheim
- Pogliani L (2000) From molecular connectivity indices to semi-empirical connectivity terms: Recent trends in graph theoretical descriptors. *Chem Rev* 100:3827–3858
- Karelson M (2000) Molecular Descriptors in QSAR/QSPR. Wiley, New York
- Garcia-Domenech R, de Julian-Ortiz JV, Besalu E (2006) True prediction of lowest observed adverse effect levels. *Mol Divers* 10:159–168
- Luco JM, Galvez J, Garcia-Domenech R, de Julian-Ortiz JV (2004) Structural invariants for the prediction of relative toxicities of polychloro dibenzo-*p*-dioxins and dibenzofurans. *Mol Divers* 8:331–342
- Garcia-Domenech R, Galvez J, de Julian-Ortiz JV, Pogliani L (2008) Some new trends in chemical graph theory. *Chem Rev* 108:1127–1169
- Galvez J, de Julian-Ortiz JV, Garcia-Domenech R (2005) Application of molecular topology to the prediction of potency and selection of novel insecticides active against malaria vectors. *Theochem* 727:107–113
- Rios-Santamarina I, Garcia-Domenech R, Cortijo J, Santamaría P, Morcillo EJ, Galvez J (2002) Natural compounds with bronchodilator activity selected by molecular topology. *Internet Electron J Mol Des* 1:70–79
- Garcia-Domenech R, Catala-Gregori A, Calabuig C, Anton-Fos GM, del Castillo L, Galvez J (2002) Predicting antifungal activity: a computational screening using topological descriptors. *Internet Electron J Mol Des* 1:339–350
- Llacer MT, Galvez J, Garcia-Domenech R, Gómez-Lechón MJ, Más-Arcas C, de Julian-Ortiz JV (2006) Topological virtual screening and pharmacological test of novel cytostatic drugs. *Internet Electron J Mol Des* 5:306–319
- Wang ZD, Song J, Chen JZ et al (2008) QSAR study of mosquito repellents from terpenoid with a six-member-ring. *Bioorg Med Chem Lett* 18:2854–2859
- Randic M (1975) Characterization of molecular branching. *J Am Chem Soc* 97:6609–6615
- Kier LB, Murray WJ, Randic M, Hall LH (1976) Molecular connectivity V: Connectivity series concept applied to density. *J Pharm Sci* 65:1226–1230
- Galvez J, Garcia R, Salabert MT, Soler R (1994) Charge indexes. New topological. Descriptors. *J Chem Inf Comput Sci* 34:520–525
- Galvez J, Garcia-Domenech R, de Julian-Ortiz JV, Soler R (1995) Topological approach to drug design. *J Chem Inf Comput Sci* 35:273–284
- Statistica 8.0 (2008) Statsoft Inc <http://www.statsoft.com>
- Hocking RR (1972) Criteria for selection of a subset regression: Which one should be used?. *Technometrics* 14:967–970
- Roy PP, Leonard JT, Roy K (2008) Exploring the impact of size of training sets for the development of predictive QSAR models. *Chemometrics Intell Lab Syst* 90:31–42
- Corvi MC (1986) Derivative of *p*-aminophenol with a mucosecretolytic fluidizing and antipyretic activity and its pharmaceutical compositions. *Eur Pat Appl EP* 166080 A1 19860102

